Characterising a novel heavy metal-sensing multikinase network in the environmental organism and opportunistic pathogen, *Burkholderia cenocepacia*

Submitted by Jack Plume, to the University of Exeter as a thesis for the degree of Doctor of Philosophy in Biological Sciences, April 2020

Acknowledgements

I have been fortunate enough to have had the help and support of many people throughout my PhD, who hopefully will be suitably acknowledged herein.

Firstly, thank you to both Dr Alan Brown and Dr Steve Porter, my PhD supervisors. Their support and guidance, scientific and otherwise, has been indispensable to my progression over the last four years. The fact that I managed to enjoy (nearly) every moment of the past few years in the lab has been largely due to their influence, and I have been extremely fortunate to have been supervised by them both.

Thank you also to my de facto third supervisor, Dr Vanessa Francis. Her patience and willingness to help, despite questions that must number into the hundreds, have been enormously appreciated. Her propensity to bring in snacks whenever she visits the petrol station has also been of great value. Thank you too to the other PhD students on the fourth floor (Cam, Georgie, Josh and Matt, collectively known as “The Brain Trust”) for many troubleshooting conversations and general comradery.

I have also been particularly fortunate to have supervised several undergraduate students during my time in Exeter, a process which I, admittedly surprisingly, found incredibly rewarding. Thank you to Emma, Jack, Becky and Ellen for being a pleasure to work alongside.

Thank you to my family for their continued encouragement, as well as reminding me that a world exists outside of metal-sensing two-component systems. Thank you to Lucy, Bess, Philly, Holly and Kia for their wagging tails, especially during troublesome attempts at molecular cloning.

And thank you to Alice, whose limitless support and love have been central to the last few years. Apologies for being 134 miles away for so long. My bad.

Abstract

Two-component systems (TCSs) are a primary means of responding to environmental cues across the bacterial domain, and usually act independently of one another, forming discrete, isolated units. Multikinase networks (MKNs) are systems of multiple TCSs which can interact to integrate numerous signals into a decided cellular output, conferring an advantage to the cell. This work focuses on a novel MKN from the opportunistic pathogen, *Burkholderia cenocepacia*.

Through purification of each putative TCS, their ability to undergo non-cognate phosphorylation with one another was assessed *in vitro* through the phosphotransfer assay. This revealed that three sensor kinases, BCAM0442, BCAM0715 and BCAS0585 are able to phosphorylate one another's response regulators. This non-cognate phosphotransfer was also possible, albeit to a lesser extent, in the presence of the cognate response regulator protein.

Deletion mutants of each TCS and investigation of TCS promoter induction revealed that BCAM0442/3 is implicated in copper resistance, and BCAM0714/5 is implicated in cadmium and zinc resistance. Exposure of *B. cenocepacia* to copper or zinc enhances resistance to imipenem, a phenomenon in which this MKN is implicated. A MKN deletion mutant is heavily attenuated in virulence in *Galleria mellonella*, linking the metal response with virulence in *B. cenocepacia*. Additionally, exploration of the copper response by RNA-seq analysis revealed substantial upregulation of the genes surrounding BCAM0442/3. A CopABCDE-like system was strongly upregulated in a BCAM0442/3-dependent manner, suggesting that BCAM0442/3 directly regulates this system.

Previous work identified that BCAM0714/5 regulates a downstream gene region, BCAM0716-21, deletion of which confers susceptibility to zinc in *B. cenocepacia*. Complementation with the BCAM0716/17 gene region restored resistance to zinc, implicating these genes in the zinc response of *B. cenocepacia*.

Given the environmental impact of heavy metal pollution and the use of metals as both an antibacterial strategy by the immune system and in medical devices, understanding the mechanisms of bacterial metal resistance is vital. This work has identified a novel metal-sensing MKN in *B. cenocepacia*, linking the cadmium, zinc and copper responses with virulence and carbapenem resistance.

Table of contents

List of figures

List of tables

List of abbreviations

ABC	ATP binding cassette
Amp	Ampicillin
Ara4N	4-amino-4-deoxy-L-arabinose
ATP	Adenosine triphosphate
BACTH	Bacterial adenylate cyclase two-hybrid system
BCC	*Burkholderia cepacia* complex
BDSF	*Burkholderia* diffusible signal factor
CA	Catalytic and ATP-binding domain
CDF	Cation diffusion facilitator
CF	Cystic fibrosis
CFTR	Cystic fibrosis transmembrane conductance regulator
CFU	Colony-forming unit
CGD	Chronic granulomatous disease
ChIP-seq	Chromatin immunoprecipitation sequencing
DBD	DNA-binding domain
ddH_2O	Double-distilled water
DHp	Histidine phosphotransfer domain
DMEM	Dulbecco's modified eagle medium
DMSO	Dimethyl sulfoxide
DTT	Dithiothreitol
EPS	Exopolysaccharides
FBS	Foetal bovine serum
Gm	Gentamicin

HPt	Histidine phosphotransferase
IPTG	Isopropyl β-D-1-thiogalactopyranoside
Kan	Kanamycin
LB	Lysogeny broth
LPS	Lipopolysaccharide
MFP	Membrane fusion protein
MIC	Minimal inhibitory concentration
MKN	Multikinase network
MOI	Multiplicity of infection
NADPH	Nicotinamide adenine dinucleotide phosphate
NRAMP1	Natural resistance-associated membrane protein 1
OCS	One-component system
OMF	Outer membrane factor
PBS	Phosphate-buffered saline
PCR	Polymerase chain reaction
Pol	Polymyxin B
RD	Receiver domain
RND	Resistance-Nodulation-Cell Division
ROS	Reactive oxygen species
RR	Response regulator
RR-P	Phosphorylated RR
SDS	Sodium dodecyl sulfate
SEM	Standard error of the mean
SK	Sensor kinase
SK-P	Phosphorylated SK

T1SS	Type I Secretion System
TCS	Two-component system
Tet	Tetracycline
Tp	Trimethoprim

Chapter 1: Introduction

1.1 – An introduction to the *Burkholderia cepacia* complex

1.1.1 – *Burkholderia* and the *Burkholderia cepacia* complex

The first *Burkholderia* species was described in 1950 as the cause of skin rot on onions bulbs, and hence given the name *Pseudomonas cepacia* [1]. This species, and six others, were transferred to the new *Burkholderia* genus in 1992, when analysis of 16S rRNA sequences justified their reclassification [2]. Belonging to the class β-proteobacteria, the genus has grown in the following decades to approximately 100 species, with members occupying a wide range of environmental niches and acting as significant mammalian pathogens [3,4].

Recent phylogenetic analyses have identified two distinct clades within the *Burkholderia* genus, with a smaller clade containing groups of clinical relevance that are able to cause a range of disease in both humans and animals, and a larger clade composed of largely environmental species, with conserved sequence indels having been identified for both clades (Fig 1.1) [5–7]. Consequently, it was proposed to transfer the larger clade into the new genus *Paraburkholderia*, leaving the smaller clade, containing mainly human, animal and plant pathogens, within *Burkholderia* [6,7]. Since this reclassification, another novel genus has been proposed to accommodate a distinct clade in this ever-growing phylogenetic tree, named *Caballeronia* [8].

As a result of the reclassification of *Burkholderia*, the genus' current members are generally considered to be either human, animal or plant pathogens. *Burkholderia* can be split into three groups, the largest of which is the *Burkholderia cepacia* complex (BCC), which is comprised of approximately 20 different species. The BCC is a highly diverse complex sitting within a highly diverse genus, with members found throughout various natural environments and are also able to act as opportunistic pathogens to the immunocompromised [9]. The *Burkholderia pseudomallei* group consists of 4 species, *B. pseudomallei*, *Burkholderia mallei*, *Burkholderia thailandensis* and *Burkholderia oklahomensis*. *B. pseudomallei* and *B. mallei* are the causative agents of melioidosis and equine glanders respectively, with *B. pseudomallei* being considered as a potential bioterror threat in the United States [10]. The final subclade consists of

phytopathogens, such as *Burkholderia glumae*, *Burkholderia gladioli* and *Burkholderia plantarii*.

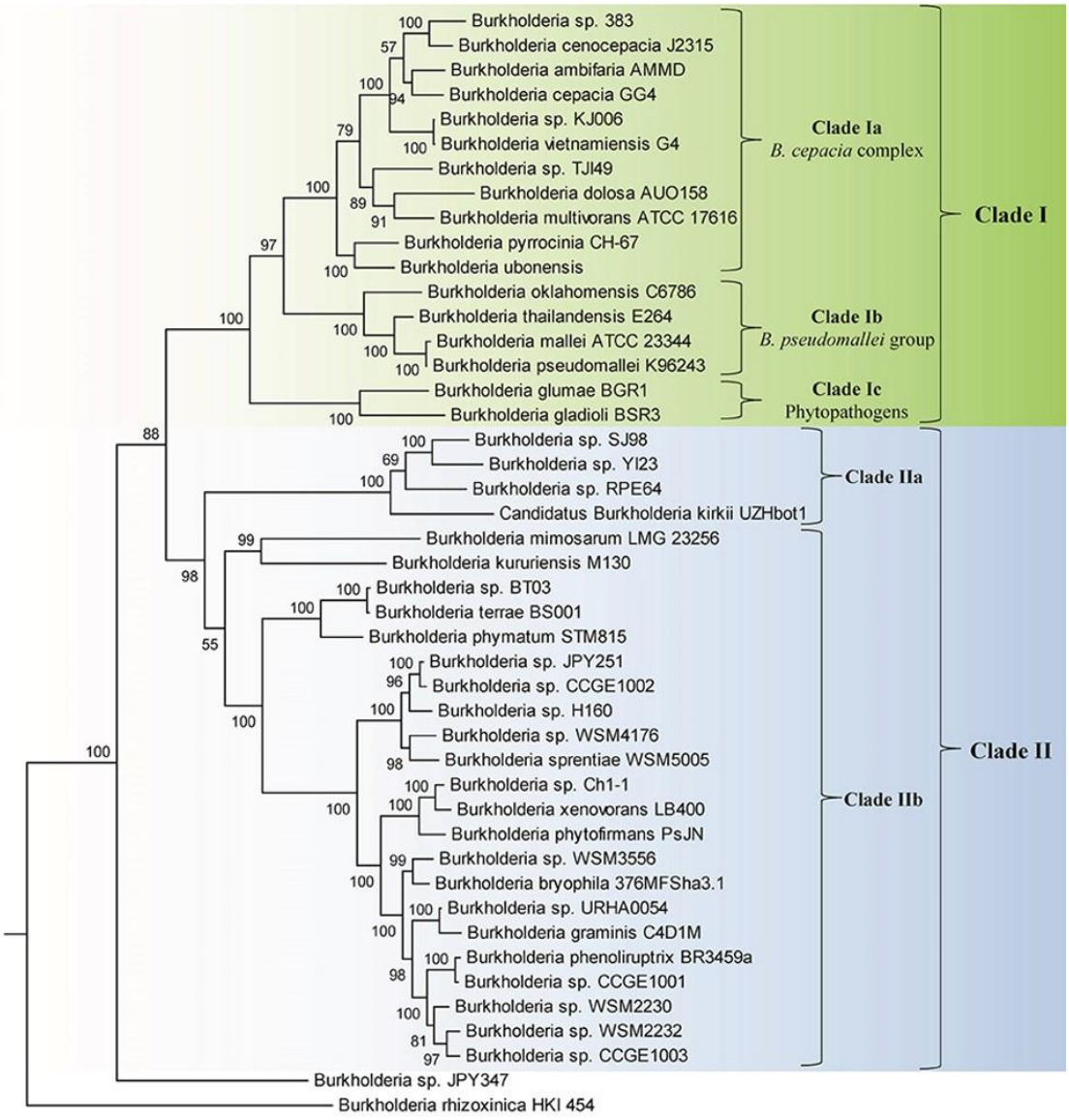

Figure 1.1: Maximum likelihood phylogenetic tree of genome-sequenced *Burkholderia* species based on sequences of 21 conserved proteins. Clade I is split into the BCC, the *B. pseudomallei* group and the phytopathogens, while Clade II is also described as the *Paraburkholderia* genus. Image taken from Sawana *et al* (2014).

Upon its formation in 1992, the *Burkholderia* genus contained 7 species, of which *Burkholderia cepacia* was the type species. However, isolates identified as *B. cepacia* were relatively heterogeneous, giving remarkably varied results in a range of biochemical and phenotypic identification tests [11–13]. A polyphasic

taxonomy study by Vandamme and colleagues (1997) looked at *B. cepacia* isolates from human samples and the environment, which ultimately resulted in the splitting of *B. cepacia* into five genomovars (I-V), collectively known as the BCC [14]. The decades since have seen the identification of several novel BCC species, and the complex currently contains at least 24 different *Burkholderia* species [7,9,15,16].

Unsurprisingly, the BCC are very closely related genetically, with levels of DNA-DNA hybridisation of 30 to 50 % (whereas levels between other *Burkholderia* species are below 30 %), and high sequence similarity in their *recA* (94 to 95 %) and 16S rRNA (98 to 99 %) genes [17–19]. Differentiating between these species is vital for accurate clinical diagnostics, however due to their phenotypic similarities in standard laboratory testing and sequence similarity in 16S and 23S rRNA genes, differentiating between BCC species is troublesome. Sequencing of the *recA* or *hisA* genes appear to be superior tools for identification of BCC species than other commonly used methodologies, though not always possible in less well-equipped laboratories [19,20].

Despite these phylogenetic similarities, the BCC are able to occupy a broad range of environmental niches, perhaps in part due to their large, multireplicon genomes, which may also contribute to their high levels of intrinsic antimicrobial resistance to aminoglycosides, polymyxins and many β-lactam antibiotics [21–24]. BCC species have been identified as both promoting plant growth and acting as phytopathogens, located in a variety of natural environments and as opportunistic pathogens to both humans and animals.

1.1.2 – The BCC in the natural environment

BCC species have been detected in several soil ecosystems, and are considered to form mutualistic relationships with plants, as well as act as phytopathogens in different situations. BCC species are reportedly commonly found in soils; 82 % of urban soil sites tested in 3 US cities reported positive for BCC via polymerase chain reaction (PCR)-based assays [25]. The BCC are particularly known for associating with the soil surrounding plant roots, known as the rhizosphere, of several crops across the globe, such as maize, rice, pea, cotton, tomato and

onion [26–31]. Additionally, some BCC species have been identified residing within plants, indicating the addition of some endophytic activity to their interactions with plants [32]. Abundance of *Burkholderia* species in rhizosphere soil was found to be over 100-fold greater than in non-rhizosphere soil, highlighting the specific interaction between *Burkholderia* and plant roots [26].

The BCC can act as phytopathogens, causing various rots against onion, banana and apricot [1,33,34]. Conversely, certain BCC species, such as *Burkholderia vietnamiensis* and *Burkholderia ambifaria*, are known promoters of plant growth, with studies demonstrating their ability to improve crop yield and protect plants from fungal infections [35–37]. Specifically, they are capable of the production of antibacterial and antifungal agents, the fixation of nitrogen and the lowering of ethylene levels in plants [37–41]. These properties, coupled with certain species' ability to degrade a range of toxic chemicals, have inclined discussions surrounding the use of the BCC as potential biocontrol or bioremediation agents [42,43]. However, concerns about the potential pathogenicity of environmental BCC strains, as well as the banning of the use of the BCC as biocontrol agents by the United States Environmental Protection Agency in 2004 has restricted discussion on this topic [29].

While BCC species are known to be found in terrestrial environments across the world, there is comparatively little information in the literature regarding their abundance in freshwater or marine environments. A handful of studies have reported the presence of BCC species in rivers and coastal waters both in Europe and the United States, and also in Mussel samples off the Croatian coast [44–48]. Despite these reports, the information surrounding BCC abundance in aquatic environments is limited, and it may be presumed that these areas do not harbour the same large BCC presence that many terrestrial environments have.

1.1.3 – The BCC and cystic fibrosis

As an opportunistic pathogen, the BCC is able to infect the immunocompromised, such as cystic fibrosis (CF) patients, but rarely affects healthy individuals. CF affects approximately 1 in every 3500 births in Caucasian populations, and is the most common autosomal recessive condition in Europe [49–51]. CF is characterised

by mutations in the cystic fibrosis transmembrane conductance regulator (CFTR), a chloride channel that is expressed in various epithelia throughout the body, such as in the lungs, intestine, kidney and pancreas, as well as in neuronal cells, though the respiratory system is the most affected [52]. The majority of patients with CF will suffer from severe chronic lung disease, often with extremely variable chronic infection statuses. Due to improvements in clinical care and availability of targeted medications, life expectancy is improving; median predicted survival age is now 47 in the UK [53]. There are potentially thousands of different CFTR mutations that may lead to CF, though empirical evidence linking mutations directly to CF exists for only a fraction of this number [54]. The ΔF508 mutation dominates in CF populations, affecting approximately 90 % with CF in the UK and USA [53,55].

The decline or absence of function of the CFTR gene leads to ineffective chloride secretion from the lung epithelia into the airway, thus depleting overall water content of the surface (periciliary) liquid by increased reuptake of water from the airway into epithelial cells [56]. This renders airway mucus thick and difficult to clear, leading to airway obstruction, trapping of microbes and eventual bronchiectasis and inflammation, a debilitating cycle that leads to the damaging of lung tissue and significantly impaired respiratory function.

CF patients usually suffer from various chronic pulmonary infections from bacteria, fungi and viruses throughout their lives, leading to a decline in lung function and ultimately respiratory failure, which serves as the primary cause of mortality in these patients [57,58]. As such, it is imperative that these chronic respiratory infections are closely managed and understood. Culture-independent methods have shed light on the sheer microbial diversity of the CF lung, with each patient having a unique bacterial profile when samples were examined using sequencing technologies [58–60]. The most common respiratory pathogens found in children with CF are *Staphylococcus aureus* and *Haemophilus influenzae*, while in adults *Pseudomonas aeruginosa* tends to dominate, being cultured from at least 44 % of adult CF patients in the UK and USA [53,55].

The BCC is comparatively less common in the CF lung, having been cultured from 1.4 % of child and 5.1 % of adult patients in the UK in 2017 [53]. Frequency is even lower in the USA, where only 2.4 % of CF patients were reported to have BCC infection [55]. Despite its relatively low prevalence, the BCC is especially

feared among the CF community due to the unpredictable nature of the infection. Many patients may be asymptomatically chronically infected with the BCC for years, however some will suffer from cepacia syndrome, a combination of bacteraemia and necrotising pneumonia, leading to an ultimately fatal decline in respiratory function [61,62]. Cepacia syndrome can occur both acutely after colonisation or after many years of chronic infection, the exact pathophysiology of which is poorly understood [63–65]. BCC species are also known to grow anaerobically in the CF lung, which contains pockets of low/no oxygen due to the presence of characteristically thick and viscous mucus [66,67].

In addition to cepacia syndrome, the high levels of transmissibility between patients and intrinsic antimicrobial resistance of the BCC renders infection with the complex a particular cause for concern for the CF community. Transmission of the BCC and other bacteria can occur between patients in close proximity (such as via direct contact or infectious droplets); as such CF patients are recommended to not meet one another if possible. An example of the threat close contact between CF patients can cause are the reports of significant cross-infection with bacteria such as the BCC and *P. aeruginosa* following summer camps that were run for those with CF around the turn of the millennium [68–72]. Infection with BCC is also a contraindication for lung transplantation, a lifesaving avenue that can bring great improvements in quality of life; patients infected with BCC prior to transplantation reportedly suffered significantly worse outcomes than those without, with *Burkholderia cenocepacia* having the greatest impact on post-transplant survival of the BCC species [73–80]. One retrospective study of CF patients between 1988 and 2012 concluded that median post-transplant survival for patients infected with BCC was 3.3 years, as opposed to 12.4 years for patients not infected with BCC [77].

Due to the particular risk of BCC infection, segregation policies were introduced in many CF centres separating patients based on BCC-infection status, which has aided in the reduction of cross-infection between patients [81]. However, there is an argument that strict segregation of patients can have detrimental mental and social impacts, such as through the reducing of contact to the support that patients can often provide one another [82,83]. Despite concerns about the negative impact of segregation, patient questionnaires have reported that on balance, patients and families strongly support segregated treatment [84,85].

In the UK, the most common BCC species to infect the CF airway are *Burkholderia multivorans* (formerly genomovar II) and *B. cenocepacia* (formerly genomovar III), consisting of 52 % and 27 % of BCC infections in adults respectively [53]. Previously, *B. cenocepacia* was the chief cause of BCC infection in CF, though the prevalence of *B. multivorans* infection is now greater in both the UK and North America [86–90]. Strains that have caused epidemics among CF populations are known to belong to several BCC species, however there are several notorious epidemic strains belonging specifically to *B. cenocepacia* – ET-12, Midwest, PHDC and ST-32, whereas *B. multivorans* infections are more sporadic, with lower incidences of epidemic transmission between patients [22,62,91]. While *B. cenocepacia* and *B. multivorans* are the predominant BCC species in CF, the vast majority of BCC species have been successfully isolated from the CF lung [9,86]. Outside of the BCC, the phytopathogen *B. gladioli* is of particular threat relative to other non-BCC *Burkholderia* species, with the frequency of infection seemingly being greater in the USA than the UK [87,88,90].

Infection control is the cornerstone of protecting against BCC infection, with strict cohort segregation reducing cross-infection in the clinic [89]. However, the number of BCC infection cases are still considerable, and the ubiquity of the BCC in the environment has led to concern that the natural environment may be a source of infection of patients with the BCC. Evidence linking environmental BCC with patient infections casts a shadow on the notion of using BCC species as bioremediation agents [29,92]. Additionally, there have been reports of BCC species isolated from the natural environment that are indistinguishable from those isolated from samples from CF patients, adding weight to the idea of acquisition of infection from the environment [93,94].

Due to the intrinsic antimicrobial resistance of the BCC, eradication of infection is troublesome and therapeutic options are limited. There is a severe lack of evidence in the literature for antimicrobial treatments of the BCC; one systematic review found no randomised or quasi-randomised trials of antibiotic treatment for CF patients infected with BCC experiencing pulmonary exacerbations, another found no trials for eradication therapy for BCC infections in CF patients, and a third assessing long-term antibiotic therapy for chronic BCC infections could only include one study in its meta-analysis [95–97]. As such there is no consensus on treatment regimens for BCC infection, and treatments are usually decided upon

using antimicrobial susceptibility data from patient samples [95,98]. Trimethoprim-sulfamethoxazole, minocycline, doxycycline, tobramycin and ceftazidime are reported to be the most effective treatments for BCC infection, though susceptibility patterns differ between isolates and between BCC species, highlighting the need for accurate species-level identification of BCC infection [91,99–104].

1.1.4 – The BCC and chronic granulomatous disease

In addition to CF patients, the BCC poses a threat to other immunocompromised individuals, such as those with chronic granulomatous disease (CGD). Affecting around 1 in every 200,000 births globally, CGD is caused by mutations in any of the five subunits of phagocyte nicotinamide adenine dinucleotide phosphate (NADPH) oxidase, an enzyme integral to the generation of superoxide and other reactive oxygen species (ROS) in immune cells [105]. These chemical species play an important role in 'respiratory burst', the process of using ROS in the degradation of internalised bacteria in immune cells. As such, patients with defective NADPH oxidase are particularly immunocompromised, and suffer from recurrent life-threatening infections throughout the body [106,107]. Diagnosis of CGD involves patient genotyping and the measuring of NADPH oxidase activity, which can aid clinicians in treatment of patients, as greater residual NADPH oxidase activity in CGD patients is linked to a better prognosis compared to those with a virtually abolished NADPH oxidase activity [107,108].

Common types of infection found in CGD populations include pneumonia, impetigo and abscesses of the skin and liver [106]. The bacteria commonly associated with CGD infection include *S. aureus*, *Serratia marcescens*, *Salmonella* species, *Norcadia* species and the BCC, while fungal infections from *Aspergillus* and *Candida* species are also common [109,110]. CGD treatment focuses on the identification of infecting microbes and the prevention and management of infection with antimicrobials [110].

As with CF patients, the BCC are not as prevalent as other bacteria are in infecting CGD patients, though they are still considerably dangerous, with BCC infection having a relatively high proportion of fatal outcomes in patient cohorts,

often causing septicaemia [109,111,112]. Contrastingly to CF, in which chronic BCC infection is usually caused by persistence of the same specific strain, BCC infection in CGD is more transient, with recurrent episodes of infection being caused by different BCC strains that aren't often shared between patients [113]. Limited data exists surrounding species-level identification of BCC infection in CGD compared to CF, though one analysis of patient isolates reported both *B. cenocepacia* and *B. multivorans* as frequent causes of BCC infection in CGD, in addition to some other BCC species that aren't often present in CF causing infection in CGD, such as *B. ambifaria* and *Burkholderia metallica* [113].

The BCC are particularly capable in resisting killing by the immune system; *B. cenocepacia* is known to be able to resist killing from respiratory burst and can produce at least one superoxide dismutase [114,115]. Additionally, *B. cenocepacia* has been demonstrated to induce necrosis in neutrophils in CGD, as well as to possess the ability to interfere with NADPH oxidase complex formation in macrophages, resulting in reduced superoxide formation compared to heat-killed control [116–118]. These factors make *B. cenocepacia* and the wider BCC particularly capable pathogens in CGD, given the already reduced capability of the immune system to destroy internalised bacteria.

1.1.5 – The wider pathogenicity of the BCC

In addition to CF and CGD patents, the BCC can pose a threat to others with a weakened immune system, such as those suffering from cancer, commonly through contaminated medical devices. Outbreaks of BCC infection often leading to bacteraemia have been reported in inpatient and outpatient units due to contamination of intravenous catheters and equipment such as ultrasound gels, mouthwash and gloves [119–127]. Although rare, the BCC has caused infections in immunocompetent individuals, with cases of pneumonia, bacteraemia and osteomyelitis among others being attributed to the complex [128–135].

The BCC has also caused infection in various animal hosts. Though feline infections have been documented due to contaminated antiseptic scrub, most origins of infection have not been traced to a nosocomial source, while there have also been cases of pyoderma in dogs, endocarditis in horses and mastitis in

sheep [136–140]. There is little evidence of the BCC residing asymptomatically in animals, though the BCC has been detected in wallaby and horse faecal samples in northern Australia, indicating a possible role for animals in the dissemination of these bacteria in the environment [141].

1.1.6 – The molecular basis of pathogenicity of the BCC

Owing to the relatively large genome size of BCC species (approximately 7-8 Mb) there are a diverse range of virulence factors that are employed in initial colonisation and survival against both antibacterial compounds and the host's immune system. The intrinsic antimicrobial resistance of BCC species renders any established infection difficult to clear. BCC species are particularly tolerant of polymyxins, with minimal inhibitory concentration (MIC) values up to 100 fold greater than those for *P. aeruginosa* or *Escherichia coli* [23]. The basis for this resistance is thought to come in part from the consistent addition of the sugar 4-amino-4-deoxy-L-arabinose (Ara4N) to lipid A of the lipopolysaccharide (LPS) structure in the outer membrane; the positive charge of the sugar is thought to reduce the net negative charge of the membrane, reducing permeability to cationic molecules such as polymyxin B [23,142]. Additionally, inactivation of a UDP-glucose dehydrogenase enzyme which is involved in the Ara4N synthesis pathway (BCAL2946) resulted in increased susceptibility to polymyxin B, supporting the importance of Ara4N in the BCC's particular resistance to this antibiotic [23,143]. Other implicated molecules in this extreme resistance include the core oligosaccharide of LPS and the alternative sigma factor RpoE [144,145].

The BCC are also intrinsically resistant to a range of other antimicrobials, such as aminoglycosides and β-lactams, though MIC values vary even between strains of the same species [24]. As with other Gram-negative bacteria, the presence of several Resistance-Nodulation-Cell Division (RND) efflux pumps is a contributory factor to broad antimicrobial resistance. Genome analysis of the J2315 genome identified 16 potential RND pumps in *B. cenocepacia*, of which at least 5 have been shown to play a role in antimicrobial resistance, though the molecular specificity of the majority of these RND pumps remains unclear [146–148].

In addition to its relatively robust antimicrobial resistance, the BCC employs a range of virulence factors to enhance its disease-causing ability. One example are bacterial secretion systems - complexes of membrane-associated proteins that extrude various molecules from the bacterial cell for reasons including nutrient scavenging, secretion of extracellular toxins and interbacterial communication and competition [149]. Genes for six secretion systems have been identified in the J2315 genome, the Type I Secretion System (T1SS), T2SS, T3SS, T4SS, T5SS and T6SS [146]. Several of these secretion systems have been implicated in BCC virulence. The T2SS exports two zinc metalloproteases, ZmpA and ZmpB, which can cleave a range of host proteins, such as immune mediators [150,151]. Mutants of the BCC T3SS have reduced virulence in the nematode model *Caenorhabditis elegans* and murine models, while genes encoding T4SSs are involved in cytotoxic protein secretion affecting onions, plasmid mobilisation and in intracellular survival within macrophages [152–156]. The T6SS is important in delaying activation of NADPH oxidase in macrophages and in inter-species bacterial competition [118,157].

Quorum sensing refers to the mechanism in which gene expression is regulated in response to population density, via the release and sensing of autoinducer molecules. Once a minimal threshold concentration of a certain autoinducer molecule is reached, gene expression is altered [158]. BCC species are able to utilise multiple QS systems, such as CepIR, a well-conserved *N*-acyl homoserine lactone-dependent QS system which regulates a broad range of genes including those involved in virulence, motility, biofilm formation and the production of extracellular proteins such as siderophores and metalloproteases [159,160]. Another QS system in the BCC involves *cis*-2-dodecenoic acid, also known as '*Burkholderia* diffusible signal factor (BDSF)', which is also implicated in the regulation of biofilm formation and virulence [161–164]. Due to their overarching role in the regulation of pathogenicity in the BCC, research has been performed into the use of QS system inhibitors, known as diketopiperazines, as potential therapeutics [165,166].

Forming part of the outer membrane of Gram-negative bacteria, the LPS is comprised of three components: Lipid A, the core oligosaccharide and the O-antigen, and is involved in interactions between bacteria and host, such as adhesion, and is also able to induce strong immune responses from the host [167].

The LPS in the BCC differs from many other Gram-negatives, such as the presence of particular disaccharides in the core oligosaccharide and the presence of Ara4N in the lipid A, altering the charge of the cell surface which has been shown to inhibit the binding of certain antibiotics to the BCC, reducing their effectiveness [23,142,168]. The BCC LPS is also able to stimulate murine macrophages to produce cytokines such as TNF-α and lL-6, contributing to host inflammation [169]. The BCC also produce a range of exopolysaccharides (EPS), the most commonly isolated being cepacian, which has been demonstrated to interfere with the production of ROS and chemotaxis in human neutrophils, and also is important in virulence in mice [170–174].

Comparative genomic analysis of clinical isolates of *B. cenocepacia* ST32 has provided insight into the adaptation of *B. cenocepacia* in cases of chronic CF infection with fatal outcomes. Indels in genes related to transition metal metabolism (particularly copper metabolism) and oxidative stress protection were frequently identified [175]. As macrophages utilise both ROS and copper in their killing of internalised pathogens, these findings suggest that evolution of strategies to overcome macrophage killing of *B. cenocepacia* may contribute to worse patient outcomes in chronic CF infection [175].

There are no clinically available vaccines to protect against the BCC, though knowledge of relevant virulence factors may lead to specific proteins being utilised in BCC vaccinations [176]. Examples of these subunit vaccines include the vaccination of mice with the bacteriocin linocin, the membrane protein OmpW or a range of outer membrane proteins from BCC species which protected mice from BCC infection, resulting in reduction of lung bacterial load [177–179]. Polysaccharides are also a focus of BCC vaccine research, as well as for vaccines of the *B. pseudomallei* group [176,180]. One study has utilised a live vaccine containing a *tonB* mutant of *B. cenocepacia*, which was deficient in the active uptake of iron, which conferred high levels of immunisation against *B. cenocepacia* in mice [181]. Bioinformatics approaches are also being utilised to aid in the search for vaccine candidates, the successful development of which may bring profound clinical benefit to a range of vulnerable individuals [182].

1.1.7 – The intracellular niche of the BCC

The respiratory epithelium acts as a physical barrier between the host and inhaled pathogens and plays a critical role in the innate immune system via the production of antimicrobial agents, stimulation of pro-inflammatory cytokines upon bacterial recognition and the trapping of bacteria in the mucosal environment [183,184]. Internalisation of respiratory pathogens by the epithelium contributes to the innate response of the host to infection, however hijacking of this process by bacterial pathogens poses a threat to the host, as certain bacteria, such as the BCC, can persist in these cells and even pass across the epithelium to the bloodstream, spreading potentially devastating infection throughout the body [185–187]. The BCC is better able to invade the CF airway than those of healthy individuals, both successfully invading and migrating across epithelial cells, so an understanding of the molecular pathophysiology behind this phenomenon is crucial for the development of therapeutics, especially for the CF population [188].

Binding of the BCC to the airway epithelium is the first step in epithelial invasion, and is reportedly mediated by a 22 kDa adhesin and cable pili; mutants lacking expression of either the adhesin or cable pili show reduced binding to cytokeratin 13, a protein with increased expression in the CF lung, and also impaired migration across squamous epithelial cells [189,190]. Isolates of *B. cenocepacia* that show greater binding of cable pili and the 22 kDa adhesin to a glycoprotein found in the lung mucus, known as mucin, are linked with a greater incidence of cepacia syndrome, suggesting a direct link between these binding proteins and pathogenicity [184,191]. Additionally, the trimeric autotransporter adhesins BCAM0223 and BCAM0224 of *B. cenocepacia* K56-2 have been associated with adherence to (and, in the case of BCAM0224, invasion of) bronchial epithelial cells, as well as biofilm formation and virulence in *Galleria mellonella*, strengthening the link between adhesins and virulence in *B. cenocepacia* [192–194]. Inhibition of glycolipid synthesis in an epithelial cell line reduced invasion of strains of both *B. multivorans* and *B. cenocepacia*, implicating glycosphingolipid receptors in BCC adhesion and invasion [195]. A number of other factors have been identified as playing a role in BCC adhesion, including OmpW, linocin and the lipoprotein pal [179,196].

Invasion of the epithelium by the BCC has been demonstrated *in vitro*, where a correlation between invasion and infection of a murine model has been shown [197]. The BCC are known to employ several methods of epithelial invasion, which can be species-specific, for example invasion by *B. multivorans* appears to depend on access to tight junctions, whereas the same was not found for *B. cenocepacia* [198]. Some species were shown to invade the epithelial layer via disruption of the actin cytoskeleton in a biofilm state, while other species penetrate the epithelium as single cells [199]. Additionally, in a CF epithelial cell line, *B. cenocepacia* invaded cells via of a process of actin rearrangement [200].

Extracellular lipase appears to play a role in invasion; application of BCC lipase to epithelial cell lines increased invasion by *B. multivorans* and *B. cenocepacia* in a tight-junction independent manner [201]. Mutants in flagellar genes *fliG* and *fliI* of *B. cepacia* showed reduced invasion of epithelial cells, suggesting motility aids invasion of these cells [202]. Additionally, the two-component system (TCS) FixLJ in the BCC species *Burkholderia dolosa* regulates invasion of epithelial cells and macrophages, as well as biofilm formation and motility [203].

The fate of the BCC following invasion into CF epithelial cells involves escaping from lysosomes and late endosomes of the cell and entering autophagosomes, where it eventually can replicate in the endoplasmic reticulum [200]. The T4SS has been implicated in the alteration of membrane trafficking in both *Legionella pneumophila* and *Brucella abortus*, and a BCC T4SS has also been identified as playing a role in avoiding degradation and aiding survival and replication within epithelial cells [155,204,205].

In addition to invading the respiratory epithelium, BCC species have been demonstrated to survive within macrophages. A zebrafish embryo model has shown *B. cenocepacia* surviving and replicating within macrophages, while deletion of an AmrAB-OprA-like efflux pump has allowed for the creation of aminoglycoside-sensitive derivatives of BCC species for use in the gentamicin-protection assay, which has displayed the ability of the BCC to replicate within murine macrophages [206–208]. The strong *in vitro* evidence for an intracellular niche of the BCC has been seen in the clinic; immunohistochemistry performed on lungs of CF patients undergoing transplant identified BCC bacteria generally being present as single cells or smaller clusters within phagocytes, while *P. aeruginosa* was identified in more biofilm-like structures [67].

Entry of *B. cenocepacia* into macrophages appears to rely on the induction of membrane ruffling and subsequent engulfment of bacterial cells (otherwise known as macropinocytosis), which is partially dependent on the T3SS [209]. Differences in internalisation rate of different BCC strains into macrophages have been observed; for example three strains of *B. multivorans* had an internalisation rate of between 1.2-5.2 % into RAW264.7 murine macrophages, while *B. cenocepacia* K56-2 had a rate of 1 % [208].

Similarly to epithelial cells, macrophages containing *B. cenocepacia* suffer from a manipulated phagosome maturation pathway. *B. cenocepacia*-containing vacuoles had significantly delayed fusion with late endosomes and lysosomes: 6 hours following internalisation for live bacteria compared to 30 minutes for heat-killed bacteria [210]. Another study found that *B. cenocepacia* does not appear to interfere with the fusion of early endosomes with phagosomes, but impaired the activation of the late phagosomal marker Rab7, which may contribute to the reduced rate of lysosomal fusion with *B. cenocepacia*-containing vacuoles [211]. *B. cenocepacia* can also interfere with autophagy, blocking maturation of the autophagosome and replicating in the cytosol [212]. While the arrest in lysosomal fusion has been observed for *B. cenocepacia*, phagosomes containing *B. multivorans* experienced normal trafficking within the macrophage, with no delay in acidification or lysosomal fusion, suggesting that while these two species share the ability to cause severe infection in the immunocompromised, their intracellular lifestyles are different [208]. Recent work using a zebrafish model suggests that rather than acting as a host defence mechanism against infection, macrophages are crucial for the spread of *B. cenocepacia* infection (as opposed to neutrophils, which played no apparent role in *B. cenocepacia* pathogenesis), indicating that targeting the intracellular stages of infection may be an avenue of exploration for the development of novel therapeutics for *B. cenocepacia* and possibly other BCC species [213].

Interestingly, while CFTR-defective macrophages display normal acidification of the phagosome, infection of these macrophages with *B. cenocepacia* confers a greater delay in acidification and lysosomal fusion compared to normal macrophages [214]. The reason for this may lie in the process of autophagy; defective CFTR reduces autophagy in macrophages, while treatment of CFTR-defective macrophages with the autophagy-stimulating rapamycin enhanced

clearance of *B. cenocepacia* through autophagy, reducing lung inflammation [215,216]. This autophagic clearance may involve the ubiquitin-binding adaptor molecular SQSTM1/p62, which has differing effects on *B. cenocepacia* survival in WT and CFTR-defective macrophages [217]. These findings shed light on the molecular mechanisms underpinning the greater ability of BCC species to infect CF macrophages compared to those from healthy individuals, an important research avenue for the CF community.

1.2 – The homeostasis, toxicity and relevance of heavy metals

1.2.1 – Heavy metals in bacterial physiology

Heavy metals are elements that typically lie within the d-block of the periodic table as transition metals, some of which are highly physiologically relevant. There is no universally accepted definition for what constitutes a 'heavy metal', with different authors utilising different thresholds for various criteria, such as density and atomic mass, for which elements are included under the term [218]. Alternative naming conventions have been suggested, such as splitting metals into Class A (oxygen-seeking), Class B (nitrogen/sulphur-seeking) and Borderline metals, although alternative terms have yet to be widely adopted in the literature [218,219]. For the sake of simplicity, the terms 'metal' and 'heavy metal' herein will refer to any element found within group 3 to group 12 inclusive in the periodic table.

Metals are fundamental to the functioning of many proteins throughout the kingdoms of life, and therefore underpin many different cellular processes [220]. Iron is an essential metal which can be found in iron-sulphur clusters, an abundant protein cofactor that plays a role in DNA replication, metabolism and respiration [221,222]. Zinc-fingers are abundant protein motifs in which zinc ions are coordinated to cysteine and histidine residues, while zinc can also be found in several bacterial ribosomal proteins and in extracellular metalloproteases [223–225]. Another common metal is copper, which can be found in several protein groups such as cytochrome oxidases and superoxide dismutases [226–228]. Other metals incorporated in metalloproteins include nickel, manganese and molybdenum [229].

In order to meet the continuous cellular demand for metals, it is necessary for bacteria to import metals from the extracellular environment into the cytoplasm. Metal transport systems import metals from the environment in a variety of ways, be it through passive transport through porins in the outer membrane, the hydrolysis of ATP in ATP binding cassette (ABC) transporters and other ATPases to actively import metals, the sequestration of metals via siderophores or co-transporting metals with other compounds such as amino acids [230,231]. However, the use of metals by organisms represents a fine balance between taking advantage of their chemical properties in the cell without exposure to their inherent toxicity at higher concentrations. If metal concentration within the cell is too high, regulatory mechanisms can downregulate the expression of import proteins and upregulate expression of efflux proteins and intracellular chelators, maintaining the delicate homeostasis of metal ion concentration [230,232,233].

Metal toxicity can arise from high concentrations of both essential and non-essential metals, which can occur if extracellular metal concentration is particularly high, or if homeostatic mechanisms are unable to overcome intracellular metal stress. In order to exhibit toxicity, metals need to accumulate in the cytoplasm, and thus penetrate the outer membrane, and for Gram-negative bacteria, the inner membrane also. While outer membrane porins are one proposed mechanism of metals penetrating into the periplasmic space, there is little clarity surrounding other potential mechanisms of passing the outer membrane [234]. The penetration of metals through the inner membrane however is somewhat more understood.

In addition to the simple mass uptake of essential metals through standard transport pathways when extracellular concentration is high, there are other mechanisms in which non-essential metals can reach the cytoplasm. One mechanism is ‘ionic mimicry’, in which metal transporters are able to facilitate the uptake of non-essential metal species that are chemically-similar to their ‘intended’ target. For example, the zinc transporters YiiP and ZipB from *E. coli* and *Bordetella bronchiseptica* respectively are able to transport the non-essential metal cadmium, albeit at a lower rate and affinity than zinc [235,236]. Siderophores may also play a role in non-essential metal uptake; the *P. aeruginosa* iron siderophore pyochelin is able to bind gallium which is eventually taken up by the FptA transporter, though at a lower rate than iron [237]. With different metals having

fundamentally different chemical properties, as well as the variety of outer and cytoplasmic membrane proteins across the bacterial domain, it is likely that while metal-uptake mechanisms may be broadly similar between species, the subtleties of metal uptake are unique to each combination of metal and bacteria.

1.2.2 – Mechanisms of metal toxicity to bacteria

There are several empirically-characterised means by which metals exert their toxicity on the bacterial cell at high concentrations; some are common to many metals, while others may only be exhibited by a single element. One toxicity mechanism is the generation of short-lived ROS, which are able to interact with and damage lipids, DNA and proteins. Several metals are able to catalyse the generation of ROS through the Fenton reaction (Fig 1.2), in which the by-products of aerobic respiration, such as superoxide and hydrogen peroxide, are able to oxidise and reduce metal species. The hydroxyl radical generated through this process poses a particular threat to the stability of the intracellular environment, due to its ability to both directly damage the cell, and also interact with biological molecules to form other radicals, such as the thiyl and peroxyl radicals [234].

1. $Fe^{2+} + H_2O_2 \rightarrow Fe^{3+} + OH^- + OH\cdot$
2. $Fe^{3+} + O_2\cdot^- \rightarrow Fe^{2+} + O_2$

---

3. $O_2\cdot^- + H_2O_2 \rightarrow O_2 + OH^- + OH\cdot$

Figure 1.2: ROS generation via the Fenton reaction. Iron is used as an example for metal-catalysed Fenton chemistry, though other metal species are also able to undergo these reactions. Equation 1 - Hydrogen peroxide (H_2O_2) is able to oxidise Fe^{2+} to produce a hydroxyl ion (OH^-) and a hydroxyl radical ($OH\cdot$). Equation 2 - Fe^{3+} is reduced by superoxide ($O_2\cdot^-$) to form Fe^{2+} and O_2, replenishing the reduced metal to react further with H_2O_2. Equation 3 - The net reaction is called the Haber-Weiss reaction.

In addition to iron, other metals have been demonstrated to undergo Fenton chemistry *in vitro*, such as chromium, cobalt, copper, nickel and vanadium [238]. As such, high intracellular concentrations of these redox-active metals may directly generate damaging ROS. Indeed, *E. coli* lacking two superoxide dismutases were more susceptible to nickel, cadmium and cobalt, and the mechanism of toxicity of chromium to *E. coli* was demonstrated to be hydroxyl radical-dependent [239,240]. Additionally, *P. aeruginosa* exposed to toxic concentrations of copper upregulated genes indicative of an oxidative stress response, and *P. aeruginosa* lacking superoxide dismutase or glutathione reductase had increased sensitivity to arsenite, implying that metal toxicity may be at least partially explained by the generation of ROS [241,242].

A more indirect mechanism of metal-catalysed ROS generation involves the targeting of exposed iron-sulphur clusters in proteins. Various metals, such as cadmium, copper, mercury, silver and zinc are able to damage [4Fe-4S] clusters in *E. coli*, resulting in the release of complexed iron into the cytoplasm [243,244]. Any release of free iron into the cytoplasm may lead to ROS generation through Fenton chemistry, regardless of whether the metal that attacks the cluster is itself redox-active. Aside from the potential generation of ROS, targeting of [4Fe-4S] clusters directly causes protein dysfunction; copper inactivates isopropylmalate dehydratase (among other proteins) in *E. coli*, an enzyme necessary for synthesis of branched-chain amino acids, leading to a growth defect [243]. This toxic effect was also present in anaerobic conditions, supporting the notion of a ROS-independent toxicity mechanism for the targeting of [4Fe-4S] clusters by metals [243]. Cadmium, mercury, silver and zinc are also able to inactivate various [4Fe-4S] dehydratases in *E. coli*, although it has been found that rather than directly target iron-sulfur clusters, copper, cobalt and zinc inhibit the biogenesis of these clusters through binding to iron-sulfur cluster assembly proteins [244–247]. As many metabolically-essential proteins contain [4Fe-4S] clusters, the targeting of these clusters, be it either directly or through their biogenesis, may also explain the toxic effects of these metals.

Another way that metals exert toxicity is through the displacement of other metal species complexed within metalloproteins. The Irving-Williams series dictates the order by which proteins tend to have affinity for essential divalent metals, which reads $Mn^{2+} < Fe^{2+} < Co^{2+} < Ni^{2+} < Cu^{2+} > Zn^{2+}$, in which proteins have the greatest

affinity for copper [229,248]. As such, intoxication with an essential metal such as copper or nickel, or a non-essential metal with relatively high affinity for protein complexes may lead to displacement of crucial metal groups in metalloproteins, leading to protein dysfunction. For example, the yeast enzyme 5-aminolaevulinate dehydratase is inhibited by the displacing of the bound zinc at its triple-cysteine site by lead, and exposure of *Saccharomyces cerervisiae* to silver led to displacement of copper bound within Cu,Zn-superoxide dismutase, rendering it dysfunctional [249,250]. In *E. coli*, nickel can displace the zinc bound to fructose-1,6-bisphosphate aldolase, leading to inhibition of enzyme activity [251].

Many metals, such as cadmium, copper, silver and zinc have been implicated in the oxidation of thiol groups, leading to disulphide bond formation in proteins and antioxidants such as glutathione [252–254]. Combined with the ROS-generating capabilities of these metals, depletion of antioxidants may compound oxidative stress, while further protein disruption through disulphide bond formation on thiol groups will increase the burden of metal toxicity upon the bacteria.

In addition to the mechanisms of metal toxicity previously mentioned, there are other mechanisms that have only been exhibited by one or two specific metals. It has been postulated that cadmium and copper are able to cause cellular damage through peroxidation of membrane lipids, and that this is the possible mechanism of copper alloy-contact killing of *E. coli* and *B. subtilis* [255–257]. Silver has been implicated in causing proton leakage and cell death in *Vibrio cholerae*, and also in inhibition of the electron transport chain in *E. coli* and *Vibrio harveyi* [258–261]. Metals may also be able to disrupt the assimilation of essential nutrients; cadmium and zinc are able to compromise the uptake of manganese in *Streptococcus pneumoniae* through binding to the lipoprotein PsaA, leading to heightened susceptibility to oxidative stress [262–264]. In essence, there are many ways in which metals can be toxic to the bacterial cell, some of which are shared across many metals, and others which have only been empirically defined for one or two metal species.

1.2.3 – The antimicrobial potential of heavy metals

Given the range of toxic effects metals can have on bacteria, it is of little surprise that metals have been used as successful antibacterial agents in a variety of ways. Examples include the use of silver nitrate to prevent gonorrhoea eye infections in newborns, the utilisation of copper sulphate in mixtures to control potato blight and the use of copper-silver ionisation in hospital water systems as a method of controlling for *Legionella* [234,265,266]. Owing to their antimicrobial properties, metals have also been incorporated in many consumer and medical products. Silver is often found in wound dressings, antimicrobial creams and catheters, copper has been postulated as an antimicrobial surface due to its contact killing capabilities, while tin and zinc have been incorporated into brands of mouthwash and toothpaste [234,267,268].

One avenue for the use of metals as antimicrobials comes in the form of metal nanoparticles. In essence, these are clusters of metal atoms below 100 nm in size and can take the form of many shapes, such as cubes, spheres and rods [269,270]. There has been particular focus on metal nanoparticles due to their particular antimicrobial properties; nanoparticles of copper oxide and zinc oxide induce ROS formation in *E. coli* and *S. aureus*, and silver nanoparticles are able to disrupt the *E. coli* plasma membrane, leading to cell death [271–275]. Given the potential for nanoparticles to associate with the bacterial membrane, controlled design of metal nanoparticles to allow for specific delivery to particular bacterial species may be a lucrative avenue of investigation for novel therapeutics [276,277].

Due to its antimicrobial properties, considerable research has been performed on the potential of incorporating copper in various surfaces in the clinical environment. Various clinically relevant bacteria, such as *Listeria monocytogenes*, *Clostridium difficile*, *S. aureus* and *E. coli* have significantly reduced survival times when grown on copper alloys compared to stainless steel [278–281]. Many trials have tested the effect of utilising copper as a hard surface in the clinic, which have found significant reduction in microbial recovery from several copper-containing surfaces, such as light switches, bed rails, taps, doors, toilet seats and pens [282–289]. Copper has also been successfully tested as an antimicrobial when incorporated into socks, bed linen, towels and clothing [290–294].

These studies strongly suggest that copper surfaces may be an effective and efficient way of reducing microbial burden in the clinical environment.

In addition to its direct toxicity to bacteria, silver is able to synergise with various antibiotics, enhancing bacterial killing compared to antibiotic alone. Silver has been shown to potentiate the toxicity of polymyxin B, vancomycin, tetracycline and multiple aminoglycosides, among others, to both Gram-positive and Gram-negative bacteria [295–300]. The mechanism of this synergy appears to be antibiotic-dependent; silver can enhance the uptake of aminoglycosides into bacterial cells, while silver has also been correlated with the blocking of the bacterial thioredoxin system, which enhances the activity of several other antibiotics [299,300]. Additionally, combinations of silver and antibiotics have been shown to be effective in the eradication of bacterial persister cells, as well as in the clearance of biofilms [295,297]. Overall, various metals, particularly copper and silver, hold promise as antimicrobial strategies, either directly or in combination with antimicrobials.

While there is potential in the use of heavy metals as antimicrobials, there is concern about the relationship between bacterial metal resistance and antibiotic resistance. Bacteria that have been isolated from metal-rich environments can often exhibit significant antibiotic resistance profiles, with there being a strong correlation between exposure to heavy metals and the presence of antibiotic resistance genes. Antibiotic/metal resistant bacteria have been isolated from many diverse environments, including drinking water systems, rivers, fields, settling basins and animal manure [301–310]. As industrial processes continue to lead to the pollution of both natural and urban environments with various heavy metals, the connection between metal resistance and antibiotic resistance is of particular significance [311–313].

There are different ways in which the link between metals and antibiotics can arise in the bacterial cell. Co-resistance refers to the situation where genes for different resistant phenotypes are located together on a genetic element, such as a plasmid [314]. There are many examples of genetic elements harbouring resistance genes to both metals and antibiotics, such as a plasmid isolated from environmental *P. aeruginosa* which harboured resistance for both tetracycline and copper, as well the linkage between the copper resistance transporter *tcrB* and resistance genes for glycopeptides and macrolides on a plasmid from

Enterococcus faecium [315,316]. A recent study of over 5000 bacterial genomes found that the linkage between the presence of metal resistant genes and antibiotic resistant genes was significantly stronger in human pathogens than environmental bacteria, reinforcing the relationship between metals and antibiotics [317]. Cross-resistance refers to when development of resistance to one agent confers resistance to another, e.g. an efflux pump extruding both metals and antibiotics [314]. For example, the MdrL efflux pump from *L. monocytogenes* confers resistance to many antibiotics, particularly cefotaxime, and the metals chromium, cobalt and zinc [318]. Resistance genes for metals and antibiotics can also be coregulated by the same regulator; the *P. aeruginosa* zinc- and copper-responsive transcriptional regulator CzcR can upregulate the heavy metal efflux pump CzcCBA and also downregulate the outer membrane porin OprD, reducing the permeability of the cell to carbapenems [319,320]. The promise that metals hold as potential antimicrobial agents should be considered alongside the risk that metal pose in the development of antibiotic resistance, and further work should be done to elucidate the relationship between metals and antibiotics.

1.2.4 – Manipulation of metal availability by the immune system

There are numerous strategies that host immune cells employ to defend against intracellular pathogens. These include acidification of the phagosome, the use of antimicrobial peptides, ROS production, and both restriction of the availability of essential metal species and intoxication with high concentrations of toxic metal ions [321,322]. Metal starvation as an antimicrobial strategy in the macrophage revolves around natural resistance-associated membrane protein 1 (NRAMP1), a metal transporter found at the phagosomal membrane which transports iron and manganese from the phagosome to the cytoplasm [323–326]. This metal export from the phagosome leads to a strongly iron- and manganese-deficient environment, limiting the supply of these essential metals to the internalised bacteria. Studies have linked NRAMP1 polymorphisms to differing susceptibilities to tuberculosis and leprosy, both caused by intracellular bacteria of the *Mycobacterium* genus, suggesting that NRAMP1, and thus iron/manganese starvation, plays a role in the defence against these bacteria [327–329]. Additionally, the role of iron in innate immunity is highlighted by the evolutionary battle between

human protein lipocalin 2, which is able to sequester bacterial siderophores and thus further restrict iron availability, and the strategies bacteria can employ to overcome this, such as production of lipocalin 2-antagonists or siderophores that evade inhibition by lipocalin 2 [330–332].

In contrast to the well-studied role of metal starvation in innate immunity, there have been more recent studies that elude to a role for copper and zinc intoxication in the defence against intracellular pathogens. For example, concentrations of copper and zinc were significantly increased over time in phagosomes containing mycobacteria, while evidence for a 'zinc burst' was found in phagosomes containing *Mycobacterium tuberculosis* [333,334]. Additionally, transcriptional profiling of intracellular *M. tuberculosis* revealed induction of several predicted heavy metal-transporting P-type ATPases, suggesting that the bacteria are exposed to intoxicating levels of metals within phagosomes [334]. Outside of mycobacteria, *E. coli* and *S. pneumoniae* deficient in the copper-transporting ATPase CopA were hypersensitive to macrophage killing, and *P. aeruginosa* with a mutated copper transporting P-type ATPase had reduced virulence in mice [335–337]. This evidence points towards a paradigm in which different metals can be extruded from or transported into the phagosome to aid in bacterial killing in various ways. Given the many mechanisms by which metals are used to kill intracellular pathogens, either through starvation or intoxication, it may be possible to produce pharmacological agents to target bacterial mechanisms of metal homeostasis that aid in the clearance of bacterial infection in the human host.

1.2.5 – Mechanisms of metal resistance in bacteria

As there are many instances in which bacteria may be exposed to metals, be it the natural environment, the clinic or within immune cells, an understanding of the molecular strategies that are employed to defend against toxic metal species is crucial. There are various mechanisms in which bacteria can resist metal intoxication, and many of these are similar to those employed to defend against antimicrobials.

Mirroring the use of metal transporters to take up metals when the intracellular concentration is too low, bacteria commonly employ efflux transporters to extrude ions from the cytoplasm out into the periplasmic/extracellular space when the concentration is too great. There are several well-characterised metal transporters, and metals have been shown to be effluxed by various families of transporters. One example are RND-family efflux pumps, tripartite complexes composed of an RND protein, a membrane fusion protein (MFP) and an outer membrane factor (OMF), which together span across both the inner and outer membranes of the bacterial cell, extruding ions from the cytoplasm directly out to the extracellular environment [338–340]. Examples include the cadmium-, cobalt- and zinc-extruding CzcCBA pump of *Alcaligenes eutrophus* and *P. aeruginosa* and the copper- and silver-extruding CusABCF system of *E. coli*, consisting of the CusABC efflux pump and the periplasmic CusF chaperone, which delivers metal ions directly to the pump from the periplasm [319,341–344].

Rather than span both membranes, cation diffusion facilitator (CDF) pumps transport substrates across a single membrane, and as such can be found in both Gram-negative and Gram-positive bacteria [230]. The zinc-transporting ZitB from *E. coli* and CzrB from *S. aureus* are two examples of metal-transporting CDF pumps [345,346]. The P1B group of P-type ATPases transport metals across the cytoplasmic membrane in an ATP-dependent manner, and have been shown to transport a range of metals, such as cadmium, cobalt, copper, lead, nickel, silver and zinc [347–349]. These ATPases are able to interact with periplasmic chaperones; the copper-transporting ATPases CopA in *E. coli* can directly deliver copper to the chaperone CusF [350]. Interestingly, certain copper-ATPases appear to not be directly involved with copper detoxification of the cytoplasm, but rather delivery of copper to the periplasm at a slower rate for incorporation into cytochrome oxidases [351,352].

Aside from efflux, there are several other mechanisms at play in defence against metals. Metal ions can undergo chemical modification into less toxic forms, for example the oxidation of Cu(I) to its less toxic form Cu(II) by multicopper oxidases, such as the periplasmic multicopper oxidase CueO from *E. coli* [353,354]. Bacteria can sequester metals within the cytoplasm through the use of storage proteins, for example bacterioferritins are used to tightly regulate free iron

concentration and prevent it from undergoing Fenton chemistry, and cysteine-rich metallothioneins sequester metals through binding to its thiol groups [355–357].

Metals can also be sequestered extracellularly; the *E. coli* secreted siderophore yersiniabactin, which usually sequesters iron, can bind extracellular Cu(II) to prevent its reduction to the more toxic Cu(I) form [358]. Additionally, yersiniabactin bound to Cu(II) can act as a superoxide dismutase, protecting the internalised *E. coli* from superoxide generated within the phagosome [359]. Other siderophores are also able to bind a range of metals, albeit at a lower affinity than they bind iron, possibly sequestering these metals in the environment [237,360]. Given the diverse environmental niches that bacterial species can occupy, it is likely that the intricacies of resistance to metal stress vary across the bacterial domain, rendering some species more tolerant to heavy metals than others.

1.2.6 – Metal resistance in the BCC

Multiple *Burkholderia* species have been isolated from metal-rich environment; *Burkholderia metallidurans* (now *Paraburkholderia metallidurans*)**,** is particularly resistant to such as cadmium, copper, lead and zinc, and a *Burkholderia* species isolated from soil contaminated by a former nuclear weapons production facility displayed heightened resistance to nickel [8,361–363]. Additionally, investigation of gallium as a potential therapeutic against the BCC found that the MIC of gallium for BCC isolates was at least four-fold greater than that for *P. aeruginosa*, concluding that the use of gallium as a therapeutic for BCC infection is limited [364]. Understanding how the BCC defends against toxic metals would inform the decision about their utilisation as bioremediation agents, as well as their pathogenic role in the CF lung, given that the concentrations of copper, iron and zinc are elevated in the CF lung compared to healthy control [365–367]. As such, characterisation of the metal response is important, though there is relatively little literature to date on the specific mechanisms employed by the BCC to resist metals.

A screen of 5000 transposon mutants of *B. cenocepacia* H111 by Schwager and colleagues (2012) identified a mutant of the P1-type ATPase CadA, which was deficient in growth on cadmium [368]. Deletion of CadA rendered *B. cenocepacia*

sensitive to cadmium, lead and zinc, while fusion of the *cadA* promoter region to *gfp* demonstrated induction of CadA in response to the same three metals [364]. The *cadA* gene is conserved both within the BCC and the wider *Burkholderia* genus; the *cadA* gene in *B. cenocepacia* H111 is 85 % similar to *cadA* from *B. multivorans* and 81 % similar to *cadA* from *B. pseudomallei* [18]. This strong conservation suggests that CadA plays an important role in resistance to cadmium, lead and zinc, and perhaps other heavy metal-resistance mechanisms are shared between *Burkholderia* species. Additionally, recent investigation of copper-resistance genes in *B. cenocepacia* H111 by transposon sequencing identified the presence of the copper-resistance system CopABCDE, which is also present in *E. coli* [369].

Aside from the aforementioned studies, there is a general lack of empirical exploration of the molecular mechanisms underpinning the metal response in the BCC. P1-type ATPases such as CadA are usually regulated by metal-responsive transcriptional repressors, in which binding of metal directly to the repressor allows expression of the protein, whereas efflux pumps such as RND-family pumps are typically regulated by TCSs [370,371]. While there are many RND-family pumps and TCSs in the BCC, their potential role in the metal response has not been described [18,146,372]. The focus of this work revolves around four putative heavy metal-sensing TCSs in *B. cenocepacia* K56-2, their individual regulons and the potential interactions between them, which will further elucidate the details of the metal response in the BCC (see section 1.3.8).

1.3 – Two-component systems and multikinase networks

1.3.1 – Introduction to the two-component system

The ability to perceive and respond to the local environment is fundamental to the survival of any living organism. TCSs are an essential means of connecting the environment to cellular homeostasis commonly employed by bacteria and some lower eukaryotes such as fungi and plants. Traditionally comprised of a membrane-bound sensor kinase (SK) and a cytoplasmic response regulator (RR), TCSs can sense and respond to a broad range of stimuli, such as pH,

temperature and the extracellular concentration of a range of compounds, and as such they are pivotal in the regulation of a number of cellular processes, such as sporulation in *Bacillus subtilis* and the acute/chronic infection switch in *P. aeruginosa* [373–375]. They are remarkably prevalent throughout the bacterial domain, with the majority of species containing dozens of TCS proteins [376,377].

Signal transduction by TCSs relies on a highly-specific phosphotransfer reaction between a SK and a cognate RR (cognate meaning the RR usually encoded directly next to the SK in the genome) (Fig 1.3). SKs are commonly bifunctional; in addition to their kinase activity, they also act as phosphatases for their cognate RRs in their basal state, ensuring that RRs are only activated upon stimulation of the SK. As such the ratio of kinase to phosphatase activity is crucial in the propagation of signal transduction, which will be affected by spatial and temporal factors [375,377]. Despite the relatively large sequence similarity between different TCSs, the phosphotransfer reaction and phosphatase activity of TCSs are specific enough to discourage crosstalk between different TCSs. While it is thought that most TCSs are distributed relatively evenly throughout the bacterial membrane, in certain situations TCSs may also be spatially separated in the cell to help overcome crosstalk in the interest of processes such as chemotaxis [378,379].

RRs contain a conserved receiver domain which, upon acceptance of the phosphoryl group from the kinase, confers a conformational change which allows for functional output to occur via the output domain. Often these domains are of ‘Winged helix’ or ‘Helix-turn-helix’ type, and their output involves the binding of DNA in the form of a homodimer, which can then positively or negatively affect regulation of transcription [380]. While DNA-binding domains account for the majority of RR function, there is a broad range of other reported functional domains of RRs, such as enzymatic domains (e.g. adenylate cyclases, c-di-GMP-synthases and methylesterases), transport domains (e.g. Mg^{2+} transporters and sulfate transporters) and protein-binding domains [380].

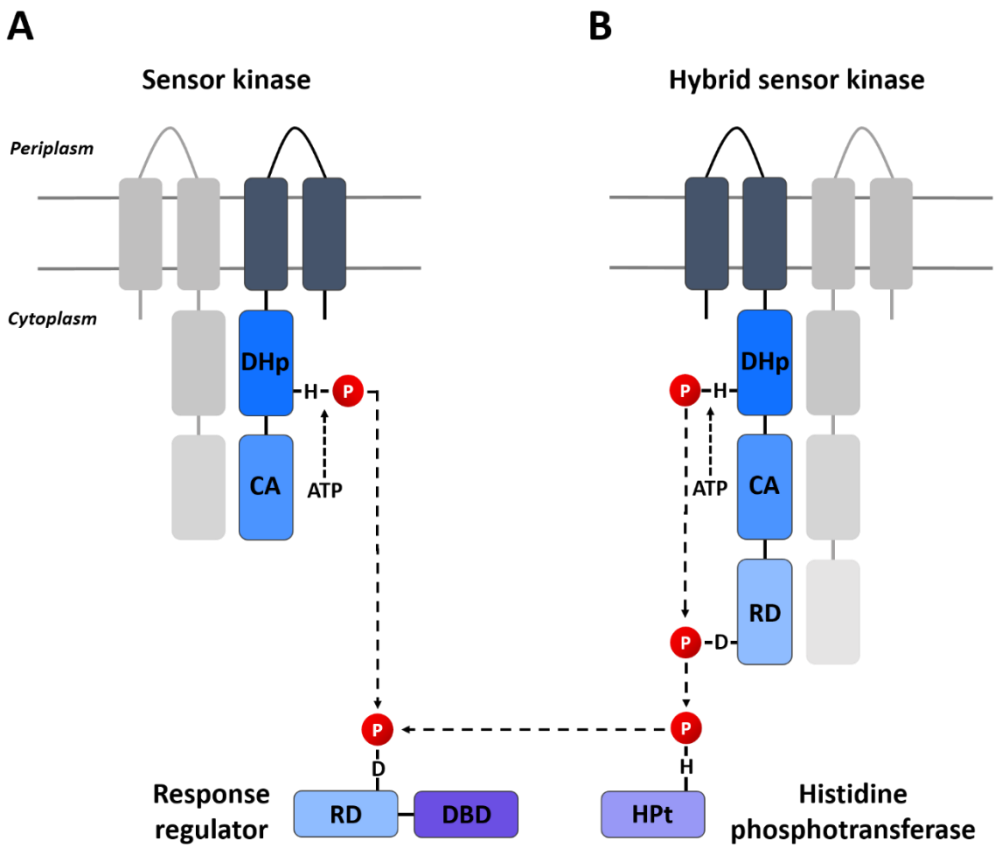

Figure 1.3: Structure of traditional TCS signalling pathways. A) A basic TCS comprised of a SK and an RR. Functioning as homodimers, SKs will sense a signal in the periplasm and undergo autophosphorylation, adding a phosphoryl group to a conserved histidine residue on the DHp domain via the catalysis of adenosine triphosphate (ATP). The conserved SK histidine residue will then donate its phosphoryl group to a conserved aspartate residue on the RR. The RR will then perform its cellular function, commonly regulation of gene transcription. Following activation, dephosphorylation of the TCS will occur through a combination of phosphatase activity of the SK and the labile phosphoryl group detaching from the RR. B) Phosphorelays consist of a hybrid SK, which contains a receiver domain as well as the usual SK domains. Phosphotransfer will occur between the DHp domain and RD of the SK and will then occur again between the RD of the SK and a conserved histidine on a Hpt protein, which can either be attached as part of the hybrid SK or as a standalone protein. This leads to phosphotransfer between the Hpt and the cognate RR in the cytoplasm. Abbreviations: CA, catalytic and ATP-binding domain; DBD, DNA-binding domain; DHp, histidine phosphotransfer domain; HPt, histidine phosphotransferase; RD, receiver domain.

As TCSs allow for the adaptation of the organism to the external environment, it is of little surprise that the number of TCS genes in a genome appears to correlate with the typical environmental habitat of a bacteria. In essence, the more diverse and changing the environment of the bacteria is, the more TCSs it typically encodes [377,380,381].

1.3.2 – Evolution of the two-component system

The evolutionary origin of the TCS is unknown, with limited information attainable from genomes analysed thus far. One suggestion arises from the shared homology of the ATP-binding domains between SKs and the GHKL superfamily of proteins, which bind ATP in ways not dissimilar to SKs, implicating a divergent event between these proteins somewhere in the evolutionary tree [377,382]. It is possible that one-component systems (OCSs), where the input and output domains are joined on a single protein, are evolutionary ancestors of TCSs, due to the similarities between sensor and DNA-binding domains of OCSs and TCSs, as well as the fact that OCSs are more widely distributed than TCSs among prokaryotes [383,384].

While TCSs are found in eukaryotes such as yeasts, fungi, amoebas and plants, they do not usually present as basic TCSs, rather the majority of TCSs in these eukaryotes are phosphorelays utilising hybrid SKs, with 90 % of plant and 100 % of fungal SKs being hybrids [377,385,386]. The absence of TCSs from the genomes of higher eukaryotes may be explained by the inherent lability of the phosphoryl group on aspartate residues. One speculation is that as cellular homeostasis became more complex in eukaryotes, the need for longer and more stable signals created an evolutionary pressure selecting for alternative residues (or proteins containing residues) that provide this stability, such as serine, threonine and tyrosine [377].

The strong sequence similarity between TCSs suggests that gene duplication is a common mechanism by which new TCSs may arise. Following a gene duplication event, provided that a duplicated TCS is able to carve out its own niche in the bacteria, thus avoiding functional redundancy and eventual deletion, novel TCSs may arise. This is supported by the finding that SKs and RRs are

some of the most common kinds of pseudogene in bacterial genomes, suggesting that these TCSs were duplicated but have not yet been removed from the genome following function-disrupting mutations [387]. An analysis of SK phylogenetic distribution found that gene duplication was a major driver of TCS evolution, though horizontal gene transfer between species also contributed significantly, with the extent of the contribution of each mechanism varying across different species [381]. Horizontal gene transfer can occur in a variety of ways, such as via plasmid conjugation or on pathogenicity islands [388–390]. While SKs and RRs often form discrete operons with each other, thus making duplication of both genes in a single event quite possible, duplicated SKs have a higher propensity to present as orphan genes, located away from a cognate RR, when compared to SKs gained through horizontal gene transfer [377,381]. This presents an interesting situation where duplicated TCS genes may retain the ability to interact with the original TCS. One example involves the five orphan kinases KinA/B/C/D/E in *B. subtilis*, which are all able to phosphorylate the RR Spo0F, which regulates sporulation [373]. Additionally, TCSs acquired through duplication events tend to have greater levels of novel domain architecture than horizontal gene transfer-acquired TCSs, supporting the idea that these mechanisms have distinct roles to play in the dissemination and evolution of TCSs [381].

1.3.3 – The therapeutic potential of targeting two-component systems

The separation between the TCS's histidine/aspartate-based phosphorylation and the serine/threonine and tyrosine-based phosphorylation cascades of higher eukaryotes presents an opportunity to develop novel antimicrobials against TCSs. As higher eukaryotes lack TCSs, compounds specifically targeting TCSs would have minimal off-target effects in the host, while the structural similarities between different SKs and RRs in bacteria implies that a targeting compound may inhibit multiple TCSs simultaneously, an ideal situation for use in clinical practice [391]. TCSs have also emerged as common regulators of various bacterial stress responses and virulence factors; targeting the upstream regulators of these processes may present an effective antimicrobial strategy when compared to targeting individual factors instead [391].

A handful of examples exist of TCSs that have been successfully targeted by pharmaceutical compounds. The TCS WalK/WalR is a master regulator of cell wall metabolism in several species including *B. subtilis* and *S. aureus*, and as such is essential for bacterial growth [392–394]. Walkmycin B, an inhibitor of the WalK SK in *B. subtilis* and *S. aureus*, significantly reduced autophosphorylation of WalK in both species [395]. Similarly, waldiomycin and singermycin B inhibited action of WalK, and waldiomycin also affected other SKs in *B. subtilis* such as PhoR and ResE [396,397]. A high-throughput screen for WalR inhibitors identified walrycin, which was bactericidal against *B. subtilis* and *S. aureus* through inhibition of cell division [398]. The example of the WalK/WalR TCS demonstrates that TCSs can be a promising avenue of novel antimicrobials, targeting both SKs and RRs.

However, examples aren't limited to just the WalKWalR system. The PhoQ/PhoP TCS in *Salmonella enterica* senses low Mg^{2+} levels and acidic pH, regulating different genes depending on the input signal received, several of which are vital for virulence [399]. A screen of 255 drug-like compounds looking to identify candidates for novel antimicrobials targeting the PhoQ/PhoP system identified eight compounds that disrupted the formation of the PhoP-DNA complex in a dose-dependent manner, thus inhibiting virulence gene regulation [400]. Mutants of *Salmonella typhimurium* with disrupted PhoP/Q regulons have demonstrated potential as live vaccine candidates in mouse models, and a PhoP mutant strain of *M. tuberculosis* has also been used as a vaccination candidate in mice and guinea pigs [401–404]. Due to the common regulation of virulence genes by TCSs, strains attenuated in particular TCS function may be promising candidates for live vaccines in the future.

1.3.4 – Cross-regulation of two-component systems

There are many situations in which TCSs can interact with one another in various ways, such as one TCS regulating the expression of another, or through phosphotransfer between non-cognate pairings of SKs and RRs. This physiologically relevant interaction is generally known as cross-regulation, as opposed to the term crosstalk, which is used to describe physiologically irrelevant non-cognate interactions between TCSs. Cross-regulation allows for networks of

TCSs to be established within the cell, providing opportunities for more intricate responses to environmental stimuli than the binary 'on/off' modality of a canonical TCS.

An example of a network of TCSs revolves around the aforementioned low Mg^{2+}-sensing PhoQ/PhoP TCS in *S. enterica* and *E. coli*. Expression of the small cytoplasmic-membrane connector protein SafA is induced by stimulation of the low pH-sensing EvgS/EvgA, which subsequently activates PhoQ/PhoP via interactions of the C-terminal domain of SafA to the sensor domain of PhoQ [394,405,406]. Additionally, PhoP directly regulates the expression of the acid-response RstB/RstA TCS through binding of its promoter, adding further complexity to the network linking the low Mg^{2+} response and the acid-response in these bacteria [394,407].

1.3.5 – Two-component systems in multikinase networks

The remainder of this section will focus on a type of cross-regulation between TCSs that utilises direct phosphosignalling-based interactions between SKs and RRs, also known as multikinase networks (MKNs). The above example of cross-regulation demonstrates some possible connections between TCSs, namely through the use of small connector proteins and direct regulation of each other's operons, whereas TCSs in MKNs specifically utilise the presence/absence of the phosphoryl group as the focus of their interactions. While the insulation between TCSs usually prevents unwanted crosstalk, there are many strong examples of non-cognate phosphorylation between TCSs that confer functional advantage to the cell in the form of sophisticated MKNs. Additionally, MKNs exist in which certain SKs can directly modulate the activity of other SKs, rather than through phosphorylation of a non-cognate RR. Essentially, in MKNs, rather than confusing different signals, the phosphosignalling-based interactions allows for higher level decision making in response to stimuli, often integrating multiple stimuli into a single, decided cellular output.

The NarXL/NarPQ system of *E. coli* is a relatively simple MKN that dictates the choice between nitrite (NO_2^-) and nitrate (NO_3^-) as alternative electron acceptors in anaerobic conditions (Fig 1.4). This MKN ensures that when the preferred

electron acceptor, NO_3^-, is present, NO_3^- reductase is expressed, but that NO_2^- reductase is only expressed when NO_2^- is present and NO_3^- is absent [408,409]. This MKN contains just two SKs and two RRs, yet provides the opportunity for higher-level decision making in the bacteria, acting as a good example of the potential for MKNs to confer evolutionary advantage to bacteria.

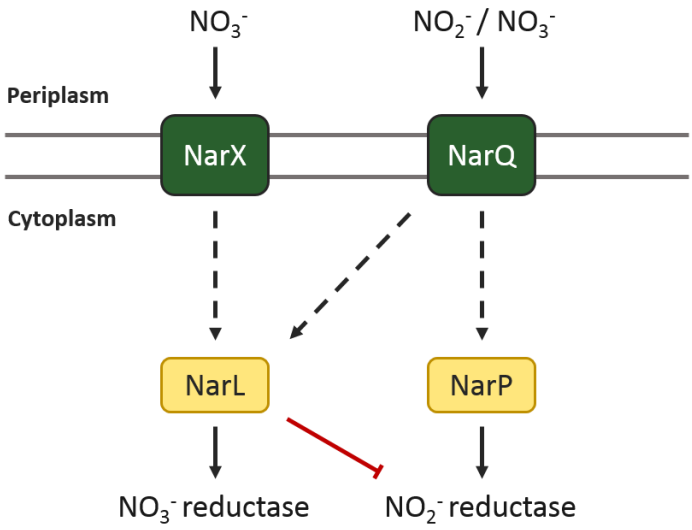

Figure 1.4: The NarXL/NarPQ MKN. NarX can phosphorylate its cognate partner NarL, while NarQ can phosphorylate both NarL and NarP, but has a slight kinetic preference for phosphorylating NarL [409]. NarL upregulates NO_3^- reductase and inhibits expression of NO_2^- reductase, while NarP upregulates NO_2^- reductase. The presence of NO_3^- leads to activation of both NarL and NarP, though the inhibiting action of NarL on NO_2^- expression means that only NO_3^- reductase is expressed. This occurs with or without the presence of NO_2^-. It is only when NO_2^- is present without NO_3^- that NO_2^- reductase is expressed, as even though NarQ can activate NarL, the cognate phosphatase activity of NarX on NarL means there is little phosphorylated NarL present. Ultimately, this MKN allows for the expression of NO_3^- reductase whenever NO_3^- is present, but only allows for the expression of NO_2^- reductase in the absence of NO_3^-. Dashed arrows signify positive interactions, the blunt-end arrow signifies inhibition. Figure adapted from Francis and Porter (2019).

In contrast to the relative simplicity of the NarXL/NarPQ MKN, The GacS network of *P. aeruginosa* is of considerable complexity, regulating the switch between the acute and chronic virulence state (Fig 1.5). This MKN consists of 7 different SKs which are able to modulate each other in a variety of ways. For example, there is extensive protein-protein interaction between the basic SK RetS and the hybrid SK GacS that utilises at least three distinct signalling mechanisms; RetS is able to receive phosphoryl groups from GacS, act as a phosphatase against the RD of GacS and also inhibit the autophosphorylation ability of GacS [410]. The MKN also includes Hpt proteins, regulatory RNAs and dual-function RRs, which come together to produce a fascinating example of the complex decision making afforded through the use of MKNs. Ultimately, the GacS MKN contains a wide variety of ways that TCSs can interact with one another, such as direct SK-SK interactions, phosphorylation of SKs and HPts and multiple SKs phosphorylating the same RR.

There are many more examples of MKNs; cell cycle control in *Caulobacter crescentus* requires the SK DivL for the recruitment of another SK, CckA, to the cell pole, and utilises multiple RRs and a HPt protein, while QS in *V. harveyi* exploits a many-to-one network of three SKs phosphorylating a single HPt protein [375,411,412]. Ultimately, while MKNs can take many forms and be of ranging complexity, they can confer great advantage to the host through allowing superior levels of decision making in response to the environment.

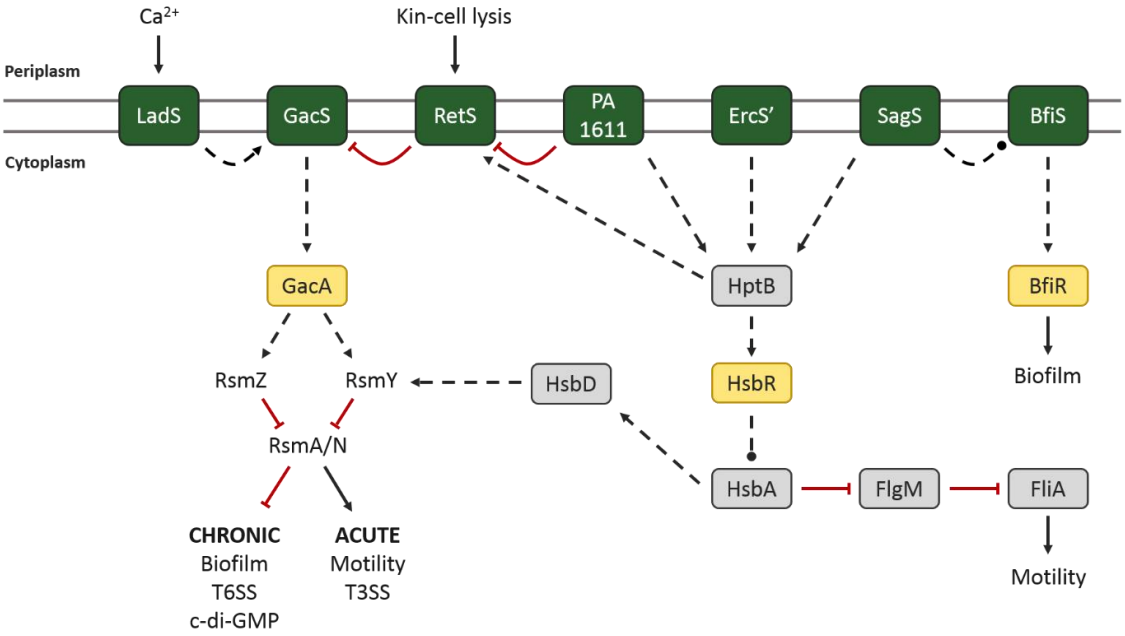

Figure 1.5: The GacS MKN of *P. aeruginosa*. The GacS MKN centres on the RR GacA, which is phosphorylated by GacS. Activated GacA promotes the chronic virulence phenotype through expression of the regulatory RNAs RsmY and RsmZ [375,413,414]. As a result, phosphorylation of GacS leads to promotion of the chronic virulence phenotype. GacS is modulated positively and negatively by LadS and RetS, and RetS is turn is regulated by PA1611 [375,410,415,416]. PA1611, SagS and ErcS' can also modulate the acute/chronic virulence switch via the Hpt protein HptB, which is part of a cascade of proteins that can increase RsmY levels to promote the chronic phenotype, or increase motility via the FlgM and FliA proteins, promoting the acute phenotype [375,417,418]. SagS can also act on BfiS, an interaction necessary for biofilm formation. Dashed arrows signify positive interactions, blunt-ended arrows signify inhibition, bulb-ended arrows signify positive or negative interactions depending on the wider state of the network. Figure adapted from Francis and Porter (2019).

1.3.6 – Molecular regulation of phosphotransfer specificity

While there are several examples of TCSs cooperating in complex MKNs, TCSs traditionally act independently of one another, with phosphotransfer between partner SKs and RRs and minimal crosstalk occurring between different TCSs. This has been demonstrated by Skerker and colleagues (2005) via systematic phosphotransfer profiling of three *E. coli* SKs against 32 *E. coli* RRs and six *C. crescentus* SKs against 44 *C. crescentus* RRs, which showed that while non-cognate phosphotransfer is possible between certain non-cognate SK-RR pairings, each SK had a starkly stronger kinetic preference for phosphorylating its cognate RR over other non-cognate RRs [419]. Given that TCSs can be present in their tens or hundreds in the cell, understanding the molecular basis of specificity between SKs and RRs is crucial in fully appreciating the nuance of how bacteria sense and respond to their environment.

Analysis of cognate TCSs pairings has revealed that there are several amino acids on SKs and RRs that coevolve together, which possibly aids in the generation of a new niche for a recently-duplicated TCS [377,420–422]. For example, a mutation in the phosphotransfer domain of a SK may require a compensatory mutation in the cognate RR, lest the TCS lose the specificity of phosphotransfer, or even the ability of the SK to phosphorylate its partner RR at all. A highly-coevolving subset of specificity residues has been identified on TCS proteins that are essential for the specificity of phosphotransfer, which surround the phosphotransfer site of TCSs; there are 6 specificity residues on SKs and 7 on RRs. As such, one can mutate these residues to rewire the specificity of the SK-RR phosphotransfer reaction [377,422,423]. For example, directed mutagenesis of three strongly coevolving specificity residues of the *E. coli* SKs EnvZ and RstB is enough to swap their phosphotransfer specificity, while the *E. coli* RR OmpR could also have its phosphotransfer specificity altered through mutagenesis of specificity residues [422]. It has been demonstrated in TCSs of *M. xanthus* that specificity residues, in addition to the specificity of phosphotransfer, also regulate binding kinetics between SKs and RRs, supporting their role as essential in avoiding unwanted crosstalk between TCSs [424]. Additionally, residues have been identified that mediate SK dimerisation specificity, promoting homodimerisation and preventing heterodimerisation [425].

1.3.7 – Characterised two-component systems in *B. cenocepacia*

There are 59 predicted SKs (9 of which are hybrid SKs) and 60 predicted RRs in *B. cenocepacia*, the majority of which are uncharacterised [18,426]. The number of TCS genes in *B. cenocepacia* is similar to that of other BCC members and to *P. aeruginosa*, though some environmental bacteria, such as *Myxococcus xanthus*, which has a total of 136 SKs and 127 RRs, have many more TCS genes [377,426]. A summary of the characterised TCSs in *B. cenocepacia* can be found in Table 1.1.

Table 1.1 – Summary of the characterised TCSs in *B. cenocepacia*.

Locus	Name	Description	Ref.
BCAL0471/2	EsaSR	Implicated in drug efflux and integrity of the cell membrane.	427
BCAL0534/5	RqpSR	Implicated in the regulation of quorum sensing and virulence.	428
BCAL2210/11	FixLJ	~95 % gene identity to the low oxygen-sensing FixLJ TCS in *B. dolosa*, implicated in virulence, biofilm formation and motility.	203
BCAL2830/31	-	Involved with transcription of the virulence factor High temperature requirement A protease, which is required for growth in osmotic and thermal stress.	429
BCAM0227/8	-	The SK BCAM0227 is involved in sensing of BDSF. Implicated in virulence in *G. mellonella* and mice.	163
BCAM0379/81	AtsRT	Phosphorelay that negatively regulates biofilm formation, quorum sensing, motility and the T6SS.	430–432
BCAM1493/4	$BceS_1R_1$	Homologous to the GacSA TCS in *P. aeruginosa*. Implicated in the regulation of protease production, motility, quorum sensing and plant pathogenesis.	433
BCAM2756-8	CblSTR	Locus of two hybrid SKs and one RR that is implicated in regulation of the cable pilus locus.	434

Currently, there is one potential example of a MKN in *B. cenocepacia*, the cable pilus-regulating *cblSTR* locus. This locus encodes two membrane-bound hybrid SKs, CblS and CblT, and the DNA-binding RR CblR. Upon autophosphorylation, the receiver domain of CblS is thought to transfer its phosphoryl group to the Hpt domain of CblT, which can then phosphorylate CblR. There is no direct evidence for phosphotransfer between the hybrid SKs CblS and CblT, however inactivation of either CblS, CblT or CblR leads to a block in transcription from the *cblBACD* locus, suggesting that all three are necessary for functional activation of the cable pilus locus [434]. Interestingly, while ectopic expression of CblS or CblR in WT *B. cenocepacia* increased the number of piliated cells, expression of CblT blocked expression of the cable pilus, perhaps indicating that CblT is able to both promote (through phosphotransfer to CblS or CblR) and inhibit (via phosphatase activity of either the Hpt domain of CblS or CblR) transcription of the *cblBACD* locus [434]. The particular stimuli that activate CblS and CblT have yet to be elucidated, and it is unclear how expression of the *cblBACD* locus is affected by the interactions between these SKs. Bioinformatic analysis of the specificity residues of CblS and CblT show their SK domains share 4 of 6 specificity residues, and their receiver domains share 5 of 7, further strengthening the idea that phosphotransfer can occur either between these SKs, or between CblS and CblT and a shared target.

1.3.8 – A potential heavy metal-sensing multikinase network in *B. cenocepacia*

Given that specificity residues regulate the exclusivity of phosphotransfer in TCSs, it may be possible to utilise specificity residues as a prediction tool for novel MKNs. If the specificity residues of multiple SKs or RRs are similar in a bacterial species, it may indicate that non-cognate phosphotransfer between these TCSs is not only kinetically possible, but is also of physiological relevance. Provided that similarities between specificity residues allows for beneficial non-cognate phosphotransfer between TCSs, evolutionary pressure may select for these similarities, and as such lead to the establishment of a physiologically relevant MKN. If novel MKNs can indeed be predicted using this method, it may lead to rapid identification of MKNs, accelerating our understanding of bacterial environmental regulation and possibly increase the number of potential targets

for novel therapeutics. As such, comparisons of the specificity residues of all SKs and RRs in *B. cenocepacia* J2315 have identified several TCS proteins that show specificity residue similarities, which may indicate the presence of novel MKNs (Table 1.2).

Table 1.2 – Summary of specificity residue similarity in TCS proteins in *B. cenocepacia*.

Gene names	Description of specificity residue similarity
	SK similarities
BCAL2012 + BCAL2605	The predicted orthologue of the *E. coli* osmolarity-sensing SK EnvZ in *B. cenocepacia*, BCAL2012, shares 5 of 6 specificity residues with BCAL2605.
BCAM0218 + BCAM0227	The BDSF-sensing hybrid SK BCAM0227 shares all 6 SK specificity residues with the hybrid SK BCAM0218. Real-time PCR and domain-swapping experiments did not reveal any BDSF-genes to be regulated by BCAM0218, hence the physiological relevance this potential interaction may have to the BDSF system of *B. cenocepacia* remains unclear [163].
	RR similarities
BCAL1350 + BCAL2011 + BCAL2606 + BCAM2175	BCAL2011, the predicted orthologue of OmpR, shares 5 specificity residues with three other RRs (BCAL2606, BCAL1350 and BCAM2175), indicating the potential presence of an osmolarity-sensing MKN in *B. cenocepacia*.
BCAL2211 + BCAM0230A	The FixJ RR and the uncharacterised BCAM0230A share 5 of 7 specificity residues.
BCAL2222 + BCAL2831	The predicted nitrogen-sensing BCAL2222 shares 5 of 7 specificity residues with BCAL2831.
BCAM0288 + BCAM0623 + BCAM1494	The GacA homologue $BceR_1$ shares 5 of 7 specificity residues with BCAM0288 and BCAM0623, potentially indicating the presence of a MKN similar to that in *P. aeruginosa*.
BCAM0443 + BCAM0714 + BCAM1418 + BCAS0586	The focus of this work. Four putative metal-sensing RRs share between 4-6 specificity residues with one another.
BCAM0820 + BCAM1161	The receiver domain of the hybrid SK BCAM0820 shares 5 of 7 specificity residues with the RR BCAM1161.
BCAM0826 + BCAM1162	Two predicted chemotaxis-specific methylesterases, BCAM0826 and BCAM1162, share 6 of 7 specificity residues.

The focus of this work revolves around four putative heavy metal-sensing TCSs in *B. cenocepacia* that share high levels of similarity between their RR specificity residues, and thus may form a novel heavy metal-sensing MKN (Fig 1.6). While the four SKs do not share great levels of similarity in their 6 specificity residues, the 7 specificity residues of the RRs are of significant similarity, particularly when focusing on BCAS0586, which shares 6 specificity residues with both BCAM0443 and BCAM0714, while four specificity residues are identical across all four RRs.

Interestingly, the overall DNA sequence similarity between these four TCSs is significantly greater than to other TCSs in the *B. cenocepacia* J2315 genome. It could therefore be argued that these TCSs originated from a single TCS via gene duplication events and have subsequently managed to establish their own functional niche in the genome. Evidence for this also lies in the specificity residues of the SKs, while not hugely similar in terms of matching residues, there are some residues that are identical across three SKs, such as the asparagine of the 2nd specificity residue, the glutamine of the 5th and the valine of the 6th.

Contrastingly, the specificity residues of the four RRs are of much greater similarity to each other than of the SKs. Given that the vast majority of RRs in the genome share between 0-2 specificity residues with other RRs, it is likely that these specificity residues have maintained their similarity to each other through some kind of evolutionary pressure, suggesting that there is physiological relevance to this potential MKN.

Previous work has established that deletion of the BCAM0714/5 TCS in *B. cenocepacia* K56-2 confers sensitivity to cadmium and zinc via disrupted expression of the CzcCBA efflux pump (Fig 1.7) (Robinson et al., Unpublished data). CzcR has been shown to regulate this CzcCBA efflux pump, its own BCAM0714/5 operon and a downstream gene region, BCAM0716-0721. Deletion of this downstream gene region confers susceptibility to zinc, albeit a lower susceptibility than deletion of CzcRS confers, indicating the presence of a novel zinc-resistance determinant in this region (Fig 1.7). Transcriptomic analysis showed that CzcCBA, BCAM0714/5 and BCAM0716-0721 were all significantly upregulated in the presence of 1.5 mM $ZnCl_2$ in comparison to LB. In essence, BCAM0714/5 confers resistance to cadmium and zinc via the CzcCBA efflux pump, while the BCAM0716-0721 region is also involved in the zinc response.

A

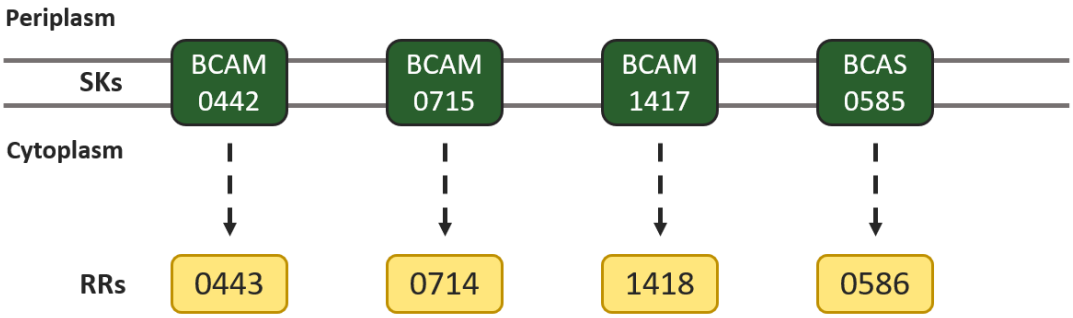

B

BCAM0442	A	N	S	S	Q	I
BCAM0715	T	N	A	A	Q	V
BCAM1417	S	I	G	Q	Q	V
BCAS0585	N	N	G	A	E	V

BCAM0443	E	K	M	Y	K	G	A
BCAM0714	E	K	T	Y	K	G	D
BCAM1418	E	K	V	Y	S	G	S
BCAS0586	E	K	T	Y	K	G	A

C

SKs	0442	0715	1417
0715	2		2
1417	1	2	
0585	1	3	2

RRs	0443	0714	1418
0714	5		4
1418	4	4	
0586	6	6	4

Figure 1.6: A potential novel heavy metal-sensing MKN in *B. cenocepacia*. A) Diagram depicting the TCSs, comprised of four basic SKs and four RRs which have DNA-binding domains. All four SKs are adjacent to their partner RRs in the genome, forming a discrete operon. Dashed arrows signify presumed cognate phosphotransfer. B) Table listing the specificity residues of the four SKs (left) and RRs (right). There are 6 specificity residues in SKs and 7 in RRs that are of particular importance in regulating specificity of phosphotransfer, and those have been selected for comparison. Yellow boxes indicate specificity residues shared across all four proteins, while green boxes indicate specificity residues which match in two or three proteins. C) A matrix table summarising the number of specificity residues which match between pairs of SKs (left) and RRs (right).

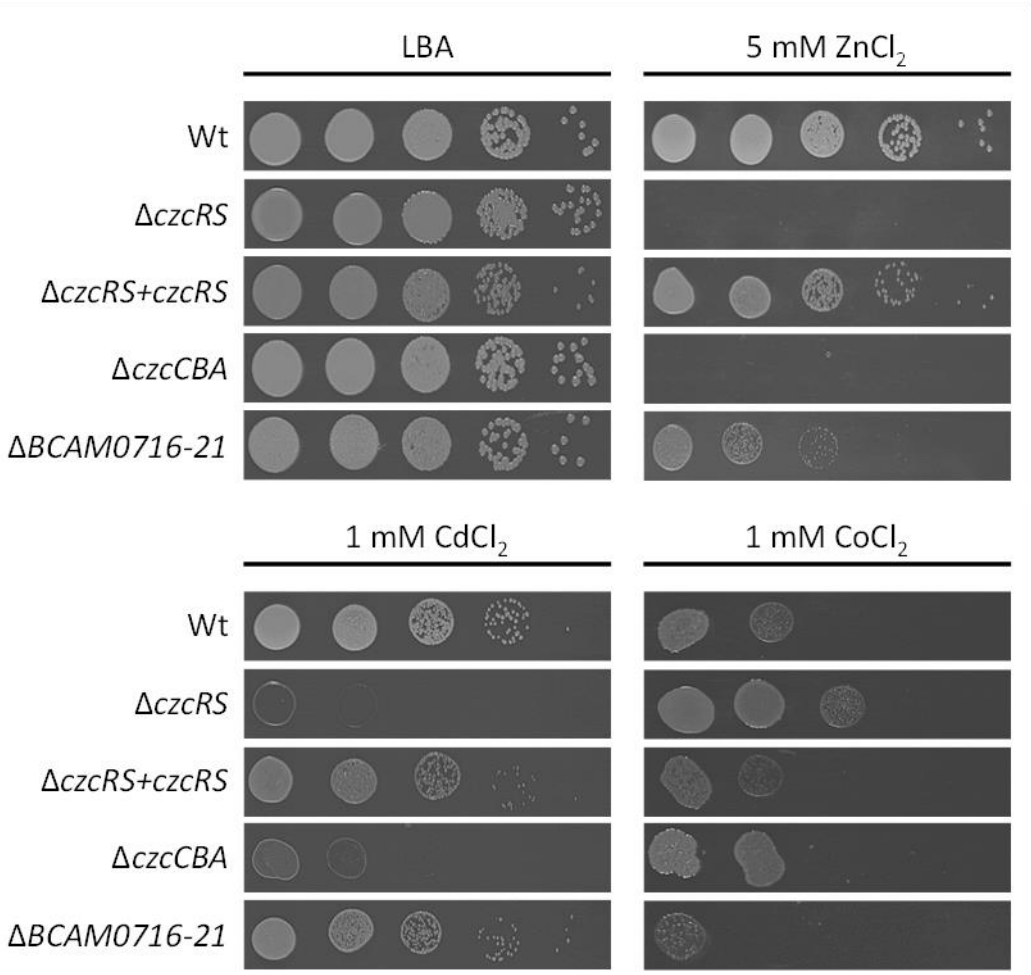

Figure 1.7: The cadmium and zinc phenotypes of CzcRS in *B. cenocepacia* K56-2. Strains were grown in LB to stationary phase, resuspended in PBS to an OD_{590} of 1 ± 0.05 and serially diluted on LB plates containing various concentrations of metal compounds. Deletion of CzcRS and CzcCBA confers susceptibility to cadmium and zinc, but not cobalt, while deletion of BCAM0716-0721 confers susceptibility to zinc. Experiment performed and figure generated by Dr Matthew Robinson.

Aside from BCAM0714/5, there is little information in the literature that sheds light on the function of the remaining TCSs. A recent paper by Higgins and colleagues (2020) identified several copper resistance genes of *B. cenocepacia* H111 via transposon sequencing, including BCAM0442/3 and the downstream BCAM0444-0450 gene region [369]. Indeed, the genomic neighbourhood of BCAM0442/3 includes apparent orthologues of the CusABCF and CopABCDE copper/silver-resistance systems, which may implicate BCAM0442/3 in copper and/or silver resistance [18,344]. Interestingly, the authors also identified the BCAM0715 and BCAS0585 SKs, but not their cognate RRs, as being involved in copper resistance, perhaps suggesting that these TCSs all contribute to the copper response of *B. cenocepacia* [369]. Aside from this transposon sequencing, little is known about what these TCSs respond to and what their wider functional role in *B. cenocepacia* may be.

This potential MKN is also conserved across the wider BCC. The other major CF BCC species, *B. multivorans*, has four putative metal-sensing TCSs which share comparable levels of specificity residue similarity in their SKs and RRs. The environmental *B. ambifaria* has three orthologous TCSs with comparable specificity residue similarities, with an orthologue of BCAM0714/5 absent. Outside of the BCC, the phytopathogen *B. glumae* has two potentially orthologous TCSs, which share four of their RR specificity residues. Both *B. pseudomallei* and *B. thailandensis* have two putative metal-sensing TCSs which share all of their SK specificity residues and 6 out of 7 RR specificity residues, both of which have high levels of similarity to BCAM0714/5, perhaps indicating a gene duplication event involving this TCS. There is evidence that a comparable MKN exists outside of the *Burkholderia* genus, as the opportunistic pathogen *P. aeruginosa* has four orthologous TCSs which also share many RR specificity residues (albeit at a slightly lower level of similarity to the *B. cenocepacia* RRs). Overall, these TCSs and the overall level of specificity residue similarity is relatively well conserved across the *Burkholderia* genus and possibly also in *P. aeruginosa*, which may have wide implications for the metal response of these bacteria, and how they respond to metal-contaminated environments and metal-containing medical devices and surfaces.

The notion that these TCSs are metal-responsive stems from the fact that the orthologue of BCAM0714/5 in *P. aeruginosa* (PA2523/4) has been implicated in

resistance to cadmium, zinc and cobalt, via upregulation of the CzcCBA RND-family efflux pump, and has thus been designated as the CzcRS system [319]. CzcRS in *P. aeruginosa* also co-regulates resistance to carbapenems via downregulation of the OprD porin, the main route of entry for these antibiotics [319,320,435]. The copper-sensing TCS CopRS (PA2809/10) is able to upregulate both CzcRS and CzcCBA, and can also downregulate OprD, linking copper, zinc, cadmium and cobalt resistance to resistance to carbapenems in *P. aeruginosa* [320]. This downregulation of OprD by both RRs has been shown to be mediated by the RNA chaperone Hfq [436]. Additionally, CzcR in *P. aeruginosa* has been identified as a regulator of pyocanin biosynthesis, several quorum sensing genes and is required for full virulence in *C. elegans*, while the IrlRS TCS in *B. pseudomallei*, which confers resistance to cadmium and zinc, is also implicated in epithelial cell invasion, further underlining the CzcRS system as a key player in regulation of virulence in addition to the metal response [437,438].

1.4 – Project aims

The overall aim of this project was to experimentally validate the putative novel heavy metal-sensing MKN in *B. cenocepacia*, through investigation of potential non-cognate phosphotransfer between TCSs of interest, and to elucidate any potential physiological relevancy that these interactions may hold. Validation of this MKN was carried out by:

- Evaluation of non-cognate interactions between TCSs via purification of SKs and RRs for phosphotransfer assays [Chapter 3].
- Generation and phenotypic characterisation of TCS deletion mutants in *B. cenocepacia* K56-2 [Chapter 4].
- Exploration of the copper response of *B. cenocepacia* K56-2 through RNA-seq analysis [Chapter 5].
- Investigation of the BCAM0716-0721 gene region through targeted complementation of the ΔBCAM0716-21 deletion mutant [Chapter 6].

Chapter 2: Materials and Methods

2.1 – General culture conditions

Strains and vectors utilised in this study can be found in Table 2.1. All *B. cenocepacia* gene names are as written in the J2315 reference genome. *E. coli* and *B. cenocepacia* K56-2 were grown at 37 °C in either a shaking incubator (200 rpm) or static incubator in lysogeny broth (LB) liquid medium or agar unless otherwise specified. A full media list can be found in Table 2.2. When suitable, filter-sterilised (0.2 µm filter) antibiotics which were added at the following concentrations and solvents: Ampicillin (Amp, 100 µg/ml, ddH_2O), Gentamicin (Gm, 25 µg/ml for *E. coli*, 50 µg/ml for *B. cenocepacia*, ddH_2O), Kanamycin (Kan, 25 µg/ml, ddH_2O), Polymyxin B (Pol, 25 µg/ml, ddH_2O), Tetracycline (Tet, 25 µg/ml for *E. coli*, 100 µg/ml for *B. cenocepacia*, 95 % EtOH), Trimethoprim (Tp, 50 µg/ml for *E. coli*, 100 µg/ml for *B. cenocepacia*, DMSO). Long term storage of strains involved storage in LB broth with relevant antibiotics and 15 % glycerol (v/v) at -80 °C.

Table 2.1: List of bacterial strains utilised in this work.

Bacterial strain	Explanation	Source/Reference
	***E. coli* strains**	
***E. coli* JM109**	Calcium-competent *E. coli*	Lab stock
***E. coli* GT115**	Calcium-competent *E. coli*	Lab stock
***E. coli* XL1-Blue**	Calcium-competent *E. coli*	Lab stock
***E. coli* pRK2013**	Helper vector for Triparental mating, Kan^R	439
***E. coli* pGPI-SceI**	(Donor) vector for 1st crossover for mutagenesis in *B. cenocepacia*, Tp^R	440
***E. coli* pDAI-SceI**	(Donor) vector for 2nd crossover for mutagenesis in *B. cenocepacia*, Tet^R	440
***E. coli* pDA17**	Expression vector, Tet^R	429
***E. coli* pSCrhaB3**	Expression vector, Tp^R	441
***E. coli* pMLS7**	Expression vector, Tp^R	442
***E. coli* pGA-G1**	Promoter probe vector, Gm^R	443/Leo Eberl group

***E. coli* M15pREP4**	Calcium-competent *E. coli* for protein expression, Kan^R	Lab stock
***E. coli* pQE80::NusA**	IPTG-inducible protein expression vector with 5' NusA gene and 6 x His tag, Amp^R	Dr Vanessa Francis
***E. coli* pQE80**	IPTG-inducible protein expression vector with 5' 6 x His tag, Amp^R	Qiagen
***E. coli* pQE60::eGFP**	IPTG-inducible protein expression vector with 5' eGFP gene Amp^R	This work
***E. coli* pQE80::eGFP**	IPTG-inducible protein expression vector with 3' eGFP gene Amp^R	This work
	***B. cenocepacia* K56-2 strains**	
***B. cenocepacia* K56-2**	WT strain	Lab stock
ΔBCAM0442/3	-	This work
ΔBCAM0714/5	-	This work
ΔBCAM1417/8	-	This work
ΔBCAS0585/6	-	This work
ΔBCAM0442/3 + ΔBCAM0714/5	-	This work
ΔBCAM0442/3 + ΔBCAS0585/6	-	This work
ΔBCAM0714/5 + ΔBCAS0585/6	-	This work
ΔBCAM0442/3 + ΔBCAM0714/5 + ΔBCAS0585/6 +	-	This work
ΔBCAM0433-0450	-	This work
ΔBCAM0716-0721	-	Dr Matthew Robinson
Δ*czcCBA*	-	Dr Matthew Robinson
Δ*czcCB*	-	Dr Matthew Robinson
***B. cenocepacia* K56-2 Gm^S**	Gentamicin-sensitive WT	Dr Matthew Robinson
ΔBCAM0442/3 Gm^S	-	This work

∆BCAM0714/5 Gm^S	-	This work
∆BCAM1417/8 Gm^S	-	This work
∆BCAS0585/6 Gm^S	-	This work

Table 2.2: List of media utilised in this work.

Media	Details	Source
LB	10 g/L Casein digest peptone, 10 g/L NaCl, 5 g/L Yeast extract	Melford
2YT	16 g/L Tryptone, 5 g/L NaCl, 5 g/L Yeast extract	Lab stock
M9	6.78 g/L Na_2HPO_4, 3 g/L KH_2PO_4, 1 g/L NH_4Cl, 0.5 g/L NaCl, 0.4 % Glucose 240.7 mg/L $MgSO_4$, 11.1 mg/L $CaCl_2$	Lab stock
SOB	20 g/L Tryptone, 0.5 g/L NaCl, 5 g/L Yeast extract, 0.75 mg/L KCl, 3.8 mg/L $MgCl_2$	Lab stock
TSB	17 g/L Pancreatic digest of casein, 3 g/L Papaic digest of soybean meal, 5 g/L NaCl, 2.5 g/L K_2HPO_4, 2.5 g/L Glucose	Oxoid

Note: Relevant agars were created by adding 1.5 % (w/v) of Agar No. 2 Bacteriological General Purpose (Neogen)

2.2 – General molecular biology techniques

2.2.1 – Crude DNA extraction

Extraction of DNA from individual bacterial colonies for the purposes of PCR involved using a 1 µl sterile loop to add a scraping of the colony to 50 µl of lysis solution (50 mM NaOH, 0.25 % Sodium dodecyl sulfate (SDS)) prior to incubation at 95 °C for 15 minutes. 180 µl of nuclease-free water was then added and the lysates spun for 10 minutes at 13,000 rpm.

2.2.2 – Genomic DNA extraction

Genomic DNA was prepared using the GenElute^{TM} Bacterial Genomic DNA Kit (Sigma-Aldrich) following manufacturer's instructions. Briefly, 5 ml overnight culture was centrifuged at 13,000 rpm for 2 minutes and resuspended in lysis

solution, followed by RNase A treatment to eliminate residual RNA. Cells were then lysed and processed through a spin column.

2.2.3 – Plasmid DNA extraction

Overnight cultures of *E. coli* containing the relevant plasmid were harvested and plasmid DNA extracted using the GeneJET Plasmid Miniprep Kit (Thermo Fisher Scientific) following manufacturer's instructions. Briefly, 5 ml overnight culture was centrifuged at 13,000 rpm for 10 minutes, resuspended, lysed and chromosomal DNA removed prior to addition to a spin column.

2.2.4 – Gel electrophoresis

Agarose gels of concentrations ranging from 1-1.5 % were made by microwaving agarose in Tris-acetate-EDTA buffer, followed by the addition of the stain Midori Green (Nippon Genetics) for the purpose of visualising nucleic acid. Samples were diluted in 6 x gel loading dye (Thermo Fisher Scientific) and loaded into wells alongside a relevant ladder, either 100 bp plus, 1 Kb or 1 Kb plus GeneRuler DNA ladder (Thermo Fisher Scientific). Gels were run at 90 V for 45 minutes, and visualised via UV light under the Gel Doc XR+ System (Bio-rad).

2.2.5 – Gel extraction of DNA

For DNA products from PCR or restriction digest that required isolating following gel electrophoresis, the relevant band was excised using a scalpel blade under UV light. The DNA was then processed using the GeneJET Gel Extraction Kit (Thermo Fisher Scientific) following manufacturer's instructions. Briefly, the agarose was melted at 60 °C in binding buffer prior to addition to a spin column.

2.2.6 – Quantification of DNA and RNA concentration

DNA concentration and quality were assessed via a NanoDrop 1000 (Thermo Fisher Scientific). RNA concentration was quantified through the Qubit™ 3.0 Fluorometer (Invitrogen), while quality was assessed using the NanoDrop 1000.

2.2.7 – Polymerase Chain Reaction (PCR)

PCR was carried out using either Taq DNA Polymerase (New England BioLabs) or Phusion High-Fidelity DNA Polymerase (using the provided High-Fidelity buffer, Thermo Fisher Scientific) depending on requirements. All primers were ordered through Eurofins Genomics. Table 2.3 lists the reaction mixture for each of these DNA polymerases, while Table 2.4 provides details of relevant cycling conditions. Following PCR, DNA was visualised via gel electrophoresis (2.2.4).

Table 2.3: Reaction mixture details for PCR.

Constituent	Taq DNA Polymerase	Phusion High-Fidelity DNA Polymerase
Relevant buffer	1 x (from 10 x stock)	1 x (from 5 x stock)
dNTPs	200 µM	200 µM
Forward primer	0.2 µM	0.5 µM
Reverse primer	0.2 µM	0.5 µM
DNA template	1 µl	1 µl
DNA polymerase	0.625 units	0.004 units
Nuclease-free H_2O	Up to 25 µl	Up to 20 µl

Note: 3 % Dimethyl sulfoxide was commonly added when amplifying from GC-rich DNA.

Table 2.4: Cycling conditions for PCR.

Cycle stage	Taq DNA Polymerase	Phusion High-Fidelity DNA Polymerase
Initial Denaturation	95 °C for 30 s	98 °C for 90 s
	Followed by 30 cycles of	
Denaturation	95 °C for 30 s	98 °C for 10 s
Annealing	Variable temperature for 30 s	Variable temperature for 30 s
Extension	68 °C for 60 s /Kb	72 °C for 20 s /Kb
	Followed by:	
Final Extension	68 °C for 600 s	72 °C for 600 s

Note: Annealing temperature was dependent on the melting temperature of the primers used. For a complete primer list see Appendix section A5.

2.2.8 – Restriction digest of DNA

Restriction digestion of DNA was carried out over an hour at 37 °C with 1 µg of DNA using FastDigest restriction enzymes (Thermo Fisher Scientific), in a total volume of 40 µl. All restriction enzymes used were active in the FastDigest buffer provided, and as such digestions using two enzymes simultaneously were commonly performed. Following digestion, DNA was visualised via gel electrophoresis and appropriate bands excised (sections 2.2.4-2.2.5).

2.2.9 – Ligation of DNA

Ligation between vector and insert DNA was carried out overnight at 16 °C using T4 DNA ligase (New England BioLabs) in a total volume of 20 µl. Generally, a molar ratio of insert:vector of 3:1 was used. A vector only control was run alongside all ligation reactions for potential troubleshooting purposes. Occasionally as a troubleshooting method, FastAP Thermosensitive Alkaline Phosphatase (Thermo Fisher Scientific) was used as per manufacturer's

instructions to dephosphorylate vector DNA prior to ligation, ensuring that no vector recircularisation occurred during the ligation process.

2.2.10 – Generation of calcium-competent *E. coli* cells

50 ml of LB broth was inoculated with 1 ml of overnight-grown *E. coli* cells (either JM109, GT115, M15pREP4 or XL1-Blue) and grown at 37 °C until an OD_{600} of 0.5-0.6 was reached. Cells were then chilled on ice for 30 minutes, then centrifuged at 3,000 rpm for 10 minutes at 4 °C. Cells were resuspended in 25 ml of chilled 100 mM $CaCl_2$, and rested on ice for 30 minutes. Cells were then spun again at 3,000 rpm for 10 minutes at 4 °C, and resuspended in 2 ml of chilled 100 mM $CaCl_2$ with 15 % glycerol (v/v). Cells were aliquoted out and stored at -80 °C until use.

2.2.11 – Transformation of DNA into calcium-competent *E. coli*

4 µl of DNA (e.g. ligation product or plasmid extracted from culture) and 50 µl of calcium-competent *E. coli* cells were added to a 1.5 ml microcentrifuge tube, gently mixed and chilled on ice for 30 minutes. Cells were heat-shocked at 42 °C for 50 s, and immediately returned to ice for 2 minutes. 250 µl of LB broth (without antibiotic) was added and cells were incubated at 37 °C, 200 rpm for 1 hour. Subsequently, 200 µl of cells were plated onto appropriate antibiotic-containing LB plates and grown at 37 °C overnight. Transformants were screened for uptake of the vector via PCR and restriction digest.

2.2.12 – Sequence verification of DNA vectors and PCR products

All sequence verification of vectors and PCR products from generated mutants was done through Eurofins Genomics (TubeSeq Service). Analysis of sequencing data was done using the Clone Manager Professional 9 software (Sci-Ed).

2.3 – Mutagenesis of *B. cenocepacia*

2.3.1 – Triparental mating of vectors into *B. cenocepacia*

Conjugation of relevant vectors into *B. cenocepacia* was performed using triparental mating through use of the pRK2013 helper vector. Donor *E. coli* strains (containing the plasmid of interest), helper *E. coli* containing pRK2013 and recipient *B. cenocepacia* were grown overnight in 5 ml SOB broth, harvested and resuspended in 5 ml SOB broth. Strains were mixed at a recipient:helper:donor ratio of 5:1:1 and 150 µl was plated without spreading onto a SOB plate (without antibiotics) and grown overnight at 37 °C.

Pools of growth were then resuspended in 2 ml PBS and plated on SOB agar plates containing appropriate antibiotics. These were a combination of either gentamicin or polymyxin B (to kill the donor and helper *E. coli*, both at a concentration of 25 µg/ml) and the relevant antibiotic for the vector of interest's resistance marker (to select for *B. cenocepacia* that had successfully taken up the vector). Plates were grown for between 24-48 hours at 37 °C. Resultant colonies were screened via PCR for a) confirmation that the colony was *B. cenocepacia* and b) successful conjugation of the vector of interest.

2.3.2 – Generation of in-frame deletion mutants of *B. cenocepacia*

Relevant deletion mutants of *B. cenocepacia* were generated using a system based on the homing endonuclease I-SceI [440]. This involved the cloning of the immediate upstream and downstream regions (approximately 700 base pairs) of the target gene(s) into the pGPI-SceI donor suicide vector, which contained a recognition site for I-SceI. The pGPI-SceI vector was conjugated into *B. cenocepacia* via triparental mating (section 2.3.1) and integrated into the genome through homologous recombination. This first crossover was subsequently PCR verified.

A second triparental mating conjugated the pDAI-SceI vector, which expressed the I-SceI endonuclease, into the first crossover. I-SceI would then cleave the

recognition site of pGPI-SceI, triggering a second recombination event in the genome, resulting in either a restored wildtype or an unmarked deletion. Second crossovers were then PCR and sequence verified through amplification of the region upstream and downstream of the sites of homologous recombination. Figure 2.1 summarises the process of mutagenesis in *B. cenocepacia*.

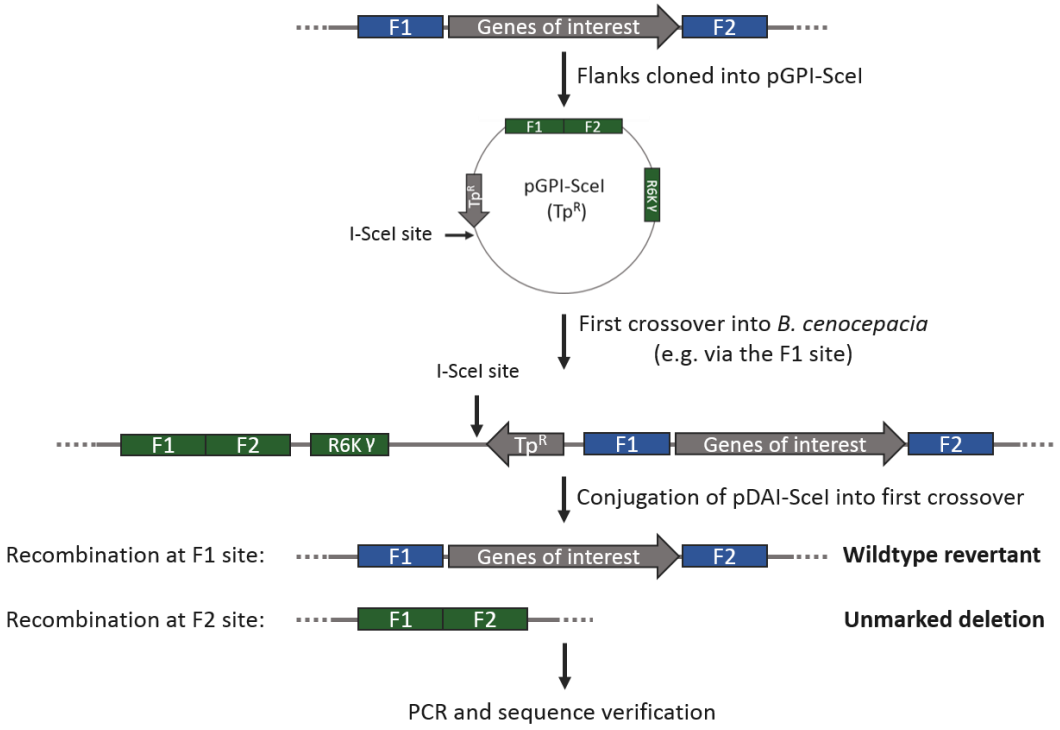

Figure 2.1: Generation of unmarked in-frame deletion mutants in *B. cenocepacia*. Upstream (F1) and downstream (F2) flanks of genes of interest are cloned into pGPI-SceI, which harbours a recognition site for the homing endonuclease I-SceI. The R6K γ origin of replication ensures that pGPI-SceI cannot be replicated within *B. cenocepacia*, and as such successful first crossovers can be selected for by plating onto trimethoprim. Conjugation of pDAI-SceI into first crossovers leads to expression of I-SceI, which will cut at the recognition site (5'-TAGGGATAACAGGGTAAT-3') leading to a double-stranded break in the chromosome. This triggers repair machinery which results in recombination at one of two sites, resulting in either a wildtype revertant or an unmarked deletion mutant. Second crossovers can then be PCR and sequence verified. Figure adapted from Flannagan *et al* (2008).

Following verification of the in-frame deletion mutants, pDAI-SceI was cured out of *B. cenocepacia* mutants. Mutants containing pDAI-SceI were grown overnight in M9 minimal media at 37 °C, with subsequent serial dilutions plated onto LB agar and grown overnight at 37 °C. Individual colonies were then screened for resistance to tetracycline to identify cured mutants, which were PCR verified for loss of pDAI-SceI.

2.3.3 – Complementation of *B. cenocepacia* deletion mutants

In the interest of attempting to complement deletion mutants with expression levels of genes similar to those found in wildtype bacteria, a modified pDA17 vector that lacked the native *dhfr* promoter was generated [429]. This allowed for the cloning of gene operons that contained the predicted upstream promoter region of those operons, leading to expression that was dictated by regulation of the promoter region, rather than an expression that was constitutively active. Following cloning of relevant inserts, pDA17 was conjugated into the deletion mutants via triparental mating (section 2.3.1).

2.4 – Purification of SK and RR proteins

2.4.1 – Construction of SK and RR expression vectors

For the purpose of ascertaining the potential for non-cognate phosphotransfer, RR genes were amplified in full and cloned into the pQE80 expression vector, however for SKs it was necessary only to purify the intracellular portion of the protein, excluding the extracellular and intramembrane portions. In order to predict the exact point in the gene at which the intracellular region began, the transmembrane region predictor TMpred was used [444]. Upon prediction of the location of the intracellular region, SK genes were amplified and cloned into the pQE80::NusA expression vector. RR genes were amplified and cloned into pQE80 (lacking the N-terminal NusA tag). Due to the similarity in size between RRs and the intracellular domains of SKs, the N-terminal NusA tag (54.9 kDa)

allowed for size discrimination on the SDS-PAGE during the phosphotransfer assay (section 2.5).

In the interest of verifying whether non-cognate phosphotransfer still occurred in the presence of the cognate RR, RR genes were also cloned into pQE60::eGFP and pQE80::eGFP vectors, to allow the tagging of eGFP onto the C-terminus and N-terminus respectively. This increased the size of the RR by approximately 28 kDa, allowing for an untagged RR, an eGFP-tagged RR and a NusA-tagged SK to be visualised on the same SDS-PAGE.

2.4.2 – Purification of SK and RR proteins

Following successful construction of relevant expression vectors, overnight culture of relevant *E. coli* strains underwent plasmid extraction and vectors were transformed into calcium-competent M15pREP4 *E. coli* cells and grown overnight in LB supplemented with 2 % glucose (v/v) to prevent leaky protein expression. Individual colonies were then grown in 25 ml of LB with 2 % glucose (v/v) overnight, and added the following morning to 500 ml of 2YT media containing ampicillin and kanamycin.

Cultures were grown at 37 °C and 200 rpm to an OD_{600} of 0.4-0.6, at which IPTG was added to a final concentration of 100 µM to induce protein expression. Cultures were then grown overnight at 18 °C at 200 rpm. Following overnight growth, cultures were spun at 8000 g for 20 minutes at 4 °C, with *E. coli* pellets resuspended in 30 ml of lysis buffer (10 % glycerol, 50 mM Tris (pH 8), 150 mM NaCl, 10 mM Imidazole, 1 mM DTT) and stored at -20 °C until further purification.

For the final stages of purification, *E. coli* cell pellets were thawed and sonicated on ice for 6 pulses of 20 seconds using a Vibra-Cell VCX 130 (Sonics). Lysates were spun at 19000 g for 30 minutes, with the resulting supernatant syringe filtered through a 0.4 µm filter. Around 1.5 ml of Ni-NTA Agarose slurry (Qiagen) was added to a column and left until separation of the ethanol and nickel solution. The ethanol was allowed to drip through, and following this 2 ml of lysis buffer was added to equilibrate the column. Subsequently supernatant was added to the column and allowed to drip through fully. This allowed the 6 x His tag-

containing SKs and RRs to bind to the column. The column was then washed with lysis buffer for 90 minutes, when finally around 5 ml of elution buffer (10 % glycerol, 50 mM Tris (pH 8), 150 mM NaCl, 200 mM Imidazole, 1 mM DTT) was added. Protein was collected in a 1.5 ml microcentrifuge tube as it passed through the column, with the majority aliquoted into 100 µl volumes and stored at -20 °C until use. The remainder of the protein was kept for analysis through SDS-polyacrylamide gel electrophoresis (SDS-PAGE) and the Bradford assay.

2.4.3 – Analysis of proteins through SDS-PAGE

Protein samples were diluted in NuPAGE LDS Sample buffer (Thermo Fisher Scientific) and heated for 5 minutes at 96 °C. NuPAGE 4-12 % Bis-Tris gels were set up in an XCell Surelock Mini-Cell tank filled with NuPAGE MES SDS Running Buffer. 20 µl of diluted samples were added to wells, with 5 µl of protein ladder added to each end of the gel. Gels were run for 30 minutes at 180 V, and subsequently washed three times in dH_2O for 5 minutes. Approximately 20 ml of SimplyBlue SafeStain (Invitrogen) was poured onto the gel and left to shake gently for 1 hour. Gels were then destained in dH_2O for at least 1 hour prior to viewing on an Odyssey CLx Imager (LI-COR)

2.4.4 – Analysis of protein concentration using the Bradford assay

The Bradford assay relies on the colour change associated with protein binding to Coomassie Brilliant Blue G-250, which can be quantified through spectrophotometry. 50 µl of various dilutions of protein sample were added to 2.5 ml of Protein Assay Dye Reagent (BIO-RAD) which had been diluted 5 x in ddH_2O. The solution was then vortexed and left for 5 minutes to allow colour change to develop, and the absorbance subsequently read at OD_{595}. The absorbance reading could be used to calculate protein concentration by comparison of optical densities to a set of standards of known concentrations of Bovine Serum Albumin.

2.5 – Phosphotransfer assay

2.5.1 – Phosphotransfer assay without pre-phosphorylated SKs

Phosphorylation assays have been widely utilised to characterise the nature of protein phosphorylation, and has been a particularly useful method of investigating phosphotransfer between proteins. The phosphotransfer assays utilised in this work were adapted based on previously described methodologies [445,446]. All phosphotransfer reactions were carried out in TGMNKD buffer (10 % glycerol, 150 mM NaCl, 50 mM Tris (pH 8), 1 mM DTT, 5 mM $MgCl_2$, 50 mM KCl). Assays were performed within 28 days of the activity date of the [γ-^{32}P] ATP (3.7 GBq/mmol, PerkinElmer), which corresponded to two half-lives of the compound. Proteins were added to 1.5 ml microcentrifuge tubes containing TGMNKD buffer at concentrations of 20 µM for SKs and 10 µM for RRs. The assay was performed at 20 °C in a total volume of 100 µl and started through addition of 2 mM [γ-^{32}P] ATP (3.7 GBq/mmol, PerkinElmer). At appropriate timepoints, 10 µl of reaction mixture was removed and quenched in 20 µl of SDS loading dye (37.5 % glycerol, 7.5 % SDS, 90 mM EDTA, 37.5 mM Tris (pH 6.8), 3 % β-mercaptoethanol) and kept on ice. Samples were loaded on 12 % polyacrylamide gels (previously prepared using the PROTEAN Multi-Casting Chamber, BIO-RAD) and run at 300 W for 1 hour at -5 °C using an anti-freeze system. Gels were then exposed to pre-bleached Phospho sheets for 1 hour and subsequently imaged with a Fujifilm FLA-7000 viewer. Any quantification of protein gels was performed using the Multi Gauge software package (Fujifilm)

2.5.2 – Phosphotransfer assay with pre-phosphorylated SKs

Depending on the particular requirements of the assay, pre-phosphorylation of the SKs occurred either immediately before the commencement of the phosphotransfer assay, or between the initial elution from the nickel column and a subsequent elution from a second nickel column. In the former case, prior to commencement of the phosphotransfer assay, SKs were incubated with [γ-^{32}P] ATP (3.7 GBq/mmol, PerkinElmer) in TGMNKD buffer for 1 hour to allow for SK

autophosphorylation. Pre-phosphorylated SKs were then used immediately in the phosphotransfer assay through addition of RRs, thus commencing the assay. The remainder of the assay was performed as per section 2.5.1.

For SKs that were to be purified away from the radiolabelled ATP, following elution from the nickel column during the protein purification process, SKs were incubated with [γ-^{32}P] ATP (3.7 GBq/mmol, PerkinElmer) in TGMNKD buffer for 1 hour to allow for SK autophosphorylation. Pre-phosphorylated SKs were then washed through and eluted off a second nickel column to separate SKs from remaining radiolabelled ATP, and subsequently stored at -20 °C. To assess concentration of pre-phosphorylated SKs, pre-bleached Phospho sheets were exposed to card containing a dilution series of each pre-phosphorylated SK for 1 hour, and subsequently imaged with a Fujifilm FLA-7000 viewer. The concentration of pre-phosphorylated SKs was then quantified against a set of standards of known radioactivity using the Multi Gauge software package (Fujifilm).

2.6 – Heavy metal sensitivity assays

For all heavy metal sensitivity assays, overnight cultures of *B. cenocepacia* strains were pelleted and resuspended in PBS to an OD_{600} 1 ± 0.05. All metals were prepared in sterile ddH_2O.

For heavy metal-supplemented agar plates, standardised strains were serially diluted in PBS down to 10^{-5}, spotted on LB plates supplemented with differing concentrations of heavy metals and grown overnight at 37 °C.

For growth curves performed in 10 ml volumes, three falcons containing LB broth and relevant heavy metal concentrations were prepared for each concentration of metal per strain. 50 µl of standardised strains were added to each falcon to a total volume of 10 ml and grown at 37 °C at 200 rpm. 1 ml was taken at relevant time points and the OD_{600} measured. For any OD_{600} > 1, culture was diluted prior to measurement.

For growth curves in 96-well plates, 190 µl of LB broth containing differing concentrations of heavy metals was added to each well of a 96-well plate. 10 µl

of standardised culture diluted to 10^{-1} was added to relevant wells. All strains were grown in each condition in triplicate. Growth curves were performed over 48 hours at 37 °C in a NanoQuant Infinite M200 PRO plate reader (Tecan). Plates were constantly shaking at 200 rpm except for approximately 5 minutes every 30 minutes to allow the plate reader to measure the OD_{600} of the wells.

For checkerboard assays [447], 190 µl of LB broth containing differing concentrations of heavy metals and/or antibiotics were added to each well of a 96-well plate. 10 µl of standardised culture diluted to 10^{-1} was added to all wells of a plate, with each strain being grown in a separate plate. An additional plate was generated that would have 10 µl of PBS added rather than bacteria, which served to generate blank values for each well. Plates were then sealed with parafilm and grown for 21 hours at 37 °C at 125 rpm. The OD_{600} of each plate was then measured on a NanoQuant Infinite M200 PRO plate reader (Tecan).

2.7 – Investigation of promoter induction via *gfp* transcriptional fusion

Promoters of interest were amplified by PCR with BamHI cut sites located on 5' and 3' ends and subsequently cloned upstream of a *gfp* gene in the pGA-G1 vector (kindly provided by the Leo Eberl group, University of Zurich, Switzerland). pGA-G1 vectors were conjugated into *B. cenocepacia* gentamicin-sensitive mutants and PCR verified for successful uptake of pGA-G1.

For all fluorescence assays, a 96-well black polystyrene plate (Corning) was used to minimise crosstalk between wells. Overnight LB cultures of strains were pelleted and resuspended in PBS to an OD_{600} 1 ± 0.05. 10 µl of standardised culture diluted to 10^{-1} was added to wells containing 190 µl of unsupplemented LB or LB supplemented with relevant metals (either 1 mM $CuCl_2$, 1 mM $ZnCl_2$, 0.25 mM $CdCl_2$, 0.25 mM $CoCl_2$ or 5 µM $AgNO_3$) and 20 µg/ml gentamicin. Plates were sealed with parafilm and incubated for 24 hours at 37 °C shaking at 125 rpm. All strains were grown in each condition in triplicate.

Following 24 hour growth, the OD_{600} and fluorescence intensity (excitation – 485 nm, emission – 528 nm) of each plate was read using a CLARIOstar *Plus* plate

reader (BMG Labtech). Fluorescence measurements were corrected for growth by division of raw fluorescence values by the OD_{600} reading for each well.

2.8 – Biofilm assay

Assessment of biofilm formation ability was based on the MBEC biofilm system, adapted for use with *B. cenocepacia* [448–451]. Strains were grown on LB plates containing appropriate antibiotics overnight at 37 °C. Strains were then restreaked on TSA plates without antibiotics and grown overnight at 37 °C. Growth was resuspended in PBS using a sterile swab to an OD_{600} 1 ± 0.05 and diluted 1:200 in TSB broth. 150 µl of diluted strains were added to the wells of a 96-well plate (8 wells per strain/condition), and an MBEC Biofilm Inoculator 96 peg-lid was added to the plate, sealed with parafilm and incubated for 24 hours at 37 °C shaking at 125 rpm. Following this, the peg-lid was added to a fresh 96-well plate containing 150 µl of TSB broth in each well, sealed with parafilm and incubated for another 24 hours under similar conditions, resulting in a total incubation time of 48 hours.

Following the second 24 hour incubation, the OD_{600} of the 96 well plate was measured to quantify growth, and the peg-lid added to a 96-well plate containing PBS for 2 minutes. The peg-lid was then left to dry at room temperature for 10 minutes, before being baked at 65 °C for 20 minutes. The peg-lid was then added to a plate containing 0.1 % crystal violet for 30 minutes on a rocker to allow staining of the biofilm on the pegs. The peg-lid was then washed in plates containing PBS three times for five minutes, before being dried at room temperature for 10 minutes. The peg-lid was subsequently added to a 96-well plate containing 95 % ethanol for 20 minutes on a rocker to remove the crystal violet from the pegs. Finally, the OD_{570} of the plate was measured. Any strains that had an OD_{570} of above 1 were diluted in 95 % ethanol and remeasured to ensure accuracy of measurement of biofilm formation.

2.9 – *Galleria mellonella* infection assay

The larvae of the greater wax moth, *G. mellonella*, were used as a model for assessing virulence of different mutants of *B. cenocepacia* [160,452,453]. All larvae were sourced from UK Waxworms Ltd (Sheffield, UK). Larvae that were within the 200-300 mg weight range were selected for use in the assay. 10 larvae were used per strain, and PBS and no-stab controls were included in every assay.

Overnight LB cultures of strains were pelleted and resuspended in 5 ml of PBS, before being pelleted again and resuspended to an OD_{600} 1 ± 0.05 in PBS. Strains were serially diluted down to 10^{-5}, followed by a further 1:4 dilution, i.e. to an approximate concentration of 2500 CFU/ml, leading to a dosage of 25 CFU/larvae.

A PB600 Gastight Repeating Dispenser (Hamilton) was prepared by rinsing in 100 % ethanol, followed by 70 % ethanol and finally PBS. This sequence of rinsing was carried out between different strains being injected. 2 x 5 µl injections were given into the upper left pro-leg of the larvae. Larvae were then incubated at 37 °C for 120 hours, with larvae being checked every 24 hours to assess the numbers of alive and dead larvae. Larvae were considered to be ‘alive’ if there was any sign of movement following a tactile stimulus with a micropipette tip.

2.10 – Establishing antibiotic MICs of *B. cenocepacia* mutants

190 µl of LB broth containing increasing concentration of antibiotics were added to wells of a 96-well plate. 10 µl of standardised culture diluted to 10^{-1} was added to relevant wells of the plate, which was subsequently sealed with parafilm and grown for 21 hours at 37 °C at 125 rpm. The OD_{600} of each plate was then measured on a NanoQuant Infinite M200 PRO plate reader (Tecan).

2.11 – Tissue culture and intracellular survival assay

2.11.1 – Culture of J774A.1 macrophages

The murine macrophage cell line J774A.1 was used for all gentamicin-protection assays. Cells were cultivated in high glucose Dulbecco's modified eagle medium (DMEM) supplemented with 10 % foetal bovine serum (FBS). Cells were grown in a T75 flask with 25 ml of DMEM media at 37 °C with 5 % CO_2. Cells were split at 1:5 ratio every 2-3 days, by washing cells in PBS and scraping adherent cells into fresh DMEM. Fresh cells were regularly resuscitated from storage in liquid nitrogen and 5 % DMSO to ensure that only cells at a passage number of between 5-15 were used for gentamicin-protection assays.

2.11.2 – Gentamicin protection assay

J774 macrophages were seeded in two 24-well plate at a density of 2.5 x 10^5 cells/well, with three wells per plate prepared for each strain (plus a negative control). These two plates would be used for a 2 hour and 24 hour post-infection timepoint during the assay [463]. The following day overnight culture of gentamicin-sensitive *B. cenocepacia* strains were pelleted, resuspended in PBS and standardised to OD_{590} 1 ± 0.05. Standardised strains were then diluted in DMEM supplemented with 10 % FBS to a multiplicity of infection (MOI) of 4, i.e. a total of 1 x 10^6 cells/ml infecting 2.5 x 10^5 macrophages.

All media used in the assay was pre-warmed at 37 °C, while all incubations were done at 37 °C with 5 % CO_2 buffering. Macrophages were washed twice in 1 ml PBS, prior to the addition of 1 ml of the relevant diluted bacterial strains (or fresh DMEM for the negative control). The inoculating dose was calculated by plating out 20 µl spots of serial dilutions of each diluted strain and counting the number of CFUs the following day. Bacteria were allowed to internalise into the macrophages through incubation for 2 hours. Macrophages were then washed once with 1 ml PBS, prior to the addition of 1 ml of DMEM containing 50 µg/ml gentamicin, in order to kill extracellular bacteria. Macrophages were then incubated for 2 hours.

Both plates were then washed three times in 1 ml PBS. Following this, the plate designated for the 24 hour timepoint had 1 ml DMEM containing 10 µg/ml gentamicin added to each well and was incubated for another 22 hours, while the macrophages of the plate designated for the 2 hour timepoint were lysed through addition and mixing of 1 ml of 0.1 % (v/v) Triton X-100 to the wells. 20 µl spots of serially diluted lysates were plated out, grown overnight at 37 °C and CFUs counted the following day. The plate designated for the 24 hour timepoint was similarly processed following the 22 hour incubation.

2.12 – RNA-seq analysis of the *B. cenocepacia* copper response

2.12.1 – Extraction of RNA from *B. cenocepacia*

Overnight LB cultures of WT and ΔBCAM0442/3 strains of *B. cenocepacia* were standardised to OD_{600} 1 ± 0.05, with 50 µl being added to a 50 ml falcon tube containing either 10 ml of LB or LB supplemented with 1 mM $CuCl_2$. 1 mM had been determined to be a sufficient sub-inhibitory concentration of $CuCl_2$ via a growth curve done under similar conditions. Each strain was added to each condition in triplicate, resulting in 12 total RNA extractions.

After 8 hours of growth, to allow cultures to reach mid log phase, 2 ml of each culture was pelleted and resuspended in 10 ml of RNA*later* stabilisation solution (Thermo Fisher Scientific) and stored at 4 °C overnight, followed by longer-term storage at -20 °C.

Extraction of total RNA was performed using the RiboPure RNA Purification Kit (Thermo Fisher Scientific) following manufacturer's instructions. RNaseZap RNase Decontamination Solution (Thermo Fisher Scientific) was applied to all work surfaces and equipment to ensure minimal degradation of total RNA.

Quality of RNA was assessed through use of a 4200 TapeStation System (Agilent), while RNA concentration was assessed with a Qubit™ 3.0 Fluorometer (Invitrogen). Samples that had an RNA integrity rating of 8 or greater were sent for RNA-seq analysis.

2.12.2 – mRNA enrichment and library preparation

Depletion of rRNA, mRNA library preparation and mapping of reads to the *B. cenocepacia* J2315 genome were performed by the Exeter Sequencing Service. ERCC spike-in control mixes (Thermo) were added to each sample according to manufacturer's instructions. rRNA was depleted from total RNA samples using the Ribo-Zero rRNA Removal Kit (Illumina), while libraries were prepared with the Tru-Seq RNA protocol (Illumina). Sequencing was performed on an Illumina HiSeq2500 platform yielding 72 million 125 bp paired end reads. Reads were checked for quality using FastQC and for contamination using Fastq_screen. Sequencing adapters and low quality bases (< Q22) were removed using cutadapt and reads shorter than 75 bp were discarded [454].

Salmon was used to quantify transcript expression against the *B. cenocepacia* J2315 genome and annotation [455]. DESeq2 was used to calculate likelihoods of differential expression between conditions and to visualise results after log normalisation [456]. An adjusted p value of $p < 0.05$ and a fold change of > 2 was used to define significantly differentially expressed genes.

2.13 – Statistical analyses

All statistical analyses barring the RNA-seq analysis were performed in GraphPad Prism 8.0. Details of statistical analyses performed and exact number of replicates can be found in relevant figure legends. All error bars show standard error of the mean (SEM). Statistical significance was taken to be $p < 0.05$.

Chapter 3: Investigation of non-cognate phosphotransfer between TCSs

3.1 – Introduction

As described in Chapter 1, there are many ways in which TCSs can interact with one another, such as through non-cognate phosphotransfer, kinase-kinase interactions, regulation of one TCS by another through intermediate proteins such as histidine phosphotransferases, or direct regulation of the regulon of one TCS by another under certain conditions. Theoretically a network of TCSs can take many different forms, some relying solely on non-cognate interactions (interactions between SKs and RRs that don't reside in the same operon), some only crossing paths at the level of regulation of DNA expression, with others being a mix of many different modalities of interaction.

The four putative heavy metal-sensing TCSs in *B. cenocepacia* share great similarity in the specificity residues of their RRs (Fig 1.6). While it is possible that these TCSs can regulate each other's regulons, or interact at the kinase-kinase level, this RR specificity residue similarity points strongly towards a model of direct non-cognate phosphotransfer being kinetically possible between the SKs and RRs of these TCSs.

The methodology employed in this chapter revolves around the phosphotransfer assay, essentially the use of radiolabelled [γ-^{32}P] ATP to assess phosphorylation of purified SKs and RRs followed by resolving of SKs and RRs via SDS-PAGE and imaging of the radiolabelled proteins. This allows the determination of *in vitro* activity and phosphotransfer capabilities of different SK-RR pairings, thus giving an insight into whether non-cognate phosphotransfer is kinetically possible between different SKs and RRs.

What the phosphotransfer assay cannot provide is an indication to how physiologically relevant any observed non-cognate phosphotransfer is. One can quantify the levels of non-cognate phosphotransfer within any SK-RR pairing, but this does not approach the dynamism of the cellular environment, which may contain tens or even hundreds of different SKs and RRs at any given time. Because of this, in addition to assays looking for evidence of non-cognate phosphotransfer between the four SKs and four RRs, assays containing a SK, its cognate RR and a non-cognate RR were performed with the aim of establishing to what extent non-cognate phosphotransfer is reduced in the presence of the

cognate partner. While this too has limitations, it does provide insight into which non-cognate interactions may be the most kinetically favourable even in the presence of the cognate partner, and as such may perhaps be of particular focus for further study.

To facilitate these phosphotransfer assays, SKs and RRs were purified with a 6 x His tag to allow for nickel affinity column purification. RRs were also purified in a His tag + eGFP-tagged form, to allow for size discrimination by SDS-PAGE against the His tag-purified form (herein referred to as 'untagged'). As phosphotransfer is not dictated by the extracellular or transmembrane portions of SKs, only the intracellular portions were purified. As the SK intracellular portions were of similar size to untagged RRs, these SKs were then tagged with an N-terminal NusA-tag (54.9 kDa), to ensure proteins were of different enough weights to observe on SDS-PAGE.

Ultimately, this chapter aims to prove whether non-cognate phosphotransfer is possible between these four TCSs. Based on the specificity residue similarity between the RRs (Fig 1.6), one may hypothesise that at least one SK of the four may be able to phosphorylate multiple RRs, forming a MKN.

3.2 – Results

3.2.1 – Prediction of SK transmembrane portions

As only the intracellular portions of SKs were required for phosphotransfer assay, transmembrane portions were predicted using TMpred (Fig 3.1) [444]. The autophosphorylation and phosphotransfer domains of SKs should follow the final intramembrane portion, hence the region immediately following the final transmembrane portion was amplified.

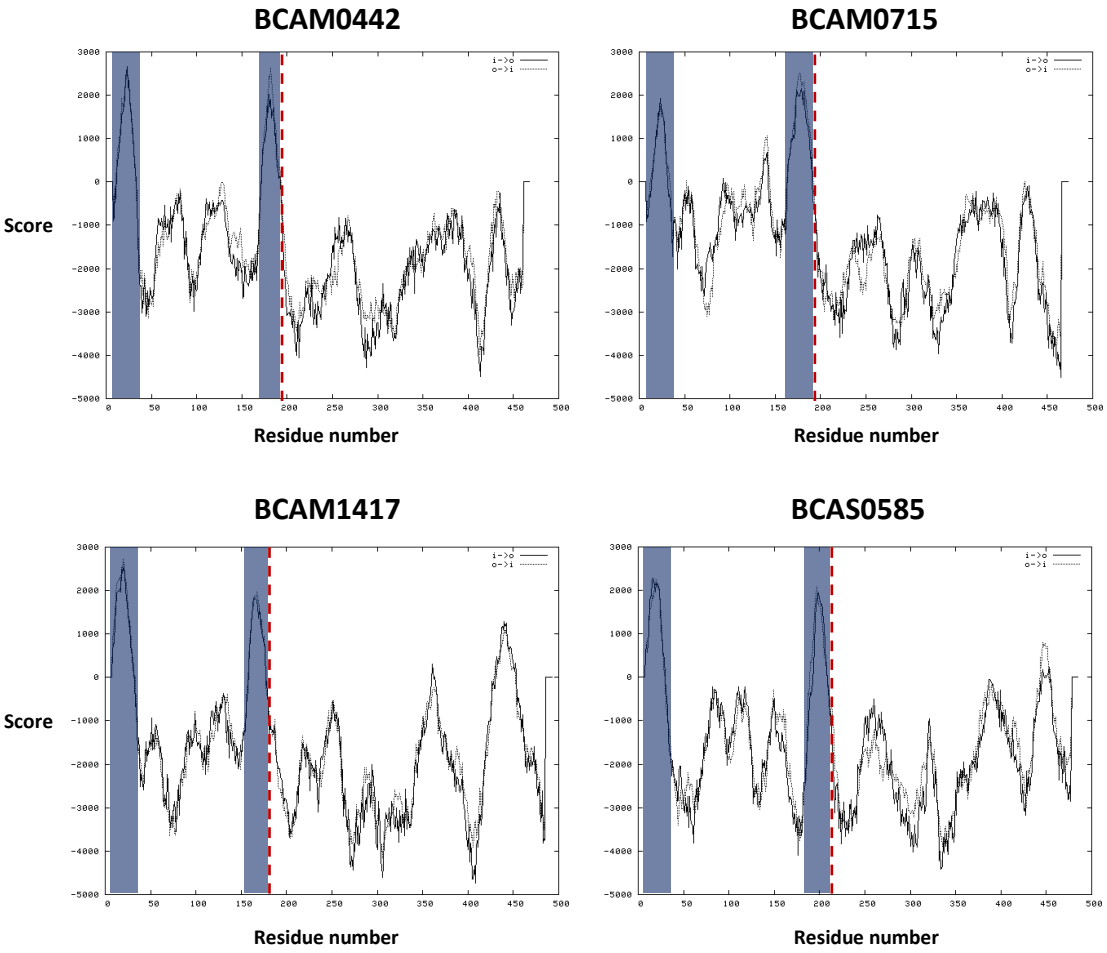

Figure 3.1: Prediction of transmembrane portions using TMpred. Each SK was inputted into the TMpred prediction tool, which provided the above four graphs as its output. Peaks highlighted in blue indicate likely intramembrane regions, while the region to the right of the red dashed line indicates the region of the SK which was amplified. For each SK, the cloned region begins at the following amino acid: BCAM0442 – S193, BCAM0714 – S192, BCAM1417 – A179, BCAS0585 – R208.

3.2.2 – Construction of SK and RR expression vectors

Primers were designed to amplify the intracellular portions of SKs and the entirety of RRs, to clone into pQE80::NusA and pQE80 respectively (Plasmid maps can be found in Figure 3.2). PCR amplification was done with Phusion High-Fidelity DNA Polymerase. SKs were cloned into the pQE80::NusA expression vector, which contained an N-terminal 55 kDa NusA tag and 6 x His tag, serving to

increase the mass of SKs to allow for size discrimination through SDS-PAGE against untagged RRs and for purification purposes through a nickel column respectively. RRs were also N-terminally tagged with a 6 x His tag through expression in the pQE80 vector (without a NusA tag).

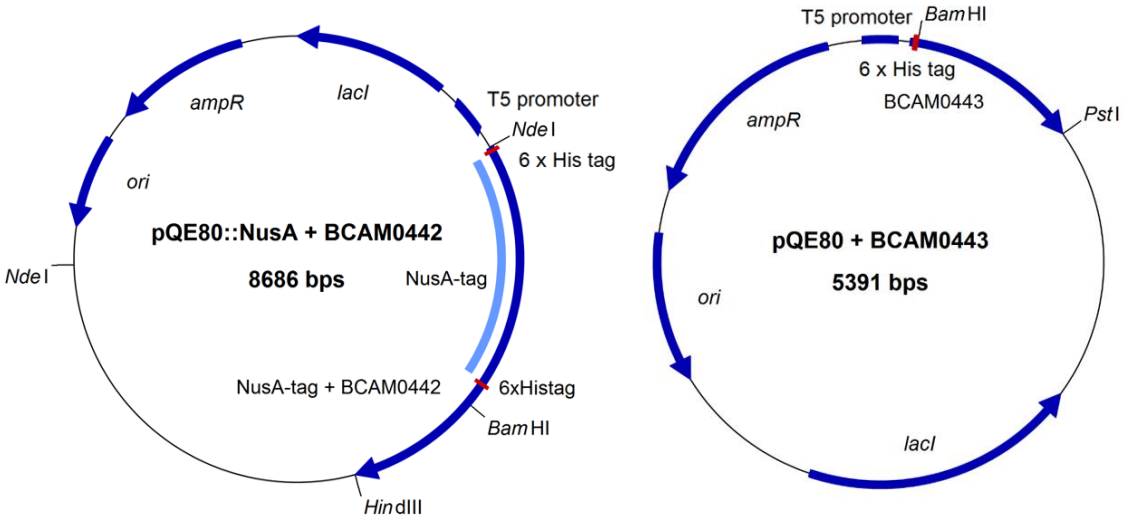

Figure 3.2: Example plasmid maps for expression of BCAM0442 and BCAM0443. Gene sequences for intracellular regions of SKs were cloned into pQE80::NusA, while RR sequences were cloned into pQE80. Relevant cloning sites for cloning of the SK BCAM0442 and the RR BCAM0443 and 6 x His tags are shown. Plasmid maps made on Clone Manager Professional 9 (Sci-Ed).

Following ligation of gene inserts into relevant plasmids, plasmids were transformed into chemically competent XL1-Blue *E. coli* cells, with successful transformants verified through restriction digest and sequencing of gene inserts.

3.2.3 – Expression of SKs and RRs

Following sequence verification of gene inserts in expression vectors, SKs and RRs were expressed through growth of *E. coli* in 2YT media and induction with IPTG. Following induction *E. coli* culture was lysed and passed through a nickel column, allowing for binding and purification of the 6 x His tag-containing proteins. SDS-PAGE of successfully purified proteins can be found in Figure 3.3. The Bradford assay was performed to assess protein concentration.

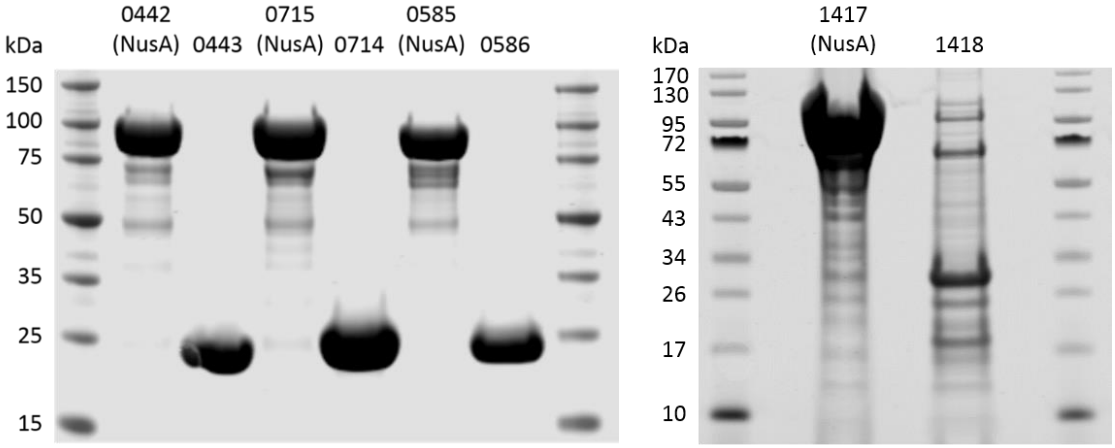

Figure 3.3: Example of SDS-PAGE of purified NusA-tagged SKs and untagged RRs. From a 1.5 ml eluate, 1 µl of protein sample was loaded in the left-hand gel, while 10 µl was loaded in the right-hand gel. Expected protein sizes (kDa): BCAM0442 (NusA) – 92.9, BCAM0443 – 26.8, BCAM0715 (NusA) – 93.2, BCAM0714 – 26.8, BCAS0585 (NusA) – 92.4, BCAS0586 – 26.7, BCAM1417 (NusA) – 96.6, BCAM1418 – 27.2.

All NusA-tagged SKs and untagged RRs expressed relatively well aside from BCAM1418, of which comparatively low yields were produced (~ 2 mg compared to averages of > 15 mg for the other untagged RRs for 500 ml culture). Final yields for NusA-tagged kinases were consistently > 10 mg. Additionally, SDS-PAGE of purified BCAM1418 consistently showed possible cleavage products alongside the RR band that were not seen when assessing the purity of the other untagged RRs. It is possible that these bands are other proteins that eluted off

the nickel column alongside BCAM1418, such as chaperone proteins, though they may also be products of cleavage and/or dimerisation of the RR.

3.2.4 – Cognate phosphotransfer between SKs and RRs

Once proteins were purified, the ability of each SK to autophosphorylate and phosphotransfer to its cognate RR was assessed through the phosphotransfer assay (Fig 3.4). All SKs were able to autophosphorylate and undergo phosphotransfer with their cognate RR. Additionally, RRs incubated alone with [γ-^{32}P] ATP displayed no phosphorylation, confirming that the phosphorylation seen in the assay is through phosphotransfer from the cognate SK.

The variations in the strength of the phosphorylated SK and RR bands (herein referred to as SK-P and RR-P respectively) suggest that the kinetics of cognate phosphotransfer differ *in vitro* for these TCSs. The lack of SK-P band for BCAM0442 and BCAM0715 when incubated alongside their cognate RR suggests that their phosphotransfer kinetics are faster than that of BCAM1417 and BCAS0585. The varying lability of the phosphoryl group on the RRs can be inferred through the intensity of the RR-P band; the weaker the band, the more labile the phosphoryl group is presumed to be on that RR. Ultimately, while cognate phosphotransfer kinetics may differ *in vitro* for these TCSs, they all display the necessary activity in the phosphotransfer assay to allow investigation of potential non-cognate phosphotransfer between these systems.

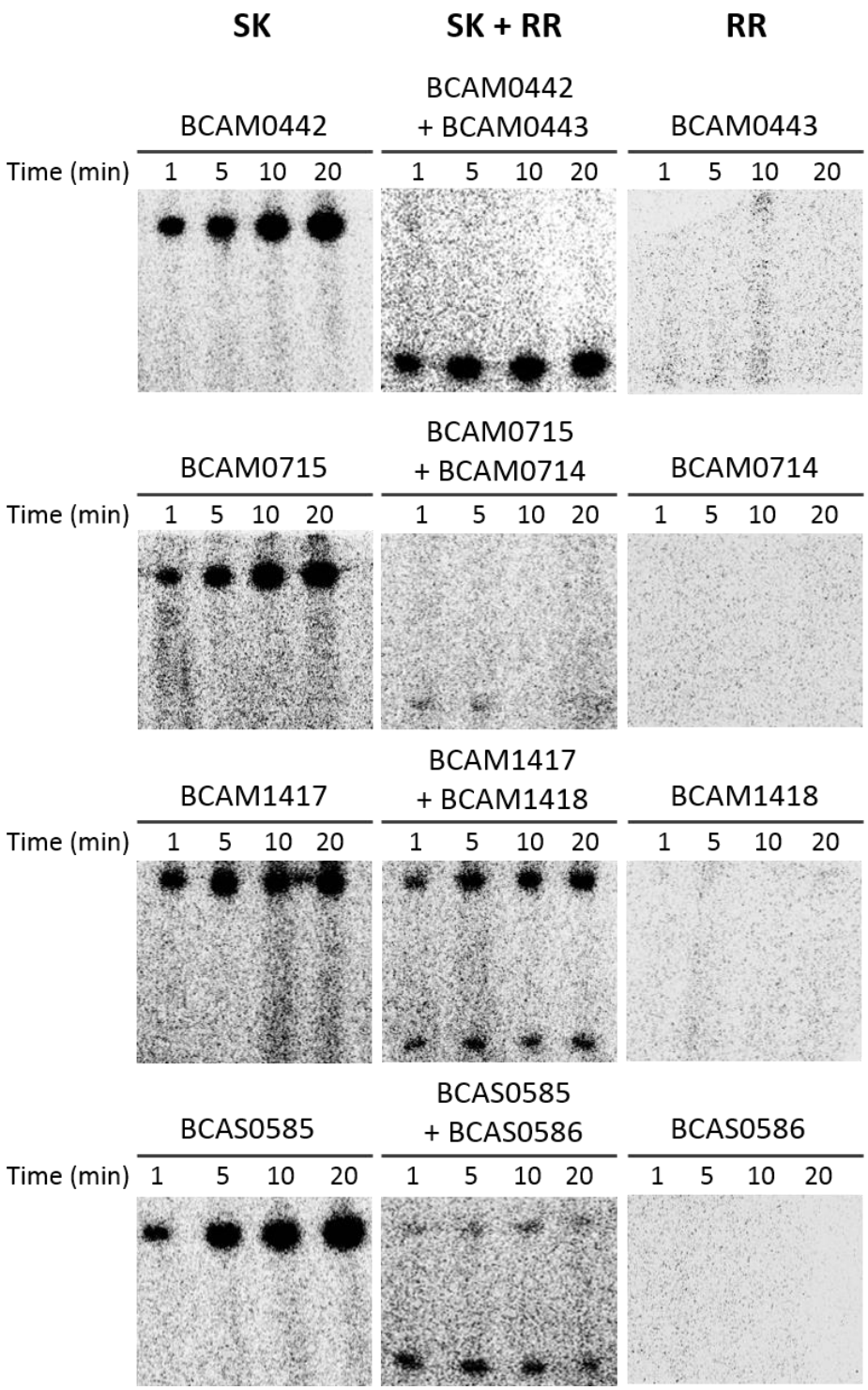

Figure 3.4: Representative gels displaying cognate phosphotransfer from the phosphotransfer assay. Reactions were performed at 20 °C and begun through addition of 2 mM [γ-^{32}P] ATP (3.7 GBq/mmol, PerkinElmer), with timepoints processed at 1, 5, 10 and 20 minutes. For each TCS shown, assays were performed containing the SK alone, the SK with its cognate RR and the RR alone.

3.2.5 – Non-cognate phosphotransfer between SKs and RRs

Following verification that each SK was able to undergo autophosphorylation and phosphotransfer to its cognate RR *in vitro*, the ability of each SK to undergo non-cognate phosphorylation was assessed. In order to assess how quickly non-cognate phosphotransfer can occur *in vitro*, timepoints were taken at earlier stages of the phosphotransfer reaction. The SKs BCAM0442, BCAM0715 and BCAS0585 were all able to phosphotransfer to each other's RRs (Fig 3.5), whereas BCAM1417 and BCAM1418 did not participate in any non-cognate phosphotransfer events (Fig 3.6). Due to continual issues with the purification of BCAM1417, the non-cognate phosphotransfer potential of BCAM1417/8 was assessed at a later date than the other three TCSs. Interestingly, the BCAM1418 RR has both the lowest sequence similarity and the lowest specificity residue similarity to the other RRs of this putative MKN, with 4 of 7 specificity residues being shared, supporting the notion that a threshold of a specificity residue similarity of 5 shared residues may be able to predict non-cognate phosphorylation between TCS proteins (Fig 1.6).

While non-cognate phosphotransfer was possible between the SKs BCAM0442, BCAM0715 and BCAS0585 and the RRs BCAM0443, BCAM0714 and BCAS0586, the reaction kinetics were observably different. For each cognate phosphotransfer interaction, the SK-P band is observably depleted across the timepoints, whereas for non-cognate interactions the SK-P band remains on the gel, getting stronger with each timepoint (Fig 3.5). This may be attributed to the preferential reaction kinetics of the cognate interaction; a depleted SK-P band indicates a faster rate of phosphotransfer reaction than a SK-P band which is increasing over time. Preferential cognate reaction kinetics can also be seen within the RR-P band; cognate interactions tend to confer a stronger RR-P band at earlier timepoints. Interestingly, RR-P bands appear to be considerably stronger for the non-cognate interactions for the BCAM0715 SK compared to the other two SKs, perhaps indicating that out of these SKs, BCAM0715 undergoes non-cognate interactions most readily.

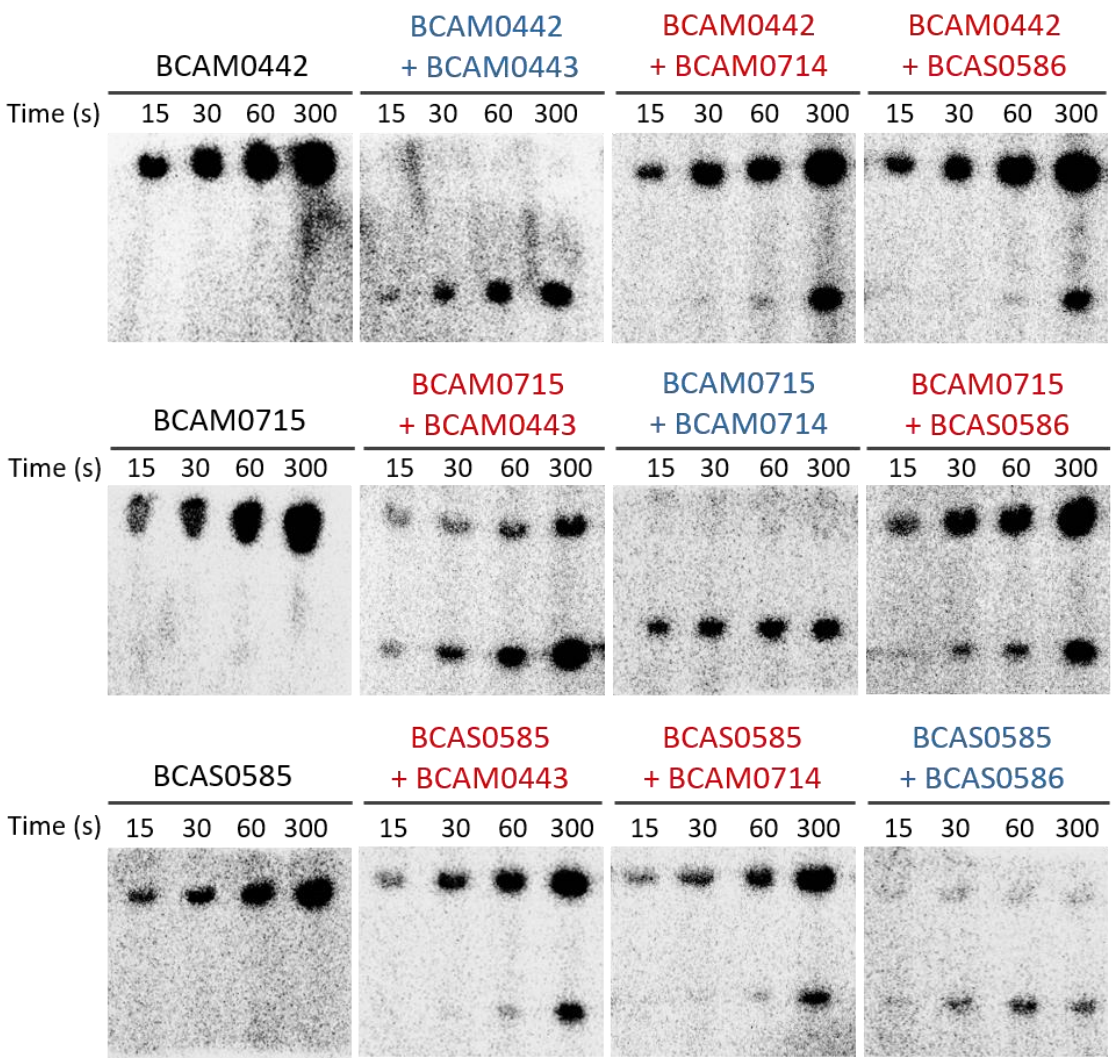

Figure 3.5: Representative gels displaying non-cognate phosphotransfer between the SKs and RRs of BCAM0442/3, BCAM0714/5 and BCAS0585/6. Labels in blue denote cognate interactions, whereas red labels denote non-cognate interactions. Within each panel, the top band represents the NusA-tagged SK-P, while the bottom band represents the untagged RR-P.

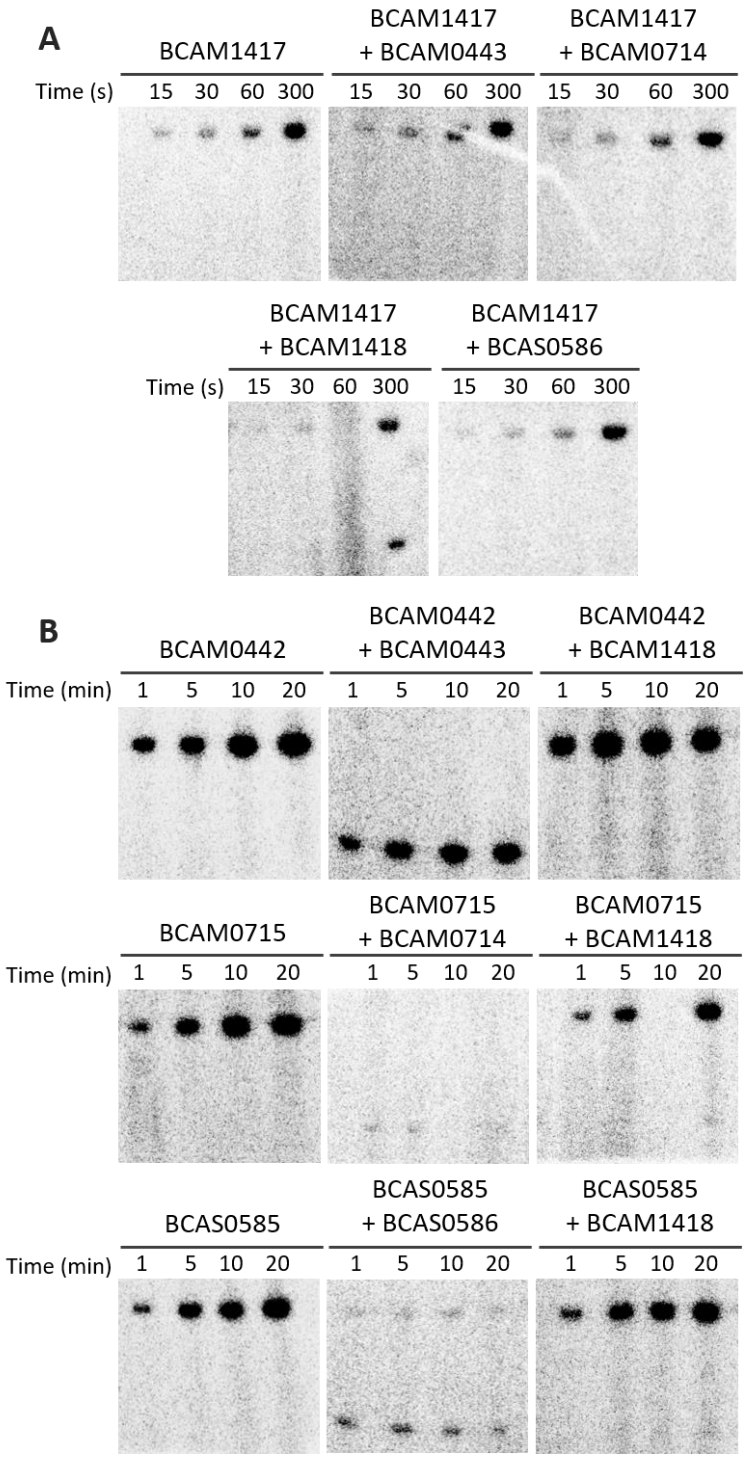

Figure 3.6: Representative gels displaying a lack of non-cognate phosphotransfer between BCAM1417/8 and the other three TCSs. A) While BCAM1417 can phosphotransfer to its cognate RR BCAM1418, no non-cognate phosphotransfer occurs. B) No other SKs can phosphorylate BCAM1418. A stacking gel error led to the 10 min timepoint of BCAM0715 + BCAM1418 not being loaded. Within all panels, the top band represents the NusA-tagged SK, while the bottom band represents the untagged RR.

3.2.6 – Generation of eGFP-tagged RRs

Following from the confirmation that three TCSs are able to undergo non-cognate phosphorylation with one another, the ability of a SK to phosphorylate a non-cognate RR whilst in the presence of its cognate RR was investigated. Due to the size similarity between RRs and the intracellular portions of SKs, it was necessary to purify RRs that contained a tag with a different molecular weight to the 55 kDa NusA tag. eGFP was chosen due to its molecular weight of 27 kDa, which would allow suitable size discrimination by SDS-PAGE. Both N-terminally and C-terminally eGFP-tagged RRs were purified through expression via pQE80 and pQE60 plasmids (plasmid maps can be found in Figure 3.7, and SDS-PAGE of purified C-terminally eGFP-tagged RRs can be found in Figure 3.8).

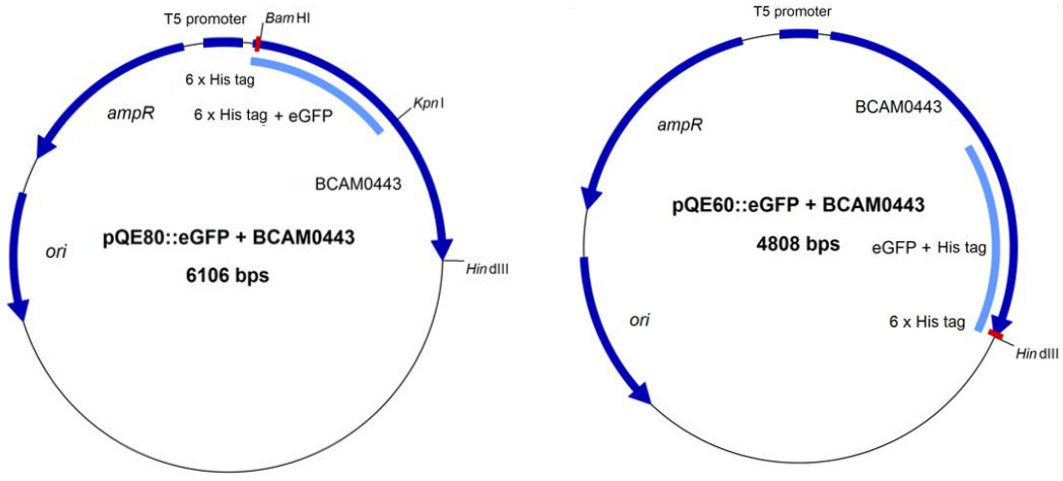

Figure 3.7: Example plasmid maps for expression of both N-terminally and C-terminally eGFP-tagged BCAM0443. eGFP was first cloned into both pQE80 and pQE60 for N-terminal and C-terminal tags respectively. Relevant cloning sites for cloning of BCAM0443 and 6 x His tags are shown. Plasmid maps made on Clone Manager Professional 9 (Sci-Ed).

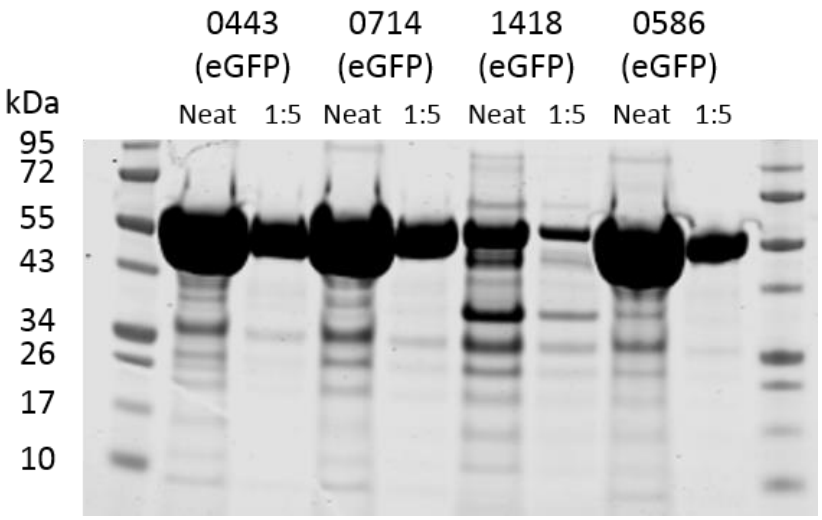

Figure 3.8: SDS-PAGE of purified C-terminally eGFP-tagged RRs. From a 1.5 ml eluate, 10 µl of both neat and a 1:5 dilution of protein was loaded for each eGFP-tagged RR. Expected protein sizes (kDa): BCAM0443 (eGFP) – 53.5, BCAM0714 (eGFP) – 53.6, BCAM1418 (eGFP) – 53.9, BCAS0586 (eGFP) – 53.5.

3.2.7 – eGFP negatively affects phosphotransfer to RRs

Following successful purification of eGFP-tagged RRs, the ability of SKs to undergo phosphotransfer to a non-cognate RR in the presence of their cognate RR was assessed. Unfortunately, the eGFP tag appeared to negatively influence the intensity of the RR-P band, either through reducing the ability of SKs to successfully phosphorylate the eGFP-tagged RR, or by increasing the lability of the phosphoryl group. The clearest example of this can be seen with BCAM0442, in which there is stronger phosphorylation of untagged BCAM0443 compared to eGFP-tagged BCAM0443 (Fig 3.9).

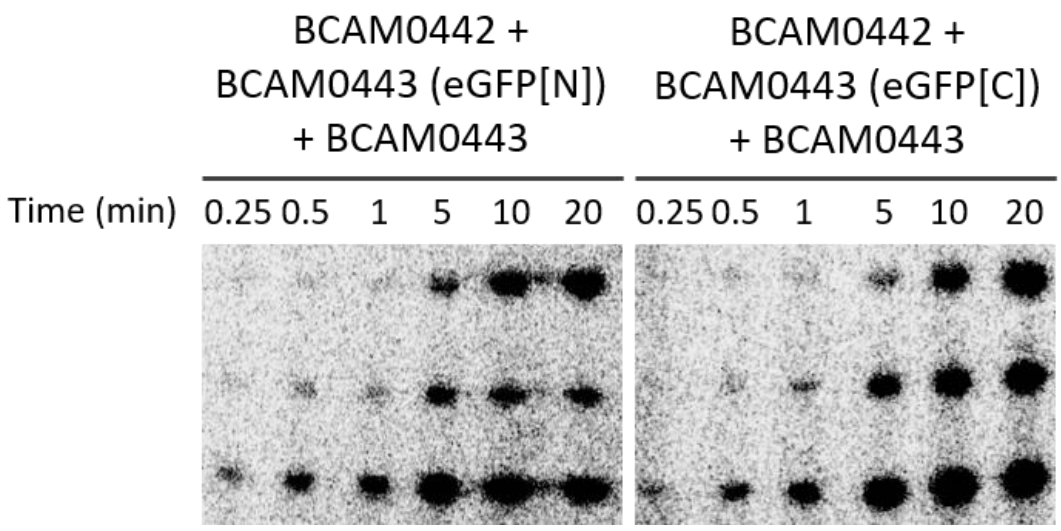

Figure 3.9: Example gels displaying that the eGFP tag negatively affects phosphotransfer from BCAM0442 to BCAM0443. Both gels contain BCAM0442 with BCAM0443 in both an untagged and eGFP-tagged form, with preferential phosphotransfer kinetics to the untagged form regardless of the relative position of the eGFP tag. Within both panels, the top band represents the SK, the middle band represents the eGFP-tagged RR, and the bottom band represents the untagged RR.

Despite the disadvantage that tagging of RRs with eGFP negatively affected their ability to be phosphorylated, phosphotransfer assays containing an SK and both its cognate RR and a non-cognate RR were carried out. Two different approaches were taken: one in which the cognate RR was tagged, and another in which the non-cognate RR was tagged. Due to the influence of the eGFP on phosphotransfer, this created a situation in which any non-cognate RR-P band was either artificially enhanced or diminished due to the eGFP tag inhibiting phosphotransfer to the cognate or non-cognate RR respectively. As such, it was not possible to gain a 'true' representation of the phosphotransfer kinetics between a SK, its cognate RR and a non-cognate RR, as the intensity of the non-cognate RR-P band would always be strengthened or diminished depending on which RR contains the eGFP tag.

3.2.8 – Non-cognate phosphotransfer in the presence of the cognate RR

Non-cognate phosphotransfer was observed in certain permutations in the presence of the cognate RR. Interestingly, when the cognate RR was tagged with eGFP, phosphotransfer was seen between certain SKs and RRs. For example, non-cognate phosphorylation was observed from the SK BCAM0442 to both BCAM0714 and BCAS0586 after 5 minutes. There is evidence to suggest that non-cognate phosphorylation can also occur between other SKs and RRs, however the relative weakness of the bands coupled with the large amount of background noise seen in Figure 3.10 renders it difficult to fully observe this phenomenon. Nonetheless, it does appear that all three of these SKs can undergo some level of non-cognate phosphorylation to each other's RRs when the eGFP tag is placed on the cognate RR. Interestingly, as can be observed for the BCAM0442 SK, even when the cognate RR is tagged with eGFP, the kinetic preference for cognate phosphorylation is significantly greater than for either of the non-cognate phosphorylation interactions, underlining the preference that SKs have for their cognate RR.

Conversely, when the assay was reversed and the non-cognate RR contained the eGFP tag, the only non-cognate RR-P band observed was phosphorylation of BCAS0586 by BCAM0442 after 20 minutes (Fig 3.11). The disparity in non-cognate RR-P bands relative to the placement of the eGFP tag highlights the significance of the negative influence that eGFP has on RR phosphorylation. It is likely that the 'true' level of non-cognate phosphotransfer *in vitro* in the presence of the cognate partner lies somewhere between these two points, however it is not currently possible to observe this directly due to the limitations of the eGFP tag.

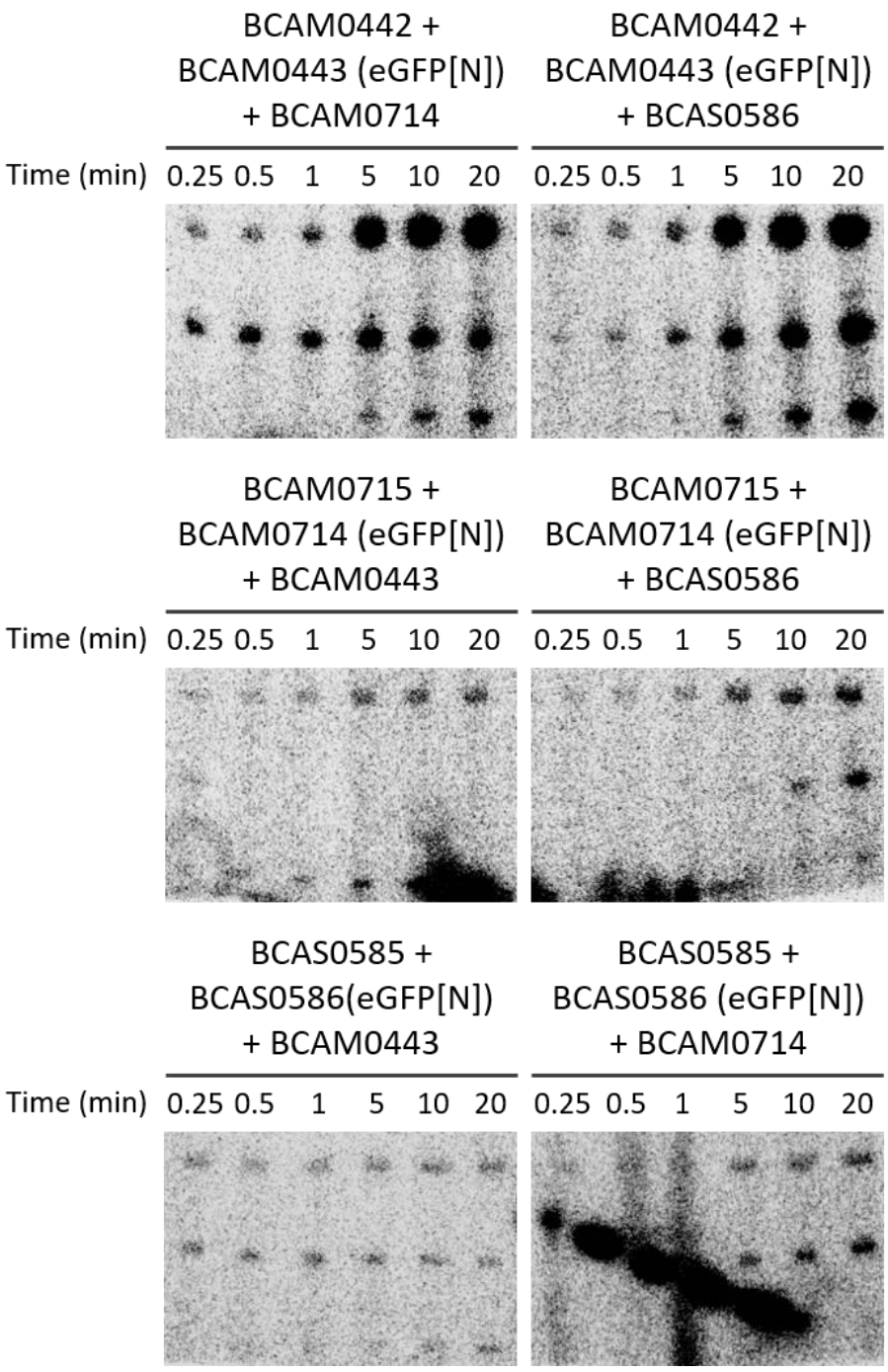

Figure 3.10: Representative gels displaying non-cognate phosphotransfer in the presence of the eGFP-tagged cognate RR. There are several examples of non-cognate phosphotransfer in the presence of the eGFP-tagged cognate RR over a 20 minute reaction, particularly for the BCAM0442 SK. Contact of the BCAS0585 + BCAS0586 (eGFP[N]) + BCAM0714 gel with the dye front led to contamination with excess radiation.

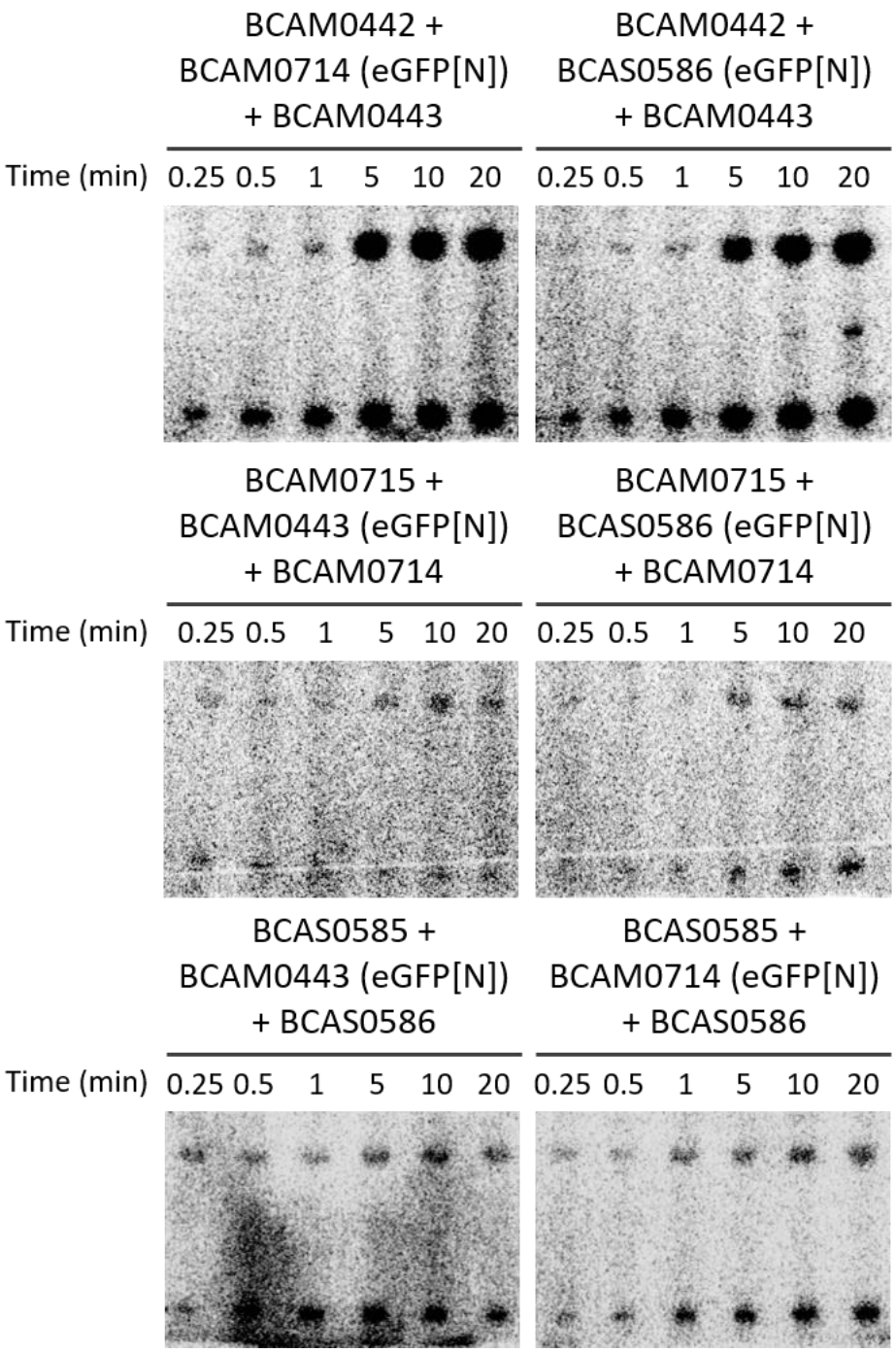

Figure 3.11: Representative gels displaying limited non-cognate phosphotransfer in the presence of the untagged cognate RR. The only observable non-cognate phosphotransfer occurs after 20 minutes between BCAM0442 and the eGFP-tagged BCAS0586.

3.2.9 – Non-cognate phosphotransfer with pre-phosphorylated SKs

While it is clear from the above data that the eGFP tag negatively influenced phosphorylation of RRs, and therefore rendered it difficult to ascertain the true rates of non-cognate phosphotransfer in the presence of the cognate RR, assays were repeated with the adjustment that SKs were pre-phosphorylated with radiolabelled ATP for 1 hour, prior to addition of RRs to begin the reaction. This alteration to the methodology would theoretically increase the rates of both cognate and non-cognate phosphotransfer, as much of the SK would be phosphorylated and ready to undergo phosphotransfer at the beginning of the reaction, reducing the impact that autophosphorylation of the SK would have on the speed of the phosphotransfer reaction. As the radiolabelled ATP is not removed from the reaction, SKs can rephosphorylate following phosphotransfer to RRs. This version of the phosphotransfer assay was carried out using an untagged cognate RR and an eGFP-tagged non-cognate RR, so that any observable non-cognate phosphorylation did not carry the caveat of being artificially enhanced by an eGFP-tagged cognate RR.

Unexpectedly, while the intensity of SK-P and RR-P bands were stronger, pre-phosphorylation of the SKs in this way did not particularly influence the strength of non-cognate RR bands (Fig 3.12). The only observable non-cognate phosphorylation over the 20 minute reaction time was between the SK BCAM0442 and the RR BCAS0586 at 20 minutes post initiation of the reaction. Interestingly, this resembles the results shown in the ‘standard’ phosphotransfer assay displayed in Figure 3.11, supporting the notion that phosphotransfer between BCAM0442 and BCAS0586 may be the fastest non-cognate interaction.

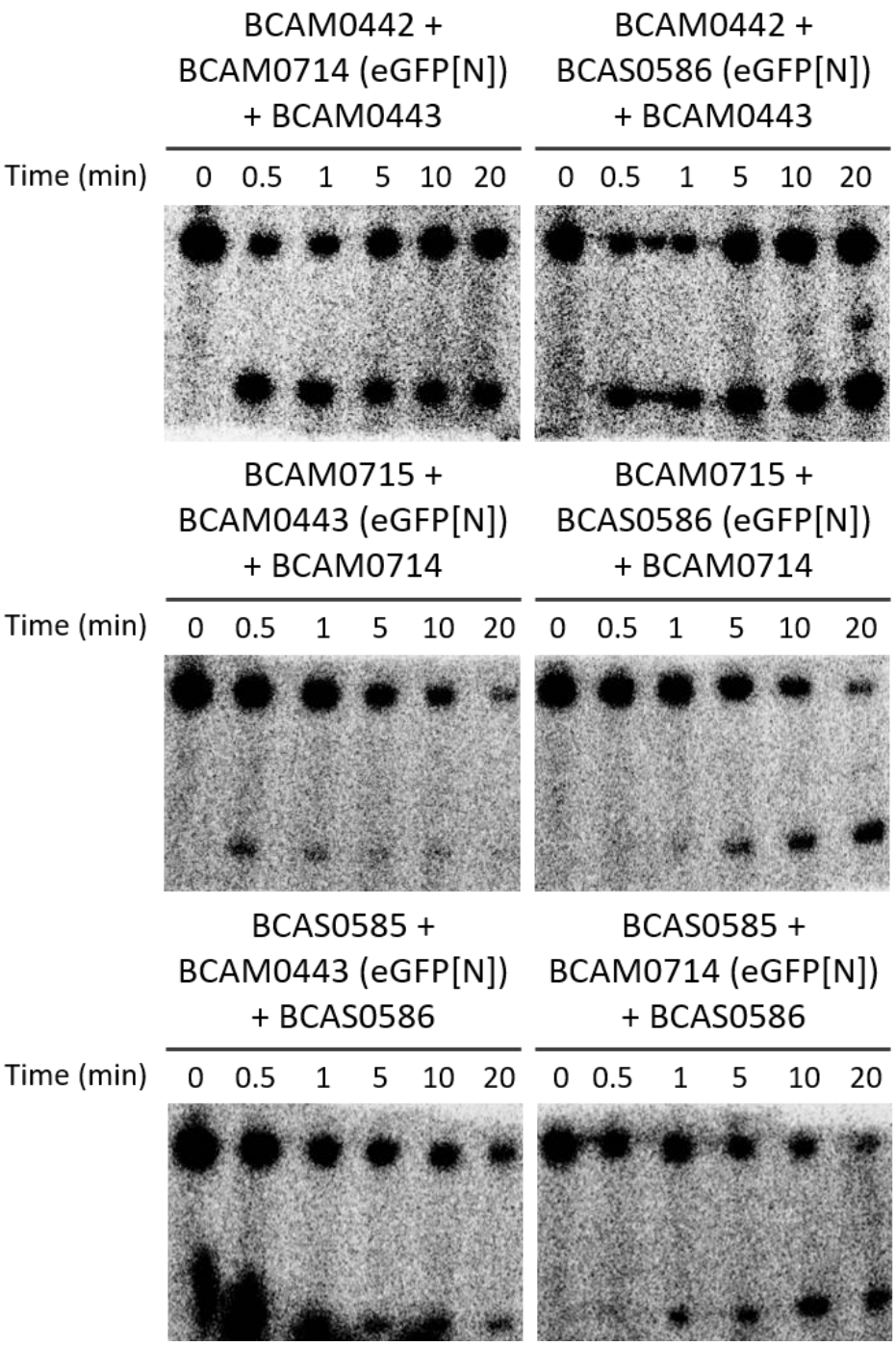

Figure 3.12: Representative gels displaying limited non-cognate phosphotransfer in the presence of the untagged cognate RR despite pre-phosphorylated SKs. The only observable non-cognate phosphotransfer occurs after 20 minutes between BCAM0442 and the eGFP-tagged BCAS0586. The 0 minute timepoint refers to the point just before both the cognate and the non-cognate RRs were added to the pre-phosphorylated SK to initiate the phosphotransfer reaction. As ATP is still present in the reaction, SKs can undergo rephosphorylation following phosphotransfer to RRs.

3.2.10 – Non-cognate phosphotransfer with pre-phosphorylated and nickel affinity column-purified SKs

It is clear from Figure 3.12 that all three SKs autophosphorylated well and gave clearly visible bands throughout the 20 minute time course. This is in contrast to examples such as Figure 3.6 B, in which certain SK and RR bands are quite weak, presumably because these reactions were initiated with the addition of the radiolabelled ATP to SKs and RRs. As such, it was decided to use this pre-phosphorylation approach of SKs to further quantify the reactions kinetics between these TCSs in a simple one SK, one RR format.

In order to focus purely on the ability of the SKs to undergo phosphotransfer to the RR, following initial purification, SKs were phosphorylated for one hour with radiolabelled ATP, and then once again washed through and eluted off a nickel resin column prior to storage at -20 °C. As such, the phosphorylated SK was purified from any remaining ATP. This resulted in the ability to perform a phosphotransfer assay in which the only available phosphoryl groups for phosphotransfer were those that were already bound to the SKs. This would therefore allow elucidation of the rate at which phosphotransfer occurs between SKs and RRs, as the ability of the SK to rephosphorylate itself, and thus undergo additional phosphotransfer, has been removed.

Similarly to when the phosphotransfer assay is performed without SK pre-phosphorylation, SKs generally had a higher kinetic preference for their cognate RR than for other RRs (Fig 3.13). For the SKs BCAM0442 and BCAM1417, only the cognate RR-P bands are clearly visible. There is some diminished SK-P band when BCAM0442 is incubated alongside BCAM0714, but non-cognate RR bands are not visible. This is in contrast to previous phosphotransfer assays (Fig 3.5), in which the RRs BCAM0714 and BCAS0586 were both heavily phosphorylated by BCAM0442.

As observed previously (Fig 3.5), BCAM0715 clearly phosphorylates BCAM0443 and BCAS0586 as well as its cognate RR. Interestingly, quantification of phosphotransfer from BCAM0715 suggests that the rate of phosphotransfer is similar to both the cognate BCAM0714 and the non-cognate BCAM0443 and BCAS0586 (Appendix Figure A1.1). Interestingly, while SK-P bands for

BCAM0442 and BCAM0715 are not visible in Figure 3.5, in Figure 3.13 the SK-P bands are clearly visible. It may be the case that in the presence of BCAM0443 or BCAM0714, autophosphorylation of BCAM0442 and BCAM0715 respectively is inhibited, which would explain the discrepancy between Figure 3.5 and Figure 3.13. Unsurprisingly, BCAM1417 does not phosphorylate any RR apart from its own cognate partner, BCAM1418. Finally, similar to the BCAM0442/3 system, BCAS0585 has quicker phosphotransfer to its cognate RR, though non-cognate bands are weakly visible for BCAM0443 and BCAM0714.

Ultimately, quantification of the rate of phosphotransfer from pre-phosphorylated SKs to RRs reaffirms the notion that cognate phosphotransfer occurs significantly quicker than non-cognate phosphotransfer for BCAM0442/3 and BCAS0585/6, though it appears that there is little difference between cognate and non-cognate phosphotransfer for the BCAM0715 SK. At least *in vitro*, BCAM0715 appears to be able to donate its phosphoryl group readily to the non-cognate BCAM0443 and BCAS0586 RRs, a phenomenon seen in both 'standard' and 'pre-phosphorylated SK' versions of the phosphotransfer assay. This readiness for non-cognate phosphorylation is not shared by BCAM0442 or BCAS0585, perhaps suggesting that the kinetics of the BCAM0715 SK allow for non-cognate phosphotransfer more easily than the other SKs. This may suggest that the BCAM0714/5 TCS has the potential to act as a central hub for this MKN.

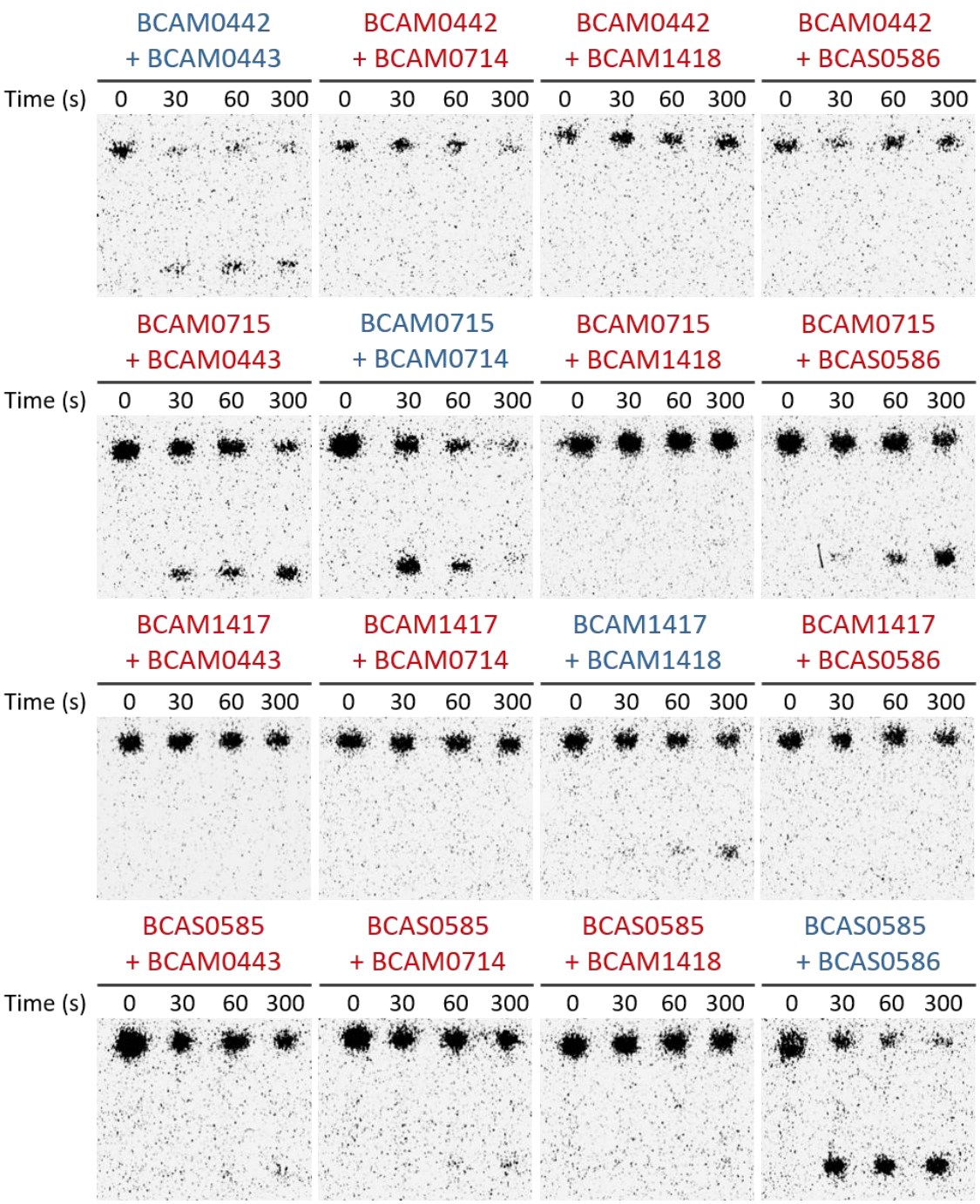

Figure 3.13: Representative gels displaying phosphotransfer from pre-phosphorylated and subsequently purified SK. Labels in blue denote cognate interactions, whereas red labels denote non-cognate interactions. There is a clear preference for cognate phosphotransfer for the pre-phosphorylated SKs, although there are many instances of non-cognate phosphotransfer. The 0 minute timepoint refers to the point just before both the cognate and the non-cognate RRs were added to the pre-phosphorylated SK to initiate the phosphotransfer reaction.

3.3 – Discussion

Through successful purification of SK intracellular portions and RRs, the potential for non-cognate phosphotransfer between all four TCSs was determined through use of the phosphotransfer assay. Each SK successfully underwent autophosphorylation and showed the potential for cognate phosphorylation with its predicted cognate RR. It is clear that non-cognate phosphotransfer is kinetically possible between BCAM0442/3, BCAM0714/5 and BCAS0585/6, whereas there is no evidence to suggest that the BCAM1417/8 TCS exhibits any non-cognate interactions with the other three TCSs. The conclusion that BCAM1417/8, the closest TCS in the *B. cenocepacia* genome to the other three TCSs in both overall sequence and specificity residue similarity, does not undergo non-cognate phosphotransfer reinforces the significance of the non-cognate interactions shared between BCAM0442/3, BCAM0714/5 and BCAS0585/6, as well as supporting the notion that 5 out of 7 shared RR specificity residues is an accurate threshold for predicting non-cognate phosphotransfer between TCSs. Though a systematic phosphotransfer profile of these three SKs has not been performed, in which every *B. cenocepacia* RR is purified and tested for potential phosphotransfer against the SKs, based on the data presented in this chapter and on the bioinformatic evidence described previously, it may be reasonably concluded that BCAM0442/3, BCAM0714/5 and BCAS0585/6 form a three-TCS MKN in *B. cenocepacia*.

Aside from the fact that phosphotransfer is kinetically possible between these TCSs, other information can be inferred from this phosphotransfer data. Based on both the ‘1 SK/1 RR’ and ‘1 SK/2 RRs’ phosphotransfer assays, it is clear that both BCAM0442 and BCAS0585 SKs hold a strong kinetic preference for their cognate RR over non-cognate RRs, whereas BCAM0715 appears to be more promiscuous. Previous data, in which the phosphotransfer profile from several SKs from both *E. coli* and *C. crescentus* was characterised, suggested a general preference for presumed cognate RRs over other non-cognate targets [419]. As such, the rate of both cognate and non-cognate phosphotransfer for BCAM0715 being similar suggests that BCAM0715 may be acting as a central hub for this MKN.

The fact that non-cognate phosphotransfer can occur between these TCSs highlights the crucial role that specificity residues hold in determining phosphotransfer specificity. The number of specificity residues shared between each RR appears to be connected to their ability to be phosphorylated by non-cognate SKs. BCAM1418 shares 4 of 7 specificity residues with the other three RRs, the lowest of all the RRs, and there is no non-cognate phosphorylation with the BCAM1417/8 TCS, suggesting that in this example there is not enough similarity to allow non-cognate interactions. The remaining RRs share either 5 or 6 specificity residues out of 7 with one another (Fig 1.6), though there appears to be no observable difference in phosphotransfer rate between those that share 5 or share 6 specificity residues. Whether 5 of 7 matching specificity residues is a 'threshold' for non-cognate phosphotransfer generally between TCSs is an interesting question worthy of further investigation. It is not known whether there are particular specificity residues that hold more influence over phosphotransfer specificity than others; this presumably would depend on the specific proteins and specificity residues in question.

The concept of specificity residue similarity between TCS proteins has focused thus far purely on whether individual specificity residues are or are not identical between proteins, without including information about specific amino acid properties. For these RRs specifically, where specificity residues do not match there is generally a large difference in their chemical properties. For example, the threonine specificity residue on BCAM0714 and BCAS0586 is smaller and more polar than the equivalent methionine on BCAM0443. However, it may be the case that different amino acids can take the place of a specificity residue without adversely impacting phosphotransfer specificity, for example it may be possible for a leucine specificity residue to be substituted for the similarly nonpolar isoleucine without affecting phosphotransfer kinetics. As such, when searching for similarities between specificity residue on TCS proteins, it may be recommended to also consider the similarities and differences between non-matching specificity residues, as this may reduce the chance of 'false-negatives' being missed by any systematic search for specificity residue similarities and MKNs.

BCAS0586 shares 6 of 7 RR specificity residues with both BCAM0443 and BCAM0714, suggesting that this single difference in specificity residues is key to

regulating phosphotransfer specificity between these TCSs. In order to ascertain that these specific residues are indeed the key to the kinetic preference for cognate phosphotransfer in these TCSs, it would be of interest to systematically mutate these residues so that one RR contained the specificity residues of another. Hypothetically, the kinetic preference for a RR would be completely swapped with whichever RR the specificity residues originated from. For example, mutation of the specificity residues on BCAM0443 to match those of BCAM0714 would hypothetically lead to BCAM0443 being much more readily phosphorylated by BCAM0715, and less readily phosphorylated by BCAM0442. If this swapping of kinetic preference did not occur as expected, it may suggest that other residues may play a role in phosphotransfer specificity between these TCSs.

Given the kinetic preference for cognate RRs by all of the SKs of interest, it is unfortunate that due to the negative impact of the eGFP tag on the RRs, it was not possible to directly observe the kinetics of non-cognate phosphotransfer in the presence of the cognate partner. While it is clear that certain non-cognate interactions can occur in the presence of the cognate partner, such as from BCAM0442 to BCAS0586 (Fig 3.11), the 'true' level of non-cognate phosphotransfer at equimolar concentrations *in vitro* is unclear. It is uncertain why the eGFP tag causes this negative impact on phosphotransfer regardless of which terminus of the RR it is placed, nor whether the tag affects either the initial phosphorylation of the RR or the lability of the phosphoryl group on the RR. It is also unknown whether any tag of similar size would similarly cause this issue, or whether this phenomenon is eGFP-specific. One possibility would be to attempt to utilise a tag that is smaller than the 27 kDa eGFP, so as to hopefully remove the negative impact on the RR, but large enough to still allow for discrimination on SDS-PAGE, such as the 12 kDa *E. coli* thioredoxin tag [457]. Successfully utilising a tag that does not have the same issues that eGFP does would allow the direct comparison of phosphotransfer from a SK to a cognate and non-cognate RR, or even between two different non-cognate RRs, further allowing the determination of which non-cognate interactions are the strongest *in vitro*.

One vital consideration to make when interpreting data from the phosphotransfer assay is that the interactions between proteins are occurring *in vitro*, at a constant concentration and temperature. While this is useful in determining what non-

cognate interactions are kinetically possible, inferring the physiological relevancy of different interactions is difficult, as the conditions of the reaction do not reflect the dynamic nature of the cellular environment. For example, it is unlikely that different TCSs are expressed at identical levels throughout the cell, and given that activation of TCSs such as BCAM0714/5 often leads to drastic alterations in their expression levels (Robinson *et al*, Unpublished data), this adds limitations to the interpretation of the phosphotransfer assay results.

Given the above constraints, one possibility for future work is to adjust the concentrations of SKs or RRs within the phosphotransfer assay. All '1 SK/2 RR' phosphotransfer assays were performed with the two RRs at an equal concentration of 10 μM. As it has previously been established that exposure of *B. cenocepacia* to 1.5 mM $ZnCl_2$ leads to an increase of BCAM0714 and BCAM0715 transcript levels by between 30-58 fold (Robinson *et al*, Unpublished data), simply doubling or tripling the concentration of a non-cognate RR or SK may be a reasonable way of further exploring non-cognate interactions between these proteins. It is not unrealistic to expect situations where the concentration of a non-cognate RR is significantly greater than that of a cognate partner, and while there are limits to the protein concentration one can achieve within the phosphotransfer assay, these possibilities may be a worthwhile avenue of exploration.

Similar to concentration, temperature is another factor that could be changed within the phosphotransfer assay. Being an environmental organism that is also capable of infecting the human host, the niches that *B. cenocepacia* may be exposed to can be of a range of different temperatures, and it may be the case that these TCSs, and thereby the kinetics of phosphotransfer between them, differ between temperatures. For example, while there is no evidence for non-cognate interactions between BCAM1417/8 and the other TCSs at room temperature, perhaps there would be evidence for such interactions at other temperatures. This could lead to interesting observations about the nature of this potential MKN in *B. cenocepacia*; for example any differences in phosphotransfer kinetics between these TCSs at 37 °C may suggest that this MKN may elicit different behaviours within the human host than in the environment.

As can be seen in Figure 3.5 and Figure 3.13, the presence of the BCAM0442-P and BCAM0715-P bands when incubated alongside BCAM0443 and BCAM0714

respectively is dependent on the particular methodology employed in the phosphotransfer reaction. Phosphotransfer initiated through the addition of radiolabelled ATP results in no observable SK-P band (Fig 3.5), whereas the addition of RR to pre-phosphorylated SK results in a strong SK-P band (Fig 3.13). One potential explanation may be that the presence of the BCAM0443 or BCAM0714 RRs inhibits autophosphorylation of BCAM0442 and BCAM0715 respectively through binding of unphosphorylated RR to the unphosphorylated SK. As such, when the SK is subsequently able to autophosphorylate, the speed of the phosphotransfer reaction to the cognate RR results in no observable SK-P band in the phosphotransfer gel. One way to explore this possibility would involve mutagenesis of the conserved aspartate residue of the RRs to an alanine, removing the ability of the RRs to be phosphorylated [458]. This would allow direct comparison of the ability of the SKs to autophosphorylate both with and without the presence of the RRs in the phosphotransfer assay, as no phosphoryl groups could be transferred from the SKs to the RRs.

Additionally, the generation of SK mutants may allow further use of the phosphotransfer assay to explore these TCSs. It has previously been established that mutation of an asparagine to an aspartate within the 'N-box' in the ATP-binding domain renders a SK unable to undergo autophosphorylation without affecting its phosphatase ability [459]. This would allow for '2 SK/1 RR' phosphotransfer assays which contained a cognate SK and RR pairing alongside a non-cognate N-box mutated SK. Comparison of RR-P bands between the '2 SK/1 RR' assay and the cognate SK and RR alone may elucidate both whether SKs can act as phosphatases to non-cognate RRs, and the relative strength of that phosphatase activity in comparison to other SKs, both important factors in the understanding of this potential MKN. A SK that could phosphorylate a non-cognate RR but not also act as a phosphatase would essentially always act as an activator for that RR and its downstream signalling pathway, rather than as the dual kinase/phosphatase protein that is standard for cognate SK/RR pairings. Alternatively, the mutation of a conserved threonine residue to an alanine residue of SKs negatively impacts its phosphatase activity, a mutation which could be repeated with these SKs of interest, directly allowing the visualisation of whether a SK could act as a phosphatase to a particular RR [460].

The work within this chapter has focused on exploring potential phosphotransfer-based interactions between these TCSs, however there are other ways in which TCS proteins may interact with one another that do not rely on the transfer of phosphoryl groups from SKs to RRs. For example, the SK RetS from *P. aeruginosa* can inhibit the autophosphorylation of the SK GacS, while the *E. coli* RR RscB can heterodimerise with the RRs MatA and DctR, adding layers of complexity to the functioning of these TCSs [410,461]. It is possible that the TCSs described in this work can interact in ways that are not visible from the phosphotransfer assay. As such, other methodologies could be employed to further explore the interactions between these TCSs.

One methodology that could be employed to explore this is the bacterial adenylate cyclase two-hybrid system (BACTH). Two proteins of interest are fused to complementary fragments of an adenylate cyclase, and if the proteins of interest associate together, the adenylate cyclase fragments can generate cAMP, leading to a functional readout [462]. The BACTH approach could therefore be used to investigate whether there is any SK-SK interaction or RR heterodimerisation between these three TCSs, which is not possible through this phosphotransfer assay. Additionally, the BACTH approach could also be used to verify the results described within this work; theoretically the three TCSs that form this putative MKN should show interaction between each SK and all three RRs. It would also be of interest to see whether there is any association between these TCSs and BCAM1417/8. Though no non-cognate phosphorylation was observed for this system, it does not limit the potential for BCAM1417/8 to interact with the other three in a non-phosphotransfer based manner.

3.4 – Conclusions

- Expression vectors for all four TCSs of interest were generated and all SKs and RRs were successfully purified.
- Three TCSs, BCAM0442/3, BCAM0714/5 and BCAS0585/6, undergo non-cognate phosphotransfer from their SKs to each other's RRs, whereas BCAM1417/8 does not, indicating that BCAM0442/3, BCAM0714/5 and BCAS0585/6 likely work together in a MKN.
- While some non-cognate phosphotransfer does occur in the presence of the cognate RR, issues with the eGFP tag prevent further investigation.

Chapter 4: Characterisation of TCS deletion mutants

4.1 – Introduction

As outlined in Chapter 3, of the four TCSs of interest within this potential metal-sensing MKN, three display non-cognate phosphotransfer to one another. Previous investigation of BCAM0714/5 has implicated this TCS in the cadmium and zinc response in *B. cenocepacia* through regulation of the CzcCBA efflux pump and a downstream gene region (Robinson *et al*., Unpublished data). Additionally, the BCAM0442/3 TCS was identified in a screen of copper resistance genes via transposon sequencing, reinforcing the idea that this TCS is metal-sensing [369]. As such, it is of interest to characterise both what the individual TCSs sense and respond to, and to what phenotypes they contribute to. Though BCAM1417/8 does not appear to be part of this MKN based on the aforementioned phosphotransfer evidence, it is still of interest to characterise its role in *B. cenocepacia*, particularly given the overall sequence similarity of BCAM1417/8 to the other three TCSs.

Characterisation of these TCSs has revolved around the construction of deletion mutants of each TCS in a *B. cenocepacia* K56-2 background. As these TCSs are predicted to be metal-sensing, these deletion mutants have then been tested for susceptibility against a range of metals. Investigation of metal-dependent induction of putative promoters of interest relied on use of a *gfp* transcriptional fusion via the pGA-G1 vector, kindly provided by the Leo Eberl group (University of Zurich, Switzerland). Additionally, deletion mutants have been investigated for a range of phenotypes of interest, such as biofilm formation, virulence in *G. mellonella* and, via the construction of gentamicin-sensitive mutants, intracellular survival within murine macrophages. Given the link between the CzcRS TCS in *P. aeruginosa* and resistance to imipenem, an equivalent link between the metal-sensing TCSs of *B. cenocepacia* and imipenem has also been investigated. Ultimately, this chapter's aim was to characterise deletion mutants of each TCS and subsequently investigate any relevant phenotypes, hence providing novel insight into the functionality of these TCSs within *B. cenocepacia*.

4.2 – Results

4.2.1 – Deletion of TCSs of interest from *B. cenocepacia*

The generation of unmarked deletion mutants within *B. cenocepacia* relied upon the methodology described previously by Flannagan and colleagues (2008), which involves upstream and downstream flanks of the genes of interest being cloned into the pGPI-SceI suicide vector, which is then conjugated into *B. cenocepacia,* resulting in a crossover event in which pGPI-SceI is incorporated into the genome (Fig 2.1) [440]. The pDAI-SceI vector, encoding for the I-SceI endonuclease, is then conjugated into these first crossovers, leading to a second recombination event in which I-SceI cuts a specific site on pGPI-SceI, resulting in the generation of either WT revertants or unmarked deletion mutants (Fig 2.1). To generate pGPI-SceI vectors for each TCS, upstream and downstream flanks were PCR amplified, spliced together and cloned into pGPI-SceI (a list of primers used can be found in Appendix section A5). In-frame unmarked deletion mutants of each TCS were then generated through the processes described in section 2.3.2. An example plasmid map of both pGPI-SceI and pDAI-SceI can be found in Figure 4.1.

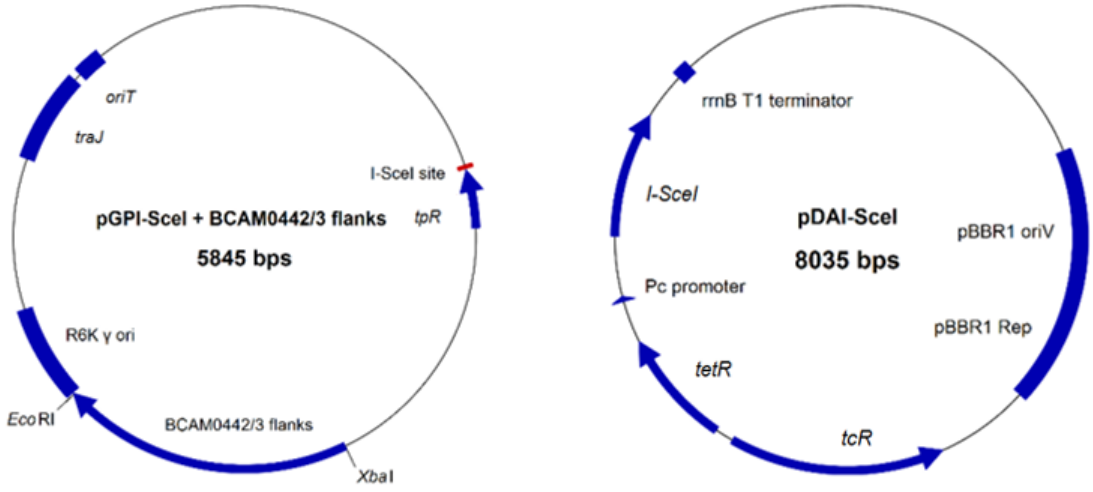

Figure 4.1: Plasmid maps for pGPI-SceI containing BCAM0442/3 flanks and for pDAI-SceI. Relevant cloning sites for cloning of BCAM0442/3 flanks into pGPI-SceI are shown. Plasmid maps made on Clone Manager Professional 9 (Sci-Ed).

Following verification of successful conjugation of pDAI-SceI into first crossovers via PCR, several verification steps were undertaken to reveal whether candidate colonies of *B. cenocepacia* were WT revertants or unmarked deletion mutants. Strains were tested for sensitivity to trimethoprim and resistance to tetracycline, which would confirm that the pGPI-SceI vector had been lost and the pDAI-SceI vector gained respectively, as well as PCR screened using primers specific to the BCC *recA* gene, to verify that colonies were indeed *B. cenocepacia*, and not *E. coli* remaining from the mutagenesis process. Various PCR screens utilising primers specific to the genes of interest and primers specific to surrounding regions were performed (example shown in Figure 4.2). Finally, to ensure that no undesired mutations had occurred during the mutagenesis process, regions containing the whole upstream and downstream flanking sites were amplified and sent for sequence verification (TubeSeq Service, Eurofins Genomics) (example shown in Figure 4.3). Overall, single deletion mutants for each TCS, double deletion mutants for each TCS pairing, and a triple ΔBCAM0442/3 + ΔBCAM0714/5 + ΔBCAS0585/6 mutant were generated (Fig 4.4). While six double TCS deletion mutants were generated, only those that are pertinent to the BCAM0442/3, BCAM0714/5 and BCAS0585/6 TCSs will be focused on, as Chapter 3 suggests that BCAM1417/8 is not part of this metal-sensing MKN.

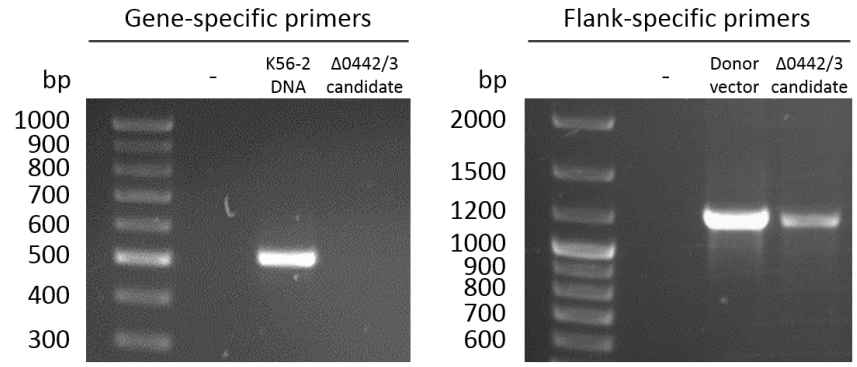

Figure 4.2: PCR verification of a ΔBCAM0442/3 deletion mutant candidate. Left – PCR using primers specific for BCAM0442 and BCAM0443. A negative band in the candidate lane suggests that these genes are not present in the candidate. Expected size – 509 bp. Right – PCR using primers specific for the flanks. A positive band in the candidate lane shows that this candidate contains flanking regions that are spliced together without the genes of interest between them. Expected size – 1201 bp.

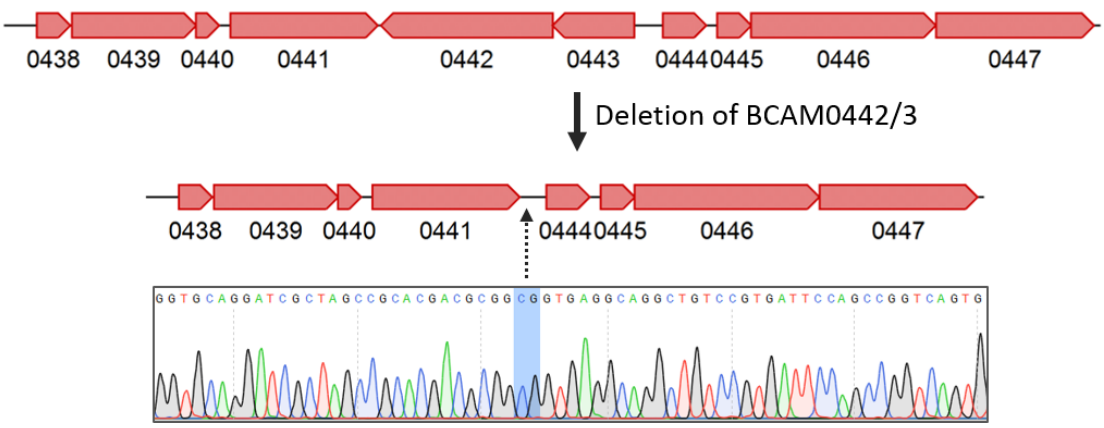

Figure 4.3: Sequence verification of a ΔBCAM0442/3 deletion mutant candidate. The genomic neighbourhood of BCAM0442/3 (top) and the unmarked ΔBCAM0442/3 deletion mutant (middle). Sequence verification of the deletion mutant is also displayed (bottom). The two bases highlighted in blue depict the point at which the upstream and downstream flanks meet.

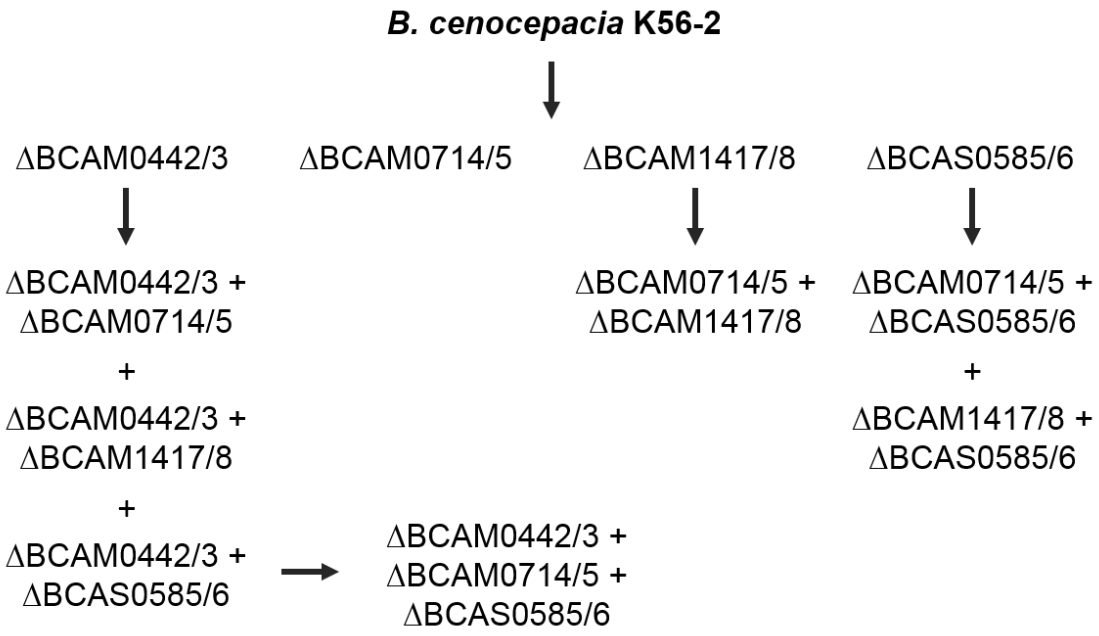

Figure 4.4: The specific combinations and order in which TCS deletion mutants were generated within this work. Four single, six double and one triple TCS deletion mutants were generated. For double and triple TCS mutants, all combinations of donor pGPI-SceI plasmid and recipient TCS deletion mutant were tested, though not all were successful. At least one mutant for each pairing was successfully generated.

4.2.2 – BCAM0442/3 and BCAM0714/5 are implicated in the copper and cadmium/zinc response respectively

Initial investigation of the TCS deletion mutants focused on whether these deletion mutants were sensitive to metals. Deletion mutants of each TCS were tested for their susceptibility to a range of metals, namely cadmium, cobalt, copper, silver and zinc. Spotting of TCS deletion mutants on metal-infused agar plates revealed that ΔBCAM0442/3 is susceptible to copper, while confirming that deletion of BCAM0714/5 confers susceptibility to cadmium and zinc (Fig 4.5). The copper and zinc phenotypes, though not the cadmium phenotype, observed for these two systems were also partially restored by complementation with a pDA17-derived vector containing the genes of interest alongside their putative promoter region. However, a previously-generated pSCrhaB3 vector containing the BCAM0714/5 genes did successfully complement both the cadmium and zinc phenotypes for ΔBCAM0714/5 (Data not shown). There is a clear metabolic burden upon *B. cenocepacia* harbouring the pDA17 vector which may explain the lack of complementation of the cadmium sensitivity of ΔBCAM0714/5 by pDA17::BCAM0714/5, due to the relatively subtle nature of the sensitivity compared to the more pronounced zinc phenotype (Fig 4.5).

The growth kinetics of these TCSs when exposed to metals of interest were further investigated through use of a 48 hour growth curve within a shaking plate reader. This revealed metal-specific differences in growth kinetics of different deletion mutants (Fig 4.6). For example, ΔBCAM0714/5 showed great sensitivity to cadmium and zinc, whereas sensitivity of the ΔBCAM0442/3 deletion mutant to copper is more subtle, with it taking longer to begin exponential growth when exposed to 5 mM $CuCl_2$ (Fig 4.6). This can also be seen in the MIC values for each single TCS deletion mutant; all strains had an MIC against $CuCl_2$ of 8 mM, despite the enhanced sensitivity of ΔBCAM0442/3 to copper (Table 4.1). Contrastingly, ΔBCAM0714/5 was significantly more sensitive to zinc than the other strains, with an MIC significantly lower than WT (Fig 4.6 and Table 4.1). Double TCS deletion mutants, as well as the triple ΔBCAM0442/3 + ΔBCAM0714/5 + ΔBCAS0585/6 deletion mutant were also tested against a range of metals, though these mutants displayed no additional metal sensitivity that was not already observed within the single TCS deletion mutants (Table 4.1).

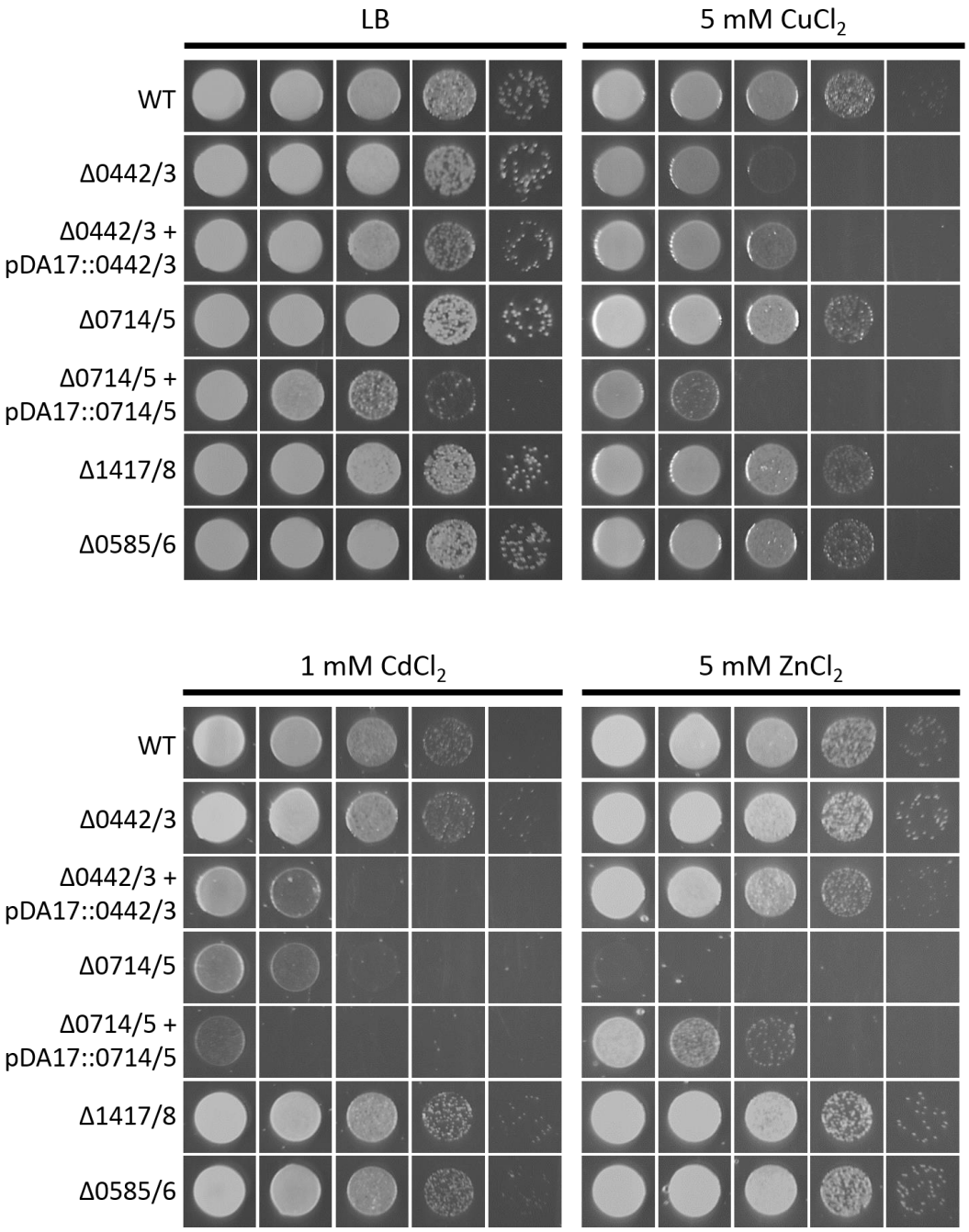

Figure 4.5: Single TCS deletion mutants spotted on copper-, cadmium- and zinc-supplemented agar plates. 10^{-1} to 10^{-5} dilutions of standardised overnight culture were spotted left to right on the plates. ΔBCAM0442/3 is sensitive to copper, whereas ΔBCAM0714/5 is sensitive to cadmium and zinc. There is no observable sensitivity to any of the metals by ΔBCAM1417/8 or ΔBCAS0585/6.

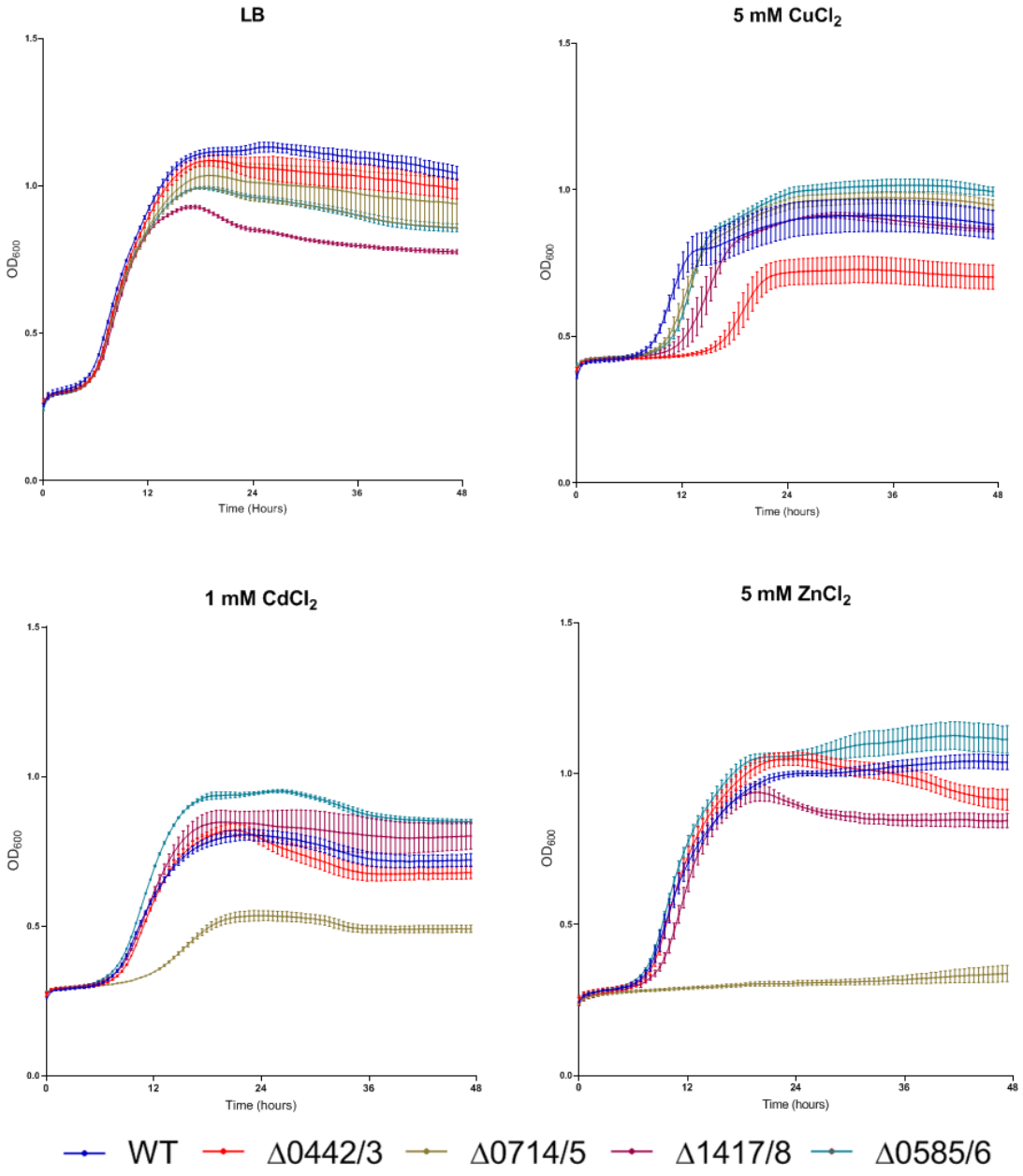

Figure 4.6: Growth of single TCS deletion mutants in LB supplemented with various heavy metals. ΔBCAM0442/3 is sensitive to copper, whereas ΔBCAM0714/5 is sensitive to cadmium and zinc. n = 3 with 3 technical replicates per assay. Error bars indicate SEM.

Table 4.1: 24 hour MICs of WT and TCS deletion mutants against doubling concentrations of a range of metals.

Strain	MIC (mM)				
	$AgNO_3$	$CdCl_2$	$CoCl_2$	$CuCl_2$	$ZnCl_2$
WT	0.016	4	1	8	16
ΔBCAM0442/3	0.016	4	1	8	16
ΔBCAM0714/5	0.016	**2**	1	8	**2**
ΔBCAM1417/8	0.016	4	1	8	16
ΔBCAS0585/6	0.016	4	1	8	16
ΔBCAM0442/3 + ΔBCAM0714/5	0.016	**2**	1	8	**2**
ΔBCAM0442/3 + ΔBCAS0585/6	0.016	4	1	8	16
ΔBCAM0714/5 + ΔBCAS0585/6	0.016	**2**	1	8	**2**
ΔBCAM0442/3 + ΔBCAM0714/5 + ΔBCAS0585/6	0.016	**2**	1	8	**2**

Note: MICs of deletion mutants highlighted in red differ from the WT

4.2.3 – Fusion of promoters of interest to *gfp* supports deletion mutant metal phenotypes

Though the metal sensitivity displayed by a TCS deletion mutant implicates that TCS in the cellular response to that metal, it does not directly support the notion of direct sensing by that TCS. It is possible that deletion of a TCS can render the cell susceptible to a toxic agent without that system directly responding to that agent. As such, to explore how these TCSs are transcriptionally activated in response to metal exposure, putative promoters of interest were cloned upstream of a *gfp* gene in the pGA-G1 vector. While BCAM0442/3 and BCAS0585/6 have clearly defined upstream regions that may contain a putative promoter, BCAM0714/5 appears to reside in a five-gene operon with *czcCBA*. As such, the upstream region of *czcC* was used as the 'BCAM0714/5 promoter'. As pGA-G1 holds a gentamicin-resistance marker, previously generated gentamicin-sensitive

deletion mutants of TCSs of interest generated for use in a gentamicin-protection assay (see section 4.2.7) were utilised.

Gentamicin-sensitive *B. cenocepacia* has been previously generated by knocking out an AmrAB-OprA-like efflux pump (BCAL1674-1676) which is crucial for resistance to aminoglycosides [207]. As such, the TCSs of interest were deleted from a previously generated gentamicin-sensitive ΔBCAL1674-76 deletion mutant of *B. cenocepacia* as described above (section 2.3.2). *B. cenocepacia* strains lacking BCAL1674-76 are hypersensitive to gentamicin; the gentamicin MIC of these mutants was < 4 μg/ml, whereas the gentamicin MIC WT *B. cenocepacia* was > 256 μg/ml (Data not shown).

To ensure that gentamicin-sensitive TCS deletion mutants had the same phenotype as the standard TCS deletion mutants, gentamicin-sensitive mutants were spotted onto metal plates, which confirmed their metal phenotypes as being the same as the previously generated mutants (Appendix Figure A2.1). Following successful verification of these mutants, pGA-G1 vectors were conjugated into gentamicin-sensitive WT, ΔBCAM0442/3, ΔBCAM0714/5 and ΔBCAS0585/6.

Overnight growth of the various mutants in LB supplemented with metals of interest revealed that the BCAM0442/3 promoter was induced in response to copper, and the BCAM0714/5 promoter was induced in response to cadmium and zinc (Fig 4.7), supporting the metal phenotypes seen in the deletion mutants (Figs 4.5 and 4.6). This induction was lost in the respective deletion mutants for each TCS, suggesting that the metal-specific induction of these promoters is dependent on the TCSs to which they belong (Fig 4.7). Though the induction of pGA-G1::0714/5$_{prom}$ in response to cadmium appears to still be present in the ΔBCAM0714/5 deletion mutant, this is due to the lower OD_{600} reached by the ΔBCAM0714/5 deletion mutant in 0.25 mM $CdCl_2$; the raw fluorescence values for this mutant were equivalent to control (Data not shown). There was no induction of the BCAS0585/6 promoter in response to the metals tested, further suggesting that BCAS0585/6 is not metal-sensing (Appendix Figure A2.2).

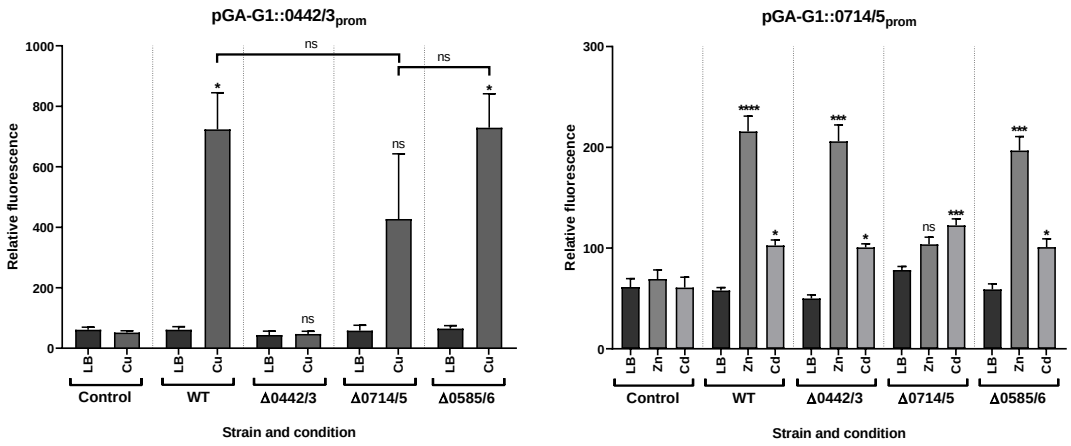

Figure 4.7: Relative fluorescence of 24 hour growth of *B. cenocepacia* TCS deletion mutants containing pGA-G1::0442/3$_{prom}$ or pGA-G1::0714/5$_{prom}$. Each graph displays fluorescence of each gentamicin-sensitive deletion mutant containing either pGA-G1::0442/3$_{prom}$ or pGA-G1::0714/5$_{prom}$. Control refers to gentamicin-sensitive WT *B. cenocepacia* containing pGA-G1 lacking a promoter. Metal concentrations are as follows: $CuCl_2$ – 1 mM, $ZnCl_2$ – 1 mM, $CdCl_2$ – 0.25 mM, $AgNO_3$ – 5 µM, $CoCl_2$ – 0.25 mM. n = 3 independent experiments with 3 technical replicates per assay. * = $p < 0.05$, *** = $p < 0.001$, **** = $p < 0.0001$. Asterisks on bars refer to one-way ANOVA comparison relative to respective metal control. Error bars indicate SEM.

As the induction of these promoters is only lost in their respective TCS deletion mutants, and not in any other TCS deletion mutant, it is suggestive that these TCSs transcriptionally regulate themselves with no observable influence from the other TCSs within this MKN. It does appear that the copper-dependent induction of the BCAM0442/3 promoter is lower in the ΔBCAM0714/5 deletion mutant, although a one-way ANOVA with multiple comparisons found no statistically significant difference between the BCAM0442/3 promoter activity in the ΔBCAM0714/5 background and that observed in either the WT or ΔBCAS0585/6 background (Fig 4.7). Conversely, while comparisons of Control vs WT and Control vs ΔBCAS0585/6 were statistically significant, there was no significant difference in the Control vs ΔBCAM0714/5 comparison (Fig 4.7). Due uncertainty surrounding this result, there is cause to further repeat these assays

in future work. Further repeats were not feasible in the course of this project due to COVID-19 restrictions forcing the cessation of lab-based research activity.

4.2.4 – A TCS-associated mechanism links copper and zinc exposure with resistance to imipenem in *B. cenocepacia*

The link between the bacterial metal response and resistance to antimicrobials has previously been discussed (section 1.2.3). As such, investigating whether these TCSs of interest had any link to how *B. cenocepacia* responds to antimicrobials was important. MIC values for *B. cenocepacia* grown overnight in different antibiotics suggest that deletion of individual TCSs does not confer susceptibility to different classes of antimicrobials (Table 4.2).

Table 4.2: 24 hour MICs of WT and single TCS deletion mutants against a range of antibiotics.

Strain	MIC (µg/ml)				
	CHL	CIP	GEN	IPM	TMP
WT	32	2	>256	32	8
Δ0442/3	32	2	>256	32	8
Δ0714/5	32	2	>256	32	8
Δ1417/8	32	2	>256	32	8
Δ0585/6	32	2	>256	32	8

CHL – Chloramphenicol, CIP – Ciprofloxacin, GEN – Gentamicin, IPM – Imipenem, TMP – Trimethoprim.

Given that exposure of *P. aeruginosa* to copper and zinc confers resistance to carbapenems through the downregulation of the OprD porin by CopRS and CzcRS [319,320], the possible presence of a similar mechanism in *B. cenocepacia* was investigated through use of the checkerboard assay (Fig 4.8). These assays confirmed that, similarly to *P. aeruginosa*, exposure of *B. cenocepacia* to copper or zinc significantly reduces its susceptibility to imipenem. While deletion of BCAM1417/8 or BCAS0585/6 did not appear to impact this phenomenon (Data

not shown), there were significant changes in this metal-dependent enhanced imipenem resistance in the ΔBCAM0442/3 and ΔBCAM0714/5 deletion mutants. While not completely removing the ability of copper to reduce susceptibility to imipenem, deletion of BCAM0442/3 did impact the extent of this copper-dependent imipenem resistance. Conversely, deletion of BCAM0714/5 appeared to completely remove the link between zinc and imipenem resistance in *B. cenocepacia*, although the heightened susceptibility of the ΔBCAM0714/5 mutant to zinc limited the granularity of the checkerboard assay in this instance. As a result, these phenotypes were further explored by performing a 48 hour growth curve of relevant strains in the presence of specific concentrations of imipenem and metals (Fig 4.9).

As seen in Figure 4.9, while exposure of both WT and ΔBCAM0442/3 *B. cenocepacia* to 0.5 mM $CuCl_2$ reduces susceptibility to 32 µg/ml imipenem, the effect is somewhat negated in ΔBCAM0442/3. There is an equivalent reduction in susceptibility to imipenem when *B. cenocepacia* is exposed to 0.25 mM $ZnCl_2$, and though deletion of BCAM0714/5 negatively impacts this phenomenon, it does not completely remove it. The combined results of Figures 4.8 and 4.9 suggest that while BCAM0442/3 and BCAM0714/5 have a role to play in the link between imipenem susceptibility and copper and zinc respectively, they are not essential to the phenomenon. As seen in the bottom half of Figure 4.9, there was variability in the ability of WT *B. cenocepacia* to grow in 32 µg/ml imipenem. This variability appeared to correlate with different batches of imipenem, suggesting batch to batch variability in the use of this antibiotic. Interestingly, in replicates that did have WT *B. cenocepacia* slightly growing in 32 µg/ml imipenem, the ΔBCAM0714/5 deletion mutant did not grow, suggesting that while the established MICs of both strains to imipenem over 24 hours is 32 µg/ml (Table 4.2), the respective MIC over a longer time course may be higher for WT *B. cenocepacia* than it is for the ΔBCAM0714/5 deletion mutant.

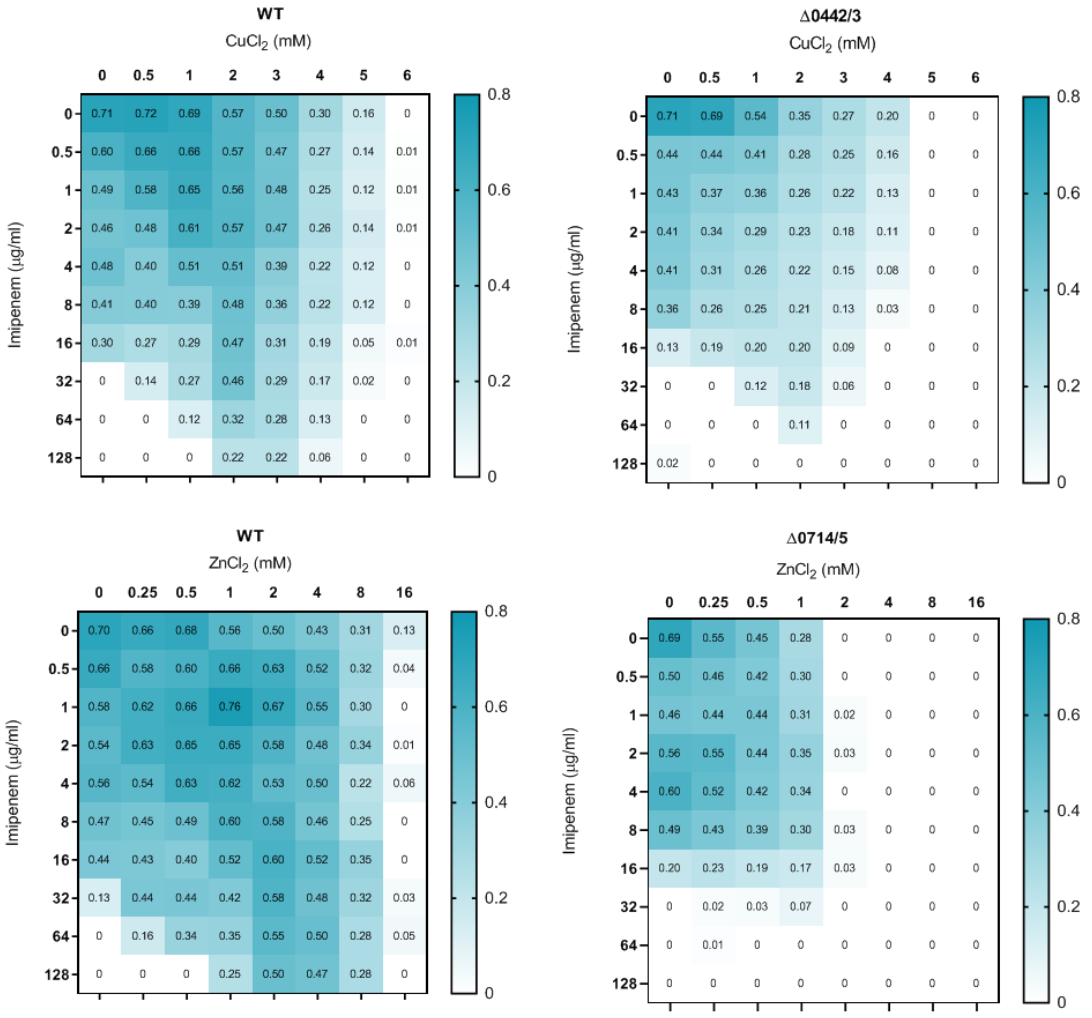

Figure 4.8: Preliminary checkerboard assays of different strains of *B. cenocepacia* grown in varying concentrations of imipenem against either copper or zinc. There is at least an eightfold increase in the imipenem MIC of *B. cenocepacia* when exposed to certain concentrations of copper or zinc. Deletion of BCAM0442/3 somewhat reduces this effect when exposed to copper, whereas deletion of BCAM0714/5 significantly inhibits this effect when exposed to zinc. Numbers shown display OD_{600} of each well with the relative blank subtracted. Blue shading is directly proportionate to OD_{600}.

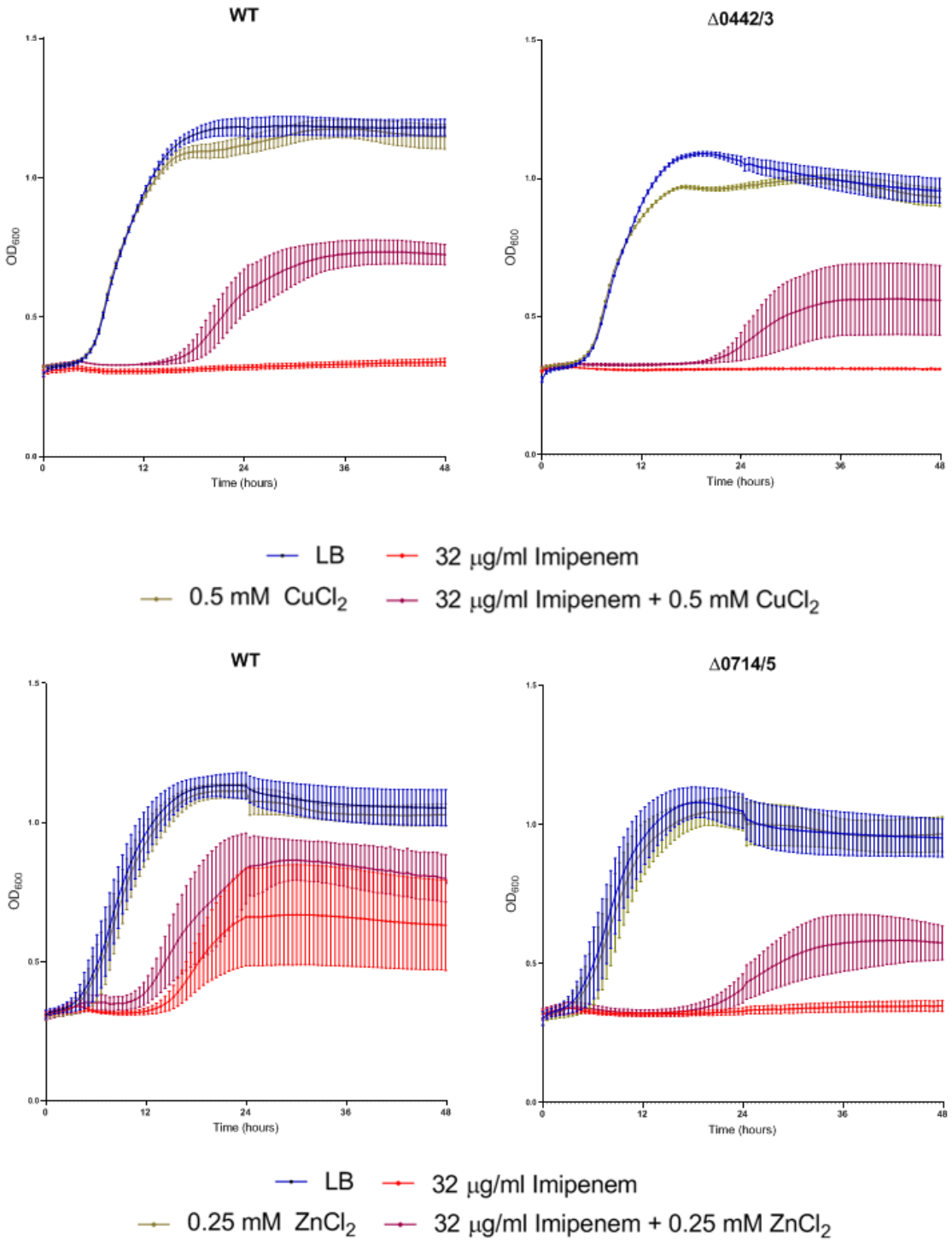

Figure 4.9: Exposure of *B. cenocepacia* to subinhibitory concentrations of copper or zinc enhances imipenem resistance. Deletion of BCAM0442/3 somewhat reduces this effect when exposed to copper, whereas deletion of BCAM0714/5 significantly inhibits this effect when exposed to zinc. n = 3 with 3 technical replicates per assay. Error bars indicate SEM.

Following on from the evidence that these TCSs are involved in enhanced resistance to imipenem, the growth kinetics of the double and triple TCS deletion mutants in imipenem were similarly investigated (Figs 4.10 and 4.11). There is a near total abolishment of the copper- and zinc-dependent enhanced imipenem resistance in the ΔBCAM0442/3 + ΔBCAM0714/5 deletion mutant, strongly suggesting that BCAM0442/3 and BCAM0714/5 interact together to aid in the facilitation of the metal-dependent enhanced imipenem resistance. Though figure 4.10 suggests that the zinc-dependent enhanced imipenem resistance is completely lost in the ΔBCAM0442/3 + ΔBCAM0714/5 mutant, preliminary checkerboard assays suggest that the effect is still present, albeit heavily diminished (Data not shown). Interestingly, whilst the metal-dependent enhanced imipenem resistance is largely abolished in the ΔBCAM0442/3 + ΔBCAM0714/5 double mutant, it is still evident in the triple deletion mutant (ΔBCAM0442/3 + ΔBCAM0714/5 + ΔBCAS0585/6). This suggests that BCAS0585/6 also has a role to play in this phenomenon, possibly acting in an opposing manner to BCAM0442/3 and BCAM0714/5.

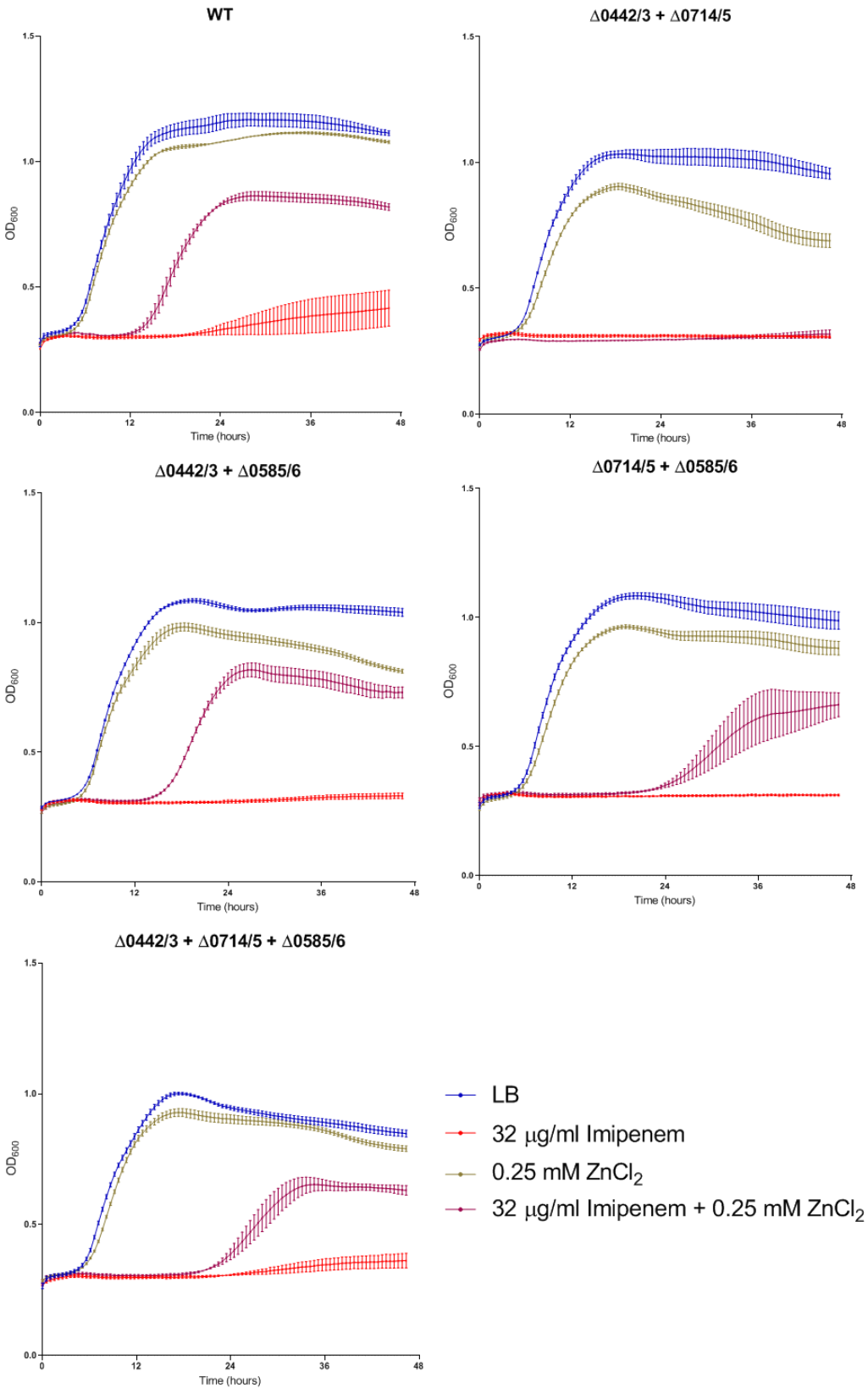

Figure 4.10: Zinc-enhanced imipenem resistance is strongly diminished in the ΔBCAM0442/3 + ΔBCAM0714/5 deletion mutant. n = 3 with 3 technical replicates per assay. Error bars indicate SEM

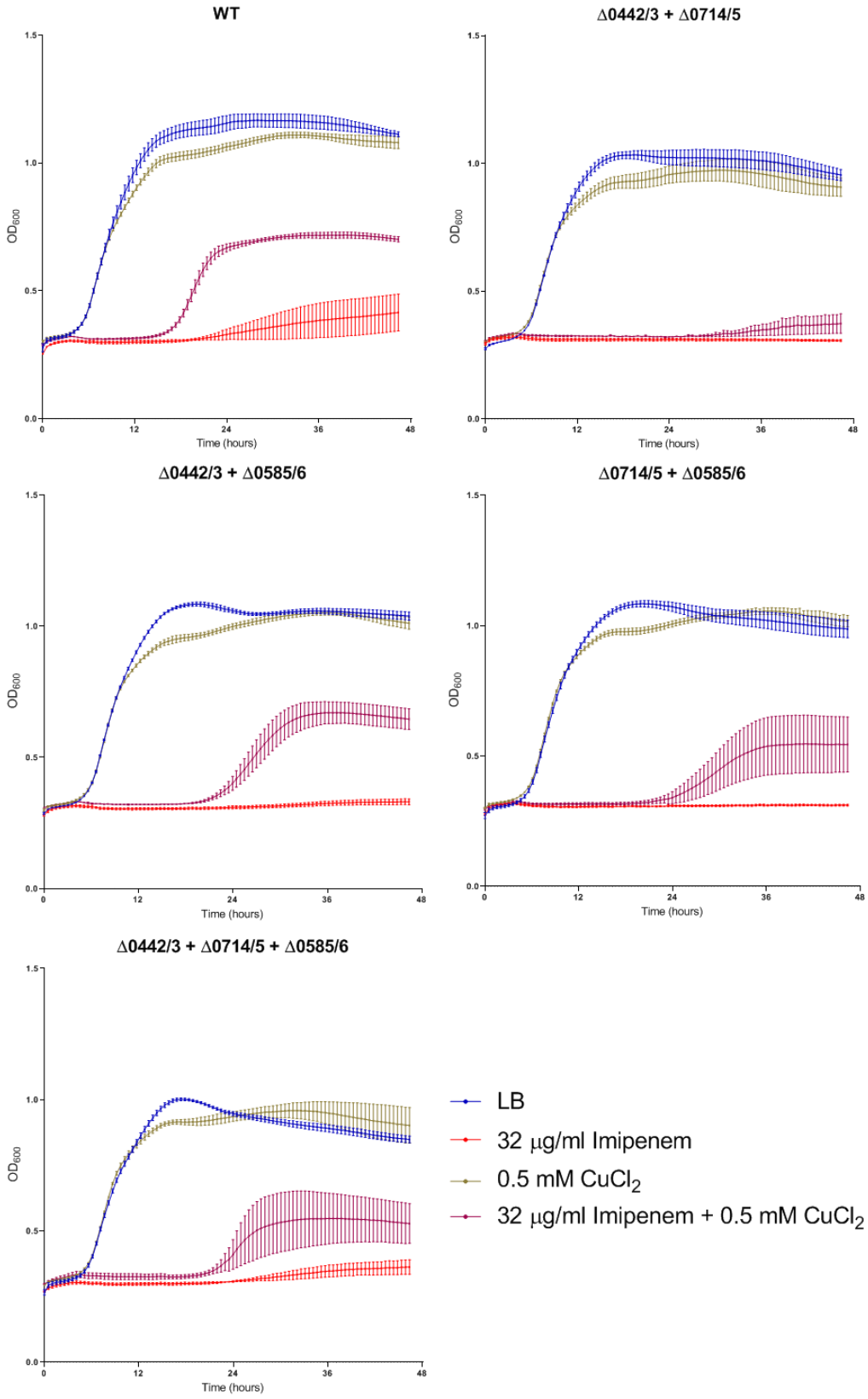

Figure 4.11: Copper-enhanced imipenem resistance is strongly diminished in the ΔBCAM0442/3 + ΔBCAM0714/5 deletion mutant. n = 3 with 3 technical replicates per assay. Error bars indicate SEM.

4.2.5 – BCAM0442/3 may be involved with biofilm formation in *B. cenocepacia*

Following on from investigations into the role of these TCSs of interest in copper- and zinc-induced resistance to imipenem in *B. cenocepacia*, the role that these TCSs may have in other virulence-associated phenotypes was investigated. The ΔBCAM0442/3 deletion mutant had a reduced ability to form biofilms, whereas deletion of any other TCS did not impact biofilm formation (Fig 4.12). However, attempts to complement this phenotype using the pDA17-derived vector containing BCAM0442/3 with its native promoter were unsuccessful (Fig 4.12).

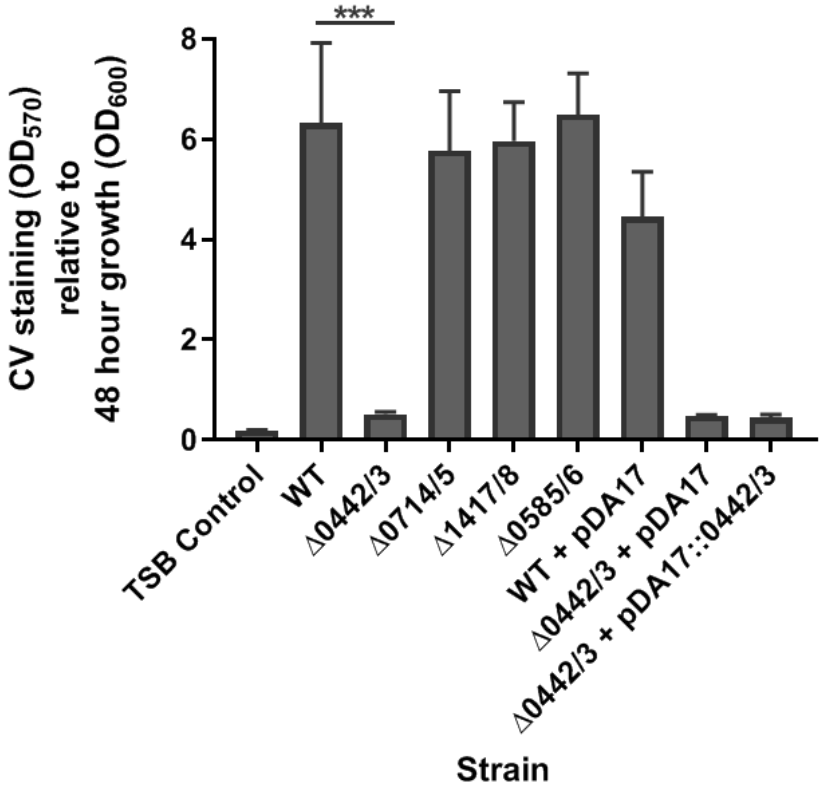

Figure 4.12: 48 hour biofilm assay of single TCS deletion mutants. ΔBCAM0442/3 has an attenuated ability to form biofilms, though attempts to complement this have been unsuccessful. Strains were grown for 48 hours on a MBEC Biofilm Inoculator 96 peg-lid, which was subsequently stained with crystal violet to quantify biofilm formation. Crystal violet staining is shown relative to growth after 48 hours. *** = $p < 0.001$, one-way ANOVA with multiple comparisons, n = 3 with 8 technical replicates per assay. Error bars indicate SEM.

Double TCS mutants were also subjected to the biofilm assay, which shows that all double TCS deletion mutants that have lost BCAM0442/3 are unable to form biofilms, appearing to suggest that BCAM0442/3 is indeed implicated in biofilm formation despite unsuccessful complementation (Fig 4.13). However, during the mutagenesis process for the double TCS deletion mutants, the successful BCAM0442/3-lacking mutants that were generated all stemmed from the original ΔBCAM0442/3 deletion mutant (Fig 4.4). As such, if an undesired mutation in the original ΔBCAM0442/3 deletion mutant was the cause of the attenuation in biofilm formation ability, that same mutation would be present in these double TCS deletion mutants. This also means that the ΔBCAM0442/3 + ΔBCAM0714/5 + ΔBCAS0585/6 triple deletion mutant would also be affected by this issue, and would presumably be attenuated in its ability to form biofilms. As such, it is currently unclear whether BCAM0442/3 has a role to play in biofilm formation in *B. cenocepacia*.

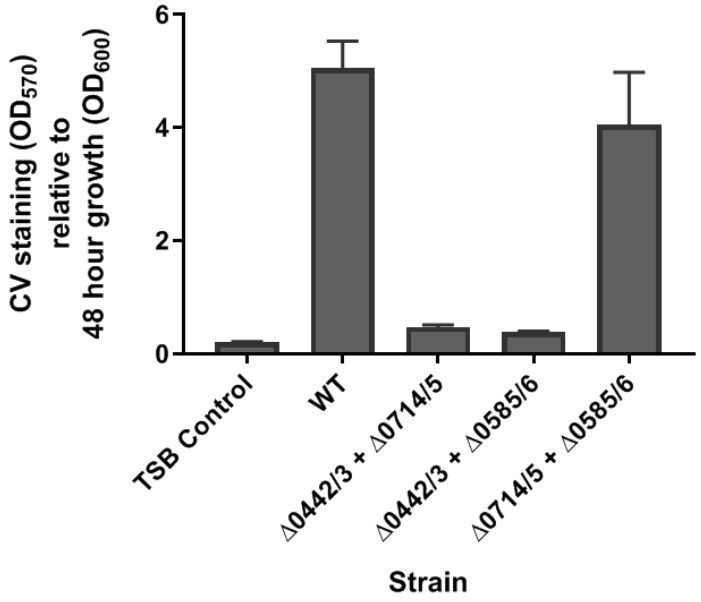

Figure 4.13: 48 hour biofilm assay of double TCS deletion mutants. All double TCS deletion mutants stemming from the original ΔBCAM0442/3 mutant have attenuated abilities to form biofilms. Strains were grown for 48 hours on a MBEC Biofilm Inoculator 96 peg-lid, which was subsequently stained with crystal violet to quantify biofilm formation. Crystal violet staining is shown relative to growth after 48 hours. n = 3 with 8 technical replicates per assay. Error bars indicate SEM.

4.2.6 – The metal-sensing MKN is important for virulence in *G. mellonella*

Given their simplicity and ease of use, the *G. mellonella* greater wax moth larva is a useful model organism for the investigation of bacterial virulence, and as such was utilised to investigate potential virulence phenotypes for each TCS deletion mutant of interest. The virulence of WT *B. cenocepacia* was consistent throughout the assays, with 0 % larvae survival beyond 48 hours (Fig 4.14). Contrastingly, both ΔBCAM0442/3 and ΔBCAM1417/8 displayed attenuated virulence in *G. mellonella* (Fig 4.14). Attempts to complement this virulence phenotype of ΔBCAM0442/3 have been unsuccessful (Fig 4.15). There is an evident fitness cost for *B. cenocepacia* in harbouring the pDA17 vector, as can be seen by the reduced virulence of WT *B. cenocepacia* carrying pDA17 (Fig 4.15).

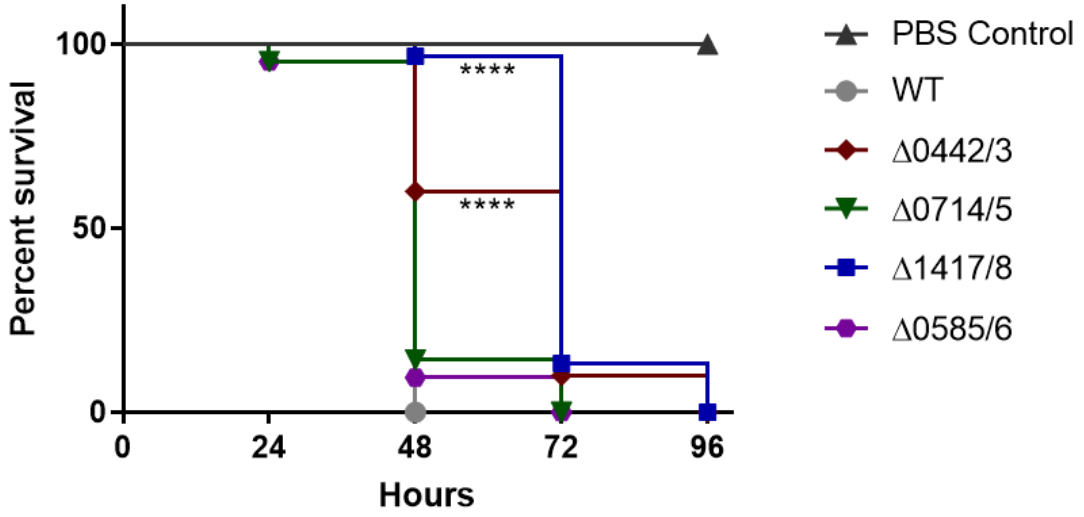

Figure 4.14: Virulence of WT and single TCS deletion mutants in *G. mellonella*. Both ΔBCAM0442/3 and ΔBCAM1417/8 display attenuated virulence in *G. mellonella* larvae. **** = $p < 0.0001$ log-rank (Mantel-Cox) test for comparison of WT and ΔBCAM0442/3 and WT and ΔBCAM1417/8 survival curves. n = 3 with 10 technical replicates per assay.

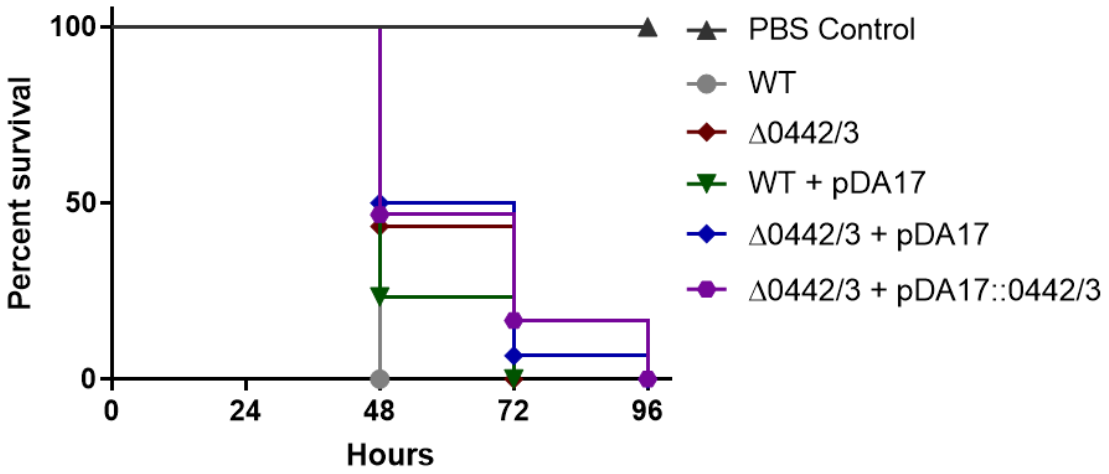

Figure 4.15: Attempts to complement the *G. mellonella* virulence phenotype of ΔBCAM0442/3. There is an observable cost to virulence when *B. cenocepacia* harbours the pDA17 vector. There is no observable complementation of the virulence phenotype of ΔBCAM0442/3. n = 3 with 10 technical replicates per assay.

Similarly to the single TCS deletion mutants, the virulence phenotypes of the double and triple TCS deletion mutants were investigated. Unsurprisingly, the deletion mutants lacking BCAM0442/3 all display attenuation in their virulence in *G. mellonella*, whereas the ΔBCAM0714/5 + ΔBCAS0585/6 deletion mutant shows only a mild reduction in virulence (Fig 4.16). Interestingly, the ΔBCAM0442/3 + ΔBCAM0714/5 + ΔBCAS0585/6 deletion mutant, i.e. a deletion mutant of the entire metal-sensing MKN, shows a stark attenuation in virulence, with 27 % of larvae surviving beyond 96 hours post-infection (Fig 4.16). This reduction in virulence in the triple TCS deletion mutant is stronger than in any of the double TCS deletion mutants, suggesting that despite the inability to complement the virulence phenotype of ΔBCAM0442/3, this MKN is indeed associated with virulence in *B. cenocepacia* (Fig 4.16).

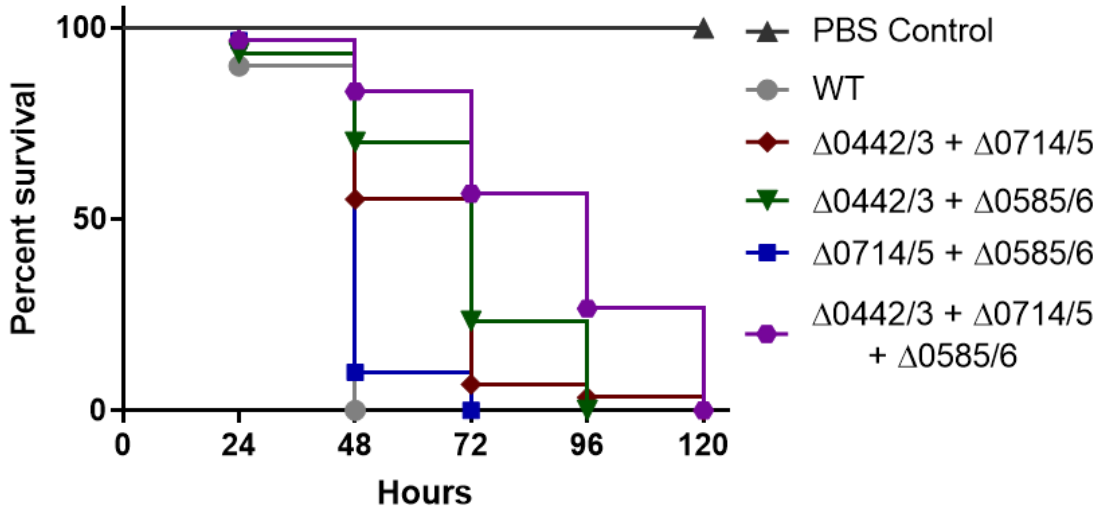

Figure 4.16: Virulence of double and triple TCS deletion mutants in *G. mellonella*. There is a stark attenuation in virulence of the ΔBCAM0442/3 + ΔBCAM0714/5 + ΔBCAS0585/6 deletion mutant in *G. mellonella* larvae. n = 3 with 10 technical replicates per assay.

4.2.7 – Investigation of intracellular survival of *B. cenocepacia* TCS deletion mutants within murine macrophages

Intracellular survival of bacteria within eukaryotic cells is commonly assessed through the gentamicin protection assay, which utilises the poor permeability of eukaryotic cells to gentamicin to kill extracellular bacteria without affecting bacteria that have been internalised by the cell [463]. Cells can then be lysed at specific timepoints to assess for intracellular survival of the bacteria in question. For this assay, the same gentamicin-sensitive deletion mutants that were employed in section 4.2.3 were used.

During the gentamicin protection assay, macrophages were lysed at two timepoints: 2 hours and 24 hours post-infection, with bacterial recovery quantified through overnight growth of serial dilutions. Bacterial recovery at 24 hours post-infection was also normalised against that at 2 hours post-infection, which aids in viewing the data in which any variations in bacterial uptake by the J774 macrophages is normalised (Fig 4.17). The bacterial load of the extracellular media at each timepoint was also checked, showing that no extracellular bacteria

survived gentamicin treatment during the assay, confirming that any recovered bacteria from the assay originated from within the macrophage (Data not shown).

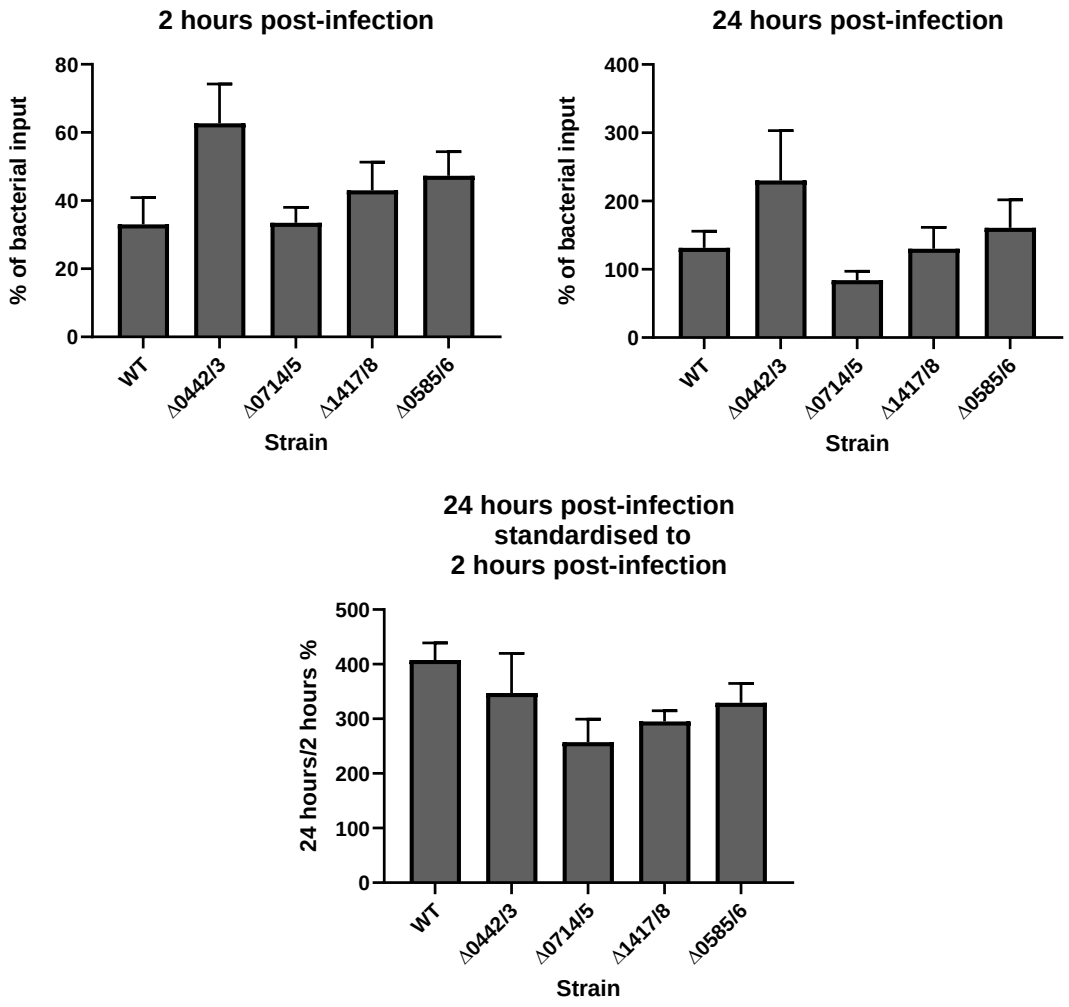

Figure 4.17: Gentamicin protection assay of WT and single TCS deletion mutants of *B. cenocepacia*. Macrophages were lysed at 2 hours and 24 hours post-infection. The bacterial recovery from 24 hours post-infection standardised to 2 hours post-infection is also shown. n = 3 with 3 technical replicates per assay.

Comparison of the bacterial recovery as a percentage of input demonstrates that greater amounts of *B. cenocepacia* are recovered at 24 hours post-infection than at 2 hours. While statistical analysis using a one-way ANOVA did not find any significant differences in bacterial recovery between strains at either 2 hours or 24 hours post-infection, there does appear to be a consistently greater recovery of the ∆BCAM0442/3 mutant than other strains. It is unclear why this may be the case, however standardising the bacterial recovery at 24 hours post-infection to the bacterial recovery at 2 hours post-infection suggests that the replication of the ∆BCAM0442/3 mutant between timepoints is no different to that of other strains. It may be possible that there is a difference either in uptake of these strains by J774 macrophages, or that the ∆BCAM0442/3 mutant is able to adapt more quickly in the initial stages of infection than other strains. Additionally, though not statistically significant, standardising bacterial recovery from 24 hours post-infection against 2 hours post-infection suggests a mild reduction in bacterial recovery from certain strains, particularly the ΔBCAM0714/5 and ΔBCAM1417/8 deletion mutants (Fig 4.17).

4.3 – Discussion

The work presented in this chapter focused on the generation and phenotypic characterisation of unmarked deletion mutants of each TCS of this metal-sensing MKN. Investigation of the sensitivity of these deletion mutants to a range of heavy metals revealed that ΔBCAM0442/3 was sensitive to copper, whereas as previously described, ΔBCAM0714/5 was sensitive to cadmium and zinc (Fig 4.5) (Robinson *et al*., Unpublished data). The metal-sensitivity phenotypes of these two TCSs were successfully complemented via use of the pDA17-derived expression vector containing the TCS genes downstream of their presumed promoter region (Fig 4.5). Conversely, ΔBCAM1417/8 and ΔBCAS0585/6 displayed no observable differences in their sensitivity to any of the heavy metals tested (copper, cadmium, zinc, cobalt and silver) compared to WT *B. cenocepacia*. None of the deletion mutants that had lost multiple TCSs had any additional sensitivity to any of the metals tested (Table 4.1). These metal phenotypes were supported by investigation of the induction of putative promoter regions via transcriptional fusion to *gfp*, which revealed induction of the BCAM0442/3 promoter by copper, and induction of the BCAM0714/5 promoter by cadmium and zinc (Fig 4.7). Induction of BCAM0442/3 in response to copper and BCAM0714/5 in response to cadmium and zinc is BCAM0442/3-dependent and BCAM0714/5-dependent respectively (Fig 4.7).

If cross regulation occurred between these TCSs in response to the metals tested, either at the protein-protein or at the transcriptional level, one may expect promoter induction to be influenced in various TCS deletion mutants. Though not fully clear from the data presented, there may be a reduction in the induction of the BCAM0442/3 promoter in response to copper in the ΔBCAM0714/5 deletion mutant, suggesting that BCAM0714/5 has a role to play in the regulation of BCAM0442/3 (Fig 4.7). Given the evidence presented in Chapter 3 that the BCAM0715 SK has the greatest propensity for non-cognate phosphotransfer, it may be that BCAM0715 can directly phosphorylate the RR BCAM0443 in response to copper, enhancing the transcriptional activation of its downstream regulon. Though there is no evidence presented in this chapter for copper-dependent activation of BCAM0714/5, section 5.2.5 explores the activation of the BCAM0714/5 genomic neighbourhood in response to copper, which may serve

as some evidence that BCAM0714/5 does indeed respond to copper. If this non-cognate phosphorylation of BCAM0443 by BCAM0715 is indeed physiologically relevant *in vivo*, it may be expected that the BCAM0443 promoter would also be induced in response to cadmium and zinc, both of which activate BCAM0714/5. However, in the presence of cadmium or zinc, the BCAM0442 SK is not activated, and would therefore presumably be acting as a phosphatase to BCAM0443, countering any non-cognate phosphorylation of the RR by BCAM0715. This phosphatase activity would not occur in the presence of copper, as the SK BCAM0442 would be activated and therefore be primarily phosphorylating BCAM0443.

Given that BCAM0442/3 and BCAM0714/5 have clear links to the metal response, it is interesting that the remaining two TCSs do not, particularly in the case of BCAS0585/6, which is a clear part of this putative MKN as described in Chapter 3. It is important to note that though deletion of BCAM1417/8 or BCAS0585/6 does not confer observable sensitivity to the metals tested, this does not eliminate the possibility that these TCSs are involved in the response of *B. cenocepacia* to these metals in some way. It is possible that a TCS can be involved in the response to a particular metal, either through direct sensing of the metal or through regulation by a separate metal-responsive element, without a deletion mutant of that TCS necessarily being sensitive to that metal. As such, though there is no observable evidence that BCAM1417/8 or BCAS0585/6 are involved in the metal response, this possibility cannot be fully excluded. Indeed, despite the lack of empirical evidence, both TCSs (particularly BCAS0585/6) show significant homology to previously characterised metal-sensing TCSs. For example, out of all the TCSs in *B. cenocepacia*, the amino acid similarity of BCAS0585/6 to CopRS from *P. aeruginosa* is the greatest (34 % similarity between the SK BCAS0585 and CopS, and 65 % similarity between the RR BCAS0586 and CopR) [146]. Despite this similarity and the high level of specificity residue similarity between BCAS0585/6 and BCAM0442/3 and BCAM0714/5 (Fig 1.6), there is no other evidence to suggest that BCAS0585/6 is metal sensing. For example, there are no clear metal-binding sites on the periplasmic domain of the SK BCAS0585, such as the ExxE iron-binding motif and the CxxC copper-binding motif [146].

As the potential role of BCAM1417/8 and BCAS0585/6 in the metal response remains unknown, different possibilities exist surrounding their role in *B. cenocepacia*. Interestingly, both BCAM1417/8 and BCAS0585/6 are located next to an RND-family efflux pump, perhaps suggesting that these TCSs are involved in the extrusion of a substance from the cell. Given that both BCAM0442/3 and BCAM0714/5 regulate genes in their immediate proximity (see Chapter 5), it may also be the case that BCAM1417/8 and BCAS0585/6 regulate their neighbouring RND-family efflux pump (BCAM1419-21 and BCAS0582-4 respectively). The inner membrane component of both of these efflux pumps is annotated with 'AcrB/AcrD/AcrF family, Interpro Accession IPR001036' on the *Burkholderia* genome database, an annotation which is shared by the inner membrane component of the CzcCBA efflux pump [18]. Interestingly, while CzcA is annotated with 'Heavy metal efflux pump: CzcA family, Interpro Accession IPR004763', there is no annotation on the BCAM1419-21 or BCAS0582-4 efflux pump that is suggestive of a role in metal extrusion [18].

The inner membrane components AcrB, AcrD and AcrF from *E. coli* are implicated in the efflux of multiple antibiotics from the cell, which given their annotation, may in turn implicate these *B. cenocepacia* efflux pumps in the resistance to antimicrobials [464]. However, though previous investigations of RND-family efflux pumps in *B. cenocepacia* implicated several in the extrusion of antimicrobials, no evidence was found for either BCAM1419-21 or BCAS0582-4 being involved in the extrusion of antimicrobials in *B. cenocepacia* [147,148]. Additionally, a screen of single TCS deletion mutants against a range of antibiotics in this work revealed no observable reduction in antibiotic MIC, potentially arguing against a link between these TCSs are antibiotic resistance (Table 4.2). However, the deletion of a TCS does not equate to the deletion of the efflux pump; it is feasible that these pumps can still be functionally regulated without the presence of the neighbouring TCS. As such, one future direction to investigate these TCSs may be to delete the BCAM1419-21 and BCAS0582-4 pumps both alone and alongside their neighbouring TCSs, allowing the direct comparison between antibiotic MICs of these deletion mutants.

The evidence for a link between metal exposure and enhanced resistance to imipenem in *B. cenocepacia* presented here further reinforces the connection between heavy metals and antimicrobial resistance as discussed previously

(section 1.2.3). This is the first time that bacterial metal-dependent enhanced imipenem resistance has been demonstrated outside of *P. aeruginosa*, perhaps suggesting that this phenomenon is more prevalent across proteobacteria than previously thought. Given the use of carbapenems in the clinic, the growing use of copper as an antimicrobial surface in the clinic and the use of other metals, such as zinc, in medical devices, the link between metals and carbapenem resistance should be further explored. This includes both further characterisation of this phenomenon in *P. aeruginosa* and *B. cenocepacia* and exploring whether metal-dependent enhanced imipenem resistance exists in other clinically-relevant bacteria.

In terms of *B. cenocepacia*, it is clear that both BCAM0442/3 and BCAM0714/5 have a role to play in this metal-dependent enhanced imipenem resistance, though the specific mechanisms at play are unclear. As the ΔBCAM0442/3 + ΔBCAM0714/5 deletion mutant has the lowest (though not totally abolished) growth in imipenem supplemented with copper or zinc, it is suggestive of these two TCSs being critical players in this phenomenon. This is in parallel with previous studies in *P. aeruginosa*, in which the CzcRS and CopRS TCSs are both implicated in enhanced resistance to imipenem [320]. Whether, as in *P. aeruginosa*, this resistance is mediated through the downregulation of an outer membrane porin is unknown. It has been shown that CzcR can directly regulate OprD through regulation of its promoter in *P. aeruginosa*, though whether CopR similarly directly regulates OprD or indirectly regulates OprD through an intermediary mechanism is unknown [320,438]. These possibilities are also present for BCAM0442/3 and BCAM0714/5 in *B. cenocepacia*, however it is clear that the presence of these two TCSs are not essential for this phenomenon, as metal-dependent resistance can still occur in the ΔBCAM0442/3 + ΔBCAM0714/5 + ΔBCAS0585/6 (see section 5.2.6 for a discussion on the transcriptional regulation of outer membrane porins in response to copper in *B. cenocepacia*).

It is of particular interest that the triple deletion mutant ΔBCAM0442/3 + ΔBCAM0714/5 + ΔBCAS0585/6, that is a deletion mutant of the entire putative MKN, shows greater levels of growth in imipenem supplemented with copper or zinc than the ΔBCAM0442/3 + ΔBCAM0714/5 deletion mutant. Though the single ΔBCAS0585/6 deletion mutant did not show any differences in this metal-dependent enhanced imipenem resistance relative to the WT (Data not shown),

the growth of the triple TCS deletion mutant suggests that BCAS0585/6 is somehow involved in this phenomenon. It may be that in the presence of BCAM0442/3 and BCAM0714/5, any impact that the loss of BCAS0585/6 has on this phenomenon is unobservable, however when BCAM0442/3 and BCAM0714/5 are not present (i.e. in the ΔBCAM0442/3 + ΔBCAM0714/5 deletion mutant), the presence of BCAS0585/6 acts to inhibit this phenomenon, again either through direct regulation of an outer membrane porin or acting via an intermediary mechanism. Evidence for regulators of this phenomenon outside of CopR and CzcR exists in *P. aeruginosa*; the MexT transcriptional regulator, which usually positively regulates an antimicrobial resistance-linked efflux pump, negatively regulates OprD, while the RNA chaperone Hfq is important for the regulation of OprD by both CzcR and CopR [320,436,465]. It is clear that this MKN has a role in the resistance of *B. cenocepacia* to carbapenems, though as in *P. aeruginosa*, the precise mechanisms by which this occurs remain unclear, and there are likely to be additional regulators of this phenomenon existing outside of this metal-sensing MKN.

Following on from the investigation of the link between this metal-sensing MKN and imipenem resistance, the role that these TCSs hold in various other cellular processes was examined. ΔBCAM0442/3, and double deletion mutants that have also lost BCAM0442/3, were heavily attenuated in their ability to form biofilms, however attempts to complement this phenotype with the pDA17-derived vector were unsuccessful (Figs 4.12 and 4.13). While the notion that all deletion mutants that have lost BCAM0442/3 are attenuated in biofilm formation ability supports the notion that BCAM0442/3 has a role to play in biofilm formation, the nature of the mutagenesis process led to both ΔBCAM0442/3 + ΔBCAM0714/5 and ΔBCAM0442/3 + BCAS0585/6 deletion mutants being generated from the ΔBCAM0442/3 single deletion mutant (Fig 4.4). As such, it is difficult to be confident in the idea that BCAM0442/3 is involved in biofilm formation, as if an undesired mutation that led to loss of biofilm formation occurred in the mutagenesis process during the generation of ΔBCAM0442/3, this undesired mutation will be present in the subsequent double and triple mutants as well.

The impact that deletion of these TCSs has on virulence was investigated through use of the *G. mellonella* larvae model. This revealed an attenuation in virulence in both ΔBCAM0442/3 and ΔBCAM1417/8 (Fig 4.14). While the presence of

pDA17 did appear to confer a fitness cost to *B. cenocepacia*, attempts to complement the virulence phenotype of ΔBCAM0442/3 were also unsuccessful (Fig 4.15). Interestingly, the ΔBCAM0442/3 + ΔBCAM0714/5 + ΔBCAS0585/6 deletion mutant was considerably more attenuated in their virulence than any other deletion mutant, providing strong evidence that this MKN is linked to virulence in *B. cenocepacia* (Fig 4.16). The reason for a link between metal-sensing TCSs and virulence is unknown, though this has previously been demonstrated in *P. aeruginosa*, as a CzcRS deletion mutant is attenuated in virulence in a *C. elegans* model [438]. The authors postulate that this is due to the positive regulation that CzcR has on quorum sensing in *P. aeruginosa*, which is an important factor in bacterial virulence [438]. However, previous work established that there is no observable quorum sensing phenotype in a ΔBCAM0714/5 deletion mutant (Robinson *et al*., Unpublished data), suggesting that this TCS is not associated with quorum sensing in *B. cenocepacia*. As BCAM0714/5 is part of a wider metal-sensing MKN, the role that BCAM0442/3 and BCAS0585/6 have in quorum sensing in *B. cenocepacia* should be further investigated, as the possibility that this MKN is associated with quorum sensing cannot be excluded. As outlined in Chapter 5, there is no clear induction of quorum sensing genes in *B. cenocepacia* in response to copper, perhaps arguing against a role for BCAM0442/3 in quorum sensing. Given that these metal-sensing TCSs are implicated in virulence, it would also be of interest to investigate whether exposure of *B. cenocepacia* to metals of interest, such as copper and zinc, affects virulence in *G. mellonella* larvae.

Given the manipulation of metal availability by the immune system in killing internalised bacteria (section 1.2.4), the link between these TCSs and survival within murine macrophages was explored via the use of the gentamicin protection assay. As such, gentamicin-sensitive single TCS deletion mutants were generated. Two timepoints were performed for processing of macrophages in the gentamicin protection assay: 2 hours and 24 hours post-infection. Comparison of bacterial recovery between these timepoints clearly demonstrates that *B. cenocepacia* can replicate within J774 murine macrophages (Fig 4.17), supporting previous studies that have demonstrated both *B. cenocepacia* and *B. multivorans* replicating within macrophages [206,208,466]. There was no statistically significant difference in bacterial recovery between these timepoints, nor when

comparing the level of bacterial recovery at the 24 hours post-infection standardised to 2 hours post-infection.

While any difference between strains did not reach the threshold for statistical significance, there does appear to be a mild reduction in bacterial recovery for several gentamicin-sensitive deletion mutants, particularly ΔBCAM0714/5, relative to the WT when standardising bacterial recovery from 24 hours post-infection against 2 hours post-infection (Fig 4.17). As this particular analysis of the data controls for any potential difference in bacterial uptake by the macrophages, any difference between strains may suggests an overall reduction in replication ability within macrophages. Given the range of toxic insults that internalised bacteria can be exposed to within the macrophage, it is unclear as to what role metal toxicity, i.e. the influx of copper and/or zinc into the phagolysosome, has to play in the killing of internalised *B. cenocepacia* cells. However, if the manipulation of metal availability in the phagolysosome is indeed a key part of killing of internalised *B. cenocepacia*, it may be that this metal-sensing MKN has some role to play in the survival of *B. cenocepacia* within macrophages. Though there was no significant difference between the single TCS deletion mutants in the gentamicin protection assay, it may be the case that double or triple deletion mutants would harbour a much greater difference in survival relative to the WT. Given the already established links between these TCSs, deletion of a single TCS may not be enough to see any observable reduction in bacterial survival, as the detoxification systems that are presumably regulated by these systems may be induced by more than one TCS. As such, the generation and characterisation of gentamicin-sensitive double and triple TCS deletion mutants should be considered, which may give a clearer picture of the role of this metal-sensing MKN in the intracellular survival of *B. cenocepacia*.

So far, the characterisation of this MKN has focused on the use of deletion mutants of each TCS, i.e. of both SK and cognate RR. The generation and characterisation of deletion mutants of the individual SK and RR proteins may reveal new insight into the functions and connections of these TCSs. For example, if the copper sensitivity phenotype of ΔBCAM0442/3 was still present in a ΔBCAM0442 deletion mutant then this would argue that activation of the regulon of BCAM0442/3 is dependent on the presence of the SK BCAM0442, i.e. that the RR BCAM0443 is not activated by any other agent in response to copper.

It would also be of benefit to assess the induction of the promoters of interest in pGA-G1 promoter vectors within these mutants. For example, is the presence of the BCAM0442 SK essential for induction of the BCAM0442/3 promoter in response to copper, or can another agent activate the BCAM0443 RR? Coupling the characterisation of single SK and single RR deletion mutants with the mutants generated within this work would provide a fuller picture of the hierarchy and connections of the proteins within this MKN.

4.4 – Conclusions

- Characterisation of TCS deletion mutants implicates BCAM0442/3 in the copper response and confirms the implication of BCAM0714/5 in the cadmium and zinc response.
- Exposure of *B. cenocepacia* to subinhibitory copper or zinc enhances resistance to imipenem. This mechanism appears to be closely associated with this metal-sensing MKN.
- There is evidence to suggest that this MKN is associated with both biofilm formation and virulence in *B. cenocepacia*, though complementation of these phenotypes has not been achieved.

Chapter 5: RNA-seq analysis of the copper response of *B. cenocepacia*

5.1 – Introduction

Given the evidence presented in earlier chapters that the cadmium/zinc and copper responses of *B. cenocepacia* are linked, exploring the transcriptomic profile of the bacterial response to different metals is of interest. As the transcriptomic response of WT and ΔBCAM0714/5 strains of *B. cenocepacia* K56-2 to zinc has previously been investigated (Robinson *et al*, Unpublished data), and as there has been no study that has investigated the transcriptomic response of *B. cenocepacia* to copper, this chapter aimed to utilise RNA-seq to assess the response of WT and ΔBCAM0442/3 *B. cenocepacia* K56-2 to copper.

Firstly, this analysis would allow the characterisation of the copper response of *B. cenocepacia*, which given the varying exposure that clinically-relevant pathogens have to copper, is of particular relevance. Additionally, comparison of the transcriptomic profiles of WT and ΔBCAM0442/3 strains would theoretically provide an indication as to what BCAM0442/3 directly regulates, and also other genes that may be indirectly affected by deletion of this TCS. Any gene that is differentially expressed in WT, but not in ΔBCAM0442/3 *B. cenocepacia*, can be thought to be regulated, either directly or indirectly, by BCAM0442/3.

While the transcriptional profile of the copper response in *B. cenocepacia* has not been previously characterised, transposon sequencing has identified several genes implicated in copper resistance [369]. This includes the BCAM0442-50 gene region, as well as the BCAM0715 and BCAS0585 SKs, potentially implicating this metal-sensing MKN in the copper response of *B. cenocepacia* [369]. Additionally, RNA-seq analysis of the copper response of *P. aeruginosa* has been performed. For example, *P. aeruginosa* grown in $CuSO_4$ had increased expression of efflux pumps and genes associated with iron homeostasis, as well as decreased expression of outer membrane porins [242]. The PA2809/10 TCS was also upregulated in response to $CuSO_4$, with subsequent further investigation confirming the role of PA2809/10 in copper homeostasis, and as such was denoted as CopRS [242]. Whether the transcriptomic profile of the copper response is similar between *B. cenocepacia* and *P. aeruginosa* is of interest, as it may provide insight into the evolutionary conservation of different strategies to withstand copper stress, and perhaps to heavy metal stress in general.

5.2 – Results

5.2.1 – Establishing conditions for bacterial growth for RNA-seq analysis

In order to assess the transcriptional profile of the copper response, it was important to select a non-lethal concentration of copper that would be sufficient to trigger the copper response, but would not trigger a larger stress response in the bacteria, and would not hamper growth. Based on growth curves (Fig 5.1), it was observed that 1 mM $CuCl_2$ did not inhibit growth of WT or ΔBCAM0442/3 *B. cenocepacia* during log phase, and was therefore considered a suitable concentration for induction of the copper response. A total growth time of 8 hours was chosen to ensure bacteria reached mid log phase prior to harvesting of RNA.

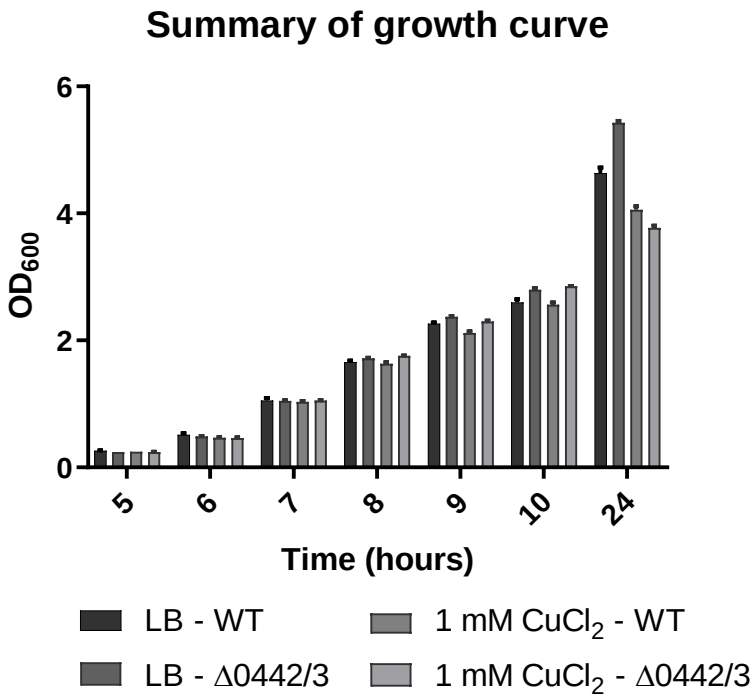

Figure 5.1: Growth of WT and ΔBCAM0442/3 *B. cenocepacia* in LB with or without 1 mM $CuCl_2$. Growth was performed in 10 ml volumes to replicate growth conditions prior to RNA harvesting. Error bars indicate SEM.

5.2.2 – Extraction of total RNA from *B. cenocepacia*

Total RNA from each replicate was extracted using the RiboPure RNA Purification Kit (Thermo Fisher Scientific). To assess quality of total RNA, samples were run on a 1 % agarose gel (Figure 5.2), and a BCC-specific PCR was performed to check for gDNA contamination (Data not shown). Total RNA samples were then analysed on a 4200 TapeStation System (Agilent). RNA integrity ratings were assigned to all samples, with samples with a rating of 8 or greater being carried forward for sequencing. The RNA extraction for sample 1 of ΔBCAM0442/3 – LB failed, and was repeated at a later date.

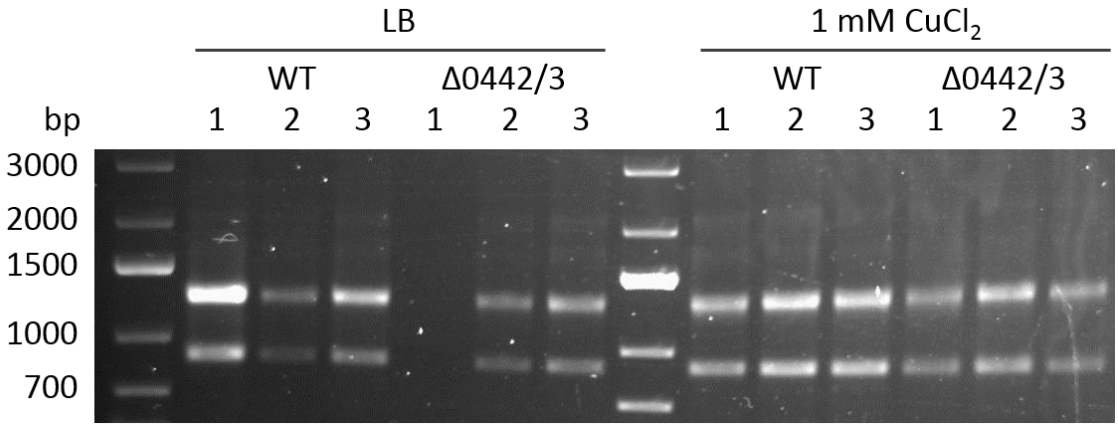

Figure 5.2: Total RNA samples run on a 1 % agarose gel. 5 µl of each sample was loaded onto the gel and run as standard. Bands indicate the presence of 23S and 16S rRNA. Due to lack of availability of an RNA-based ladder, the ladder shown is a DNA-ladder. Expected size (bp): 23S rRNA – 2876, 16S rRNA – 1531 bp.

5.2.3 – Illumina sequencing results for the *B. cenocepacia* copper response

Following sequencing and quantification of transcript levels by the Exeter Sequencing Service, replicates were clustered to assess for similarity. There is an outlier in the ∆0442/3_LB group of replicates, which does not cluster with any of the other groups (The TapeStation report can be found in Figure 5.3, while cluster analysis of replicates can be found in Figure 5.4). Interestingly, this outlier is the sample that was prepared separately to the other 11 samples due to the extraction of total RNA from a ∆0442/3_LB replicate failing. The large difference between this replicate and the remaining two raises questions surrounding why a bacterial culture grown in standard LB broth to a similar timepoint has a transcriptomic profile that is different to the remaining replicates. Nonetheless, the Δ0442/3_LB_A outlier passed all quality control checks (Fig 5.3). The remaining groups cluster well together (Fig 5.4). For all statistical analysis of the transcriptomic dataset, the ∆0442/3_LB_A outlier was included. While the presence of the outlier does reduce the number of significantly differentially expressed genes overall, the increased confidence in the data by including all three replicates warrants its inclusion. Table 5.1 lists the number of significantly differentially expressed genes in relevant comparisons of *B. cenocepacia*.

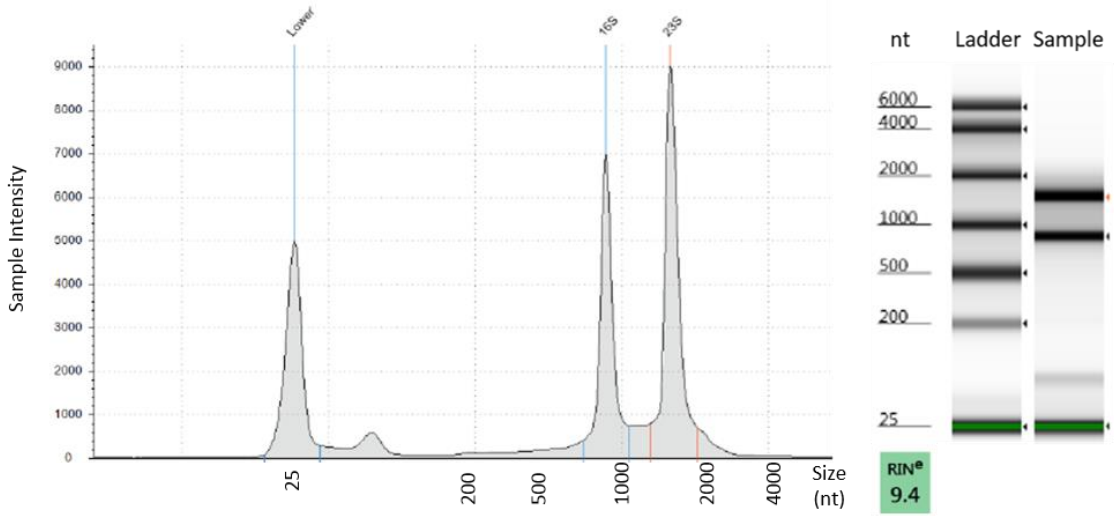

Figure 5.3: Quality of RNA for ∆BCAM0442/3 – LB #1. Left – 23S and 16S rRNA peaks alongside nucleotide markers. The 23S:16S peak area ratio serves as an indicator of RNA sample quality. In this example, the ratio is 1.4. Right – Gel displaying both 16S and 23S rRNA, alongside the RNA integrity rating of 9.4.

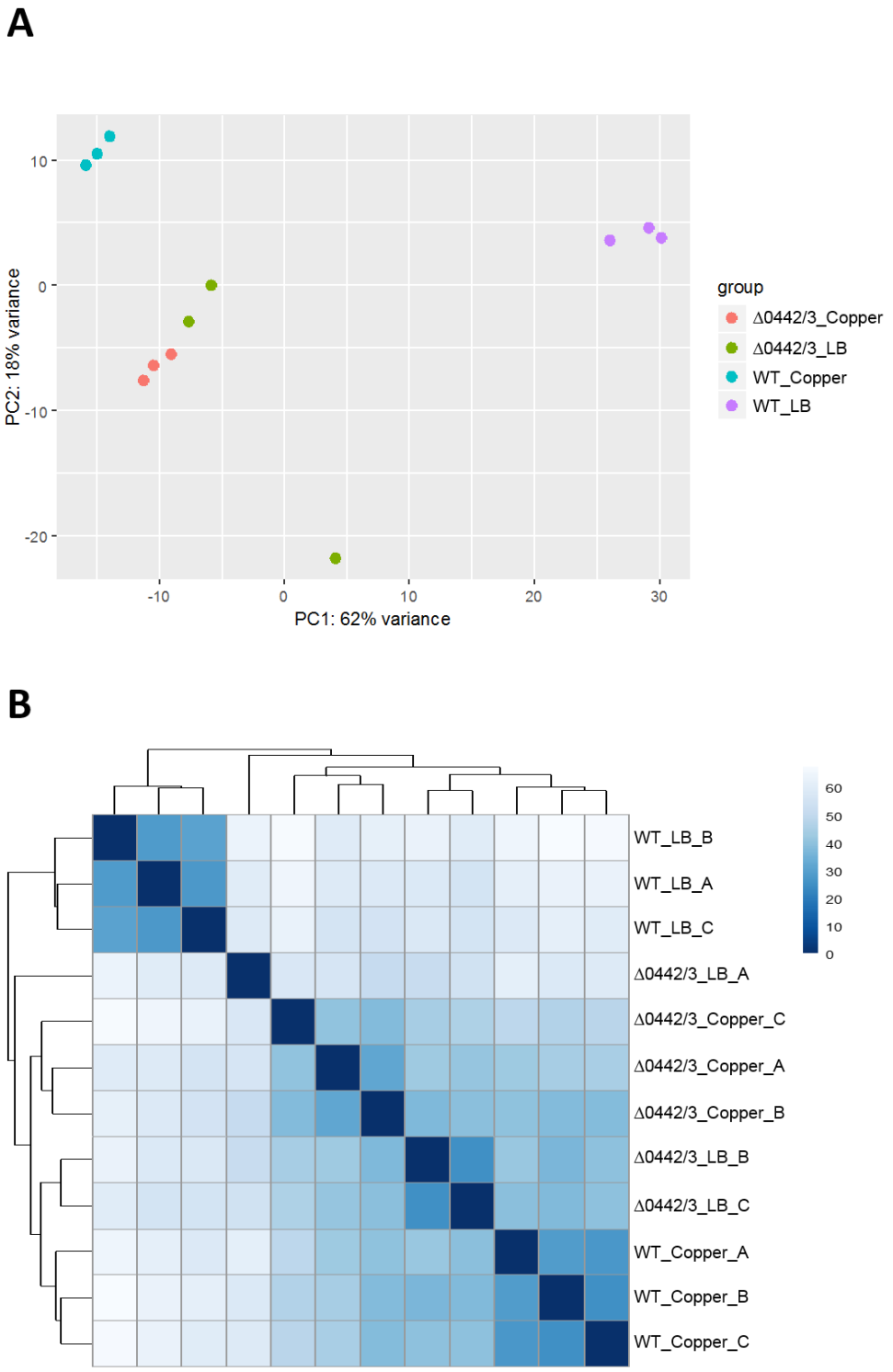

Figure 5.4: Analysis of similarity of transcriptomic replicates. A) Principal component analysis of individual samples. Each group of samples clusters well apart from 0442_LB, which contains an outlier. B) Heatmap displaying the hierarchical clustering of samples. 0442_LB_A does not cluster with its replicates, while other groups cluster together.

Table 5.1: Number of significantly differentially expressed genes of WT and ∆BCAM0442/3 *B. cenocepacia* when grown in LB with and without 1 mM $CuCl_2$.

Sample comparison	Significantly differentially regulated genes		
	Upregulated	Downregulated	Total
WT_Copper vs. WT_LB	551	551	1102
∆0442/3_Copper vs. ∆0442/3_LB	68	106	174
∆0442/3_LB vs. WT_LB	517	478	995
∆0442/3_Copper vs. WT_Copper	83	106	189

Note: Significantly differentially expressed genes are defined as having an adjusted p-value of < 0.05 and a fold change of > 2.

There is a large transcriptomic response to copper in WT *B. cenocepacia*, with 1102 out of 7125 genes/pseudogenes being significantly differentially expressed, representing 15 % of the genome. The copper response of the ∆BCAM0442/3 mutant appears more modest, though this has been negatively influenced by the outlier. Excluding the outlier from the analysis increases the total number of significantly differentially expressed genes between ∆0442/3_Copper and ∆0442/3_LB from 174 to 250, suggesting that there is a loss of granularity of the ∆BCAM0442/3 copper response due to this outlier. Surprisingly, there is also a large difference in transcriptomic profile between WT and ∆BCAM0442/3 when both are grown in LB without $CuCl_2$, suggesting that the role of BCAM0442/3 in *B. cenocepacia* extends beyond the copper response.

Out of 1102 differentially expressed genes in the WT_Copper to WT_LB comparison, 942 were successfully assigned a COG value using eggNOG-mapper v1 [467]. 175 of these COG-assigned genes were assigned as ‘function unknown’, the majority of which were annotated in the J2315 genome as ‘conserved hypothetical protein’ or as ‘putative exported/membrane protein’, while an additional 9 were ambiguously assigned two COG values. The COG values of remaining 758 differentially expressed genes can be seen in Figure 5.5.

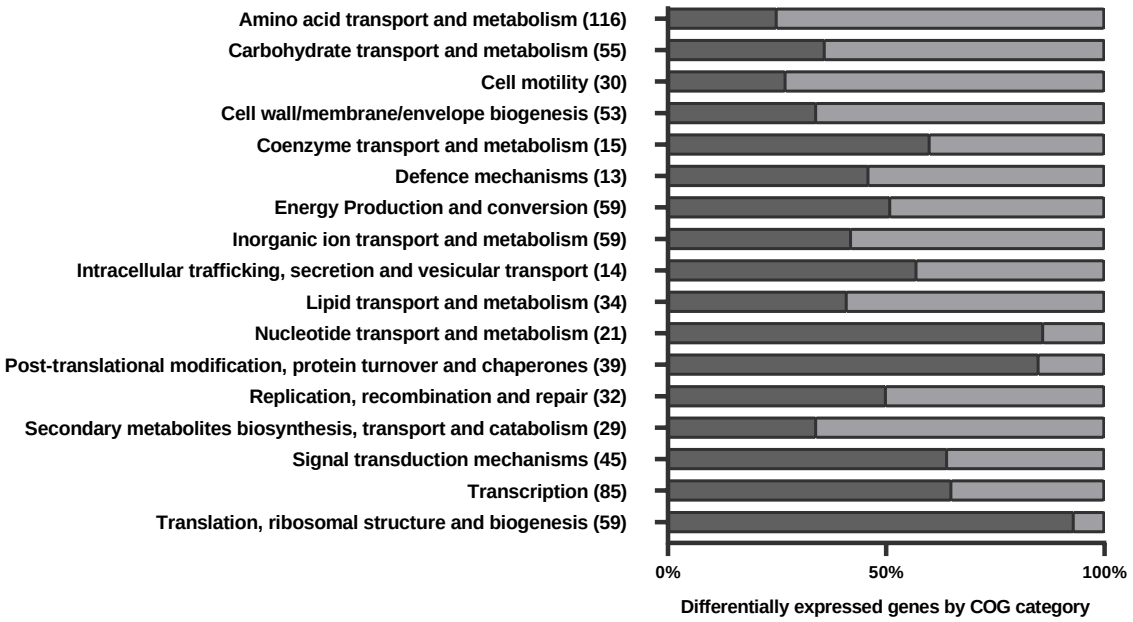

Figure 5.5: Significantly differentially expressed genes in WT *B. cenocepacia* in response to growth in LB with 1 mM $CuCl_2$ relative to growth in LB. Out of 1102 differentially expressed genes, 758 were assigned single COG values (excluding genes assigned 'Function unknown'). The number of genes in each COG category is given in brackets on the y-axis. Each bar is split into upregulated genes (dark grey) and downregulated genes (light grey), with the total number of genes in each COG category shown in brackets.

As displayed in Table 5.1, there are a large number of genes that are significantly differentially expressed in the comparison of both WT and ΔBCAM0442/3 *B. cenocepacia* grown in LB. A total of 995 genes are significantly differentially expressed, representing 14 % of the genome (Table 5.1). Removal of the Δ0442/3_LB_A outlier increases this total to 1100 genes, suggesting that the outlier is not the cause of this difference in transcriptional profile to growth in LB. Of these 995 differentially expressed genes, 669 were also significantly differentially expressed in the comparison between WT grown with and without 1 mM $CuCl_2$. Interestingly, 667 of these 669 genes were differentially expressed in the same 'direction', i.e. within these 667 genes, the genes that were upregulated were upregulated in both comparisons. Unsurprisingly, the remaining genes were BCAM0442 and BCAM0443. This similarity suggests that the transcriptional

profile of ΔBCAM0442/3 grown in LB shares particular similarity to WT *B. cenocepacia* grown in 1 mM $CuCl_2$. In other words, for *B. cenocepacia* grown in LB, deletion of BCAM0442/3 confers a copper response-like state to the bacteria. This can also be seen when comparing the COG values of differentially expressed genes between both comparisons, which presents a similar transcriptional profile of differentially expressed genes (Figures 5.5 and 5.6).

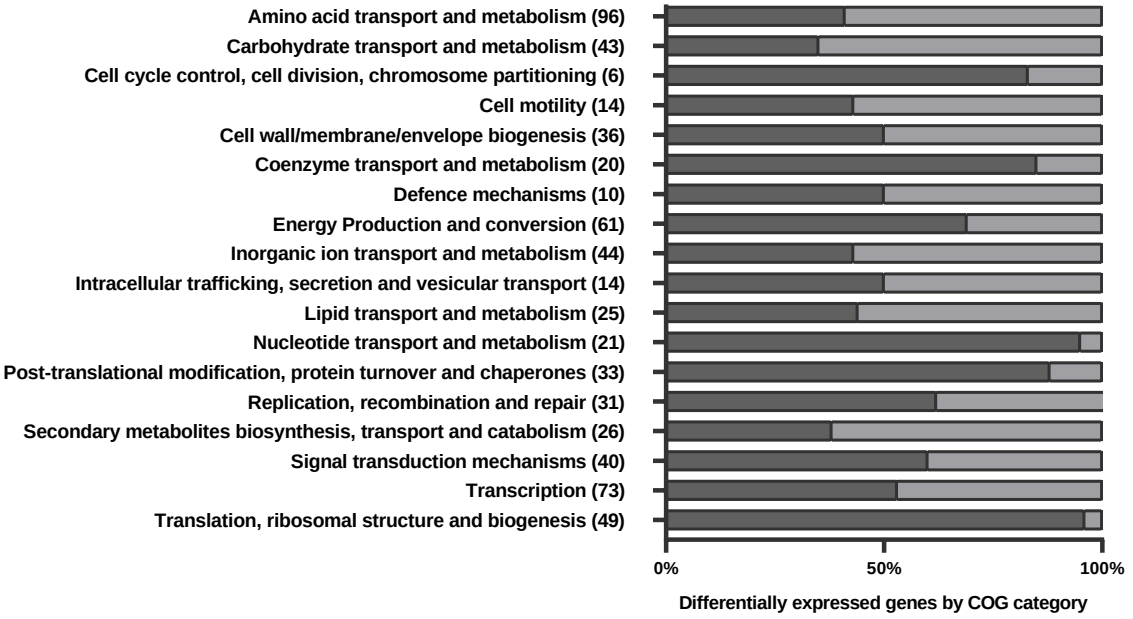

Figure 5.6: Significantly differentially expressed genes in ΔBCAM0442/3 *B. cenocepacia* in response to growth in LB relative to growth of WT *B. cenocepacia* in LB. Out of 995 genes, 814 were assigned single COG values (excluding genes assigned 'Function unknown'). The number of genes in each COG category is given in brackets on the y-axis. Each bar is split into upregulated genes (dark grey) and downregulated genes (light grey), with the total number of genes in each COG category shown in brackets.

5.2.4 – Upregulation of the BCAM0442/3 genomic neighbourhood

The genes that underwent the greatest amount of upregulation in response to copper are those that are downstream of the BCAM0442/3 TCS (Table 5.2). The

genes that are upregulated in the BCAM0442/3 gene region of WT *B. cenocepacia* can generally be split into two groups: BCAM0433-0436, which are orthologues of the CusABCF system, and BCAM0446-0450, orthologous to the Cop/PcoABCDE system (Fig 5.7).

Table 5.2: Fold changes of significantly differentially expressed genes in the neighbourhood of BCAM0442/3 in WT and ΔBCAM0442/3 *B. cenocepacia* in response to copper.

Gene name	Predicted protein function	Fold change (Copper vs LB)		Fold change (Δ0442/3 vs WT)	
		WT	Δ0442/3	LB	$CuCl_2$
BCAM0432	Hypothetical protein	1.53	1.32	1.31	1.12
BCAM0433	Outer membrane protein (CusC)	33.8	15.8	3.73	1.74
BCAM0434	Cation efflux protein (CusB)	46.5	25.5	3.25	1.78
BCAM0435	Cation efflux system (CusA)	12.4	24.9	0.75	1.51
BCAM0436	Periplasmic protein (CusF)	126.8	64.3	1.00	0.50
BCAM0437	Na^+/Ca^{2+} exchanger protein	3.01	2.14	2.03	1.44
BCAM0438	Conserved hypothetical protein	2.18	0.91	2.10	0.88
BCAM0439	Cation efflux protein	1.75	1.15	1.67	1.10
BCAM0440	Conserved hypothetical protein	0.39	1.83	0.30	1.41
BCAM0441	Major Facilitator Superfamily protein	1.38	2.99	0.52	1.12
BCAM0442	Response regulator (CopR)	21.0	1.00	0.07	0.01
BCAM0443	Sensor kinase (CopS)	33.2	1.00	0.01	0.00
BCAM0444	Hypothetical protein	1030.2	1.00	1.00	0.00
BCAM0445	Hypothetical protein	62.4	1.00	1.00	0.03
BCAM0446	Outer membrane efflux protein (CopB)	1464.7	0.24	7.00	0.00
BCAM0447	Exported multicopper oxidase (CopA)	1460.5	2.07	4.19	0.01
BCAM0448	Periplasmic protein (CopE)	1754.6	0.48	3.43	0.00
BCAM0449	Copper-resistance exported protein (CopC)	352.3	1.68	1.86	0.01
BCAM0450	Copper-resistance membrane protein (CopD)	231.3	1.00	1.00	0.01

BCAM0451	Extracellular endo/exonuclease	23.0	1.23	0.59	0.03

Note: Gene names in brackets are suggested notations based on RNA-seq and sequence analysis. Shaded cells indicate genes that are not significantly differentially expressed in that comparison. Significantly differentially expressed genes are defined as having an adjusted p-value of < 0.05 and a fold change of > 2.

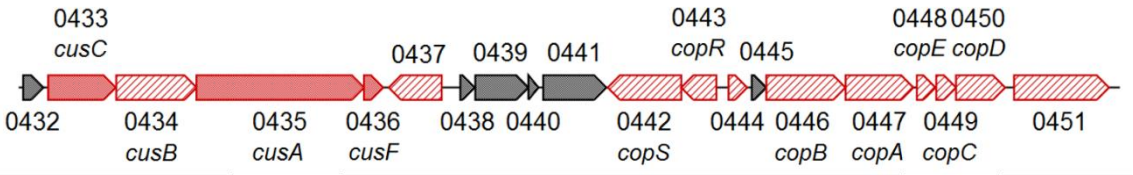

Figure 5.7: Genomic neighbourhood of BCAM0442/3. Dark red arrows denote genes significantly differentially expressed in response to 1 mM $CuCl_2$ relative to growth in unsupplemented LB in both WT and ΔBCAM0442/3 *B. cenocepacia*. Striped light red arrows denote genes significantly differentially expressed in WT but not ΔBCAM0442/3 *B. cenocepacia*. Grey arrows denote genes that are not significantly differentially expressed.

The CusABCF system in *E. coli* confers resistance to both copper and silver, consisting of an RND-family efflux pump and a periplasmic copper chaperone [343,344]. The CusABCF system in *E. coli* is regulated by the upstream CusRS TCS [468,469]. The central transport protein CusA is an inner membrane protein that complexes with CusB, the MFP, which in turn complexes with the OMF CusC, ultimately allowing the transport of copper and silver ions from the cytoplasm out to the extracellular environment [343,344,470]. CusF is a periplasmic metallochaperone that is able to bind Ag(I) and Cu(I) (but not Cu(II)) and deliver it to CusB, aiding to reduce copper and silver levels in the periplasm [344,471–473].

Parts of the BCAM0433-0436 region share significant similarity to this CusABCF system of *E. coli*; the protein sequences of BCAM0434 and BCAM0435 share 31.0 % and 62.6 % similarity to CusB and CusA respectively. In contrast, BCAM0433 shares just 17 % protein sequence similarity to CusC. This difference may be explained by the finding that, in contrast to CusA, CusB and CusF, the

crystal structure of the *E. coli* CusC has no detectable Cu(I) or Ag(I) binding sites, implying that CusC does not contribute to the substrate specificity of the CusCBA RND-family pump [474]. This may therefore allow significant variation in protein sequence of the OMF without hampering the ability of the RND pump as a whole to extrude copper or silver. This discrepancy in sequence similarity may mean that BCAM0433 in *B. cenocepacia* serves a functional purpose that CusC in *E. coli* does not, such as alteration of substrate specificity or variation in ion extrusion rate. It is also possible that an OMF of greater similarity to CusC lies elsewhere in the genome and is recruited to BCAM0434 and BCAM0435 in response to copper, however the proteins of greatest similarity to CusC in *B. cenocepacia* are not upregulated in response to copper. As such, it is likely that BCAM0433-0435 together form a CusCBA-like RND-family efflux pump.

The *E. coli* CusF shares 27 % protein sequence similarity with BCAM0436 and 22 % with BCAM0448. Both BCAM0436 and BCAM0448 are upregulated in response to copper, however BCAM0448 is upregulated much more strongly than BCAM0436 (1754.6 vs 126.8 fold change). Additionally, BCAM0448 is not upregulated in the ΔBCAM0442/3 mutant, whereas BCAM0436 is. Interestingly, BCAM0436 and BCAM0448 share 49 % protein sequence identity and are both predicted to be found in the periplasm, implying that they may share a similar function. Due to the higher sequence similarity, being within the same operon as CusCBA and also being upregulated in the ΔBCAM0442/3 mutant, it is likely that BCAM0436 fulfils the copper chaperone role in the CusABCF-like system, whereas BCAM0448 is part of a separate, BCAM0442/3-regulated system.

It is clear that the CusABCF-like system in *B. cenocepacia* is still upregulated in the ΔBCAM0442/3 mutant. While the fold change of BCAM0434 in the ΔBCAM0442/3 mutant is approximately in line with the operon as a whole, it is considered not significantly differentially expressed. This is due to the number of normalised counts for BCAM0434 in this comparison being below the threshold set in analysis, and therefore the upregulation cannot be considered significant. Despite this, it is fair to conclude that the CusABCF-like system is not directly regulated by the BCAM0442/3 TCS, and must be regulated by a separate copper-responsive system.

The Cop/Pco system of *E. coli* consists of seven proteins, Cop/PcoABCDERS. The system was originally identified on the pRJ1004 plasmid from *E. coli* isolated

from pigs fed a copper sulphate-supplemented diet, and denoted the Pco (plasmid-borne copper resistance) system [475,476]. The Pco and Cop systems are homologous, and the names can be used interchangeably (the 'Cop' notation will be used herein to refer to Cop/PcoABCDERS). CopA is a periplasmic multicopper oxidase that oxidises Cu(I) into its less toxic Cu(II) form, while CopB is an outer membrane protein channel [353,477]. CopC and CopE are periplasmic copper chaperones, whereas CopD is an inner membrane protein [477–479]. These five proteins are regulated by the CopRS TCS [344,477]. The particular interplay between these proteins within copper homeostasis is not fully clear, however expression of CopC and CopD together without the other components of the system in *Pseudomonas syringae* led to copper hypersensitivity, implicating these proteins in copper uptake [480]. Additionally, fusion proteins of CopC and CopD have been identified in Gram-positive bacteria, reinforcing the idea of their shared functional aim [481]. It therefore may be the case that CopC and CopD play a role in import of copper into the cell, while CopA, CopB and CopE ensure that potentially harmful excess copper is sequestered and extruded from the cell.

The BCAM0446-0450 gene region is heavily expressed in response to copper in the WT, and contains proteins of predicted function similar to those found in the CopABCDE system. There are two membrane channels, one in the outer membrane (BCAM0446), and one in the inner membrane (BCAM0450), that are similar to CopB and CopD respectively. BCAM0447 is a periplasmic multicopper oxidase, BCAM0448 shares 49 % protein similarity to BCAM0436 (CusF) and BCAM0449 also may sit in the periplasm, making these genes candidates for the respective roles of CopA, CopC and CopE. Unlike the CusABCF system, there is no great protein sequence similarity between the *E. coli* CopABCDE genes and BCAM0446-0450. CopC shares 34 % similarity to BCAM0449, with the second greatest similarity being between CopD and BCAM0450 at 22 %. Nonetheless, given that the predicted function of the genes is similar to that of other CopABCDE systems, their proximity to each other in the genome and strong upregulation in response to copper, it is reasonable to conclude that these five genes form a CopABCDE-like system in *B. cenocepacia*.

It is clear from Table 5.2 that while the CusABCF-like system is still upregulated in response to copper in the ΔBCAM0442/3 mutant, the CopABCDE-like system is not. The fold change difference when comparing the responses of both WT and

∆BCAM0442/3 *B. cenocepacia* to 1 mM $CuCl_2$ is stark. As there is strong evidence to suggest that the BCAM0442/3 TCS directly regulates the CopABCDE-like system in *B. cenocepacia*, and that there are no other candidates for a CopABCDE-like system in *B. cenocepacia,* it is proposed that the BCAM0442/3 TCS should be denoted as CopRS. This annotation complements the suggestion that the BCAM0442/3 TCS and the downstream CopABCDE-like system in *B. cenocepacia* H111 are implicated in copper resistance via transposon sequencing analysis, reinforcing the significance of this gene region in the copper response of *B. cenocepacia* [369].

Aside from the CusABCF-like and CopABCDE-like systems, other genes in this region are upregulated in response to copper. BCAM0437 is a predicted Na^+/Ca^{2+} antiporter which is upregulated 3-fold in WT *B. cenocepacia*, however any potential role this may have in copper homeostasis is unclear. BCAM0444 is a hypothetical protein lying between BCAM0443 and another hypothetical protein which is strongly upregulated in WT *B. cenocepacia* in response to copper, however there is no evidence to suggest what its function may be. Given the RR BCAM0443-dependent stark upregulation of its neighbouring genes, it is perhaps surprising that the upregulation of the hypothetical protein BCAM0445 did not reach significance, particularly when considering that BCAM0445 appears to form an operon with the strongly upregulated CopB and CopA. BCAM0451, a predicted endonuclease/exonuclease that sits at the downstream end of the BCAM0442/3 neighbourhood, is another gene that undergoes BCAM0443-dependent upregulation in response to copper, albeit not to the same extent as the CopABCDE-like system. Again, the potential involvement of BCAM0451 in the copper response is unclear.

In order to assess the importance of the genomic neighbourhood of BCAM0442/3 to copper resistance in *B. cenocepacia*, a ΔBCAM0433-50 deletion mutant was generated and tested for susceptibility to copper (Fig 5.8). Surprisingly, though ΔBCAM0433-50 was sensitive to copper, there was no greater susceptibility than in the ΔBCAM0442/3 deletion mutant (Fig 5.8). Given that the transcription of CopABCDE is BCAM0443-dependent, the major difference between these two deletion mutants lies in the CusABCF system, which is still fully active in ΔBCAM0442/3, but deleted in ΔBCAM0433-50. This suggests that CopABCDE

may play a more significant role in resistance to copper than CusABCF in *B. cenocepacia*.

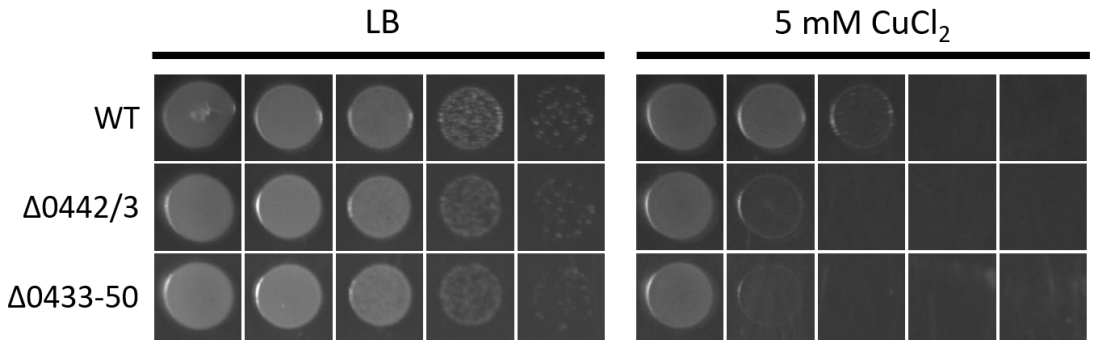

Figure 5.8: ΔBCAM0433-50 shows similar copper sensitivity to ΔBCAM0442/3. 10^{-1} to 10^{-5} dilutions of standardised overnight culture were spotted left to right on the plates.

Overall, it can be concluded that *B. cenocepacia* employs both a CusABCF-like and a CopABCDE-like system in response to copper, of which the latter is controlled by the BCAM0442/3 TCS, now denoted CopRS. There are other genes that may appear to be directly regulated by CopRS in *B. cenocepacia*, but due to the issues with the outlier in the Δ0442/3_LB samples, it is difficult to infer with great certainty that this is the case outside of the downstream CopABCDE-like system.

5.2.5 – Upregulation of the BCAM0714/5 genomic neighbourhood

Interestingly, while the BCAM1417/8 and BCAS0585/6 TCSs were not significantly differentially expressed in response to copper, BCAM0714/5 was (Table 5.3). The upregulation of BCAM0714/5 was considerably milder than the upregulation of the BCAM0442/3 gene region, though there was greater upregulation of the downstream genes BCAM0716 and BCAM0718, as well as the upstream BCAM0711-13 efflux pump. The magnitude of the differential expression of these genes is largely linked to their orientation in the genome, and thus point towards the potential operons that they are composed of (Fig 5.9).

BCAM0709 displays downregulation in WT and upregulation in the ΔBCAM0442/3 mutant, and though the differential expression of BCAM0710 does not reach significance, the raw fold changes show a similar pattern of expression. The BCAM0711-13 CzcCBA efflux pump and the BCAM0714/5 CzcRS TCS are upregulated in both WT and ΔBCAM0442/3 *B. cenocepacia*, though the fold change of the RR BCAM0714 in WT *B. cenocepacia* is below the threshold for significance. The BCAM0716-21 downstream gene region shows considerable variation in gene expression in response to copper; the hypothetical protein BCAM0716 is upregulated in response to copper in both WT and the ΔBCAM0442/3 mutant, whereas BCAM0717 is not, suggesting they form distinct operons. Interestingly, BCAM0715 and BCAM0716 were identified as being essential to the growth of *B. cenocepacia* H111 in copper by transposon sequencing, which reinforces the notion that these genes are involved in the response of *B. cenocepacia* to copper [369]. The only other gene upregulated within the BCAM0716-21 region in WT *B. cenocepacia* is BCAM0718, while BCAM0721 is downregulated in ΔBCAM0442/3 *B. cenocepacia*. The physiological benefit of this upregulation is unclear, though it supports the findings of the copper response in *P. aeruginosa*, which also had upregulation of both CzcRS and CzcCBA in response to copper [242].

Table 5.3: Fold changes of significantly differentially expressed genes in the neighbourhood of BCAM0714/5 in WT and ΔBCAM0442/3 *B. cenocepacia* in response to copper.

Gene name	Predicted protein function	Fold change (Copper vs LB)		Fold change (Δ0442/3 vs WT)	
		WT	Δ0442/3	LB	$CuCl_2$
BCAM0709	Hypothetical protein	0.50	2.51	0.34	1.72
BCAM0710	Metallopeptidase	0.53	2.31	0.36	1.56
BCAM0711	RND-family efflux pump (CzcC)	8.20	12.9	0.43	0.67
BCAM0712	RND-family efflux pump (CzcB)	4.97	11.7	0.48	1.12
BCAM0713	RND-family efflux pump (CzcA)	5.12	10.7	0.78	1.63
BCAM0714	Response regulator (CzcR)	1.95	2.64	0.95	1.29
BCAM0715	Sensor kinase (CzcS)	4.39	6.25	0.78	1.12

BCAM0716	Hypothetical protein	88.7	15.0	0.89	0.15
BCAM0717	Putative Gram-negative porin	2.60	8.80	0.79	2.68
BCAM0718	Hypothetical protein	21.3	4.91	0.49	0.11
BCAM0719	Hypothetical protein	36.3	0.89	1.85	0.05
BCAM0720	Hypothetical membrane protein	1.00	1.53	0.92	1.41
BCAM0721	O-acetylhomoserine thiol-lyase	0.98	0.44	1.22	0.54

Note: Gene names in brackets are suggested notations based on RNA-seq and sequence analysis. Shaded cells indicate genes that are not significantly differentially expressed in that comparison. Significantly differentially expressed genes are defined as having an adjusted p-value of < 0.05 and a fold change of > 2.

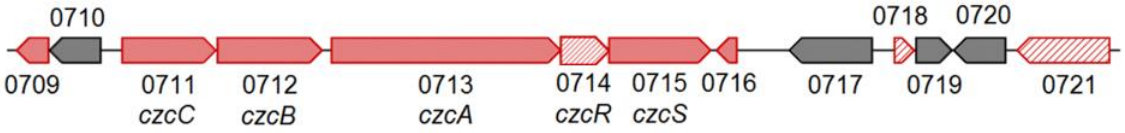

Figure 5.9: Genomic neighbourhood of BCAM0714/5. Dark red arrows denote genes significantly differentially expressed in response to 1 mM $CuCl_2$ relative to growth in unsupplemented LB in both WT and ΔBCAM0442/3 *B. cenocepacia*. Striped light red arrows denote genes significantly differentially expressed in either WT or ΔBCAM0442/3 *B. cenocepacia*. Grey arrows denote genes that are not significantly differentially expressed in response to 1 mM $CuCl_2$.

5.2.6 – The expression of other genes of interest in response to copper

Aside from the CusABCF and CopABCDE systems in *E. coli*, the Cue system is another characterised copper-responsive system. This is comprised of the MerR family cytosolic regulator CueR, which directly senses copper and activates the expression of an inner membrane P-type ATPase CopA (not to be confused with the multicopper oxidase CopA of the CopABCDE system) and a periplasmic multicopper oxidase CueO [482–484]. It is unknown whether a similar system also exists in *B. cenocepacia*, however possible orthologues for each gene are present in the genome. The predicted orthologues of CueR, CueO and CopA in

B. cenocepacia, BCAL2309, BCAL2733 and BCAM2683, share 41 %, 29 % and 35 % protein sequence similarity respectively to their predicted *E. coli* counterparts. BCAL2309 and BCAL2733 are not significantly differentially expressed in response to copper, whereas the predicted orthologue of the P-type ATPase CopA, BCAM2683, is strongly upregulated (Table 5.4). If a similar CueR system to *E. coli* exists in *B. cenocepacia*, it would be expected that the entire system is upregulated in response to copper, rather than a single component. Aside from BCAM0447, no other multicopper oxidase appears to exist within the *B. cenocepacia* genome, and while two other MerR family proteins are upregulated in response to copper, BCAL0054 and BCAL0602, neither show any particular sequence similarity to CueR from *E. coli*, arguing against the possibility of other genes being playing the role of CueO and CueR in a *B. cenocepacia* Cue-like system. Despite the uncertainties surrounding the mechanisms of its regulation, the CopA orthologue BCAM2683 is clearly heavily induced in response to copper, presumably aiding in detoxification of the cell through extrusion of copper from the cytoplasm into the periplasm.

Another upregulated putative copper-resistance protein is BCAM2215, which is annotated as a 'copper resistance protein C precursor'. Indeed, BCAM2215 shares 40 % protein sequence similarity with BCAM0449, suggesting it may indeed act as a copper chaperone similar to CopC in *B. cenocepacia*. BCAM2215 also shares 52 % similarity with BCAM2696, although BCAM2696 is not significantly differentially expressed in response to copper (Table 5.4). The neighbouring protein BCAM2216 is also upregulated in response to copper, though there is no clear link between BCAM2216 and any other copper-resistance protein within *B. cenocepacia*. As such, while BCAM2215 likely acts as a copper chaperone within *B. cenocepacia*, the role of BCAM2216 in the copper response remains unclear.

Table 5.4: Fold changes of other various genes of interest in response to copper.

Gene name	Predicted protein function	Fold change (Copper vs LB)		Fold change (Δ0442/3 vs WT)	
		WT	Δ0442/3	LB	$CuCl_2$
BCAL2309	Orthologue of CueR	0.70	1.31	0.62	1.16
BCAL2733	Orthologue of CueO	1.90	0.64	2.99	1.01
BCAM2683	Orthologue of CopA P-type ATPase	194.1	30.3	4.29	0.67
BCAM2215	Copper resistance protein C precursor	11.2	2.31	5.66	1.16
BCAM2216	Hypothetical protein	14.3	2.96	21.1	4.37
BCAL2696	Putative copper resistance protein	1.06	0.31	1.34	0.39
BCAL0604	Putative heavy metal binding protein	102.4	58.8	0.73	0.42
BCAL0055	Orthologue of CadA P-type ATPase	2.67	1.75	3.03	1.99
BCAM0318	Putative cation-transporting ATPase	3.22	0.71	5.17	1.14
BCAL0534	Response regulator (RqpR)	4.81	1.09	4.90	1.11
BCAL0535	Sensor kinase (RqpS)	3.67	0.58	5.81	0.92
BCAM1493	Response regulator ($BceR_1$)	2.14	1.68	1.60	1.26
BCAM1494	Sensor kinase ($BceS_1$)	1.55	1.43	1.79	1.64
BCAM2723	Putative outer membrane porin	0.14	0.89	0.27	1.72

Note: Shaded cells indicate genes that are not significantly differentially expressed in that comparison. *Significantly differentially expressed genes are defined as having an adjusted p-value of < 0.05 and a fold change of > 2.*

Surprisingly, the CadA P-type ATPase, BCAL0055, is also upregulated in response to copper, albeit at a level much lower than the CopA P-type ATPase (Table 5.4). This is in contrast to the characterisation of CadA performed by Schwager and colleagues (2012), which found that the expression of CadA in *B. cenocepacia* H111 was induced by the presence of cadmium, lead and zinc, but not copper, and that deletion of the *cadA* gene did not result in an observable sensitivity to copper [368]. Given the relatively mild upregulation of CadA in response to copper, it is likely that it does not play a significant role in the detoxification of the cell to copper, and deletion of this gene does not affect overall

sensitivity to copper. It is possible that the upregulation of CadA in response to copper serves a similar purpose to the upregulation of CzcCBA, that is the hypothesis that general extrusion of metal ions from the cytoplasm aids to reduce overall metal stress, thereby increasing the ability of the cell to withstand toxic concentrations of single metal species, in this case copper.

Another heavily upregulated gene in response to copper is BCAL0604, a putative heavy metal binding protein. BCAL0604 shares 26 % protein sequence similarity with CopZ from *B. subtilis*, a copper chaperone known to interact with the P-type ATPase CopA, and also shares 31 % and 42 % similarity with cytoplasmic copper chaperones CopZ1 and CopZ2 from *P. aeruginosa* [485,486]. Given this similarity, and the strong upregulation of BCAL0604 in response to copper, it is possible that BCAL0604 serves to sequester copper in the cytoplasm and deliver it to the CopA ATPase, where it is extruded into the periplasm. In addition to CadA and CopA, another putative ATPase is upregulated in response to copper, BCAM0318 (Table 5.4). While the upregulation of BCAM0318 is relatively mild at a 3 fold increase in expression in response to copper, this upregulation is lost in the ΔBCAM0442/3 *B. cenocepacia* mutant, perhaps indicating that the BCAM0442/3 system directly or indirectly regulates the expression of this ATPase.

Of the characterised TCSs in *B. cenocepacia* listed in Table 1.1, two undergo some level of differential expression in response to copper (Table 5.4). The most notable of these is the RqpR RR BCAL0534, which is upregulated 4.8-fold in WT *B. cenocepacia* in response to copper but is not differentially expressed in the ΔBCAM0442/3 mutant. The upregulation of the RqpS SK BCAL0535 did not reach the threshold for significance, but follows a similar pattern to BCAL0534. Given the role that RqpSR has in quorum sensing and pathogenicity, this upregulation, while mild, may point toward a link between the copper and/or wider metal response and these phenotypes in *B. cenocepacia* [428].

Several gene loci that are pertinent to a range of important pathogenic phenotypes in *B. cenocepacia* are significantly differentially expressed in response to copper (Appendix Table A3.1). The BCAL0337-51 gene region, which encodes many putative T6SS proteins, is downregulated between 2-fold and 4-fold in response to copper in WT but not ΔBCAM0442/3 *B. cenocepacia*. Additionally, BCAL3517 and BCAL3525-6, which encode for T2SS proteins, are

also downregulated to a similar degree in response to copper, though surrounding T2SS genes are not. There is also differential expression of genes involved in chemotaxis and motility; gene loci including BCAL0520-27, BCAL0561-72 and BCAL3501-07 contain many genes associated with flagellar biosynthesis that are downregulated in response to copper, whereas many chemotaxis-associated genes, including genes within the BCAL0126-32 gene region, are upregulated in response to copper. Additionally, of 14 genes annotated with 'putative universal stress protein' or similar in *B. cenocepacia*, four were upregulated (BCAM0290-92 and BCAM1829), while one was downregulated (BCAL2268), perhaps suggesting that these genes are involved in the wider stress response to copper.

There are numerous predicted outer membrane porins in *B. cenocepacia*; analysis of the J2315 genome encodes at least 45 putative porins, of which 7 are downregulated and 1 upregulated in response to copper in WT *B. cenocepacia* [146]. Given that the presence of certain metals leads to enhanced resistance to carbapenems in *P. aeruginosa* through downregulation of the OprD porin, and that this metal-inducible carbapenem resistance is also present in *B. cenocepacia* (Fig 4.8), it is possible that at least one of these downregulated porins is the equivalent route of entry for carbapenems in *B. cenocepacia*, and as such is responsible for this resistance to imipenem [319,320]. Of these 7 downregulated porins, only BCAM2723 displays any particular similarity to OprD in *P. aeruginosa,* sharing 32 % protein sequence similarity to OprD. BCAM2723 undergoes a fold change of 0.14-fold in response to copper in WT, but is not differentially expressed in response to copper in the ΔBCAM0442/3 mutant (Table 5.4). Given the similarity to OprD and downregulation in response to copper, it is feasible to suggest that BCAM2723 serves the same role in carbapenem entry in *B. cenocepacia* as OprD does in *P. aeruginosa*. However, BCAM2723 is not differentially expressed in response to 1.5 mM $ZnCl_2$ (Robinson *et al*, Unpublished data), a concentration that does lead to enhanced imipenem resistance (Fig 4.8). It is possible that a different porin serves this role that does not share any particular similarity to the OprD porin of *P. aeruginosa*, or that a separate mechanism that links the presence of metals with carbapenem resistance exists that is porin-independent.

Many genes within the low-oxygen-activated locus (BCAM0275a-0323), which contain genes associated with the viability of *B. cenocepacia* in low-oxygen environments, were upregulated in response to copper [487]. Interestingly, the abundance of several proteins encoded by this locus was increased in sequential isolates from chronically infected CF patients, while deletion of this gene region also significantly reduces the attachment of *B. cenocepacia* to epithelial cells, suggesting that these genes are associated with adaptation of *B. cenocepacia* to the CF lung [488]. Two genes within the flp type pilus-encoding BCAL1525-32 region were also upregulated in response to copper, further linking adhesion to host surfaces and the copper response in *B. cenocepacia*.

Perhaps unexpectedly, given the ability of copper to undergo Fenton chemistry and generate ROS, there is little evidence for upregulation of oxidative stress-related genes. No putative oxidative stress-genes are differentially expressed in response to copper in WT or ΔBCAM0442/3 *B. cenocepacia*. As the growth condition of 1 mM $CuCl_2$ does not negatively affect growth of *B. cenocepacia* (Fig 5.1), it is possible that this copper concentration is not high enough to induce an oxidative stress response, as the previously discussed copper-detoxification systems, such as CusABCF and CopABCDE, can detoxify the cell without the need for the upregulation of oxidative stress-specific genes.

Aside from genes that have been characterised at least in part in the literature, there are several uncharacterised genes that undergo significant upregulation or downregulation in response to copper in *B. cenocepacia* (Table 5.5). It is noteworthy that the genes that undergo the greatest levels of upregulation and downregulation in WT *B. cenocepacia* in response to copper often aren't significantly differentially expressed in ΔBCAM0442/3 *B. cenocepacia*. This pattern is still true if the anomalous 0442_LB_A replicate is excluded from the relevant comparison, suggesting that this stark contrast between WT and ΔBCAM0442/3 *B. cenocepacia* is a genuine phenomenon of the data. It is relatively unlikely that these genes are all within the direct BCAM0443 RR regulon, rather this data suggests that BCAM0443 acts as a global regulator for copper stress, both directly regulating the CopABCDE-like system and indirectly regulating a myriad of other genes. It is also of interest that no other genes in *B. cenocepacia* are upregulated as greatly as the BCAM0442/3 genomic

neighbourhood and the CopA P-type ATPase in response to copper, underlining their importance in copper homeostasis.

Table 5.5: Fold changes of various uncharacterised genes that undergo the highest levels of differential expression in response to copper.

Gene name	Predicted protein function	Fold change (Copper vs LB)		Fold change (Δ0442/3 vs WT)	
		WT	Δ0442/3	LB	$CuCl_2$
Upregulated genes					
BCAL1458	Putative exported protein	47.6	0.46	20.9	0.2
BCAM0626	Putative DNA-binding protein	41.0	1.49	29.5	1.08
BCAL0883	TetR family regulatory protein	37.6	3.27	8.67	0.75
BCAM2461	Putative inosine-uridine nucleoside hydrolase	34.7	2.02	16.4	0.96
BCAM1669	Putative exported protein	33.7	2.17	9.47	0.61
BCAL1921	Hypothetical protein	30.1	1.03	29.7	1.02
BCAL3362	Putative oxidoreductase	30.1	1.37	30.7	1.41
BCAM1259	RNA polymerase sigma factor	25.8	1.63	29.2	1.85
Downregulated genes					
BCAM0628	Putative phosphotyrosine protein phosphatase	0.014	0.62	0.053	2.38
BCAM1745	Putative magnesium-transporting ATPase	0.025	0.67	0.094	2.52
BCAL2352	Putative carbonic anhydrase	0.027	1.03	0.12	4.70
BCAL1055	Histidine transport system permease protein	0.031	0.43	0.13	1.85
BCAL3502	Flagellar biosynthetic protein	0.045	0.26	0.59	3.33
BCAL1056	Histidine transport system permease protein	0.049	0.51	0.24	2.54
BCAM2145	Putative GABA permease	0.059	0.78	0.16	2.2

Note: Shaded cells indicate genes that are not significantly differentially expressed in that comparison. *Significantly differentially expressed genes are defined as having an adjusted p-value of < 0.05 and a fold change of > 2.*

5.3 – Discussion

Given the presence of copper in the environment, its use in intoxicating internalised pathogens in the phagolysosome and as an antimicrobial surface in the clinic, bacteria are commonly exposed to copper in various situations, and understanding the mechanisms underpinning how bacteria respond to and resist this exposure is essential. While there have been transcriptomic analyses of the copper response in the environmental organism, *P. aeruginosa*, there is a lack of literature surrounding how the BCC responds to metal stress [242,486]. This research presents the first transcriptomic profiling of the response of *B. cenocepacia* to copper, as well as the characterisation of the potential regulon of the copper-sensing BCAM0442/3 TCS.

Through harvesting, purification and sequencing of mRNA from both WT and ΔBCAM0442/3 *B. cenocepacia* K56-2 grown to mid log phase in LB with and without 1 mM $CuCl_2$, a concentration that did not negatively affect growth (Fig 5.1), the response of *B. cenocepacia* to copper was characterised. In contrast to previous data of the response of *B. cenocepacia* to 1.5 mM $ZnCl_2$, in which only 54 genes were significantly differentially expressed (Robinson *et al*., Unpublished data), the response to 1 mM $CuCl_2$ was much greater, with 1102 genes being differentially expressed, representing 15 % of the genome. In contrast, only 174 genes were significantly differentially expressed in response to copper in the ΔBCAM0442/3 deletion mutant, suggesting that this TCS is a key regulator in the *B. cenocepacia* copper response. However, an outlier in the LB-grown ΔBCAM0442/3 mutant condition appeared to negatively affect the interpretation of the ΔBCAM0442/3 data; exclusion of the outlier from the analysis increased the number of significantly differentially expressed genes from 174 to 250, suggesting that the granularity of the data has been impacted by the presence of this outlier. Additionally, the comparison between the copper-exposed ΔBCAM0442/3 deletion mutant and copper-exposed WT only contained 189 differentially expressed genes, which is lower than may be expected if BCAM0442/3 does indeed play a key role in the response of *B. cenocepacia* to copper. It is therefore difficult to ascertain to what degree the BCAM0442/3 TCS acts as a central regulator in response to copper in *B. cenocepacia*, though the

role it plays in regulating individual genes can still be assessed on a case by case basis.

Despite the uncertainty surrounding the data arising from the ΔBCAM0442/3 deletion mutant, a large number of genes are significantly differentially expressed in the comparison of the transcriptomic profiles of both the deletion mutant and WT *B. cenocepacia* grown in LB. 67 % of these significantly differentially expressed genes were similarly differentially expressed in the WT_Copper vs WT_LB comparison, suggesting that, when grown in LB, deletion of BCAM0442/3 leads to copper response-like transcriptional changes in *B. cenocepacia*. This suggests that BCAM0442/3 appears to indeed act as a central regulator of the copper response in *B. cenocepacia*. However, the mechanism by which it fulfils this role is unclear. Rather than be essential for the transcriptional activation of many of these genes, it may be the case that the RR BCAM0443 acts to repress transcription. That is not to say that BCAM0443 directly represses these genes, it may be the case that BCAM0443 acts as an upstream player in a larger, unknown copper-responsive signalling pathway. One possibility is that phosphorylation of BCAM0443 by BCAM0442 leads to the negation of this repression, allowing the wider transcriptional response that is observable in the WT_Copper vs WT_LB comparison. If this is indeed the case, it is interesting that the CusABCF system and the BCAM0711-21 gene region do not seem to fall under this hypothetical system, as these genes are not significantly differentially expressed in the 0442_LB vs WT_LB comparison.

Several copper-responsive genes that have previously been described in the literature in *E. coli* appear to also both exist and respond to copper in *B. cenocepacia*. Based on this work, nomenclature for several genes is proposed, namely the CusABCF system, the CopRS TCS and the CopABCDE system. The genes that showed the greatest upregulation constituted the CopABCDE system downstream of BCAM0442/3; genes within this region were upregulated between 230-fold and 1754-fold in response to copper in WT *B. cenocepacia*, but were not significantly differentially expressed in response to copper in the ΔBCAM0442/3 mutant or in the 0442_LB vs WT_LB comparison, suggesting that the BCAM0442/3 TCS directly regulates the CopABCDE system in *B. cenocepacia*. Another copper-associated system is the CusABCF system found upstream of BCAM0442/3, upregulated between 12-fold and 126-fold in response to copper

in WT *B. cenocepacia*. While there was some variation in the level of upregulation between WT and ΔBCAM0442/3 *B. cenocepacia*, this system was generally upregulated in both strains, suggesting that it is not under the direct regulation of BCAM0442/3.

Outside of the BCAM0442/3 regulon, other copper-responsive genes are upregulated, such as the CopA P-type ATPase, CopC-like proteins and a CopZ orthologue. Surprisingly, the cadmium-extruding P-type ATPase CadA was mildly upregulated, suggesting that CadA is linked to the survival of *B. cenocepacia* to copper, perhaps through the extrusion of other heavy metals to reduce the overall metal stress on the cell. A summary of the major proteins associated with detoxification of *B. cenocepacia* to copper can be found in Figure 5.10.

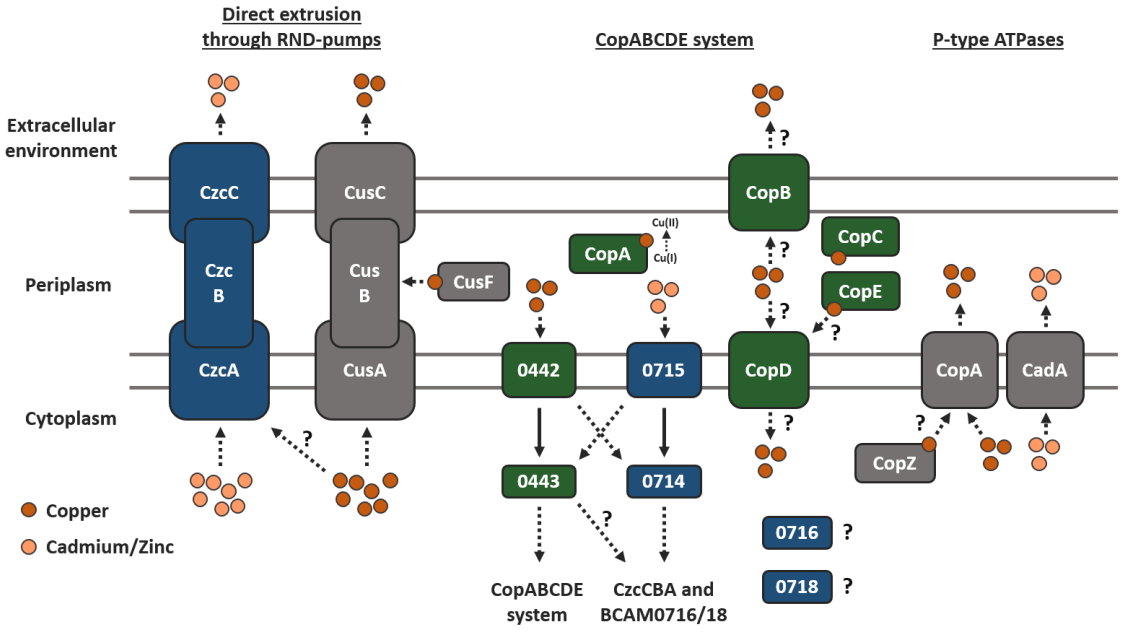

Figure 5.10: Proteins of interest that are upregulated in response to copper in *B. cenocepacia*. Proteins are given three colours; green for those directly regulated by BCAM0442/3, blue for those directly regulated by BCAM0714/5, and grey for proteins not thought to be directly regulated by either. Protein-protein interactions or protein localisation that is unclear are labelled with question marks.

The upregulation of the BCAM0711-13 CzcCBA efflux pump and the BCAM0714/5 CzcRS TCS in response to copper raises interesting questions surrounding their role in the copper response. As shown in Chapter 6, the CzcCBA efflux pump does appear to be implicated in the resistance of *B. cenocepacia* to toxic copper concentrations; one suggestion is that CzcCBA extrudes copper in addition to cadmium and zinc. Alternatively, the general extrusion of metals may benefit the cell in situations of copper stress through the reduction of overall metal stress, particularly in environments that contain high levels of multiple metals [320]. It may be the case that exposure of *B. cenocepacia* to copper 'primes' the cell into preparing for the likely possibility of exposure to other toxic metals in the environment through upregulation of general detoxification systems. In *P. aeruginosa*, the expression of CzcCBA and CzcRS is also induced by copper, thought to be a result of the CopR RR binding to a 'cop box' upstream of the *czcRS* operon, thus inducing expression of the CzcRS TCS and the subsequent expression of CzcCBA [320]. As the upregulation of CzcCBA and CzcRS in *B. cenocepacia* in response to copper remains in the ΔBCAM0442/3 mutant, it can be concluded this upregulation in *B. cenocepacia* is not BCAM0443-dependent, and another mechanism links the copper response to the expression of these genes.

The notion that upregulation of CzcCBA and BCAM0714/5 is BCAM0443-independent raises various possibilities for how this upregulation occurs. Firstly, the SK BCAM0715 could directly sense the presence of copper and activate the RR BCAM0714, which would then upregulate the entire BCAM0711-21 gene region. Secondly, BCAM0714 could be phosphorylated by a non-cognate phosphodonor, be it a SK or a separate protein. Finally, a different transcription factor could bind and transcribe these genes in response to copper. The lack of sensitivity that the ΔBCAM0714/5 deletion mutant has to copper may argue against direct regulation of these genes by BCAM0714 in response to copper, though the relatively modest upregulation of these genes in response to copper may indicate that these genes are not particularly essential to the resistance of *B. cenocepacia* to copper, and deletion of BCAM0714/5 may not provide an observable copper-sensitive phenotype. Additionally, in response to zinc the upregulation of the genes within the BCAM0716-19 gene region are relatively similar (Robinson *et al*, Unpublished data), whereas there are significant

discrepancies in differential expression of these genes in response to copper, arguing against a direct regulation by BCAM0714. This latter point also suggests that it is unlikely that this upregulation is due to the phosphorylation of BCAM0714 by a non-cognate donor in response to copper. This is also supported by the fact that no other predicted metal-sensing TCS is differentially expressed in response to copper. This somewhat questions the relevance of the non-cognate phosphotransfer observed in Chapter 3; if non-cognate phosphotransfer does indeed occur *in vivo* between BCAM0442 and BCAM0714, then it is unclear as to why BCAM0442/3-dependent upregulation of the regulon of BCAM0714 in response to copper is not observed. Perhaps the growth condition of 1 mM $CuCl_2$ is not great enough to stimulate the upregulation of BCAM0442 to a point in which phosphotransfer from BCAM0442 to BCAM0714 can overcome the presumed phosphatase ability of BCAM0715 to BCAM0714, and as such the BCAM0442/3-dependent upregulation of these genes was not observed in these conditions. Equally, while there is upregulation of the SK BCAM0442 in response to copper, the RR BCAM0443 is also upregulated, meaning there are considerable levels of cognate RR available to sequester any phosphoryl groups from BCAM0442, hampering any potential non-cognate phosphotransfer to BCAM0714.

As such, the possibility that remains is that a different transcription factor aside from the RRs BCAM0714 and BCAM0443 is responsible for the upregulation of these genes. The other RRs of interest, BCAM1418 and BCAS0586, are not differentially expressed in response to copper, suggesting that a transcription factor outside of these TCS may be responsible for this upregulation. Overall, while the expression of CzcCBA and CzcRS in *B. cenocepacia* in response to copper is similar to that in *P. aeruginosa*, these data suggest that the mechanisms by which this occurs are not shared between these species.

As another environmental organism and opportunistic pathogen, it is of interest to compare the copper response of *P. aeruginosa* to the data presented above for *B. cenocepacia*. Due to differences in copper concentration and exposure times between previous studies exploring the copper response of *P. aeruginosa* and the work presented here, it is difficult to directly compare the transcriptional profiles of these bacteria in response to copper, though specific comparisons can still be informative. The proportion of genes that are differentially expressed appears to be larger in *B. cenocepacia* than *P. aeruginosa*; 7.5 % of *P.*

aeruginosa genes were differentially expressed (with a fold change of > 2) after 2 hours of exposure to 0.5 mM $CuSO_4$, whereas 15.5 % of *B. cenocepacia* genes were differentially expressed with a similar fold change [486]. Similarly, following exposure of *P. aeruginosa* to 10 mM $CuSO_4$ for 6 hours, 5.9 % of the genome was differentially expressed (with a fold change of > 3), compared to 7.6 % of the *B. cenocepacia* genome [242]. While the differences in concentration and exposure times between these studies need to be considered, there is evidence to suggest that the copper response of *B. cenocepacia* is more extensive than that of *P. aeruginosa*.

There are several similarities in the copper response between these bacteria, for example exposure to copper leads to upregulation of several efflux proteins and the downregulation of outer membrane porins [242,486]. Interestingly, *P. aeruginosa* exposed to a 'shock' of 10 mM $CuSO_4$ for 45 minutes upregulated several oxidative stress-associated genes, whereas *P. aeruginosa* which was 'adapted' to the same concentration for 6 hours did not, suggesting that induction of oxidative stress genes may be an acute response to the presence of high levels of copper, and that over time intracellular concentrations of copper decrease to the point at which oxidative stress genes are no longer upregulated [242]. This notion is supported by the fact that *B. cenocepacia* that had been exposed to 1 mM $CuCl_2$ for 8 hours did not show induction of an obvious oxidative stress response, albeit the 10-fold lower copper concentration may alternatively suggest that oxidative stress response genes are not necessary at subinhibitory concentrations of copper. Another similarity between the copper response of *P. aeruginosa* and *B. cenocepacia* is the induction of PA2523/4, the orthologue of the BCAM0714/5 TCS, and PA2520-22, the orthologue of the CzcCBA efflux pump in *B. cenocepacia* in response to copper [242,486].

While there are several similarities between the published *P. aeruginosa* copper response and the data presented here on *B. cenocepacia*, there are differences also. Iron homeostasis genes appear to be tightly regulated in *P. aeruginosa* in response to high levels of copper; pyoverdine biosynthesis was upregulated whereas genes associated with pyochelin were downregulated in response to 10 mM $CuSO_4$ [242]. Contrastingly, these genes were not differentially expressed in response to copper when *P. aeruginosa* was exposed to 0.5 mM $CuSO_4$, suggesting that regulation of these genes in response to copper is concentration-

dependent [486]. While exposure of *B. cenocepacia* to 1 mM $CuCl_2$ did not induce any differential expression of iron homeostasis genes, it is not to say that they would not be induced at higher levels of copper stress, though it appears that iron homeostasis genes do not play a critical role in the response of *B. cenocepacia* to copper. Interestingly, two genes associated with ornibactin, PvdA and OrbA, were upregulated in response to 1.5 mM $ZnCl_2$ in *B. cenocepacia* (Robinson *et al*, Unpublished data). The reason for the discrepancy in iron homeostasis genes between the copper and zinc response of *B. cenocepacia* is unclear, though it does suggest that iron homeostasis has a role to play in the response to zinc, but not to copper, and it is of interest whether these genes would be induced by exposure to other metals.

Comparing the transcriptional response of *B. cenocepacia* to copper and to zinc highlights the stark difference in magnitude of the two responses. With the same threshold for significance of having a fold change > 2, 15 % of the *B. cenocepacia* genome was differentially expressed in response to 1 mM $CuCl_2$, yet only 0.76 % of the genome was differentially expressed in response to 1.5 mM $ZnCl_2$ (Robinson *et al*., Unpublished data). Given the general lack of transcriptomic data sets of the copper and zinc responses of various bacteria in the literature, it is unclear whether the copper response is usually considerably greater in magnitude than the zinc response. There is no current published transcriptomic data on the zinc response of *P. aeruginosa*, though exposure of *Pseudomonas putida* to 1.5 mM $ZnSO_4$ led to differential expression of 10.4 % of the genome [489]. While there are likely to be interspecies differences, comparison of the zinc response of *P. putida* to the copper response of *P. aeruginosa* discussed above suggests that there is not a stark difference in the magnitude of the zinc and copper responses in these bacteria. If this is the case, then it raises interesting questions surrounding why the zinc response of *B. cenocepacia* is considerably milder than its copper response.

Though the data presented above provides insight into both the overall response of *B. cenocepacia* to copper and the role that the BCAM0442/3 TCS has to play in such a response, interpretation of the data must consider that it provides a specific snapshot of how *B. cenocepacia* responds to a particular concentration (1 mM $CuCl_2$) at a particular length of time (8 hours). As shown previously for *P. aeruginosa*, the transcriptomic profile in response to copper can vary significantly

depending on the particular conditions of growth; the concentration of copper used and the length of time of exposure to copper strongly influence the overall response and therefore the interpretation of any RNA-seq output [242,486]. As such, it would be valuable to perform similar transcriptomic analyses at varying concentrations of copper. 1 mM $CuCl_2$ was chosen as it did not confer any inhibitory effect on growth (Fig 5.1), thus implying that *B. cenocepacia* is not under significant levels of stress at this concentration. Alongside this data, observing how the transcriptomic response of *B. cenocepacia* changes with increasing levels of copper, particularly at levels which are inhibitory to the ΔBCAM0442/3 mutant but not WT *B. cenocepacia*, would enhance our understanding of how *B. cenocepacia* adapts to copper-containing environments and the role of BCAM0442/3 in this adaptation.

In addition to various copper concentrations, observing the early-stages of the transcriptomic response to copper would also be of value. As demonstrated for oxidative stress genes in *P. aeruginosa*, many genes may be differentially regulated in the initial stages of copper exposure, but not in the later stages of exposure [242]. One reason for this may be that the initial regulation of these genes allows the cell to deal with the sudden presence of copper, while simultaneously enhancing the expression of specific copper-detoxification systems, such as CusABCF and CopABCDE. Understanding the different 'phases' of the copper response is crucial to building a greater picture of how bacteria are able to respond to this clinically-relevant metal, and future transcriptomic analysis of the copper response in *B. cenocepacia* should consider the utilisation of various copper concentrations and exposure times to account for these phases.

Comparing the transcriptomic response of both WT and ΔBCAM0442/3 *B. cenocepacia* to copper has provided insight into the regulon of the BCAM0442/3 TCS and the links between the copper and zinc response in *B. cenocepacia*. As such, comparing how different TCS deletion mutants respond to copper would provide further insight into whether individual TCSs have a role to play in the copper response, even if they don't directly sense copper themselves, and to what degree the various metal responses of *B. cenocepacia* are linked. For example, while the BCAM0714/5 gene region is upregulated in response to copper in both the WT and ΔBCAM0442/3 mutant *B. cenocepacia*, it is uncertain whether that copper-induced upregulation would still be present in the

ΔBCAM0714/5 mutant. Any upregulation of the CzcCBA efflux pump or the downstream BCAM0716-21 gene region in response to copper in the ΔBCAM0714/5 mutant would suggest that these genes are under the regulation of a different transcription factor, possibly linking the metal response to other cellular processes.

In addition to assessing the copper response, exploration of the response of different mutants of *B. cenocepacia* to various metals is also a useful avenue of investigation. Given the upregulation of cadmium- and zinc-detoxifying genes in the presence of copper in *B. cenocepacia*, it may be the case that a number of systems are upregulated in response to a range of different metals, leading to a general detoxification of metals within the cell in order to reduce overall metal stress. Given the similarities between how different metals exert their toxic effects on bacteria, this general detoxification may be of benefit to many different instances of metal exposure.

While transcriptomic profiling is an inherently powerful technique for understanding how a bacteria responds to a certain stimulus, its use for the elucidation of the regulon of specific TCSs is limited. Genes that are upregulated in a bacteria which are not in a TCS deletion mutant could be described as being under the regulation of that TCS, however as is seen above for the copper response of the ΔBCAM0442/3 mutant, there are hundreds of genes that are not differentially expressed in the mutant which are upregulated in the WT. As such, it is difficult to be truly confident in claiming that certain genes are or are not under the direct regulation of a TCS based on transcriptomic profiling alone.

One methodology that could be employed to address this issue is chromatin immunoprecipitation sequencing (ChIP-seq), which allows the investigation of the DNA binding sites of proteins. Cross-linking between DNA and bound proteins, and eventual sequencing of bound DNA, enables the characterisation of which particular DNA sites a protein binds to under different conditions. For TCSs, a RR that binds to the putative promoter region upstream of a gene can be thought to directly regulate that gene under the conditions that the analysis took place in. ChIP-seq analysis has been used previously to assess the regulon of the BCAM0714 RR, which demonstrated that BCAM0714 regulates the CzcCBA efflux pump and the downstream BCAM0716-21 gene region in response to 1.5 mM $ZnCl_2$ (Robinson *et al*, Unpublished data). A similar approach could be taken

with the remaining RRs of this putative metal-sensing MKN; elucidation of the binding sites of each RR under various conditions would allow further insight into the regulon of each TCS, which would be of particular interest for the yet uncharacterised BCAS0585/6 TCS. When coupled with the RNA-seq data generated here, use of ChIP-seq may be a natural next step for investigation of this MKN.

5.4 – Conclusions

- The response of *B. cenocepacia* to copper is stark, with 15 % of the genome being differentially expressed in response to 1 mM $CuCl_2$.
- The genes that undergo the highest levels of upregulation form a CopABCDE-like system, which appears to be under the direct regulation of BCAM0442/3.
- The CzcCBA efflux pump, BCAM0714/5 TCS and BCAM0716/18 are upregulated in response to copper in a BCAM0442/3-independent manner.

Chapter 6: Investigation of a novel zinc resistance determinant within the BCAM0716-21 gene region

6.1 – Introduction

In the course of assessing the transcriptomic profile of *B. cenocepacia* K56-2 to 1.5 mM $ZnCl_2$, regions both upstream and downstream of the BCAM0714/5 TCS were shown to be heavily upregulated in response to zinc (Robinson *et al.,* Unpublished data). The genes encoding the CzcCBA efflux pump, lying upstream of BCAM0714/5, were upregulated between 40-72 fold, and aid in the extrusion of cadmium and zinc from the cell (Robinson *et al*., Unpublished data). Contrastingly, the downstream BCAM0716-21 gene region, comprised mainly of hypothetical proteins, was upregulated between 6-256 fold (Table 6.1) (Robinson *et al*., Unpublished data). Additionally, ChIP-seq analysis of the BCAM0714 RR identified enrichment of this BCAM0716-21 region, suggesting that BCAM0714 may regulate some or all of the genes within this region (Robinson *et al*., Unpublished data). Deletion of the BCAM0716-21 gene region conferred stark zinc sensitivity to *B. cenocepacia*, suggesting that a novel BCAM0714-regulated zinc-resistance determinant is present within this region (Robinson *et al*., Unpublished data).

Though the putative Gram-negative porin BCAM0717 displays the greatest level of upregulation in response to 1.5 mM $ZnCl_2$ of the genes in this region, BCAM0717 within *B. cenocepacia* K56-2 contains a 2 nucleotide deletion approximately 28 % along the coding region relative to the *B. cenocepacia* J2315 reference sequence, resulting in a considerably longer transcript (386 amino acids in J2315 vs 581 in K56-2) (Fig 6.1) [146]. As such, it is thought that BCAM0717 does not act as a functional porin in *B. cenocepacia* K56-2.

A motif search using MEME [490] identified a distinct motif upstream of BCAM0716 and BCAM0717/8, as well as a closely-related motif upstream of *czcC* (Robinson *et al*., Unpublished data) (Appendix Figure A4.1). If this motif corresponds to a BCAM0714 binding site, this suggests that while BCAM0714 can regulate the BCAM0716-19 gene region, BCAM0720 and BCAM0721 are regulated by a separate zinc-responsive system (Fig 6.2) (Robinson *et al*., Unpublished data). This is supported by the fact that the fold changes of BCAM0720 and BCAM0721 in response to zinc are considerably lower than the genes within the BCAM0716-19 gene region (Table 6.1) (Robinson *et al*., Unpublished data).

Table 6.1: Differentially expressed genes in the BCAM0711-21 region in *B. cenocepacia* in response to 1.5 mM $ZnCl_2$ (Robinson *et al*., Unpublished data).

Gene name	Predicted protein function	Fold change
BCAM0711	RND-family efflux pump (CzcC)	72.3
BCAM0712	RND-family efflux pump (CzcB)	40.5
BCAM0713	RND-family efflux pump (CzcA)	40.4
BCAM0714	Response regulator (CzcR)	58.1
BCAM0715	Sensor kinase (CzcS)	29.5
BCAM0716	Hypothetical protein	136.2
BCAM0717	Putative Gram-negative porin	255.6
BCAM0718	Hypothetical protein	122.3
BCAM0719	Hypothetical protein	132.6
BCAM0720	Hypothetical membrane protein	44.0
BCAM0721	O-acetylhomoserine thiol-lyase	6.4

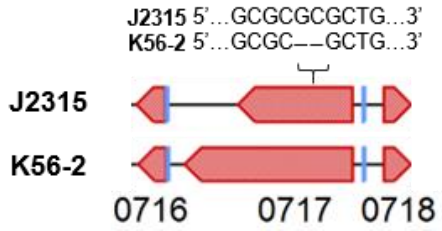

Figure 6.1: Differences between BCAM0717 in *B. cenocepacia* J2315 and K56-2. A 2 bp deletion within the BCAM0717 coding region in K56-2 increases the length of the BCAM0717 transcript. Binding motifs identified by MEME for BCAM0714 are denoted in blue. See appendix Figure A4.2 for the full alignment of DNA sequences of BCAM0717 from both *B. cenocepacia* J2315 and K56-2.

Figure 6.2: The BCAM0716-21 gene region of *B. cenocepacia* J2315. Binding motifs identified by MEME for BCAM0714 are denoted in blue.

The work presented within this chapter surrounds the further investigation of this BCAM0716-21 gene region with the aim to identify the potential novel zinc-resistance determinant that resides within it. This encompasses complementation of the ΔBCAM0716-21 deletion mutant with various combinations of genes alongside their native promoters in an attempt to identify which genes are necessary for restoration of the ability of ΔBCAM0716-21 to grow on zinc. Part of the work presented herein, namely conjugation of pDA17 containing various pairs of genes within this region into the ΔBCAM0716-21 deletion mutant, and the subsequent validation of these complemented strains, was performed in conjunction with Rebecca Tooze, an undergraduate project student whose work aligned closely with the focus of this chapter.

6.2 – Results

6.2.1 – Complementation of ΔBCAM0716-21 with the BCAM0716-21 gene region

In the aim of complementing the zinc-sensitivity phenotype of the ΔBCAM0716-21 deletion mutant, the BCAM0716-21 gene region was amplified and subsequently cloned into the pDA17 vector, replacing the native *dhfr* promoter of pDA17. An agarose gel displaying a digested pDA17::BCAM0716-21 vector can be found in Figure 6.3. Following successful sequence verification, the pDA17::BCAM0716-21 vector was conjugated into the ΔBCAM0716-21 deletion mutant. The conjugation of pDA17::BCAM0716-21 into ΔBCAM0716-21 partially restored the zinc sensitivity phenotype of the deletion mutant, confirming the notion that a novel zinc resistance determinant resides within the BCAM0716-21 gene region (Fig 6.4).

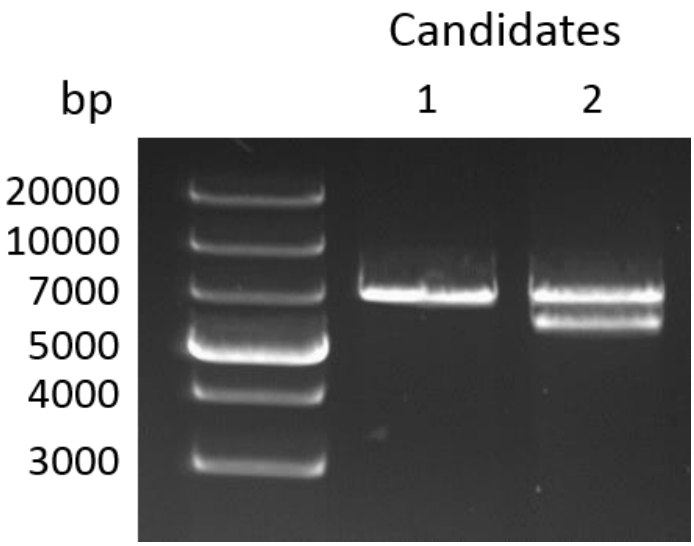

Figure 6.3: Restriction digests of two pDA17::BCAM0716-21 candidates on a 1 % agarose gel. Following transformation into *E. coli* JM109 cells, transformant colonies were grown overnight and subsequently underwent plasmid extraction. The resultant plasmids were then digested with XbaI and NheI for one hour. Both candidates hold pDA17, though only candidate 2 contains the BCAM0716-21 gene insert. Expected sizes (bp): pDA17 – 6939, BCAM0716-21 – 5903. Ladder = GeneRuler 1 kb plus.

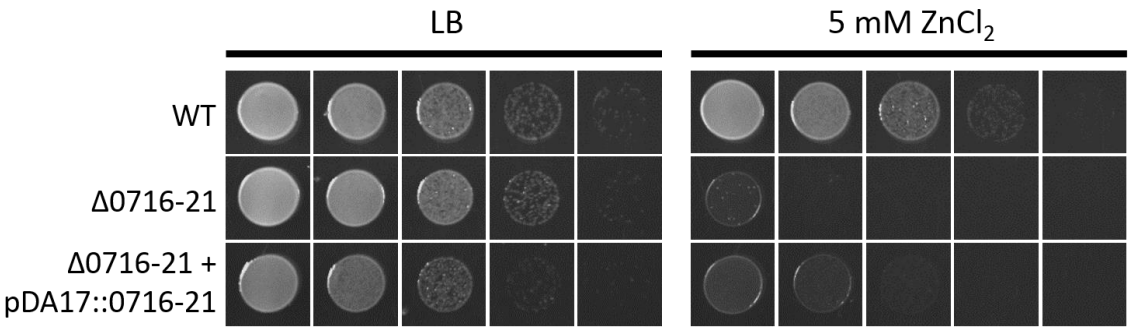

Figure 6.4: Conjugation of pDA17::BCAM0716-21 into the ΔBCAM0716-21 deletion mutant partially restores the ability to grow on zinc. 10^{-1} to 10^{-5} dilutions of standardised overnight culture were spotted left to right on the plates.

6.2.2 – Complementation of ΔBCAM0716-21 with single genes within the BCAM0716-21 gene region

Following on from the successful partial complementation of the zinc sensitivity phenotype of ΔBCAM0716-21, the role that the individual genes within the BCAM0716-21 region held in this phenotype was explored. The individual genes, barring BCAM0717 due to the frameshift within its coding region, were each cloned into pDA17 downstream of the native *dhfr* promoter. While the generation of the pDA17::BCAM0720 vector was unsuccessful, the remaining four pDA17 vectors were successfully generated and conjugated into ΔBCAM0716-21. None of the pDA17 vectors containing the individual genes (BCAM0716, BCAM0718, BCAM0719 and BCAM0721) complemented the zinc sensitivity phenotype of ΔBCAM0716-21 (Fig 6.5). While it may be possible that complementation with BCAM0720 alone could restore the ability to grow on zinc, previous insertional inactivation of BCAM0720 in *B. cenocepacia* did not confer any zinc sensitivity, meaning that it is unlikely that BCAM0720 alone has a major role to play in this novel zinc resistance determinant (Robinson *et al*., Unpublished data). Additionally, complementation with individual genes using different means of expression via the alternative vectors pMLS7 (containing the P_{s7} promoter) and the rhamnose-inducible pSCrhaB3 vector (both with and without 0.2 % rhamnose) was attempted, though this also did not result in any restoration of the ability to grow on zinc (Data not shown).

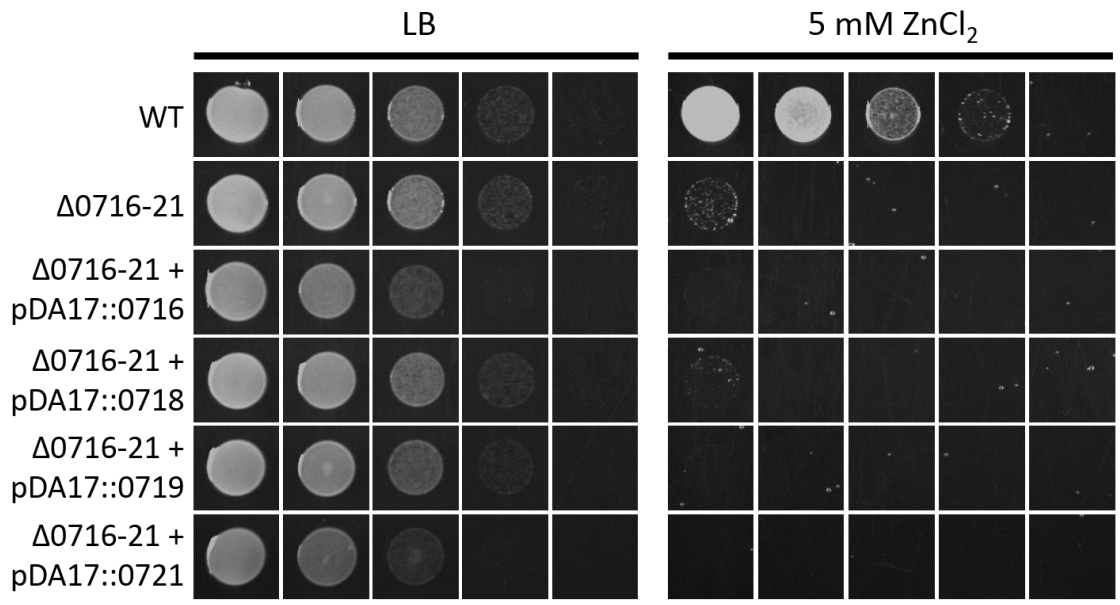

Figure 6.5: Conjugation of pDA17 containing individual genes within the BCAM0716-21 gene region into the ∆BCAM0716-21 deletion mutant does not restore the ability to grow on zinc. 10^{-1} to 10^{-5} dilutions of standardised overnight culture were spotted left to right on the plates

6.2.3 – Complementation of ∆BCAM0716-21 with pairings of genes within the BCAM0716-21 gene region

As conjugation of pDA17 vectors containing individual genes into the ΔBCAM0716-21 deletion mutant did not restore the ability to grow on zinc, larger portions of the gene region were cloned into pDA17 in an attempt to identify the general region of the novel zinc resistance determinant. As shown in Figure 6.2, the BCAM0716-21 gene region can be split into three portions based on gene orientation: BCAM0716-17, BCAM0718-19 and BCAM0720-21. As such, these three portions, as well as any upstream region that may contain a putative promoter, were cloned into pDA17 lacking the native *dhfr* promoter and subsequently conjugated into ΔBCAM0716-21.

Interestingly, pDA17::BCAM0716-17 successfully restored the ability of ΔBCAM0716-21 to grow on zinc, whereas pDA17::BCAM0718-19 and pDA17::BCAM0720-21 did not (Fig 6.6). Though this does not exclude the

possibility of the BCAM0718-21 gene region holding a role in the zinc response, there is a strong suggestion that the novel zinc resistance determinant within BCAM0716-21 lies within the BCAM0716-17 gene region.

Further investigation of the BCAM0716-17 gene region revealed inconsistencies in the annotation of the *B. cenocepacia* J2315 and the *B. cenocepacia* K56-2 genomes. In addition to the 2 nucleotide deletion within BCAM0717 in the K56-2 genome relative to the J2315 reference genome, resulting in a longer BCAM0717 protein than is annotated (580 amino acids in K56-2 compared to 368 amino acids in J2315) (Fig 6.1), a gene residing between BCAM0716 and BCAM0717 is annotated in the K56-2 genome, but not the J2315 genome, despite this gene region being identical in sequence between the two strains. Additionally, though annotated in the K56-2 genome as a 306 bp gene beginning with a GTG codon, an in frame ATG codon lies further upstream of this gene, which may potentially act as the start site, increasing its length to 444 bp. This gene is herein referred to as BCAM0716A. The current annotations of both the J2315 and K56-2 genomes, and recommended alterations to the annotation of the BCAM0716-17 gene region, can be found in Figure 6.7.

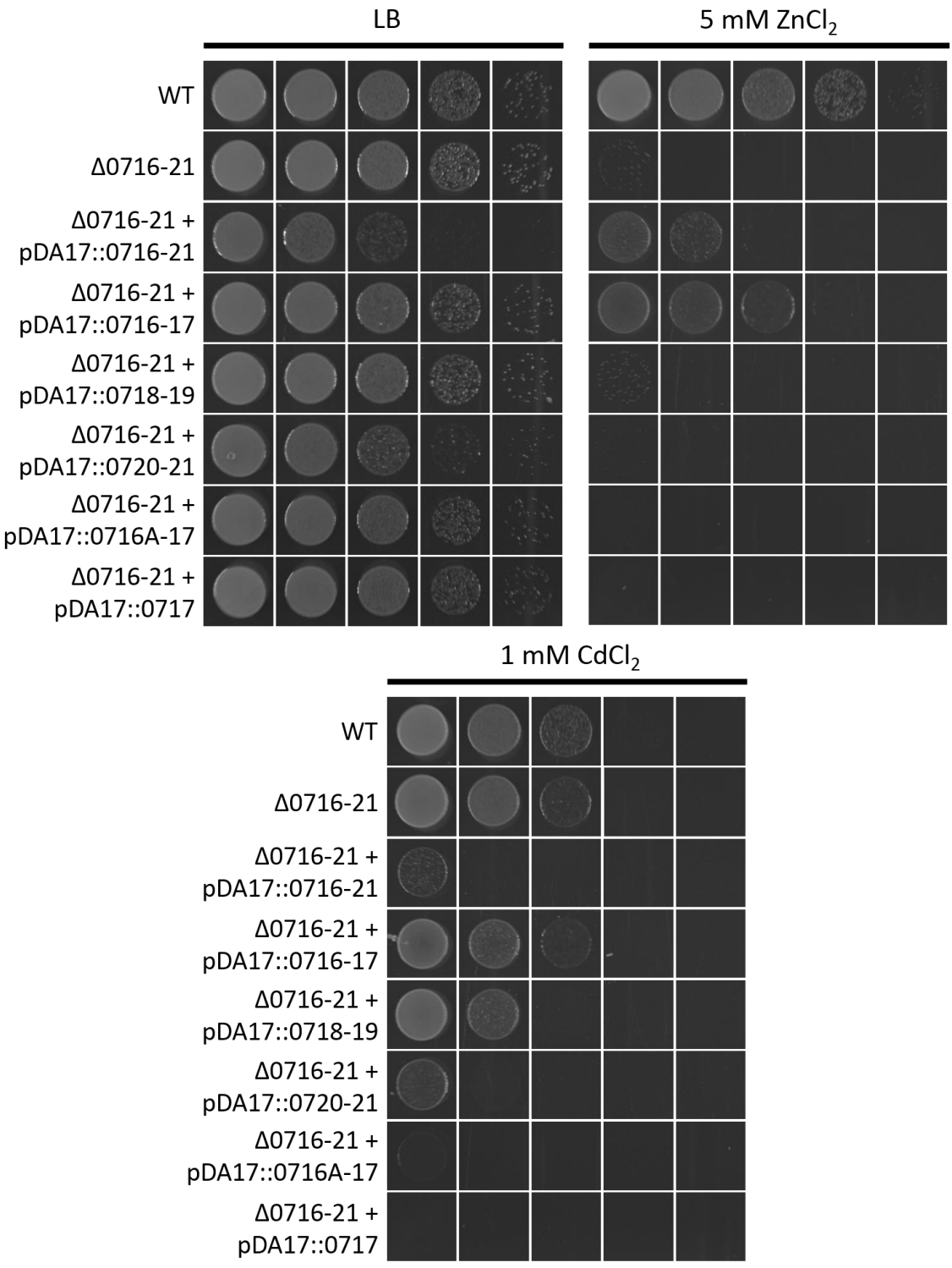

Figure 6.6: pDA17::BCAM0716-17 successfully restores the ability of ΔBCAM0716-21 to grow on zinc. 10^{-1} to 10^{-5} dilutions of standardised overnight culture were spotted left to right on the plates

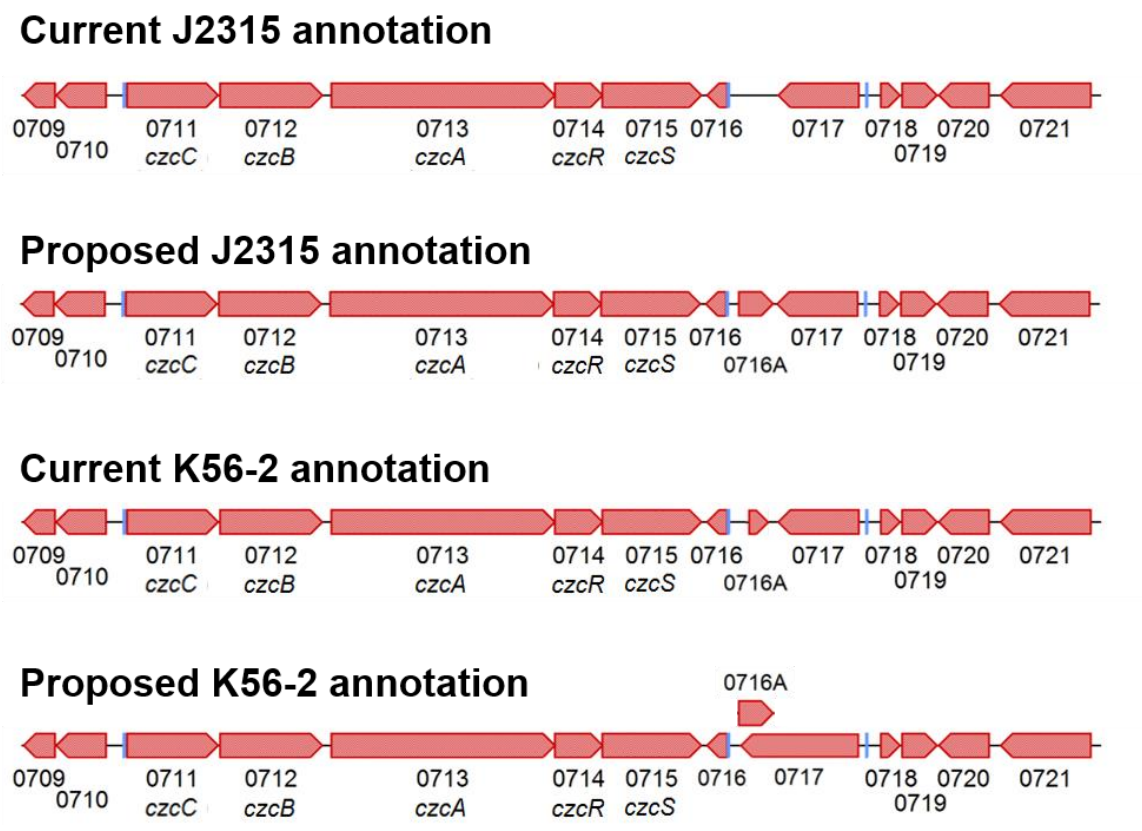

Figure 6.7: Current and proposed annotations of the BCAM0716-21 gene region. The putative gene BCAM0716A should be included between BCAM0716 and BCAM0717 in the J2315 genome, while the length of BCAM0716A and BCAM0717 should be extended in the K56-2 genome. Binding motifs identified by ChIP-seq for BCAM0714 are denoted in blue.

Given that conjugation of the BCAM0716-17 region into the ΔBCAM0716-21 deletion mutant restored the ability to grow on zinc, the generation of pDA17 vectors containing different portions of the BCAM0716-17 region was attempted. Unfortunately, while pDA17::BCAM0716A-17 was successfully generated, attempts to create a vector containing just BCAM0716 downstream of its native promoter were unsuccessful. A pDA17::BCAM0717 vector was also created, which due to being in the opposite orientation, also included BCAM0716A from its 'original' GTG start site (though not with the 'new' ATG start site). As such, it 'is unclear whether pDA17::BCAM0717 encodes just BCAM0717 or also BCAM0716A. While previous conjugation of pDA17::BCAM0716 into ΔBCAM0716-21 did not restore the ability to grow on zinc, this BCAM0716 gene

was downstream of the native *dhfr* promoter rather than its upstream gene region (Fig 6.5).

Interestingly, conjugation of the BCAM0716A-17 gene region into ΔBCAM0716-21 did not restore the ability to grow on zinc. This strongly suggests that either BCAM0716 alone is responsible for this resistance to zinc, and that complementation with the previous pDA17::BCAM0716 was not successful due to differences in expression level, or that the entire BCAM0716-17 gene region is necessary to restore the ability to grow on zinc. Strikingly, conjugation of BCAM0716A-17 into ΔBCAM0716-21 conferred sensitivity to cadmium, a phenotype also seen when pDA17::BCAM0717 was conjugated into the deletion mutant (Fig 6.6). The fact that cadmium sensitivity is not seen when BCAM0716 is conjugated alongside BCAM0717 into ΔBCAM0716-21 suggests that BCAM0716 interacts with BCAM0716A or BCAM0717 in *B. cenocepacia* K56-2, preventing the cadmium sensitivity that is seen when BCAM0716A/17 are expressed on their own.

The sensitivity to cadmium that conjugation of BCAM0716A-17 into ΔBCAM0716-21 confers led to the investigation of whether this phenomenon was unique to cadmium, or whether an equivalent sensitivity to zinc was also present. As ΔBCAM0716-21 showed limited growth on 5 mM $ZnCl_2$, thus making it difficult to assess whether any complemented strains were more sensitive to zinc, relevant strains were spotted onto a 1.25 mM $ZnCl_2$ plate (Fig 6.8). There is a clear sensitivity to zinc in the ΔBCAM0716-21 deletion mutant when conjugated with pDA17::BCAM0716A-17 and pDA17::BCAM0717, a sensitivity which is not seen when conjugated with the entire BCAM0716-17 gene region (Fig 6.8). This strongly suggests that either BCAM0716A is involved in sensitising the cell to these metals or, despite the large frameshift in its coding region, BCAM0717 is still involved with cadmium and zinc homeostasis in *B. cenocepacia* K56-2, perhaps through facilitating the influx of cadmium and zinc through the outer membrane. Additionally, as pDA17::BCAM0716-17 did not confer any metal sensitivity, it is likely that BCAM0716 is able to counteract this BCAM0716A/0717-induced metal sensitivity (Figs 6.6 and 6.8).

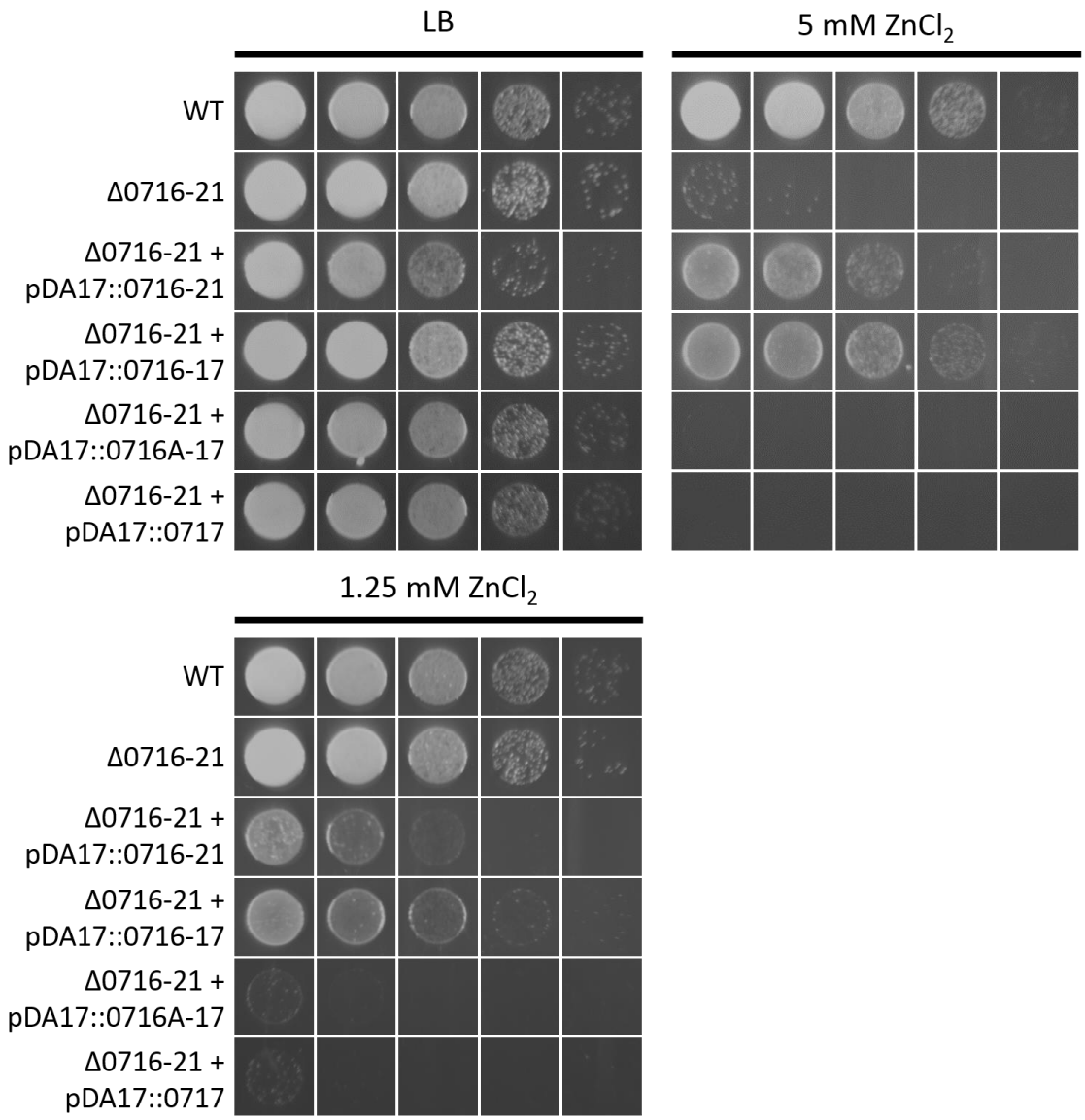

Figure 6.8: Conjugation of BCAM0716A-17 into ΔBCAM0716-21 confers stark sensitivity to zinc. 10^{-1} to 10^{-5} dilutions of standardised overnight culture were spotted left to right on the plates

6.2.4 – A potential non-coding RNA between BCAM0715 and BCAM0716 is not involved with zinc resistance

A genomics-based search for non-coding RNAs (ncRNA) in *B. cenocepacia* J2315 by Coenye and colleagues (2007) identified a potential 85 nucleotide-long ncRNA spanning the intergenic region between BCAM0715 and BCAM0716 [491]. This potential ncRNA is poorly conserved across the BCC, perhaps suggesting that it has no particular role in cellular function [491]. Nonetheless, as the pDA17::BCAM0716-17 and pDA17::BCAM0716-21 constructs include this potential ncRNA, the role that this ncRNA may hold in the zinc resistance conferred by these gene regions was investigated. Two equivalent constructs lacking the potential ncRNA (i.e. starting at the final codon of BCAM0716, rather than continuing until the final codon of BCAM0715) were generated, denoted pDA17::BCAM0716-17 -ncRNA and pDA17::BCAM0716-21 -ncRNA. Both vectors lacking this potential ncRNA complemented the zinc sensitivity of ΔBCAM0716-21 with equivalent efficacy to their ncRNA-containing counterparts, suggesting that this potential ncRNA does not have a major role to play in the zinc resistance determinant within BCAM0716-17 (Fig 6.9).

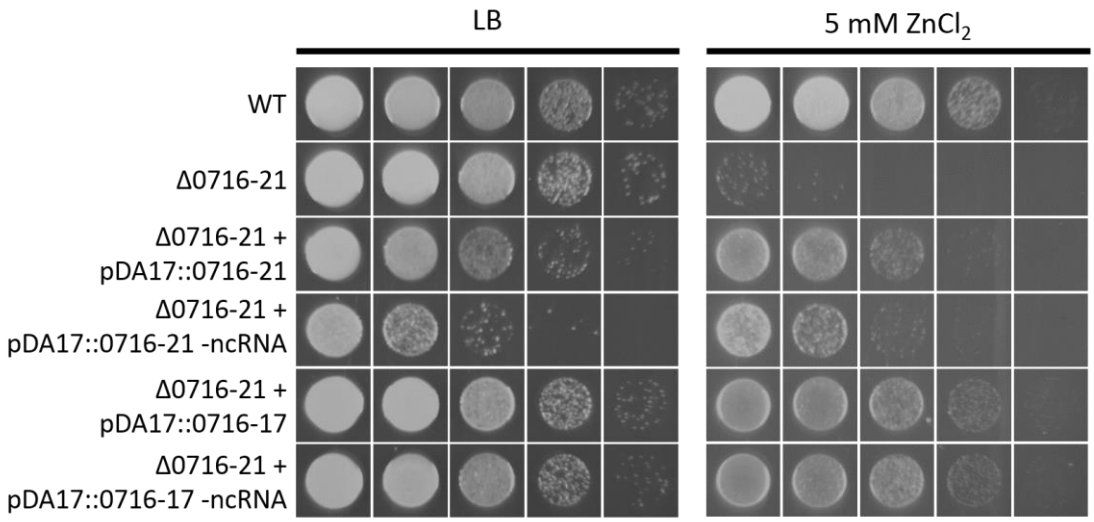

Figure 6.9: The potential ncRNA does not appear to affect complementation of the zinc sensitivity phenotype of ΔBCAM0716-21. 10^{-1} to 10^{-5} dilutions of standardised overnight culture were spotted left to right on the plates

6.2.5 - Δ*czcCBA*, but not ΔBCAM0716-21, is sensitive to copper

Based on the upregulation of the genes in the BCAM0711-21 gene region in response to copper outlined in Chapter 5 (Table 5.3), the ability of various deletion mutants related to this gene region to grow on copper was investigated. Surprisingly, while ΔBCAM0714/5 and ΔBCAM0716-21 showed no reduction in growth on copper, the previously generated Δ*czcCBA* mutant was sensitive to copper to a similar extent as the ΔBCAM0442/3 mutant (Fig 6.10). Interestingly, though a previously generated Δ*czcCB* mutant was also sensitive to copper, the sensitivity of Δ*czcCB* was lower than that of Δ*czcCBA*, suggesting that CzcA can function without CzcC or CzcB, either by itself or alongside other proteins, to extrude copper (Fig 6.11). While there is no complemented strain of Δ*czcCBA*, a Δ*czcCB* mutant conjugated with a previously generated pDA17::*czcCB* vector appears to be slightly complemented in its ability to grow on copper (Fig 6.11).

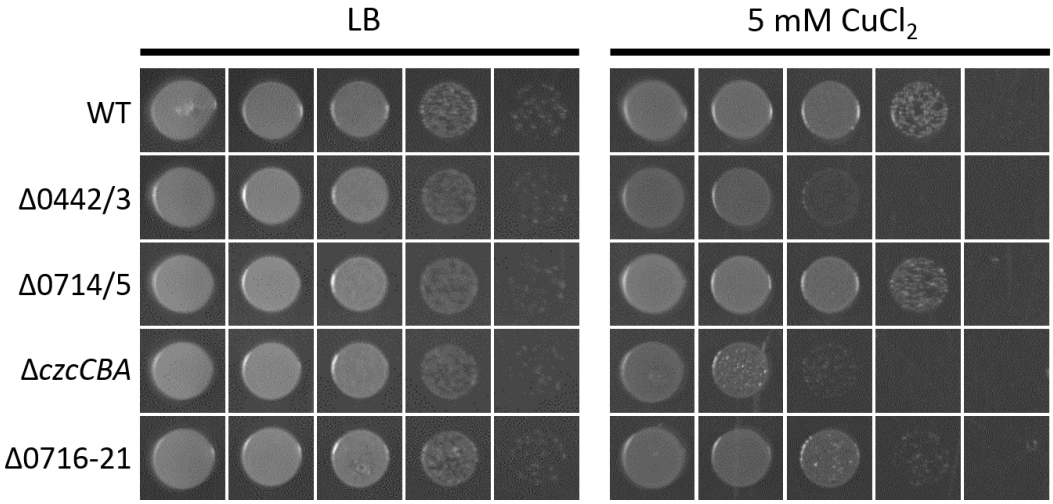

Figure 6.10: Δ*czcCBA* has a similar copper sensitivity phenotype to ΔBCAM0442/3. 10^{-1} to 10^{-5} dilutions of standardised overnight culture were spotted left to right on the plates

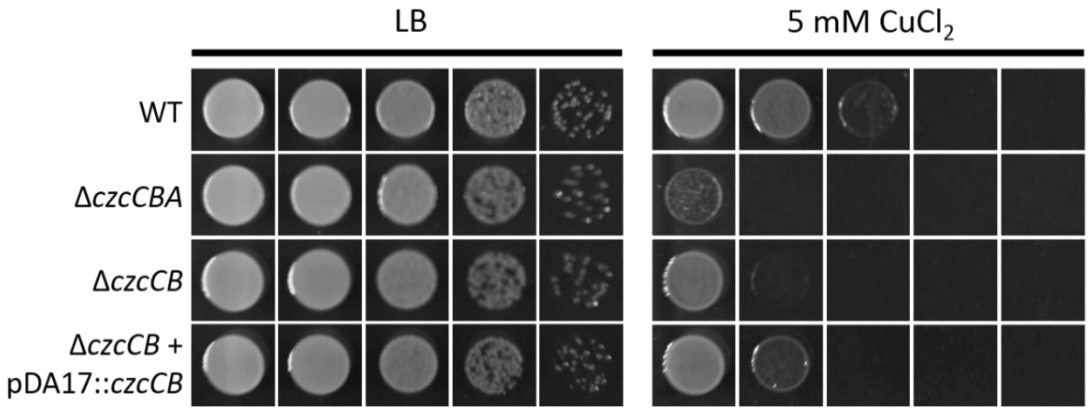

Figure 6.11: Δ*czcCBA* has greater sensitivity to copper than Δ*czcCB*. Conjugation of pDA17::*czcCB* into Δ*czcCB* appears to partially complement the copper sensitivity phenotype. 10^{-1} to 10^{-5} dilutions of standardised overnight culture were spotted left to right on the plates.

6.3 - Discussion

Previous work has established that the BCAM0714/5 TCS directly regulates parts of the BCAM0716-21 gene region, and that deletion of this region resulted in stark zinc sensitivity to *B. cenocepacia* (Robinson *et al*., Unpublished data). Through systematic complementation of the ΔBCAM0716-21 deletion mutant, the work presented in this chapter provides further insight into the novel zinc resistance determinant located within this gene region.

Conjugation of pDA17 vectors containing various pairings of genes within this BCAM0716-21 gene region resulted in identification of the BCAM0716-17 gene region as being likely to hold a novel zinc resistance determinant. There are three genes located within this region, BCAM0716, BCAM0716A and BCAM0717, the latter two of which overlap in opposite orientations within the genome. As conjugation of BCAM0716A/BCAM0717 into ΔBCAM0716-21 did not restore the ability to grow on zinc (Fig 6.6), it is likely that BCAM0716 is central to the novel zinc resistance determinant, acting either alone or in conjunction with BCAM0716A and/or BCAM0717.

Annotated within the J2315 genome as a 'Hypothetical protein', the potential role that BCAM0716 holds in the zinc response is unclear. Interestingly, BCAM0716 shares 41 % protein sequence identity with BCAM0718, and both are predicted to have a 'Domain of unknown function (DUF4148), Interpro Accession IPR025421' as listed on the *Burkholderia* genome database [18]. Two other genes within *B. cenocepacia*, BCAL1236 and BCAS0573, are predicted to contain the DUF4148 domain, though neither gene is differentially expressed in response to copper or zinc, so their potential link to the metal response is unclear. Genes with the DUF4148 domain appear to exist throughout the *Burkholderia* genus and the wider *Burkholderiales* order, though there is no evidence to suggest what role this domain has to play either in the zinc response or wider cellular function [492].

Being a relatively small protein at 95 amino acids in length, one possible explanation for the function of BCAM0716 (and possibly BCAM0718) may be that it acts as a zinc metallochaperone in *B. cenocepacia*. However, bacterial zinc chaperones are considered to be involved more in the shuttling of zinc to metalloproteins in situations of zinc limitation, such as ZigA from *Acinetobacter*

baumannii, [493,494] rather than situations of zinc toxicity, arguing against the idea that zinc metallochaperones may hold a role in protection of *B. cenocepacia* against zinc. Alternatively, BCAM0716 may act as a protein-folding chaperone, and given its proximity to the putative outer membrane porin BCAM0717 in the genome, it may be the case that BCAM0716 aids in the folding of BCAM0717 within the periplasm. Given that the 2 nucleotide deletion of BCAM0717 in *B. cenocepacia* K56-2 results in only the first 109 amino acids of BCAM0717 in *B. cenocepacia* K56-2 matching that of the J2315 genome (out of a total of 386 amino acids in J2315), it is relatively unlikely that BCAM0717 in *B. cenocepacia* K56-2 acts as a functional outer membrane porin [146]. Indeed, no conserved domains of BCAM0717 in *B. cenocepacia* K56-2 were identified bar outer membrane porin domains residing in the original 28 % of the protein [495].

That being said, given the evidence in Figure 6.6 that the BCAM0716-17 gene region is able to restore the ability of ΔBCAM0716-21 to grow on zinc, it may be the case that the longer transcript of BCAM0717 in *B. cenocepacia* K56-2 encodes a protein that is still able to contribute to zinc resistance provided that BCAM0716 is also present, even if it is non-functional as a porin. Additionally, given that conjugation of BCAM0716A-17 into ΔBCAM0716-21 confers cadmium and zinc sensitivity, it may be the case that despite the large frameshift within *B. cenocepacia* K56-2, BCAM0717 can still facilitate the influx of cadmium and zinc (Figs 6.6 and 6.8). As this sensitivity is not seen when BCAM0716 is also conjugated alongside BCAM0717 and BCAM0716A it is likely that BCAM0716 contributes to cadmium and zinc resistance, potentially through interacting either directly with BCAM0716A and/or BCAM0717 or through interactions with the metals of which BCAM0717 presumably facilitates the influx. This supports the idea that BCAM0716 assists the correct folding of BCAM0717, with BCAM0717 contributing to cadmium and zinc resistance alongside BCAM0716, though without BCAM0716, the presence of BCAM0717 confers sensitivity.

The other gene within the BCAM0716-17 gene region, BCAM0716A, is not currently annotated within the J2315 genome, despite being annotated in the K56-2 genome. Additionally, the annotation of BCAM0716A in the K56-2 genome may be missing the initial 138 bp of the gene, as an in frame ATG codon lies upstream of the currently annotated GTG start codon. As such it is not particularly clear whether BCAM0716A is a genuine gene or rather a potential open reading

frame that is not actually transcribed. As seen in Figure 6.7, a BCAM0714 binding motif lies between BCAM0716 and BCAM0716A, potentially meaning that BCAM0716A could be regulated by the BCAM0714 RR. However, BLAST searches of the protein sequence of BCAM0716A do not indicate any similarity with known protein sequences, nor does the annotated BCAM0716A in the *B. cenocepacia* K56-2 genome contain any particular functional or protein motif predictions, potentially signifying that BCAM0716A is not a genuine, transcribed gene [18]. If BCAM0716A were a genuine protein, its function in the zinc response is unclear. If BCAM0716A does indeed play a role in the response to zinc then it presumably must be reliant on the presence of BCAM0716, as conjugation of BCAM0716A and BCAM0717 does not restore the ability of ΔBCAM0716-21 to grow on zinc (Fig 6.6).

While there has been much focus on the BCAM0716-17 gene region, given the suggestion that a novel zinc resistance determinant resides within it, there is still the possibility that BCAM0718-21 also has a role to play in the response to zinc. While conjugation of the individual genes and orientation-guided pairings into ΔBCAM0716-21 did not restore the ability to zinc, it is possible that these genes work in conjunction with one another beyond the confines of their presumed operons to aid in the response to zinc. As such, complementation with a pDA17 vector containing all four genes within BCAM0718-21 should be considered in the future to ascertain whether these genes do in fact have any relation to the novel zinc resistance determinant located within the BCAM0716-21 gene region.

The work presented in this chapter has focused on complementation of the ΔBCAM0716-21 deletion mutant as the primary means of investigating the novel zinc resistance determinant in this region. In order to confirm whether the BCAM0716-17 region is indeed central to this determinant, deletion mutants of various genes and gene regions should be generated to assess the impact that loss of these genes has on the ability of *B. cenocepacia* to grow on zinc. Coupling data generated from relevant deletion mutants to the work presented here would hopefully refine the knowledge of the zinc resistance determinant within BCAM0716-21, as well as the potential contribution of other genes in this region to wider cellular function.

Given the upregulation of various genes within the genomic neighbourhood of the BCAM0714/5 TCS in response to 1 mM $CuCl_2$, including BCAM0716 and

BCAM0718 (Table 5.3), the ability of the ΔBCAM0716-21 deletion mutant to grow on copper was tested (Fig 6.10). While deletion of the BCAM0716-21 region does not confer sensitivity to copper, the previously generated Δ*czcCBA* and Δ*czcCB* mutants were sensitive to copper (Figs 6.10 and 6.11). As discussed in section 5.3, functional explanations for the upregulation of cadmium- and zinc-effluxing genes in response to copper include the general detoxification of heavy metals from the cell, in order to reduce general metal stress in response to the presence of one metal, and also to anticipate and prepare for the presence of one metal in an environment which contains another. However, the stark sensitivity of Δ*czcCBA* to copper suggests that the CzcCBA efflux pump plays a much more central role in the detoxification of *B. cenocepacia* to copper than previously thought; presumably an efflux pump that was upregulated to specifically detoxify cadmium and zinc, even in the aim of reducing metal stress, would not be as essential to resistance to copper as CzcCBA appears to be in Figure 6.10. As such, it may be that CzcCBA directly extrudes copper from the cell, in addition to cadmium and zinc. Given that the Δ*czcCBA* mutant appears more sensitive to copper than the Δ*czcCB* mutant, it may also be the case that the inner membrane-bound CzcA may be able to function to extrude copper without forming the full RND-family efflux pump with CzcCB (Fig 6.11).

As BCAM0714/5 is known to directly regulate CzcCBA (Robinson *et al*., Unpublished data), it is surprising that while BCAM0714/5 is indeed upregulated in response to 1 mM $CuCl_2$ (Table 5.3), the ΔBCAM0714/5 deletion mutant does not share the sensitivity to copper that Δ*czcCBA* does (Fig 6.10). This suggests that the transcription of the *czcCBA* genes is not under the sole regulation of BCAM0714, and that a separate transcription factor enables the upregulation of these genes in response to copper. As the upregulation of the CzcCBA efflux pump in response to 1 mM $CuCl_2$ still occurs in the ΔBCAM0442/3 deletion mutant (Table 5.3), and that there is no evidence that BCAS0585/6 is involved in the response of *B. cenocepacia* to copper, it is likely that this additional control of CzcCBA lies outside of this heavy metal-sensing MKN.

6.4 – Conclusions

- The novel zinc resistance determinant residing within BCAM0716-21 is located in the BCAM0716-17 region.
- Alterations to the annotations of BCAM0716-17 gene region within the *B. cenocepacia* J2315 and K56-2 genomes are recommended.
- The CzcCBA efflux pump has a role to play in the response to *B. cenocepacia* to copper, and its copper-dependent regulation is controlled by an unknown mechanism.

Chapter 7: Final discussion and concluding remarks

7.1 – Final discussion and concluding remarks

The work described here has surrounded four putative metal-sensing TCSs in *B. cenocepacia*, predicted to form a wider MKN based on specificity residue analysis. Previous work has characterised the BCAM0714/5 TCS as being implicated in the cadmium and zinc response (Robinson *et al*., Unpublished data), while BCAM0442/3 was identified in a screen of copper-resistance genes in *B. cenocepacia* H111 [369]. Various methodologies have been employed in the aim of identifying whether these TCSs do indeed form a MKN, and what individual role these TCSs have in the metal response of *B. cenocepacia*. A visual summary of the current information known about this MKN can be found in Figure 7.1.

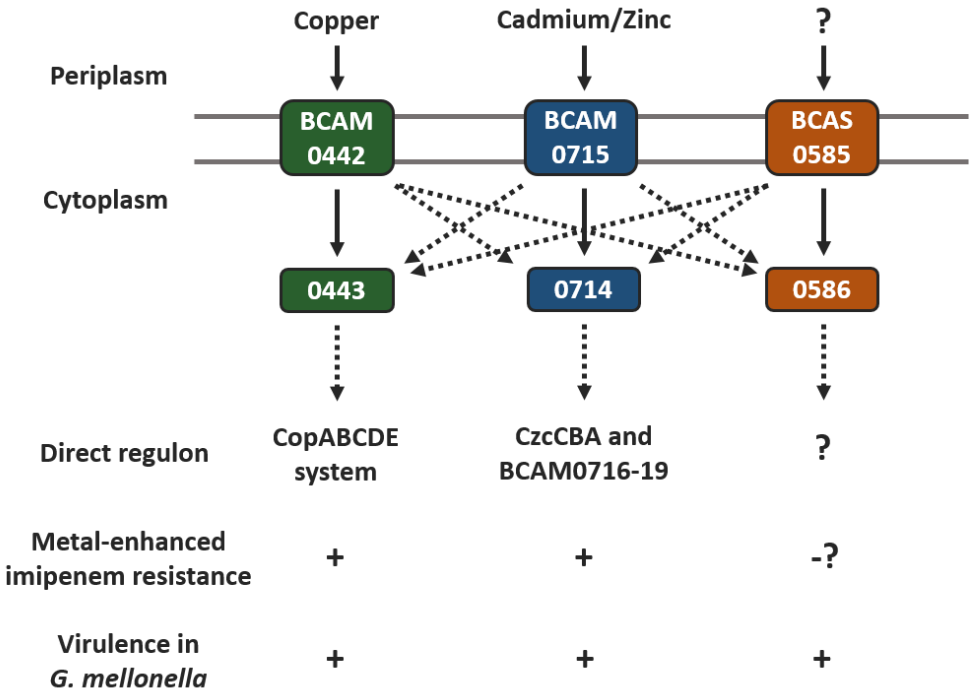

Figure 7.1: The current model for the metal-sensing MKN in *B. cenocepacia*. Three TCSs in which non-cognate phosphotransfer is possible form a metal-sensing MKN in *B. cenocepacia*. Though this MKN links the copper, cadmium and zinc responses of *B. cenocepacia* through BCAM0442/3 and BCAM0714/5, the role of BCAS0585/6 is unclear. This MKN is associated with metal-enhanced imipenem resistance, though it appears that BCAS0585/6 acts in an opposing manner to the other two TCSs. Additionally, this MKN is important for virulence of *B. cenocepacia* to *G. mellonella* larvae.

By purifying relevant SKs tagged with NusA and untagged RRs, the potential for non-cognate phosphotransfer between these TCSs was investigated using the phosphotransfer assay. This led to the finding that non-cognate phosphotransfer is kinetically possible between the SKs and RRs of three of the four TCSs, BCAM0442/3, BCAM0714/5 and BCAS0585/6, suggesting that these three TCSs form a MKN. This also validates the notion that specificity residue analysis is a reliable tool of predicting non-cognate phosphotransfer between SKs and RRs. Additionally, the BCAM0715 SK appeared to have the greatest propensity for non-cognate phosphotransfer, with rates of phosphotransfer being similar for cognate and non-cognate RRs, perhaps signifying that BCAM0714/5 may act as a central hub within this metal-sensing MKN.

Following on from the identification of the three TCSs that form a MKN, single, double and triple TCS deletion mutants were generated. This confirmed that BCAM0714/5 is implicated in the cadmium and zinc response, and also identified that the BCAM0442/3 TCS is implicated in the copper response. Transcriptional fusion of TCS putative promoters to *gfp* identified that BCAM0442/3 and BCAM0714/5 are induced by copper and cadmium/zinc respectively; this induction was lost in their respective TCS deletion mutants. Additionally, there appears to be a reduction of copper-dependent induction of the BCAM0442/3 promoter in the ΔBCAM0714/5 deletion mutant, suggesting that transcriptional activation of BCAM0442/3 in response to copper is partially mediated by BCAM0714/5. As is the case with *P. aeruginosa*, growth curve analysis revealed that exposure of *B. cenocepacia* to subinhibitory copper or zinc reduces sensitivity to imipenem, and that this MKN plays a crucial role, but is not absolutely necessary, in this phenomenon. It also appears to be the case that the TCSs within this MKN play a role in virulence in the *G. mellonella* larvae model, with a deletion mutant of the entire MKN showing a stark attenuation in virulence compared to other deletion mutants.

To further explore the role of BCAM0442/3 in *B. cenocepacia*, RNA-seq analysis was conducted on WT and ΔBCAM0442/3 *B. cenocepacia* grown with and without 1 mM $CuCl_2$. This identified a large transcriptional response to copper, with 15.5 % of the genome being significantly differentially expressed. While concentration of copper and time of exposure were not identical to this study, this level of transcriptional response is comparatively larger than that observed for *P.*

aeruginosa, in which two studies demonstrated a transcriptional response involving 6-8 % of the genome [242,486]. Several genes surrounding BCAM0442/3 that are heavily upregulated in response to copper, including a CopABCDE-like system, the upregulation of which appears to be BCAM0442/3-dependent. As such, it is recommended that BCAM0442/3 now be denoted as CopRS. Many other genes were identified as being upregulated in response to copper, including the BCAM0714/5 genomic neighbourhood, perhaps suggesting that the general detoxification of the cell of heavy metals may confer protection against high concentrations of a single metal.

Previous work identified that deletion of the downstream gene region of the BCAM0714/5 TCS, BCAM0716-21, conferred stark zinc sensitivity to *B. cenocepacia*. Chapter 6 of this work focused on the complementation of the ΔBCAM0716-21 deletion mutant with the aim of identifying the novel zinc resistance determinant located within. Conjugation of the BCAM0716-17 gene region, which also contains the hypothetical protein BCAM0716A, into ΔBCAM0716-21 restored the ability to grow on zinc, suggesting that the novel zinc resistance determinant resides within this gene region. Additionally, it was identified that the previously generated Δ*czcCBA* mutant was sensitive to copper, suggesting either that CzcCBA extrudes copper in addition to cadmium or zinc, or that detoxification of cadmium or zinc from the cell is crucial in the response of *B. cenocepacia* to copper. Surprisingly, ΔBCAM0714/5 was not sensitive to copper, suggesting that the copper-dependent upregulation of *czcCBA* is BCAM0714/5-independent. Additionally, the upregulation of *czcCBA* was still observed in the ΔBCAM0442/3 deletion mutant, suggesting that this upregulation is also BCAM0442/3-independent.

Though this work has provided the first evidence that a metal-sensing MKN exists in *B. cenocepacia*, there are questions surrounding what the evolutionary advantage is to the cell in having a network of three TCSs that are able to undergo non-cognate phosphorylation with each other, rather than having three discrete, independent TCSs. The data presented here, such as the metal phenotypes of the TCS deletion mutants, the induction of the promoters via *gfp* transcriptional fusion vectors, the virulence phenotypes of each TCS and the RNA-seq analysis of the copper response, do not provide clear evidence that alludes to why this network exists. It is presumably the case that the stark similarity in specificity

residues between the RRs of these TCSs is due to evolutionary pressure to maintain this non-cognate phosphotransfer. Indeed, specificity residue similarity between putative metal-sensing TCSs is found throughout the BCC and the wider *Burkholderia* genus, suggesting that this MKN is indeed evolutionarily conserved. As such, there must be some benefit to the cell in maintaining non-cognate phosphotransfer, rather than allowing these TCSs to drift apart, forming three independent systems. Though this work has uncovered the key players in this network, future work should primarily focus on investigating why this metal-sensing network exists in *B. cenocepacia*.

For that objective, there are several avenues of investigation that could be followed to refine our knowledge of this network. To further explore the non-cognate interactions that these TCSs share, several protein mutants could be generated, such as SKs that lack the ability to autophosphorylate, and SKs that are unable to act as phosphatases to their RRs. This would allow the investigation of whether SKs can act as phosphatases not just to their own RRs, but also to non-cognate RRs through use of the phosphotransfer assay; a concept which would further aid our understanding of the dynamics of this MKN. Additionally, employment of the BACTH methodology would permit the study of whether any non-phosphotransfer based interactions occur between these proteins, such as SK or RR heterodimerisation.

One important further focus should be the generation and characterisation of deletion mutants of individual SKs and RRs, to further refine what contribution particular proteins provide to this MKN. All assays presented here that utilise TCS deletion mutants should be further performed with single SK or single RR deletion mutants. For example, a ΔBCAM0442 SK deletion mutant that is not sensitive to copper would strongly suggest activation of the RR BCAM0443 in a BCAM0442-independent manner. Additionally, double and triple TCS deletion mutants that are gentamicin-sensitive could be generated, to further explore what function these TCSs have in the survival within immune cells. ChIP-seq analysis of each RR would allow the definition of the specific regulon of each TCSs, which coupled to RNA-seq analysis and *gfp* transcriptional fusion of putative promoters would give invaluable insight into the functioning of this MKN. Ultimately, there are many different avenues that could be taken in the future that would aid in the understanding of this novel heavy metal-sensing MKN.

Given the environmental impact of heavy metal pollution, the use of metals as an antibacterial strategy by the immune system and the clinical use of metals such as copper, understanding the regulators and effectors of bacterial metal resistance is vital. Overall, this work has generated evidence for the existence of a novel heavy metal-sensing MKN in *B. cenocepacia*, which is implicated in both resistance to carbapenems and in virulence.

Appendices

A1 – Figures/Tables pertinent to Chapter 3

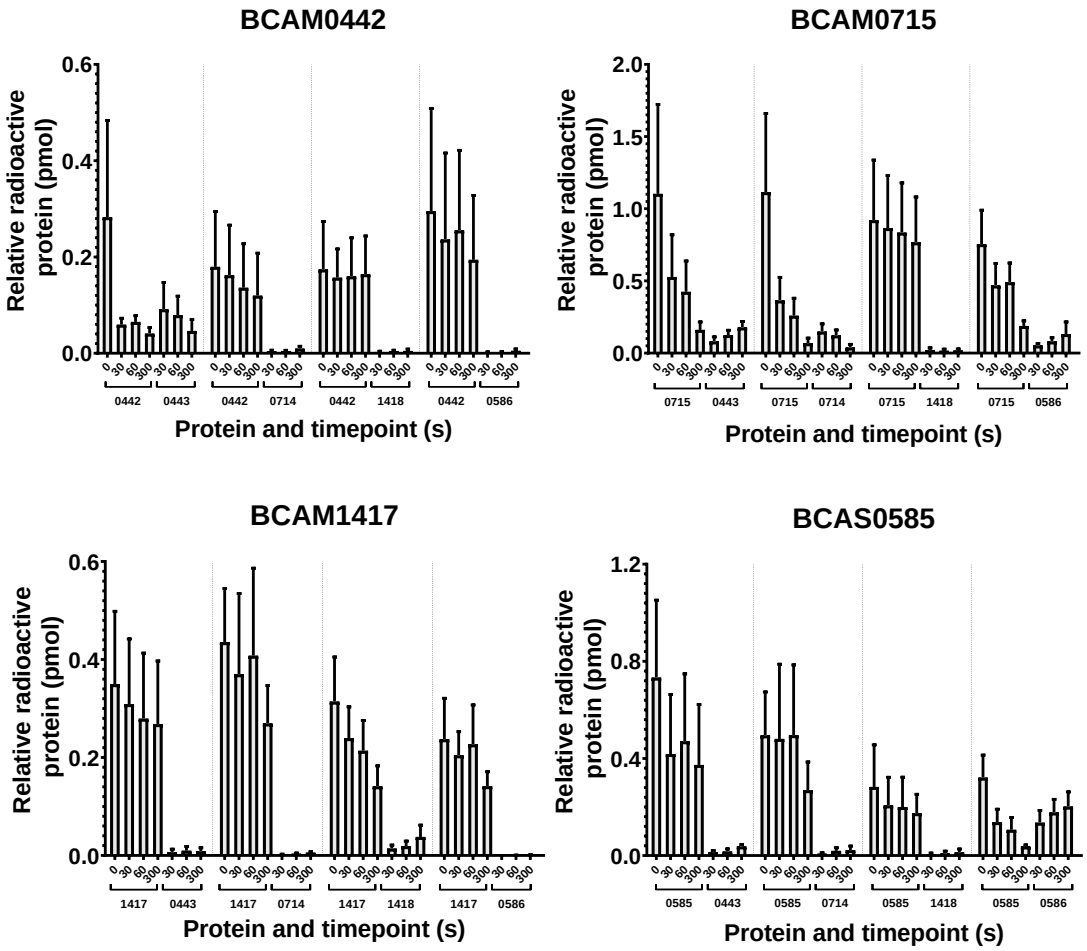

Figure A1.1: Quantification of phosphotransfer from pre-phosphorylated and subsequently purified SK. Each graph displays phosphotransfer from a single SK to multiple RRs in '1 SK-1 RR' phosphotransfer reactions. n = 3 independent experiments. Error bars indicate SEM.

A2 – Figures/Tables pertinent to Chapter 4

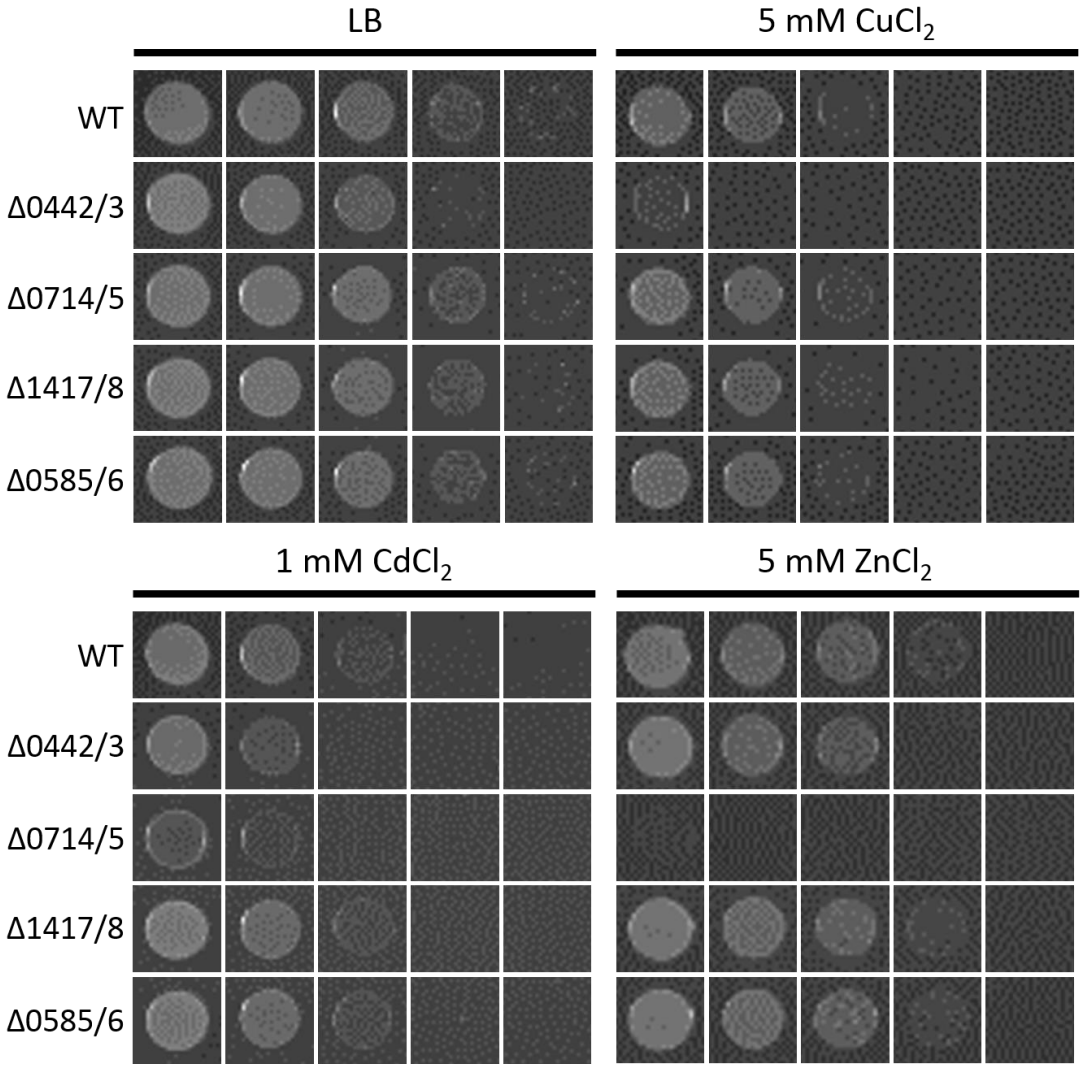

Figure A2.1: Gentamicin-sensitive single TCS deletion mutants spotted on copper-, cadmium- and zinc-supplemented agar plates. 10^{-1} to 10^{-5} dilutions of standardised overnight culture were spotted left to right on the plates. The metal sensitivity of the gentamicin-sensitive mutants matches that of the regular single TCS deletion mutants (Fig 4.5).

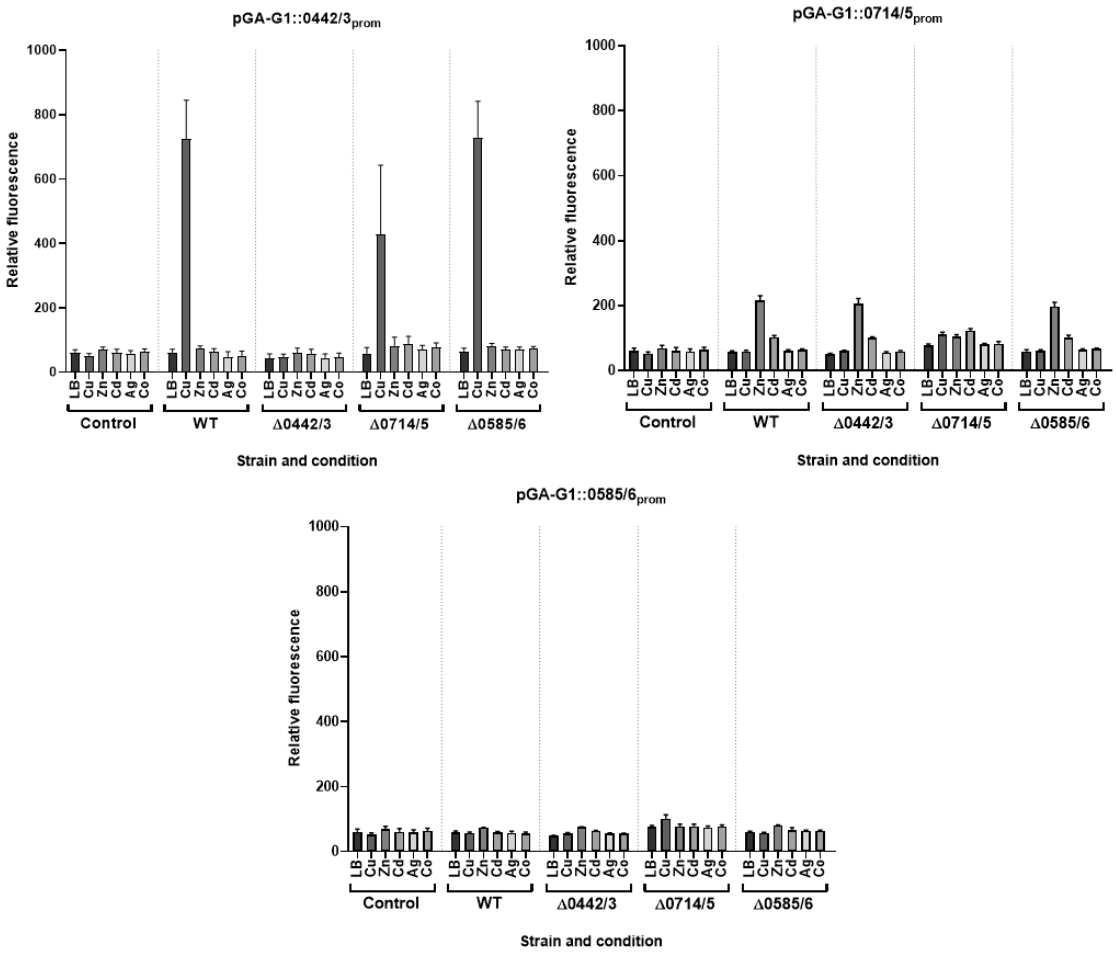

Figure A2.2: Relative fluorescence of 24 hour growth of *B. cenocepacia* TCS deletion mutants containing all pGA-G1 promoter vectors. Control refers to gentamicin-sensitive WT *B. cenocepacia* containing pGA-G1 lacking a promoter. Metal concentrations are as follows: $CuCl_2$ – 1 mM, $ZnCl_2$ – 1 mM, $CdCl_2$ – 0.25 mM, $AgNO_3$ – 5 µM, $CoCl_2$ – 0.25 mM. n = 3 independent experiments with 3 technical replicates per assay. Error bars indicate SEM.

A3 – Figures/Tables pertinent to Chapter 5

Table A3.1: Fold changes of various genes that are pertinent to a range of virulence phenotypes in response to copper.

Gene name	Predicted protein function	Fold change (Copper vs LB)		Fold change (Δ0442/3 vs WT)	
		WT	Δ0442/3	LB	$CuCl_2$
Bacterial secretion systems					
BCAL0337	T6SS protein (TssL)	0.26	0.55	0.59	1.26
BCAL0338	T6SS protein (TssK)	0.34	0.71	0.60	1.25
BCAL0339	T6SS protein (TssJ)	0.30	1.10	0.41	1.49
BCAL0340	Putative lipoprotein	0.53	0.70	0.71	0.94
BCAL0341	T6SS protein (TssB)	0.51	0.68	0.83	1.12
BCAL0342	T6SS protein (TssC)	0.38	0.78	0.58	1.17
BCAL0343	T6SS protein (TssD)	0.34	0.80	3.30	7.75
BCAL0344	T6SS protein (TssE)	0.33	1.07	0.42	1.36
BCAL0345	T6SS protein (TssF)	0.33	0.91	0.49	1.35
BCAL0346	T6SS protein (TssG)	0.32	0.68	0.65	1.40
BCAL0347	T6SS protein (TssH)	0.35	0.85	0.63	1.53
BCAL0348	T6SS protein (TssA)	0.34	0.83	0.64	1.58
BCAL0349	Putative outer membrane protein	0.31	1.12	0.52	1.87
BCAL0350	Hypothetical protein	0.24	0.83	0.41	1.41
BCAL0351	T6SS protein (TssM)	0.25	0.97	0.36	1.39
BCAL3515	T2SS protein N (GspN)	0.55	0.59	1.42	1.52
BCAL3516	T2SS protein M (GspM)	0.90	0.38	2.49	1.05
BCAL3517	T2SS protein L	0.39	0.88	1.01	2.28
BCAL3519	T2SS protein K (GspK)	0.83	0.59	1.11	0.79
BCAL3520	T2SS protein J (GspJ)	1.30	0.12	4.19	0.39
BCAL3521	T2SS protein I (GspI)	0.91	0.68	2.51	1.87

BCAL3522	T2SS protein H (GspH)	3.26	0.32	4.39	0.43
BCAL3523	T2SS protein G (GspG)	0.73	0.51	1.48	1.03
BCAL3524	Putative T2SS protein	0.86	0.52	2.26	1.35
BCAL3525	T2SS protein F (GspF)	0.29	1.56	0.43	2.30
BCAL3526	T2SS protein E (GspE)	0.34	0.98	0.66	1.90
BCAL3527	T2SS potein D (GspD)	0.56	0.85	0.58	0.91
Flagella-associated genes					
BCAL0520	Flagellar hook-length control protein (FliK)	0.40	0.30	1.23	0.95
BCAL0521	Flagellar protein (FliJ)	0.60	0.65	0.84	0.91
BCAL0522	Flagellum-specific ATP synthase (FliI)	0.22	0.73	0.35	1.13
BCAL0523	Flagellar assembly protein (FliH)	1.07	0.27	1.83	0.46
BCAL0524	Flagellar motor switch protein (FliG)	0.14	0.41	0.58	1.74
BCAL0525	Flagellar M-ring protein (FliF)	0.17	0.28	0.54	0.85
BCAL0526	Flagellar hook-basal body complex protein (FliE)	0.14	0.24	0.44	0.77
BCAL0527	Flagellar protein (FliS)	3.48	0.33	2.91	0.27
BCAL0561	Flagella synthesis protein (FlgN)	2.46	0.74	1.68	0.50
BCAL0562	Negative regulator of flagellin synthesis (anti-sigma-28 factor)	3.80	0.64	2.06	0.35
BCAL0563	Flagellar basal body P-ring formation protein (FlgA)	0.41	0.19	1.14	0.53

BCAL0564	Flagellar basal-body rod protein (FlgB)	0.18	0.26	0.54	0.76
BCAL0565	Flagellar basal-body rod protein (FlgC)	0.13	0.24	0.61	1.14
BCAL0566	Basal-body rod modification protein (FlgD)	0.086	0.35	0.45	1.80
BCAL0567	Flagellar hook protein 1 (FlgE1)	0.13	0.36	0.59	1.56
BCAL0568	Flagellar basal-body rod protein (FlgF)	0.12	0.51	0.51	2.26
BCAL0569	Flagellar basal-body rod protein (FlgG)	0.14	0.59	0.44	1.84
BCAL0570	Flagellar L-ring protein precursor (FlgH)	0.16	0.65	0.56	2.28
BCAL0571	Flagellar P-ring protein precursor (FlgI)	0.26	0.53	0.61	1.26
BCAL0572	Peptidoglycan hydrolase (FlgJ)	0.47	0.68	0.68	0.99
BCAL3501	Flagellar biosynthetic protein (FliR)	0.094	0.81	0.22	1.94
BCAL3502	Flagellar biosynthetic protein (FliQ)	0.045	0.26	0.59	3.33
BCAL3503	Flagellar biosynthetic protein (FliP)	0.080	0.52	0.30	1.98
BCAL3504	Flagellar protein (FliO)	0.20	0.22	2.29	2.55
BCAL3505	Flagellar motor switch protein (FliN)	0.14	0.24	0.50	0.86
BCAL3506	Flagellar motor switch protein (FliM)	0.13	0.25	0.43	0.81
BCAL3507	Flagellar protein (FliL)	0.27	0.20	0.65	0.49
Chemotaxis-associated genes					

BCAL0126	Chemotaxis protein (MotA)	4.67	1.10	2.54	0.60
BCAL0127	Chemotaxis protein (MotB)	4.45	0.92	2.59	0.54
BCAL0128	Chemotaxis two-component RR (CheY)	6.83	0.49	3.44	0.25
BCAL0129	Chemotaxis two-component SK (CheA)	2.88	0.66	2.20	0.50
BCAL0130	Chemotaxis protein (CheW)	1.66	0.87	1.21	0.64
BCAL0131	Methyl-accepting chemotaxis protein	1.64	0.65	1.47	0.58
BCAL0132	Chemotaxis protein methyltransferase (CheR)	1.74	1.01	1.30	0.75
Putative universal stress proteins					
BCAM0290	Putative universal stress protein	4.20	0.46	7.72	0.84
BCAM0291	Putative universal stress protein	3.45	0.98	4.08	1.16
BCAM0292	Putative universal stress protein	4.29	0.65	4.97	0.75
BCAM1829	Putative universal stress protein	3.56	1.96	1.99	1.09
BCAL2268	Putative stress protein	0.17	1.13	0.27	1.81
Putative outer membrane porins					
BCAL0584	Putative outer membrane porin	0.19	0.54	0.51	1.40
BCAL2615	Putative outer membrane porin	0.24	1.60	0.19	1.28
BCAL3008	Putative outer membrane porin	0.16	1.27	2.49	0.92
BCAM1015	Putative porin	0.50	0.66	1.00	1.32

BCAM2063	Putative carbohydrate-selective porin	0.10	0.39	0.43	1.77
BCAM2462	Putative Gram-negative porin	3.37	2.62	2.97	2.30
BCAM2723	Putative outer membrane porin	0.14	0.89	0.27	1.72
BCAS0256	Putative porin protein	0.14	1.20	0.18	1.57
Low-oxygen-activated locus genes					
BCAM0275a	Hypothetical protein	1.17	0.83	1.69	1.20
BCAM0276	Putative universal stress protein	1.78	0.71	2.74	1.10
BCAM0277	Hypothetical protein	4.56	0.79	5.35	0.92
BCAM0278	Putative heat shock protein	8.08	1.59	4.69	0.92
BCAM0279	Hypothetical protein	1.84	0.51	4.11	1.14
BCAM0280	Putative phospholipid-binding protein	4.76	1.03	5.23	1.13
BCAM0280A	Conserved hypothetical protein	5.17	1.15	5.38	1.20
BCAM0281	Putative sulfate transporter family protein	2.48	1.41	1.65	0.94
BCAM0282	Conserved hypothetical protein	3.09	1.14	2.46	0.91
BCAM0283	Putative lysine decarboxylase	2.29	1.19	2.46	1.29
BCAM0284	Putative cytochrome c	2.33	0.62	4.60	1.23
BCAM0285	Hypothetical protein	1.84	0.58	2.93	0.91
BCAM0286	Putative alcohol dehydrogenase	3.17	0.90	2.55	0.73
BCAM0287	CRP family regulatory protein	0.57	0.58	1.26	1.28

BCAM0288	Two-component regulatory system, RR protein	1.09	1.10	1.13	1.13
BCAM0289	Two-component regulatory system, SK protein	1.43	1.27	1.26	1.12
BCAM0290	Putative universal stress protein	4.20	0.46	7.72	0.84
BCAM0291	Putative universal stress protein	3.45	0.98	4.08	1.16
BCAM0292	Putative universal stress protein	4.29	0.65	4.97	0.75
BCAM0293	Putative acetate kinase	1.95	0.75	3.32	1.28
BCAM0294	Putative universal stress protein	1.34	0.71	2.39	1.27
BCAM0295	Hypothetical protein	2.74	0.64	4.06	0.94
BCAM0296	Acetoacetyl-CoA reductase	2.32	0.84	3.76	1.36
BCAM0297	Putative poly(3-hydroxyalkanoate) polymerase	3.03	1.13	3.17	1.19
BCAM0298	Putative phosphate acetyl/butyryl transferase	4.79	1.13	4.53	1.07
BCAM0299	Putative zinc-binding alcoholdehydrogenase	15.38	1.18	12.19	0.93
BCAM0300	Metallo-beta-lactamase superfamily protein	1.42	0.66	2.59	1.20
BCAM0301	Putative membrane protein	3.37	1.17	1.95	0.68
BCAM0302	Putative ABC transporter protein	14.22	1.15	8.64	0.70

BCAM0303	ABC transporter ATP-binding membrane protein	7.01	1.33	5.73	1.08
BCAM0304	Transporter system transport protein	6.54	0.99	8.23	1.24
BCAM0305	Outer membrane transport system protein	4.57	0.74	5.60	0.90
BCAM0306	Putative membrane protein	1.98	0.34	3.24	0.56
BCAM0307	Hypothetical protein	3.59	0.85	4.54	1.08
BCAM0308	Hypothetical protein	3.56	1.20	4.44	1.50
BCAM0309	Putative cell division-related metallo peptidase	3.62	1.43	3.65	1.44
BCAM0310	Putative ribonucleotide reductase	2.08	0.57	2.47	0.67
BCAM0311	Putative 6-phosphofructokinase	2.60	0.38	5.10	0.74
BCAM0312	Putative polysaccharide deacetylase	2.02	0.47	3.95	0.93
BCAM0313	Putative exported protein	1.94	0.68	3.83	1.34
BCAM0314	Hypothetical protein	2.34	0.19	2.33	0.19
BCAM0315	Putative exported protein	3.47	1.45	4.49	1.87
BCAM0316	Hypothetical protein	2.37	0.60	3.17	0.80
BCAM0317	Putative membrane protein	1.53	0.52	2.12	0.72
BCAM0318	Putative cation-transporting ATPase	3.22	0.71	5.17	1.14

BCAM0319	Putative universal stress protein	0.87	0.50	2.21	1.27
BCAM0320	Putative cytochrome b561	1.52	1.17	1.24	0.96
BCAM0321	Hypothetical protein	1.04	0.95	0.99	0.91
BCAM0322	Two-component regulatory system, RR protein	0.99	1.08	0.86	0.93
BCAM0323	Two-component regulatory system, SK protein	0.78	1.09	0.85	1.19
Flp type pilus genes					
BCAL1525	Flp type pilus subunit	1.50	1.19	0.78	0.62
BCAL1525a	Putative flp type pilus leader peptidase	1.92	1.01	1.38	0.72
BCAL1526	Putative flp type pilus assembly protein	1.84	1.05	1.12	0.64
BCAL1527	Flp type pilus assembly protein	1.25	0.74	1.11	0.66
BCAL1528	Flp type pilus assembly protein	1.80	0.78	2.07	0.91
BCAL1529	Flp pilus type assembly-related protein	1.43	1.07	1.47	1.10
BCAL1530	Flp pilus type assembly protein	1.88	0.90	1.96	0.94
BCAL1531	Flp type pilus assembly protein	2.05	1.09	1.74	0.92
BCAL1532	Flp type pilus assembly protein	2.28	1.02	1.56	0.70

Note: Shaded cells indicate genes that are not significantly differentially expressed in that comparison. *Significantly differentially expressed genes are defined as having an adjusted p-value of < 0.05 and a fold change of > 2.*

A4 – Figures/Tables pertinent to Chapter 6

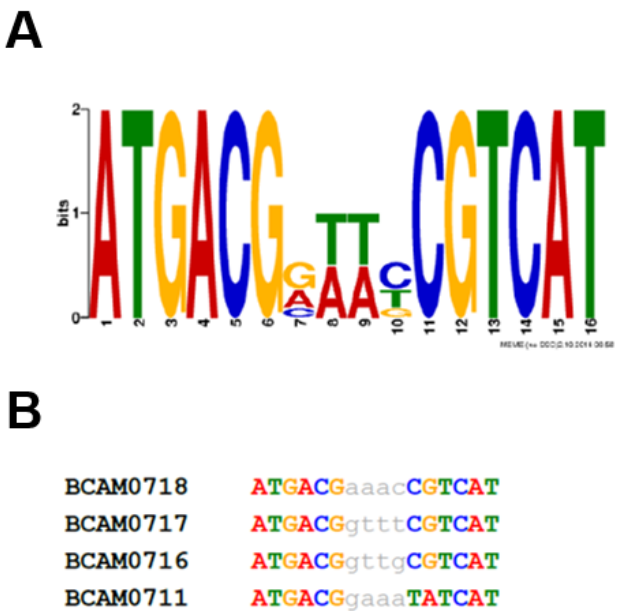

Figure A4.1: A conserved motif upstream of BCAM0714-potentially regulated genes. A) A fully-conserved 6 bp inverted repeat is separated by a non-conserved sequence of 4 bp. B) A motif upstream of *czcC* is similar to the motif upstream of both BCAM0716 and BCAM0717/8. Analysis performed and figure generated by Dr Matthew Robinson using MEME [490].

Figure A4.2: Alignment of BCAM0717 from *B. cenocepacia* J2315 and K56-2. The two bp deletion within BCAM0717 from *B. cenocepacia* K56-2 is denoted with red bars. While BCAM0717 from *B. cenocepacia* J2315 is 1161 bp in length, BCAM0717 in *B. cenocepacia* K56-2 continues to the next in frame stop codon, resulting in an open reading frame of 1745 bp in length. Alignment created using Clustal Omega 1.2.4 [496].

A5 – List of primers

Table A5.1 – List of primers pertinent to Chapter 3.

Name	Sequence (5’ – 3’)	Enzyme site
BCAM0442 F	acgcggatcctcgcgcggcctgcgcccg	BamHI
BCAM0442 R	acgcaagcttctaacgatcggcgccgcgcgga	HindIII
BCAM0443 F	acgcggatcccggatactgatagtcgaagacg	BamHI
BCAM0443 R	acgcaagctttcacgaacgatcctcgagcac	HindIII
BCAM0714 F	acgcggatcccgaattctgattgtcgaggatg	BamHI
BCAM0714 R	acgcaagctttcatgcggccgcgcc	HindIII
BCAM0715 F	acgcggatccagcccgctgcggcggttcgc	BamHI
BCAM0715 R	acgcaagctttcaggtgctgatggcggccgg	HindIII
BCAM1417 F	acgcagatctgcgcgcttcgggctcg	BglII
BCAM1417 R	acgcaagctttcagtgcagcgcgcgc	HindIII
BCAM1418 F	acgcggatccaaagtgctgatcgtcgaagac	BamHI
BCAM1418 R	acgcaagctttcatgcgcgccgctccg	HindIII
BCAS0585 F	acgcggatcccgcacggcgctcgcgccg	BamHI
BCAS0585 R	acgcaagctttcacgcagccggcggccggt	HindIII
BCAS0586 F	acgcagatctcgcatcctgatagtcgaag	BglII
BCAS0586 R	acgcaagctttcatgcgtcgtccttcgg	HindIII
BCAM0443 eGFP F	acgcggtaccggtcggatactgatagtcgaagacg	KpnI
BCAM0443 eGFP R	acgcaagctttcacgaacgatcctcgagcac	HindIII
BCAM0714 eGFP F	acgcggtaccggtcgaattctgattgtcgaggatg	KpnI
BCAM0714 eGFP R	acgcaagctttcatgcggccgcgcc	HindIII
BCAM1418 eGFP F	acgcggtaccggtaaagtgctgatcgtcgaagac	KpnI
BCAM1418 eGFP R	acgcaagctttcatgcgcgccgctccg	HindIII
BCAS0586 eGFP F	acgcggtaccggtcgcatcctgatagtcgaag	KpnI
BCAS0586 eGFP R	acgcaagctttcatgcgtcgtccttcgg	HindIII
eGFP F	acgcggatccgtgagcaagggcgaggag	BamHI
eGFP R	acgcggtaccttgtacagctcgtccatgc	KpnI
NusA F	gaacgccagcacatggac	-
pQE80 F	atcgggagaaattaactatgagaggatcgc	-
pQE80 R	atcgctggatctatcaacaggagtccaag	-

Note: Restriction site sequences are underlined.

Table A5.2 – List of primers pertinent to Chapter 4.

Name	Sequence (5' – 3')	Enzyme site
Flanking primers utilised for generation of pGPI-SceI vectors		
BCAM0442/3 F1	agcttctagagagccgcgcgtcaatccgatccg	XbaI
BCAM0442/3 R1	gccgcgtcgtgcggctagc	-
BCAM0442/3 F2	gctagccgcacgacgcggcggtgaggcaggctgtccgtg	-
BCAM0442/3 R2	agctgaattcggtcgatgccgccgg	EcoRI
BCAM0714/5 F1	agcttctagaggccagttcgagcagttg	XbaI
BCAM0714/5 R1	tcacgcattacccttgaagaaacc	-
BCAM0714/5 F2	ggtttcttcaagggtaatgcgtgacagcgcgggcggctacg	-
BCAM0714/5 R2	agctgcatgcgcggcaggcttcatgttccgc	SphI
BCAM1417/8 F1	agcttctagagtatttcccgcgcatcacg	XbaI
BCAM1417/8 R1	tccgcgtaaccggttaagg	-
BCAM1417/8 F2	ccttaaccggttacgcggatgcactgacggcggtcgcg	-
BCAM1417/8 R2	agctgaattcagcatgcgatcgacgcgaag	EcoRI
BCAS0585/6 F1	agcttctagactcgaaagttcgttcttcgc	XbaI
BCAS0585/6 R1	tcgtgctcacgttcaacc	-
BCAS0585/6 F2	ggttgaacgtgagcacgacgtcgcattcgtggggacatg	-
BCAS0585/6 R2	agctgaattcatgcacatgctgatctcgatca	EcoRI
Primers for PCR and sequence validation of deletion mutants		
BCAM0442/3 ScrnF	cttggcggagatctcgatgtc	-
BCAM0442/3 ScrnR	gaattcctcgcccgtatccgctc	-
BCAM0714/5 ScrnF	gttgaccgtcaacctcgacc	-
BCAM0714/5 ScrnR	cggcatagtcgatttgctcg	-
BCAM1417/8 ScrnF	gctgctgtcgttgagctggtag	-
BCAM1417/8 ScrnR	aagctgctgcacacgatcc	-
BCAS0585/6 ScrnF	tcgaggaatcgggtttcagcgtc	-
BCAS0585/6 ScrnR	gtgtcgctgtcgaaattcatgtccc	-

dhfr F	gagtgccacctttggcttag	-
dhfr R	aatgcttaggccacacgttc	-
pGPI-SceI F	tgctcaatcaatcaccggatcc	-
pGPI-SceI R	gaacacttaacggctgacatgg	-
pDA17 F	ttgttgtggggtaggcagtc	-
pDA17 R	accgcttctgcgttctgat	-
BCR1 [497]	tgaccgccgagaagagcaa	-
BCR2 [497]	ctcttcttcgtccatcgcctc	-
Primers for the generation of the pDA17::0442/3 complementation vector		
BCAM0442/3 C F	acgtgctagctggatgcgaaatcgggcagacag	NheI
BCAM0442/3 C R	acgtggtaccacgcgctaacgatcggc	KpnI
Primers for the generation of pGA-G1 promoter-*gfp* fusion vectors		
BCAM0442/3 Pr F	agctggatccggatgcgaaatcgggcagacagcgatc	BamHI
BCAM0442/3 Pr R	agctggatccggtgaggcaggctgtccgtgattccag	BamHI
BCAM0714/5 Pr F	agctggatcctgattcaaagtctcgattcgtaggttttcaagc	BamHI
BCAM0714/5 Pr R	agctggatccgttcggttctgcggtaacgg	BamHI
BCAS0585/6 Pr F	agctggatcctgcgcgagccggcggcgttag	BamHI
BCAS0585/6 Pr R	agctggatcccgccggctccgtcgcattcgtgg	BamHI
pGA-G1 F	ccttcaccctctccactgacag	-
pGA-G1 R	gctttactaagctgatccggtgg	-

Note: Restriction site sequences are underlined.

Table A5.3 – List of primers pertinent to Chapter 5.

Name	Sequence (5’ – 3’)	Enzyme site
BCAM0433-50 F1	acgttctagacgcacgagcatcccttcgt	XbaI
BCAM0433-50 R1	gggacgatctagcggcgg	-
BCAM0433-50 F2	ccgccgctagatcgtccccccaaatcggaacccaaaggg	-
BCAM0433-50 R2	acgtgaattcgactggatgcgctcgg	EcoRI
BCAM0433-50 ScrnF	tcgaggatcaggcggttgcg	-
BCAM0433-50 ScrnR	gcgcagtatctcgcggacc	-

Note: Restriction site sequences are underlined.

Table A5.4 – List of primers pertinent to Chapter 6.

Name	Sequence (5' – 3')	Enzyme site
BCAM0716 F	atcggaattcatgaaaacggcaaaactcgca	EcoRI
BCAM0716 R	atcgtctagacatgtggccggtcatcattg	XbaI
BCAM0718 F	atcggaattcatgaacatcccgcgtccg	EcoRI
BCAM0718 R	atcgtctagaacgttcaaagcaccgcgaa	XbaI
BCAM0719 F	atcggaattcatgcgcaatgtcgcgaag	EcoRI
BCAM0719 R	atcgtctagaatcggtgaaagcctgacgc	XbaI
BCAM0720 F	atcggaattcatgacaccgaccgcgaa	EcoRI
BCAM0720 R	atcgtctagacgtcaggctttcaccga	XbaI
BCAM0721 F	atcggaattcatgaccgatcaggccaagc	EcoRI
BCAM0721 R	atcgtctagagttgcgctcaaagctgcg	XbaI
BCAM16-21 F	atcggctagcccggtcgatcatggacaatc	NheI
BCAM16-21 R	atcgtctagactggttccaccgatcctgatc	XbaI
pDA17 F	ttgttgtggggtaggcagtc	-
pDA17 R	accgcttctgcgttctgat	-
pMLS7 F	gaatcgggttagttggtggc	-
pMLS7 R	catgcctgcaggtcgac	-
pSCrhaB3 F	gtcagtaacgagaaggtcgc	-
pSCrhaB3 R	gtcgtcgtcgtccttgtagtc	-
BCAM16-17 R	agctggtaccgttggggctccttgctgg	KpnI
BCAM18-19 F	agctgctagccatggtgtgtccctgaagttc	NheI
BCAM18-19 R	atcgtctagaatcggtgaaagcctgacgc	XbaI
BCAM20-21 F	agctgctagcacgacctggtagccgtcg	NheI
BCAM0717 R	agctggtacccgcgtgctctccttgatctggg	KpnI

Note: Restriction site sequences are underlined.

Reference List

1. Burkholder, W. H. Sour skin, a bacterial rot of Onion bulbs. *Phytopathology* **40**(1), 115–117 (1950).

2. Yabuuchi, E. *et al.* Proposal of *Burkholderia* gen. nov. and transfer of seven species of the genus *Pseudomonas* homology group II to the new genus, with the type species *Burkholderia cepacia* (Palleroni and Holmes 1981) comb. nov. *Microbiol Immunol* **36**(12), 1251–1275 (1992).

3. Euzéby, J. P. List of bacterial names with standing in nomenclature: A folder available on the internet. *Int. J. Syst. Bacteriol.* **47**(2), 590–592 (1997).

4. Parte, A. C. LPSN - List of prokaryotic names with standing in nomenclature (Bacterio.net), 20 years on. *Int. J. Syst. Evol. Microbiol.* **68**(6), 1825–1829 (2018).

5. Zuleta, L. F. G. *et al.* The complete genome of *Burkholderia phenoliruptrix* strain BR3459a, a symbiont of *Mimosa flocculosa*: Highlighting the coexistence of symbiotic and pathogenic genes. *BMC Genomics* **15**, 535 (2014).

6. Sawana, A., Adeolu, M. & Gupta, R. S. Molecular signatures and phylogenomic analysis of the genus *Burkholderia*: proposal for division of this genus into the emended genus *Burkholderia* containing pathogenic organisms and a new genus *Paraburkholderia* gen. nov. harboring env. *Front Genet* **5**, 429 (2014).

7. Estrada-de los Santos, P., Rojas-Rojas, F. U., Tapia-Garcia, E. Y., Vasquez-Murrieta, M. S. & Hirsch, A. M. To split or not to split: an opinion on dividing the genus *Burkholderia*. *Ann. Microbiol.* **66**(3), 1303–1314 (2016).

8. Dobritsa, A. P. & Samadpour, M. Transfer of eleven species of the genus *Burkholderia* to the genus *Paraburkholderia* and proposal of *Caballeronia* gen. nov. to accommodate twelve species of the genera *Burkholderia* and *Paraburkholderia*. *Int. J. Syst. Evol. Microbiol.* **66**(8), 2836–2846 (2016).

9. Vandamme, P. & Dawyndt, P. Classification and identification of the *Burkholderia cepacia* complex: Past, present and future. *Syst Appl Microbiol* **34**(2), 87–95 (2011).

10. Nandi, T. & Tan, P. Less is more: *Burkholderia pseudomallei* and chronic melioidosis. *MBio* **4**(5), e00709-13 (2013).

11. Bevivino, A. *et al.* Phenotypic comparison between rhizosphere and clinical isolates of *Burkholderia cepacia*. *Microbiology* **140**(5), 1069–77 (1994).

12. Tabacchioni, S. *et al.* Molecular characterization of rhizosphere and clinical isolates of *Burkholderia cepacia*. *Res. Microbiol.* **146**(7), 531–42 (1995).

13. Yohalem, D. S. & Lorbeer, J. W. Multilocus Isoenzyme Diversity Among Strains of *Pseudomonas cepacia* isolated from Decayed Onions, Soils, and Clinical Sources. *Syst. Appl. Microbiol.* **17**(1), 116–124 (1994).

14. Vandamme, P. *et al.* Occurrence of Multiple Genomovars of *Burkholderia cepacia* in Cystic Fibrosis Patients and Proposal of *Burkholderia multivorans* sp. nov. *Int. J. Syst. Bacteriol.* **47**(4), 1188–200 (1997).

15. Martina, P. *et al. Burkholderia puraquae* sp. nov., a novel species of the *Burkholderia cepacia* complex isolated from hospital settings and agricultural soils. *Int. J. Syst. Evol. Microbiol.* **68**(1), 14–20 (2018).

16. Weber, C. F. & King, G. M. Volcanic soils as sources of novel CO-oxidizing *Paraburkholderia* and *Burkholderia*: *Paraburkholderia hiiakae* sp. nov., *Paraburkholderia metrosideri* sp. nov., *Paraburkholderia paradisi* sp. nov., *Paraburkholderia peleae* sp. nov., and *Burkholderia alpina* sp. . *Front. Microbiol.* **8**, 207 (2017).

17. Ramette, A., LiPuma, J. J. & Tiedje, J. M. Species abundance and diversity of *Burkholderia cepacia* complex in the environment. *Appl. Environ. Microbiol.* **71**(3), 1193–1201 (2005).

18. Winsor, G. L. *et al.* The *Burkholderia* Genome Database: Facilitating flexible queries and comparative analyses. *Bioinformatics* **24**(23), 2803–2804 (2008).

19. Devanga Ragupathi, N. K. & Veeraraghavan, B. Accurate identification and epidemiological characterization of *Burkholderia cepacia* complex: an update. *Ann. Clin. Microbiol. Antimicrob.* **18**, 7 (2019).

20. Furlan, J. P. R., Pitondo-Silva, A., Braz, V. S., Gallo, I. F. L. & Stehling, E. G. Evaluation of different molecular and phenotypic methods for identification of environmental *Burkholderia cepacia* complex. *World J. Microbiol. Biotechnol.* **35**(3), 39 (2019).

21. Vermis, K., Vandamme, P. A. R. & Nelis, H. J. *Burkholderia cepacia* complex genomovars: utilization of carbon sources, susceptibility to antimicrobial agents and growth on selective media. *J. Appl. Microbiol.* **95**(6), 1191–9 (2003).

22. Drevinek, P. & Mahenthiralingam, E. *Burkholderia cenocepacia* in cystic fibrosis: epidemiology and molecular mechanisms of virulence. *Clin Microbiol Infect* **16**(7), 821–830 (2010).

23. Loutet, S. A. & Valvano, M. A. Extreme Antimicrobial Peptide and Polymyxin B Resistance in the Genus *Burkholderia*. *Front. Microbiol.* **2**, 159 (2011).

24. Nzula, S. Influence of taxonomic status on the in vitro antimicrobial susceptibility of the *Burkholderia cepacia* complex. *J. Antimicrob. Chemother.* **50**(2), 265–9 (2002).

25. Miller, S. C. M., LiPuma, J. J. & Parke, J. L. Culture-based and non-growth-dependent detection of the *Burkholderia cepacia* complex in soil environments. *Appl. Environ. Microbiol.* **68**(8), 3750–58 (2002).

26. Pallud, C., Viallard, V., Balandreau, J., Normand, P. & Grundmann, G. Combined use of a specific probe and PCAT medium to study *Burkholderia* in soil. *J. Microbiol. Methods* **47**(1), 25–34 (2001).

27. Zhang, L. & Xie, G. Diversity and distribution of *Burkholderia cepacia* complex in the rhizosphere of rice and maize. *FEMS Microbiol. Lett.* **266**(2), 231–35 (2007).

28. Knee, E. M. *et al.* Root Mucilage from Pea and Its Utilization by Rhizosphere Bacteria as a Sole Carbon Source. *Mol. Plant-Microbe*

Interact. **14**(6), 775–84 (2001).

29. Vial, L., Chapalain, A., Groleau, M. C. & Deziel, E. The various lifestyles of the *Burkholderia cepacia* complex species: a tribute to adaptation. *Environ. Microbiol.* **13**, 1–12 (2011).

30. Vanlaera, E. *et al. Burkholderia latens* sp. nov., *Burkholderia diffusa* sp. nov., *Burkholderia arboris* sp. nov., *Burkholderia seminalis* sp. nov., and *Burkholderia metallica* sp. nov., novel species within the *Burkholderia cepacia* complex. *Int. J. Syst. Evol. Microbiol.* **58**(7), 1580–90 (2008).

31. Jacobs, J. L. *et al.* Identification and onion pathogenicity of *Burkholderia cepacia* complex isolates from the onion rhizosphere and onion field soil. *Appl. Environ. Microbiol.* **74**(10), 3121–9 (2008).

32. Compant, S., Nowak, J., Coenye, T., Clement, C. & Ait Barka, E. Diversity and occurrence of *Burkholderia* spp. in the natural environment. *Fems Microbiol. Rev.* **32**(4), 607–626 (2008).

33. Lee, Y.-A. & Chan, C.-W. Molecular Typing and Presence of Genetic Markers Among Strains of Banana Finger-Tip Rot Pathogen, *Burkholderia cenocepacia*, in Taiwan. *Phytopathology* **97**(2), 195–201 (2007).

34. Fang, Y. *et al.* Bacterial fruit rot of apricot caused by *Burkholderia cepacia* in China. *Plant Pathol. J.* **25**(4) (2009).

35. Trân Van, V., Berge, O., Ngô Kê, S., Balandreau, J. & Heulin, T. Repeated beneficial effects of rice inoculation with a strain of *Burkholderia vietnamiensis* on early and late yield components in low fertility sulphate acid soils of Vietnam. *Plant Soil* **218**, 273–284 (2000).

36. Ji, X. *et al.* Colonization of *Morus alba* L. by the plant-growth-promoting and antagonistic bacterium *Burkholderia cepacia* strain Lu10-1. *BMC Microbiol.* **10**, 243 (2010).

37. Bevivino, A., Dalmastri, C., Tabacchioni, S. & Chiarini, L. Efficacy of *Burkholderia cepacia* MCI 7 in disease suppression and growth promotion of maize. *Biol. Fertil. Soils* **31**(3), 225–231 (2000).

38. Rojas-Rojas, F. U. *et al.* Broad-spectrum antimicrobial activity by *Burkholderia cenocepacia* TATL-371, a strain isolated from the tomato

rhizosphere. *Microbiology* **164**, 1072–1086 (2018).

39. Simonetti, E. *et al.* A novel *Burkholderia ambifaria* strain able to degrade the mycotoxin fusaric acid and to inhibit Fusarium spp. growth. *Microbiol. Res.* **206**, 50–59 (2018).

40. Tang, S.Y., Hara, S., Melling, L., Goh, K.J. & Hashidoko, Y. *Burkholderia vietnamiensis* Isolated from Root Tissues of Nipa Palm (*Nypa fruticans*) in Sarawak, Malaysia, Proved to Be Its Major Endophytic Nitrogen-Fixing Bacterium. *Biosci. Biotechnol. Biochem.* **74**(9), 1972–5 (2010).

41. Onofre-Lemus, J. *et al.* ACC (1-Aminocyclopropane-1-Carboxylate) Deaminase Activity, a Widespread Trait in *Burkholderia* Species, and Its Growth-Promoting Effect on Tomato Plants. *Appl. Environ. Microbiol.* **75**(20), 6581–6590 (2009).

42. Radway, J. C., Santo Domingo, J. W., Hazen, T. C. & Wilde, E. W. Evaluation of biodegradation potential of foam embedded *Burkholderia cepacia* G4. *Biotechnol. Lett.* **20**(7), 663–666 (1998).

43. Field, J. A. & Sierra-Alvarez, R. Microbial transformation and degradation of polychlorinated biphenyls. *Environ. Pollut.* **155**(1), 1–12 (2008).

44. Vermis, K., Brachkova, M., Vandamme, P. & Nelis, H. Isolation of *Burkholderia cepacia* Complex Genomovars from Waters. *Syst. Appl. Microbiol.* **26**(4), 595–600 (2003).

45. Olapade, O. A. *et al.* Abundance of Three Bacterial Populations in Selected Streams. *Microb. Ecol.* **49**(3), 461–467 (2005).

46. Wang, Y., Yin, B., Hong, Y., Yan, Y. & Gu, J.-D. Degradation of dimethyl carboxylic phthalate ester by *Burkholderia cepacia* DA2 isolated from marine sediment of South China Sea. *Ecotoxicology* **17**, 845–852 (2008).

47. Maravić, A. *et al.* Occurrence and antibiotic susceptibility profiles of *Burkholderia cepacia* complex in coastal marine environment. *Int. J. Environ. Health Res.* **22**(6), 531–542 (2012).

48. Venter, J. C. *et al.* Environmental Genome Shotgun Sequencing of the Sargasso Sea. *Science.* **304**(5567), 66–74 (2004).

49. Ratjen, F. & Döring, G. Cystic fibrosis. *Lancet* **361**(9358), 681–689 (2003).

50. Farrell, P. M. The prevalence of cystic fibrosis in the European Union. *J. Cyst. Fibros.* **7**(5), 450–453 (2008).

51. Salvatore, D. *et al.* An overview of international literature from cystic fibrosis registries. Part 3. Disease incidence, genotype/phenotype correlation, microbiology, pregnancy, clinical complications, lung transplantation, and miscellanea. *J. Cyst. Fibros.* **10**(2), 71–85(2011).

52. Guo, Y., Su, M., McNutt, M. A. & Gu, J. Expression and distribution of cystic fibrosis transmembrane conductance regulator in neurons of the human brain. *J. Histochem. Cytochem.* **57**(12), 1113–20 (2009).

53. UK Cystic Fibrosis Registry. UK Cystic Fibrosis Registry Annual Data Report 2017. (2018).

54. Sosnay, P. R. *et al.* Defining the disease liability of variants in the cystic fibrosis transmembrane conductance regulator gene. *Nat. Genet.* **45**(10), 1160–7 (2013).

55. Cystic Fibrosis Foundation Patient Registry. 2017 Annual Data Report. (2018).

56. Tarran, R. *et al.* Normal and Cystic Fibrosis Airway Surface Liquid Homeostasis. *J. Biol. Chem.* **280**(42), 35751–35759 (2005).

57. Ciofu, O., Hansen, C. R. & Høiby, N. Respiratory bacterial infections in cystic fibrosis. *Curr. Opin. Pulm. Med.* **19**(3), 251–258 (2013).

58. Filkins, L. M. & O'Toole, G. A. Cystic Fibrosis Lung Infections: Polymicrobial, Complex, and Hard to Treat. *PLOS Pathog.* **11**(12), e1005258 (2015).

59. Rogers, G. B. *et al.* Bacterial diversity in cases of lung infection in cystic fibrosis patients: 16S ribosomal DNA (rDNA) length heterogeneity PCR and 16S rDNA terminal restriction fragment length polymorphism profiling. *J. Clin. Microbiol.* **41**(8), 3548–58 (2003).

60. Cécile, F. B. *et al.* Fungal and Bacterial Diversity of Airway Microbiota in

Adults with Cystic Fibrosis: Concordance Between Conventional Methods and Ultra-Deep Sequencing, and Their Practical use in the Clinical Laboratory. *Mycopathologia* **183**(1), 171–183 (2018).

61. Isles, A. *et al. Pseudomonas cepacia* infection in cystic fibrosis: An emerging problem. *J. Pediatr.* **104**(2), 206–210 (1984).

62. Mahenthiralingam, E., Urban, T. A. & Goldberg, J. B. The multifarious, multireplicon *Burkholderia cepacia* complex. *Nat. Rev. Microbiol.* **3**(2), 144–56 (2005).

63. Hindo, H., Sigley, C. & Karlson, K. Cepacia Syndrome in an Adolescent With Cystic Fibrosis. *Infect. Dis. Clin. Pract.* **16**(3), 198–200 (2008).

64. Shafiq, I., Carroll, M. P., Nightingale, J. A. & Daniels, T. V. W. Cepacia syndrome in a cystic fibrosis patient colonised with *Burkholderia multivorans*. *BMJ Case Rep.* **2011**, bcr0820103296 (2011).

65. Gilchrist, F. J., Webb, A. K., Bright-Thomas, R. J. & Jones, A. M. Successful treatment of *cepacia* syndrome with a combination of intravenous cyclosporin, antibiotics and oral corticosteroids. *J. Cyst. Fibros.* **11**(5), 458–460 (2012).

66. Worlitzsch, D. *et al.* Effects of reduced mucus oxygen concentration in airway *Pseudomonas* infections of cystic fibrosis patients. *J. Clin. Invest.* **109**(3), 317–25 (2002).

67. Schwab, U. *et al.* Localization of *Burkholderia cepacia* complex bacteria in cystic fibrosis lungs and interactions with *Pseudomonas aeruginosa* in hypoxic mucus. *Infect. Immun.* **82**(11), 4729–45 (2014).

68. Tümmler, B. *et al.* Nosocomial acquisition of *Pseudomonas aeruginosa* by cystic fibrosis patients. *J. Clin. Microbiol.* **29**(6), 1265–7 (1991).

69. Pegues, D. A. *et al.* Acquisition of *Pseudomonas cepacia* at summer camps for patients with cystic fibrosis. Summer Camp Study Group. *J. Pediatr.* **124**(5), 694–702 (1994).

70. Ojeniyi, B., Frederiksen, B. & Hoiby, N. *Pseudomonas aeruginosa* cross-infection among patients with cystic fibrosis during a winter camp. *Pediatr. Pulmonol.* **29**(3), 177–81 (2000).

71. Scoffone, V. C. *et al. Burkholderia cenocepacia* Infections in Cystic Fibrosis Patients: Drug Resistance and Therapeutic Approaches. *Front. Microbiol.* **8**, 1592 (2017).

72. Brimicombe, R. W. *et al.* Transmission of *Pseudomonas aeruginosa* in children with cystic fibrosis attending summer camps in The Netherlands. *J. Cyst. Fibros.* **7**(1), 30–36 (2008).

73. Chaparro, C. *et al.* Infection with *Burkholderia cepacia* in Cystic Fibrosis: Outcome Following Lung Transplantation. *Am. J. Respir. Crit. Care Med.* **163**(1), 43–48 (2001).

74. Aris, R. M., Routh, J. C., Lipuma, J. J., Heath, D. G. & Gilligan, P. H. Lung Transplantation for Cystic Fibrosis Patients with *Burkholderia cepacia* Complex. Survival linked to genomovar type. *Am. J. Respir. Crit. Care Med.* **164**(11), 2102–2106 (2001).

75. Alexander, B. D. *et al.* Survival After Lung Transplantation of Cystic Fibrosis Patients Infected with *Burkholderia cepacia* Complex. *Am. J. Transplant.* **8**(5), 1025–1030 (2008).

76. Murray, S., Charbeneau, J., Marshall, B. C. & LiPuma, J. J. Impact of *Burkholderia* Infection on Lung Transplantation in Cystic Fibrosis. *Am. J. Respir. Crit. Care Med.* **178**(4), 363–371 (2008).

77. Stephenson, A. L. *et al.* Clinical and demographic factors associated with post-lung transplantation survival in individuals with cystic fibrosis. *J. Hear. Lung Transplant.* **34**(9), 1139–45 (2015).

78. Chaparro, C. & Keshavjee, S. Lung transplantation for cystic fibrosis: an update. *Expert Rev. Respir. Med.* **10**(12), 1269–1280 (2016).

79. Gilljam, M., Nyström, U., Dellgren, G., Skog, I. & Hansson, L. Survival after lung transplantation for cystic fibrosis in Sweden. *Eur. J. Cardio-Thoracic Surg.* **51**(3), 571–576 (2016).

80. Boussaud, V. *et al.* Clinical outcome following lung transplantation in patients with cystic fibrosis colonised with *Burkholderia cepacia* complex: results from two French centres. *Thorax* **63**(8), 732–737 (2008).

81. Conway, S. Segregation is good for patients with cystic fibrosis. *J. R. Soc.*

Med. **1**, 101 (2008).

82. Duff, A. J. A. Psychological consequences of segregation resulting from chronic *Burkholderia cepacia* infection in adults with CF. *Thorax* **57**, 756–8 (2002).

83. Geddes, D. Segregation is not good for patients with cystic fibrosis. *J. R. Soc. Med.* **1**, 101 (2008).

84. Griffiths, A. L., Armstrong, D., Carzino, R. & Robinson, P. Cystic fibrosis patients and families support cross-infection measures. *Eur. Respir. J.* **24**, 449–452 (2004).

85. Russo, K., Donnelly, M. & Reid, A. J. M. Segregation—the perspectives of young patients and their parents. *J. Cyst. Fibros.* **5**(2), 93–99 (2006).

86. Reik, R., Spilker, T. & Lipuma, J. J. Distribution of *Burkholderia cepacia* complex species among isolates recovered from persons with or without cystic fibrosis. *J. Clin. Microbiol.* **43**(6), 2926–8 (2005).

87. Lipuma, J. J. The changing microbial epidemiology in cystic fibrosis. *Clin. Microbiol. Rev.* **23**(2), 299–323 (2010).

88. Salsgiver, E. L. *et al.* Changing Epidemiology of the Respiratory Bacteriology of Patients With Cystic Fibrosis. *Chest* **149**(2), 390–400 (2016).

89. Zlosnik, J. E. A. *et al. Burkholderia* Species Infections in Patients with Cystic Fibrosis in British Columbia, Canada. 30 Years' Experience. *Ann. Am. Thorac. Soc.* **12**(1), 70–78 (2015).

90. Kenna, D. T. D. *et al.* Prevalence of *Burkholderia* species, including members of *Burkholderia cepacia* complex, among UK cystic and non-cystic fibrosis patients. *J. Med. Microbiol.* **66**(4), 490–501 (2017).

91. Abbott, F. K., Milne, K. E. N., Stead, D. A. & Gould, I. M. Combination antimicrobial susceptibility testing of *Burkholderia cepacia* complex: significance of species. *Int. J. Antimicrob. Agents* **48**(5), 521–527 (2016).

92. Ramsay, K. A. *et al.* Factors Influencing Acquisition of *Burkholderia cepacia* Complex Organisms in Patients with Cystic Fibrosis. *J. Clin.*

Microbiol. **51**(12), 3975–3980 (2013).

93. LiPuma, J. J., Spilker, T., Coenye, T. & Gonzalez, C. F. An epidemic *Burkholderia cepacia* complex strain identified in soil. *Lancet* **359**(9322), 2002–2003 (2002).

94. Baldwin, A. *et al.* Environmental *Burkholderia cepacia* complex isolates in human infections. *Emerg. Infect. Dis.* **13**(3), 458–61 (2007).

95. Horsley, A., Jones, A. M. & Lord, R. Antibiotic treatment for *Burkholderia cepacia* complex in people with cystic fibrosis experiencing a pulmonary exacerbation. *Cochrane Database Syst. Rev.* **1** (2016).

96. Regan, K. H. & Bhatt, J. Eradication therapy for *Burkholderia cepacia* complex in people with cystic fibrosis. **4** *Cochrane Database Syst. Rev.* (2019).

97. Frost, F., Shaw, M. & Nazareth, D. Antibiotic therapy for chronic infection with *Burkholderia cepacia* complex in people with cystic fibrosis. *Cochrane Database Syst. Rev.* **6** (2019).

98. Horsley, A., Webb, K., Bright-Thomas, R., Govan, J. & Jones, A. Can early *Burkholderia cepacia* complex infection in cystic fibrosis be eradicated with antibiotic therapy? *Front. Cell. Infect. Microbiol.* **1**, 18 (2011).

99. Kitt, H., Lenney, W. & Gilchrist, F. J. Two case reports of the successful eradication of new isolates of *Burkholderia cepacia* complex in children with cystic fibrosis. *BMC Pharmacol. Toxicol.* **17**, 14 (2016).

100. El-Halfawy, O. M., Naguib, M. M. & Valvano, M. A. Novel antibiotic combinations proposed for treatment of *Burkholderia cepacia* complex infections. *Antimicrob. Resist. Infect. Control* **6**, 120 (2017).

101. Sfeir, M. M. *Burkholderia cepacia* complex infections: More complex than the bacterium name suggest. *J. Infect.* **77**(3), 166–170 (2018).

102. Van Dalem, A. *et al. In Vitro* Susceptibility of *Burkholderia cepacia* Complex Isolated from Cystic Fibrosis Patients to Ceftazidime-Avibactam and Ceftolozane-Tazobactam. *Antimicrob. Agents Chemother.* **62**(9) (2018).

103. Tamma, P. D. *et al.* Successful Treatment of Persistent *Burkholderia cepacia* Complex Bacteremia with Ceftazidime-Avibactam. *Antimicrob. Agents Chemother.* **62**(4) (2018).

104. Garcia, B. A. *et al.* Implementation of a successful eradication protocol for *Burkholderia* Cepacia complex in cystic fibrosis patients. *BMC Pulm. Med.* **18**(1), 35 (2018).

105. Rider, N. L., Jameson, M. B. & Creech, C. B. Chronic Granulomatous Disease: Epidemiology, Pathophysiology, and Genetic Basis of Disease. *J. Pediatric Infect. Dis. Soc.* **7**, S2–S5 (2018).

106. Roos, D. Chronic granulomatous disease. *Br. Med. Bull.* **118**(1), 50–63 (2016).

107. Roos, D. & de Boer, M. Molecular diagnosis of chronic granulomatous disease. *Clin. Exp. Immunol.* **175**(2), 139–149 (2014).

108. Kuhns, D. B. *et al.* Residual NADPH Oxidase and Survival in Chronic Granulomatous Disease. *N. Engl. J. Med.* **363**(27), 2600–2610 (2010).

109. Winkelstein, J. A. *et al.* Chronic granulomatous disease. Report on a national registry of 368 patients. *Medicine (Baltimore).* **79**(3), 155–69 (2000).

110. Song, E. *et al.* Chronic granulomatous disease: a review of the infectious and inflammatory complications. *Clin. Mol. Allergy* **9**(1), 10 (2011).

111. Marciano, B. E. *et al.* Common Severe Infections in Chronic Granulomatous Disease. *Clin. Infect. Dis.* **60**(8), 1176–1183 (2015).

112. Berg, J. M. van den *et al.* Chronic Granulomatous Disease: The European Experience. *PLoS One* **4**(4), (2009).

113. Greenberg, D. E. *et al.* Recurrent *Burkholderia* Infection in Patients with Chronic Granulomatous Disease: 11-Year Experience at a Large Referral Center. *Clin. Infect. Dis.* **48**(11), 1577–1579 (2009).

114. John, M. A. *et al.* Intracellular survival of *Burkholderia cepacia* complex isolates in the presence of macrophage cell activation. *Microbiology* **145**(12), 3465–3475 (1999).

115. Keith, K. E. & Valvano, M. A. Characterization of SodC, a periplasmic superoxide dismutase from *Burkholderia cenocepacia*. *Infect. Immun.* **75**(5), 2451–60 (2007).

116. Bylund, J., Campsall, P. A., Ma, R. C., Conway, B. A. & Speert, D. P. *Burkholderia cenocepacia* induces neutrophil necrosis in chronic granulomatous disease. *J Immunol* **174**(6), 3562–3569 (2005).

117. Keith, K. E., Hynes, D. W., Sholdice, J. E. & Valvano, M. A. Delayed association of the NADPH oxidase complex with macrophage vacuoles containing the opportunistic pathogen *Burkholderia cenocepacia*. *Microbiology* **155**(4), 1004–1015 (2009).

118. Rosales-Reyes, R., Skeldon, A. M., Aubert, D. F. & Valvano, M. A. The Type VI secretion system of *Burkholderia cenocepacia* affects multiple Rho family GTPases disrupting the actin cytoskeleton and the assembly of NADPH oxidase complex in macrophages. *Cell. Microbiol.* **14**(2), 255–73 (2012).

119. Abe, K. *et al.* Outbreak of *Burkholderia cepacia* Bloodstream Infection at an Outpatient Hematology and Oncology Practice. *Infect. Control Hosp. Epidemiol.* **28**(11), 1311–1313 (2007).

120. Heo, S. T. *et al.* Hospital outbreak of *Burkholderia stabilis* bacteraemia related to contaminated chlorhexidine in haematological malignancy patients with indwelling catheters. *J. Hosp. Infect.* **70**(3), 241–245 (2008).

121. Mann, T. *et al.* An outbreak of *Burkholderia cenocepacia* bacteremia in immunocompromised oncology patients. *Infection* **38**(3), 187–194 (2010).

122. Souza Dias, M. B. *et al.* Multi-institutional outbreak of *Burkholderia cepacia* complex associated with contaminated mannitol solution prepared in compounding pharmacy. *Am. J. Infect. Control* **41**(11), 1038–1042 (2013).

123. Singhal, T., Shah, S. & Naik, R. Outbreak of *Burkholderia cepacia* complex bacteremia in a chemotherapy day care unit due to intrinsic contamination of an antiemetic drug. *Indian J. Med. Microbiol.* **33**(1), 117–9 (2015).

124. Sommerstein, R. *et al. Burkholderia stabilis* outbreak associated with contaminated commercially-available washing gloves, Switzerland, May 2015 to August 2016. *Euro Surveill.* **22**(49) (2017).

125. Marquez, L. *et al.* An Outbreak of *Burkholderia cepacia* Complex Infections Associated with Contaminated Liquid Docusate. *Infect. Control Hosp. Epidemiol.* **38**(5), 567–573 (2017).

126. Rastogi, N. *et al.* Epidemiological investigation and successful management of a *Burkholderia cepacia* outbreak in a neurotrauma intensive care unit. *Int. J. Infect. Dis.* **79**, 4–11 (2019).

127. Song, J. E. *et al.* Outbreak of *Burkholderia cepacia* pseudobacteraemia caused by intrinsically contaminated commercial 0.5% chlorhexidine solution in neonatal intensive care units. *J. Hosp. Infect.* **98**(3), 295–299 (2018).

128. Waterer, G. W., Jones, C. B. & Wunderink, R. G. Bacteremic community-acquired pneumonia in an immunocompetent adult due to *Burkholderia cepacia*. *Chest* **116**(6), 1842–3 (1999).

129. Hsu, C.-C. *et al.* Urachal abscess: a cause of adult abdominal pain that cannot be ignored. *Am. J. Emerg. Med.* **23**(2), 229–230 (2005).

130. Bayram, M., Babalık, M., Bakan, N. D. & Döngel, I. Community-acquired *Burkholderia cepacia* pneumonia: a report of two immunocompetent patients. *Tuberk. Toraks* **59**(4), 380–3 (2011).

131. Karanth, S. S., Regunath, H., Chawla, K. & Prabhu, M. A rare case of community acquired *Burkholderia cepacia* infection presenting as pyopneumothorax in an immunocompetent individual. *Asian Pac. J. Trop. Biomed.* **2**(2), 166–168 (2012).

132. Hsieh, C.-T., Hsu, S.-K. & Chang, C.-J. Thoracic Vertebral Osteomyelitis Caused by *Burkholderia cepacia* in an Immunocompetent Adult. *Surg. Infect. (Larchmt).* **14**(5), 476–479 (2013).

133. Hauser, N. & Orsini, J. Cepacia Syndrome in a Non-Cystic Fibrosis Patient. *Case Rep. Infect. Dis.* **2015**, 1–4 (2015).

134. Ishtiaq, R. *et al.* Ceftazidime-Resistant *Burkholderia cepacia*: An Unusual

Case in a Pregnant Patient. *Cureus* **9**(11) (2017).

135. Ranjan, R., Chowdhary, P. & Kamra, A. Community Acquired *Burkholderia cepacia* Bacteraemia Presenting as MODS in an Immunocompetent Individual: An Unusual Case. *J. Clin. Diagn. Res.* **11**(3), DD01–DD02 (2017).

136. Wong, J. K. *et al.* Cellulitis caused by the *Burkholderia cepacia* complex associated with contaminated chlorhexidine 2% scrub in five domestic cats. *J. Vet. Diagnostic Investig.* **30**(5), 763–769 (2018).

137. Banovic, F., Koch, S., Robson, D., Jacob, M. & Olivry, T. Deep pyoderma caused by *Burkholderia cepacia* complex associated with ciclosporin administration in dogs: a case series. *Vet. Dermatol.* **26**(4), 287-e64 (2015).

138. Cain, C. L., Cole, S. D., Bradley, C. W., Canfield, M. S. & Mauldin, E. A. Clinical and histopathological features of *Burkholderia cepacia* complex dermatitis in dogs: a series of four cases. *Vet. Dermatol.* **29**(5), 457-e156 (2018).

139. Travers, C. W. & van den Berg, J. S. *Pseudomonas* spp. associated vegetative endocarditis in two horses. *J. S. Afr. Vet. Assoc.* **66**(3), 172–6 (1995).

140. Berriatua, E. *et al.* Outbreak of subclinical mastitis in a flock of dairy sheep associated with *Burkholderia cepacia* complex infection. *J. Clin. Microbiol.* **39**(3), 990–994 (2001).

141. Höger, A. C. R. *et al.* The melioidosis agent *Burkholderia pseudomallei* and related opportunistic pathogens detected in faecal matter of wildlife and livestock in northern Australia. *Epidemiol. Infect.* **144**(9), 1924–1932 (2016).

142. Vinion-Dubiel, A. D. & Goldberg, J. B. Lipopolysaccharide of *Burkholderia cepacia* complex. *J. Endotoxin Res.* **9**(4), 201–13 (2003).

143. Loutet, S. A., Bartholdson, S. J., Govan, J. R. W., Campopiano, D. J. & Valvano, M. A. Contributions of two UDP-glucose dehydrogenases to viability and polymyxin B resistance of *Burkholderia cenocepacia*.

Microbiology **155**(6), 2029–39 (2009).

144. Ortega, X. *et al.* Biosynthesis and structure of the *Burkholderia cenocepacia* K56-2 lipopolysaccharide core oligosaccharide: Truncation of the core oligosaccharide leads to increased binding and sensitvity to polymyxin B. *J. Biol. Chem.* **284**(32), 21738–51 (2009).

145. Loutet, S. A., Mussen, L. E., Flannagan, R. S. & Valvano, M. A. A two-tier model of polymyxin B resistance in *Burkholderia cenocepacia*. *Environ. Microbiol. Rep.* **3**(2), 278–85 (2011).

146. Holden, M. T. G. *et al.* The genome of *Burkholderia cenocepacia* J2315, an epidemic pathogen of cystic fibrosis patients. *J. Bacteriol.* **191**(1), 261–77 (2009).

147. Buroni, S. *et al.* Differential Roles of RND Efflux Pumps in Antimicrobial Drug Resistance of Sessile and Planktonic *Burkholderia cenocepacia* Cells. *Antimicrob. Agents Chemother.* **58**(12), 7424–9 (2014).

148. Podnecky, N. L., Rhodes, K. A. & Schweizer, H. P. Efflux pump-mediated drug resistance in *Burkholderia*. *Front. Microbiol.* **6**, 305 (2015).

149. Green, E. R. & Mecsas, J. Bacterial Secretion Systems: An Overview. *Microbiol. Spectr.* **4**(1) (2016).

150. Corbett, C. R., Burtnick, M. N., Kooi, C., Woods, D. E. & Sokol, P. A. An extracellular zinc metalloprotease gene of *Burkholderia cepacia*. *Microbiology* **149**(8), 2263–2271 (2003).

151. Kooi, C. & Sokol, P. A. *Burkholderia cenocepacia* zinc metalloproteases influence resistance to antimicrobial peptides. *Microbiology* **155**(9), 2818–2825 (2009).

152. Tomich, M., Griffith, A., Herfst, C. A., Burns, J. L. & Mohr, C. D. Attenuated virulence of a *Burkholderia cepacia* type III secretion mutant in a murine model of infection. *Infect. Immun.* **71**(3), 1405–15 (2003).

153. Markey, K. M., Glendinning, K. J., Morgan, J. A. W., Hart, C. A. & Winstanley, C. *Caenorhabditis elegans* killing assay as an infection model to study the role of type III secretion in *Burkholderia cenocepacia*. *J. Med. Microbiol.* **55**(7), 967–9 (2006).

154. Engledow, A. S., Medrano, E. G., Mahenthiralingam, E., LiPuma, J. J. & Gonzalez, C. F. Involvement of a plasmid-encoded type IV secretion system in the plant tissue watersoaking phenotype of *Burkholderia cenocepacia*. *J. Bacteriol.* **186**(18), 6015–24 (2004).

155. Sajjan, S. U., Carmody, L. A., Gonzalez, C. F. & Lipuma, J. J. A type IV secretion system contributes to intracellular survival and replication of *Burkholderia cenocepacia*. *Infect. Immun.* **76**(12), 5447–55 (2008).

156. Zhang, R., LiPuma, J. J. & Gonzalez, C. F. Two type IV secretion systems with different functions in *Burkholderia cenocepacia* K56-2. *Microbiology* **155**(12), 4005–13 (2009).

157. Spiewak, H. L. *et al. Burkholderia cenocepacia* utilizes a type VI secretion system for bacterial competition. *Microbiologyopen* e774 (2019).

158. Miller, M. B. & Bassler, B. L. Quorum sensing in bacteria. *Annu. Rev. Microbiol.* **55**, 165–99 (2001).

159. Eberl, L. Quorum sensing in the genus *Burkholderia*. *Int. J. Med. Microbiol.* **296**(2-3), 103–10(2006).

160. Uehlinger, S. *et al.* Identification of specific and universal virulence factors in *Burkholderia cenocepacia* strains by using multiple infection hosts. *Infect. Immun.* **77**(9), 4102–10 (2009).

161. Boon, C. *et al.* A novel DSF-like signal from *Burkholderia cenocepacia* interferes with *Candida albicans* morphological transition. *ISME J.* **2**(1), 27–36 (2008).

162. Ryan, R. P., McCarthy, Y., Watt, S. A., Niehaus, K. & Dow, J. M. Intraspecies signaling involving the diffusible signal factor BDSF (cis-2-dodecenoic acid) influences virulence in *Burkholderia cenocepacia*. *J. Bacteriol.* **191**(15), 5013–9 (2009).

163. McCarthy, Y. *et al.* A sensor kinase recognizing the cell-cell signal BDSF (cis-2-dodecenoic acid) regulates virulence in *Burkholderia cenocepacia*. *Mol. Microbiol.* **77**(5), 1220–1236 (2010).

164. Deng, Y. *et al.* Cis-2-dodecenoic acid receptor RpfR links quorum-sensing signal perception with regulation of virulence through cyclic dimeric

guanosine monophosphate turnover. *Proc. Natl. Acad. Sci.* **109**(38), 15479–84 (2012).

165. Scoffone, V. C. *et al.* Discovery of new diketopiperazines inhibiting *Burkholderia cenocepacia* quorum sensing in vitro and in vivo. *Sci. Rep.* **6**, 32487 (2016).

166. Buroni, S. *et al.* Investigating the mechanism of action of diketopiperazines inhibitors of the *Burkholderia cenocepacia* quorum sensing synthase CepI: A site-directed mutagenesis study. *Front. Pharmacol.* **9**, 836 (2018).

167. Maldonado, R. F., Sá-Correia, I. & Valvano, M. A. Lipopolysaccharide modification in Gram-negative bacteria during chronic infection. *FEMS Microbiol. Rev.* **40**(4), 480–93(2016).

168. De Soyza, A., Silipo, A., Lanzetta, R., Govan, R. J. & Molinaro, A. Chemical and biological features of *Burkholderia cepacia* complex lipopolysaccharides. *Innate Immun.* **14**(3), 127–44 (2008).

169. Shimomura, H. *et al.* Lipopolysaccharide of *Burkholderia cepacia* and its unique character to stimulate murine macrophages with relative lack of interleukin-1β-inducing ability. *Infect. Immun.* **69**(6), 3663–9 (2001).

170. Cunha, M. V. *et al.* Studies on the involvement of the exopolysaccharide produced by cystic fibrosis-associated isolates of the *Burkholderia cepacia* complex in biofilm formation and in persistence of respiratory infections. *J. Clin. Microbiol.* **42**(7), 3052–8 (2004).

171. Bylund, J., Burgess, L. A., Cescutti, P., Ernst, R. K. & Speert, D. P. Exopolysaccharides from *Burkholderia cenocepacia* inhibit neutrophil chemotaxis and scavenge reactive oxygen species. *J. Biol. Chem.* **281**(5), 2526–32 (2006).

172. Herasimenka, Y. *et al.* Exopolysaccharides produced by clinical strains belonging to the *Burkholderia cepacia* complex. *J. Cyst. Fibros.* **6**(2), 145–52 (2007).

173. Sousa, S. A. *et al.* Virulence of *Burkholderia cepacia* complex strains in gp91phox−/− mice. *Cell. Microbiol.* **9**(12), 2817–2825 (2007).

174. Cuzzi, B. *et al.* Versatility of the *Burkholderia cepacia* complex for the biosynthesis of exopolysaccharides: A comparative structural investigation. *PLoS One* **9**(4), e94372 (2014).

175. Nunvar, J., Capek, V., Fiser, K., Fila, L. & Drevinek, P. What matters in chronic *Burkholderia cenocepacia* infection in cystic fibrosis: Insights from comparative genomics. *PLoS Pathog.* **13**(12), e1006762 (2017).

176. Pradenas, G., Ross, B. & Torres, A. *Burkholderia cepacia* Complex Vaccines: Where Do We Go from here? *Vaccines* **4**(2), 10 (2016).

177. Bertot, G. M. *et al.* Nasal immunization with *Burkholderia multivorans* outer membrane proteins and the mucosal adjuvant adamantylamide dipeptide confers efficient protection against experimental lung infections with *B*. *multivorans* and *B. cenocepacia*. *Infect. Immun.* **75**(6), 2740–52 (2007).

178. Makidon, P. E. *et al.* Induction of immune response to the 17 kDa OMPA *Burkholderia cenocepacia* polypeptide and protection against pulmonary infection in mice after nasal vaccination with an OMP nanoemulsion-based vaccine. *Med. Microbiol. Immunol.* **199**(2), 81–92 (2010).

179. McClean, S. *et al.* Linocin and OmpW Are Involved in Attachment of the Cystic Fibrosis-Associated Pathogen *Burkholderia cepacia* Complex to Lung Epithelial Cells and Protect Mice against Infection. *Infect. Immun.* **84**(5), 1424–37 (2016).

180. Cloutier, M., Muru, K., Ravicoularamin, G. & Gauthier, C. Polysaccharides from *Burkholderia* species as targets for vaccine development, immunomodulation and chemical synthesis. *Nat. Prod. Rep.* **35**(12), 1251–93 (2018).

181. Pradenas, G., Myers, J. & Torres, A. Characterization of the *Burkholderia cenocepacia* TonB Mutant as a Potential Live Attenuated Vaccine. *Vaccines* **5**(4), 33 (2017).

182. Sousa, S., Seixas, A. & Leitão, J. Postgenomic Approaches and Bioinformatics Tools to Advance the Development of Vaccines against Bacteria of the *Burkholderia cepacia* Complex. *Vaccines* **6**(2), 34 (2018).

183. Parker, D. & Prince, A. Innate immunity in the respiratory epithelium. *Am. J. Respir. Cell Mol. Biol.* **15**, 147–163 (2011).

184. Ganesan, S. & Sajjan, U. S. Host Evasion by *Burkholderia cenocepacia*. *Front. Cell. Infect. Microbiol.* **1**, 25 (2012).

185. Burns, J. L. *et al.* Invasion of respiratory epithelial cells by *Burkholderia* (*Pseudomonas*) *cepacia*. *Infect. Immun.* **64**(10), 4054–9 (1996).

186. Saldías, M. S. & Valvano, M. A. Interactions of *Burkholderia cenocepacia* and other *Burkholderia cepacia* complex bacteria with epithelial and phagocytic cells. *Microbiology* **155**(9), 2809–17 (2009).

187. Bertuzzi, M., Hayes, G. E. & Bignell, E. M. Microbial uptake by the respiratory epithelium: outcomes for host and pathogen. *FEMS Microbiol. Rev.* **43**(2), 145–161(2019).

188. Sajjan, U., Keshavjee, S. & Forstner, J. Responses of well-differentiated airway epithelial cell cultures from healthy donors and patients with cystic fibrosis to *Burkholderia cenocepacia* infection. *Infect. Immun.* **72**(7), 4188–99 (2004).

189. Sajjan, U., Wu, Y., Kent, G. & Forstner, J. Preferential adherence of cable-piliated *Burkholderia cepacia* to respiratory epithelia of CF knockout mice and human cystic fibrosis lung explants. *J. Med. Microbiol.* **49**(10), 875–885 (2000).

190. Urban, T. A., Goldberg, J. B., Forstner, J. F. & Sajjan, U. S. Cable pili and the 22-kilodalton adhesin are required for *Burkholderia cenocepacia* binding to and transmigration across the squamous epithelium. *Infect. Immun.* **73**(9), 5426–37 (2005).

191. Sajjan, U. *et al.* Binding of nonmucoid *Pseudomonas aeruginosa* to normal human intestinal mucin and respiratory mucin from patients with cystic fibrosis. *J. Clin. Invest.* **89**(2), 657–65 (1992).

192. Mil-Homens, D., Rocha, E. P. C. & Fialho, A. M. Genome-wide analysis of DNA repeats in *Burkholderia cenocepacia* J2315 identifies a novel adhesin-like gene unique to epidemic-associated strains of the ET-12 lineage. *Microbiology* **156**(4), 1084–1096 (2010).

193. Mil-Homens, D. & Fialho, A. M. A BCAM0223 mutant of *Burkholderia cenocepacia* is deficient in hemagglutination, serum resistance, adhesion to epithelial cells and virulence. *PLoS One* **7**(7), e41747 (2012).

194. Mil-Homens, D., Leç, M. I., Fernandes, F., Pinto, S. N. & Fialho, A. M. Characterization of BCAM0224, a multifunctional trimeric autotransporter from the human pathogen *Burkholderia cenocepacia*. *J. Bacteriol.* **196**(11), 1968–1979 (2014).

195. Mullen, T., Callaghan, M. & McClean, S. Invasion of *Burkholderia cepacia* complex isolates into lung epithelial cells involves glycolipid receptors. *Microb. Pathog.* **49**(6), 381–7 (2010).

196. Dennehy, R. *et al.* The *Burkholderia cenocepacia* peptidoglycan-associated lipoprotein is involved in epithelial cell attachment and elicitation of inflammation. *Cell. Microbiol.* **19**(5) (2017).

197. Cieri, M. V, Mayer-Hamblett, N., Griffith, A. & Burns, J. L. Correlation between an in vitro invasion assay and a murine model of *Burkholderia cepacia* lung infection. *Infect. Immun.* **70**(3), 1081–6 (2002).

198. Duff, C., Murphy, P. G., Callaghan, M. & McClean, S. Differences in invasion and translocation of *Burkholderia cepacia* complex species in polarised lung epithelial cells in vitro. *Microb. Pathog.* **41**(4-5), 183–92 (2006).

199. Schwab, U. *et al.* Patterns of epithelial cell invasion by different species of the *Burkholderia cepacia* complex in well-differentiated human airway epithelia. *Infect. Immun.* **70**(8), 4547–55 (2002).

200. Sajjan, U. S., Yang, J. H., Hershenson, M. B. & LiPuma, J. J. Intracellular trafficking and replication of *Burkholderia cenocepacia* in human cystic fibrosis airway epithelial cells. *Cell. Microbiol.* **8**(9), 1456–66 (2006).

201. Mullen, T., Markey, K., Murphy, P., McClean, S. & Callaghan, M. Role of lipase in *Burkholderia cepacia* complex (Bcc) invasion of lung epithelial cells. *Eur. J. Clin. Microbiol. Infect. Dis.* **26**(12), 869–77 (2007).

202. Tomich, M., Herfst, C. A., Golden, J. W. & Mohr, C. D. Role of flagella in host cell invasion by *Burkholderia cepacia*. *Infect. Immun.* **70**(4), 1799–

1806 (2002).

203. Schaefers, M. M. *et al.* An Oxygen-Sensing Two-Component System in the *Burkholderia cepacia* Complex Regulates Biofilm, Intracellular Invasion, and Pathogenicity. *PLoS Pathog.* **13**(1), e1006116 (2017).

204. Vogel, J. P., Andrews, H. L., Wong, S. K. & Isberg, R. R. Conjugative transfer by the virulence system of *Legionella pneumophila*. *Science.* **279**(5352), 873–6 (1998).

205. Comerci, D. J., Martínez-Lorenzo, M. J., Sieira, R., Gorvel, J. P. & Ugalde, R. A. Essential role of the virB machinery in the maturation of the *Brucella abortus*-containing vacuole. *Cell. Microbiol.* **3**(3), 159–68 (2001).

206. Vergunst, A. C., Meijer, A. H., Renshaw, S. A. & O'Callaghan, D. *Burkholderia cenocepacia* creates an intramacrophage replication niche in zebrafish embryos, followed by bacterial dissemination and establishment of systemic infection. *Infect. Immun.* **78**(4), 1495–1508(2010).

207. Hamad, M. A., Skeldon, A. M. & Valvano, M. A. Construction of Aminoglycoside-Sensitive *Burkholderia cenocepacia* Strains for Use in Studies of Intracellular Bacteria with the Gentamicin Protection Assay. *Appl. Environ. Microbiol.* **76**(10), 3170–3176 (2010).

208. Schmerk, C. L. & Valvano, M. A. *Burkholderia multivorans* survival and trafficking within macrophages. *J. Med. Microbiol.* **62**(2), 173–84 (2013).

209. Rosales-Reyes, R., Sánchez-Gómez, C., Ortiz-Navarrete, V. & Santos-Preciado, J. I. *Burkholderia cenocepacia* Induces Macropinocytosis to Enter Macrophages. *Biomed Res. Int.* **2018**, 4271560 (2018).

210. Lamothe, J., Huynh, K. K., Grinstein, S. & Valvano, M. A. Intracellular survival of *Burkholderia cenocepacia* in macrophages is associated with a delay in the maturation of bacteria-containing vacuoles. *Cell. Microbiol.* **9**(1), 40–53 (2007).

211. Huynh, K. K., Plumb, J. D., Downey, G. P., Valvano, M. A. & Grinstein, S. Inactivation of macrophage Rab7 by *Burkholderia cenocepacia*. *J. Innate Immun.* **2**(6), 522–33 (2010).

212. Al-Khodor, S. *et al. Burkholderia cenocepacia* J2315 escapes to the cytosol and actively subverts autophagy in human macrophages. *Cell. Microbiol.* **16**(3), 378–395 (2014).

213. Mesureur, J. *et al.* Macrophages, but not neutrophils, are critical for proliferation of *Burkholderia cenocepacia* and ensuing host-damaging inflammation. *PLoS Pathog.* **13**(6), e1006437 (2017).

214. Lamothe, J. & Valvano, M. A. *Burkholderia cenocepacia*-induced delay of acidification and phagolysosomal fusion in cystic fibrosis transmembrane conductance regulator (CFTR)-defective macrophages. *Microbiology* **154**(12), 3825–3834 (2008).

215. Luciani, A. *et al.* Defective CFTR induces aggresome formation and lung inflammation in cystic fibrosis through ROS-mediated autophagy inhibition. *Nat. Cell Biol.* **12**(9), 863–75 (2010).

216. Abdulrahman, B. A. *et al.* Autophagy stimulation by rapamycin suppresses lung inflammation and infection by *Burkholderia cenocepacia* in a model of cystic fibrosis. *Autophagy* **7**(11), 1359–70 (2011).

217. Abdulrahman, B. A. *et al.* Depletion of the ubiquitin-binding adaptor molecule SQSTM1/P62 from macrophages harboring cftr △F508 Mutation Improves the Delivery of *Burkholderia cenocepacia* to the Autophagic Machinery. *J. Biol. Chem.* **288**(3), 2049–58 (2013).

218. Hübner, R., Astin, K. B. & Herbert, R. J. H. 'Heavy metal' - Time to move on from semantics to pragmatics? *J. Environ. Monit.* **12**(8), 1511–4 (2010).

219. Hodson, M. E. Heavy metals - Geochemical bogey men? *Environ. Pollut.* **129**(3), 341–3 (2004).

220. Dupont, C. L., Yang, S., Palenik, B. & Bourne, P. E. Modern proteomes contain putative imprints of ancient shifts in trace metal geochemistry. *Proc. Natl. Acad. Sci. U. S. A.* **103**(47), 17822–7 (2006).

221. Py, B., Moreau, P. L. & Barras, F. Fe-S clusters, fragile sentinels of the cell. *Curr. Opin. Microbiol.* **14**(2), 218–23 (2011).

222. Blanc, B., Gerez, C. & Ollagnier de Choudens, S. Assembly of Fe/S

proteins in bacterial systems. Biochemistry of the bacterial ISC system. *Biochim. Biophys. Acta - Mol. Cell Res.* **1853**(6), 1436–47 (2015).

223. Chen, K., Roberts, E. & Luthey-Schulten, Z. Horizontal gene transfer of zinc and non-zinc forms of bacterial ribosomal protein S4. *BMC Evol. Biol.* **9**, 179 (2009).

224. Wu, J. W. & Chen, X. L. Extracellular metalloproteases from bacteria. *Appl. Microbiol. Biotechnol.* **92**(9), 253–62 (2011).

225. Cassandri, M. *et al.* Zinc-finger proteins in health and disease. *Cell Death Discov.* **3**, 17071 (2017).

226. Tainer, J. A., Getzoff, E. D., Richardson, J. S. & Richardson, D. C. Structure and mechanism of copper, zinc superoxide dismutase. *Nature* **306**(5940), 284–7 (1983).

227. Tsukihara, T. *et al.* Structures of metal sites of oxidized bovine heart cytochrome c oxidase at 2.8 Å. *Science.* **269**(5227), 1069–74 (1995).

228. Ridge, P. G., Zhang, Y. & Gladyshev, V. N. Comparative genomic analyses of copper transporters and cuproproteomes reveal evolutionary dynamics of copper utilization and its link to oxygen. *PLoS One* **3**(1), e1378 (2008).

229. Waldron, K. J. & Robinson, N. J. How do bacterial cells ensure that metalloproteins get the correct metal? *Nat. Rev. Microbiol.* **7**(1), 25–35 (2009).

230. Ma, Z., Jacobsen, F. E. & Giedroc, D. P. Coordination chemistry of bacterial metal transport and sensing. *Chem. Rev.* **109**(10), 4644–81 (2009).

231. Porcheron, G., Garénaux, A., Proulx, J., Sabri, M. & Dozois, C. M. Iron, copper, zinc, and manganese transport and regulation in pathogenic Enterobacteria: Correlations between strains, site of infection and the relative importance of the different metal transport systems for virulence. *Front. Cell. Infect. Microbiol.* **3**, 90 (2013).

232. Blindauer, C. A. *et al.* Multiple bacteria encode metallothioneins and SmtA-like zinc fingers. *Mol. Microbiol.* **45**(5), 1421–32 (2002).

233. Bitoun, J. P., Wu, G. & Ding, H. *Escherichia coli* FtnA acts as an iron buffer for re-assembly of iron-sulfur clusters in response to hydrogen peroxide stress. *BioMetals* **21**(6), 693–703 (2008).

234. Lemire, J. A., Harrison, J. J. & Turner, R. J. Antimicrobial activity of metals: Mechanisms, molecular targets and applications. *Nat. Rev. Microbiol.* **11**, 371–384 (2013).

235. Wei, Y. & Fu, D. Selective metal binding to a membrane-embedded aspartate in the *Escherichia coli* metal transporter YiiP (FieF). *J. Biol. Chem.* **280**(40), 33716–24 (2005).

236. Lin, W., Chai, J., Love, J. & Fu, D. Selective electrodiffusion of zinc ions in a Zrt-, Irt-like protein, ZIPB. *J. Biol. Chem.* **285**(50), 39013–20 (2010).

237. Braud, A., Hannauer, M., Mislin, G. L. A. & Schalk, I. J. The *Pseudomonas aeruginosa* pyochelin-iron uptake pathway and its metal specificity. *J. Bacteriol.* **191**(11), 3517–25 (2009).

238. Strlič, M., Kolar, J., Šelih, V. S., Kočar, D. & Pihlar, B. A comparative study of several transition metals in fenton-like reaction systems at circum-neutral pH. *Acta Chim. Slov.* **50**(4), 619–32 (2003).

239. Itoh, M. *et al.* Mechanism of chromium(VI) toxicity in *Escherichia coli*: Is hydrogen peroxide essential in Cr(VI) toxicity? *J. Biochem.* **117**(4), 780–6 (1995).

240. Geslin, C., Llanos, J., Prieur, D. & Jeanthon, C. The manganese and iron superoxide dismutases protect *Escherichia coli* from heavy metal toxicity. *Res. Microbiol.* **152**(10), 901–5 (2001).

241. Parvatiyar, K. *et al.* Global analysis of cellular factors and responses involved in *Pseudomonas aeruginosa* resistance to arsenite. *J. Bacteriol.* **187**(14), 4853–64 (2005).

242. Teitzel, G. M. *et al.* Survival and growth in the presence of elevated copper: Transcriptional profiling of copper-stressed *Pseudomonas aeruginosa*. *J. Bacteriol.* **188**(20), 7242-56 (2006).

243. Macomber, L. & Imlay, J. A. The iron-sulfur clusters of dehydratases are primary intracellular targets of copper toxicity. *Proc. Natl. Acad. Sci. U. S.*

A. **106**(20), 8344–9 (2009).

244. Xu, F. F. & Imlay, J. A. Silver(I), mercury(II), cadmium(II), and zinc(II) target exposed enzymic iron-sulfur clusters when they toxify *Escherichia coli*. *Appl. Environ. Microbiol.* **78**(10), 3614–21 (2012).

245. Ranquet, C., Ollagnier-de-Choudens, S., Loiseau, L., Barras, F. & Fontecave, M. Cobalt stress in *Escherichia coli*: The effect on the iron-sulfur proteins. *J Biol Chem* **282**(42), 30442–51 (2007).

246. Tan, G. *et al.* Anaerobic copper toxicity and iron-sulfur cluster biogenesis in *Escherichia coli*. *Appl. Environ. Microbiol.* **83**(16), e00867-17 (2017).

247. Li, J. *et al.* Zinc toxicity and iron-sulfur cluster biogenesis in *Escherichia coli*. *Appl. Environ. Microbiol.* **85**(9), e01967-18 (2019).

248. Irving, H. & Williams, R. J. P. Order of stability of metal complexes. *Nature* **162**, 746–7 (1948).

249. Ciriolo, M. R. *et al.* Purification and characterization of Ag,Zn-superoxide dismutase from *Saccharomyces cerevisiae* exposed to silver. *J. Biol. Chem.* **269**(41), 25783–7 (1994).

250. Erskine, P. T. *et al.* X-ray structure of 5-aminolaevulinate dehydratase, a hybrid aldolase. *Nat. Struct. Biol.* **4**, 1025–31 (1997).

251. Macomber, L., Elsey, S. P. & Hausinger, R. P. Fructose-1,6-bisphosphate aldolase (class II) is the primary site of nickel toxicity in *Escherichia coli*. *Mol. Microbiol.* **82**(5), 1291–300 (2011).

252. Helbig, K., Bleuel, C., Krauss, G. J. & Nies, D. H. Glutathione and transition-metal homeostasis in *Escherichia coli*. *J. Bacteriol.* **190**(15), 5431–8 (2008).

253. Helbig, K., Grosse, C. & Nies, D. H. Cadmium toxicity in glutathione mutants of *Escherichia coli*. *J. Bacteriol.* **190**(15), 5439–54 (2008).

254. Harrison, J. J. *et al.* Chromosomal antioxidant genes have metal ion-specific roles as determinants of bacterial metal tolerance. *Environ. Microbiol.* **11**(10), 2491–509 (2009).

255. Howlett, N. G. & Avery, S. V. Induction of lipid peroxidation during heavy

metal stress in *Saccharomyces cerevisiae* and influence of plasma membrane fatty acid unsaturation. *Appl. Environ. Microbiol.* **63**(8), 2971–6 (1997).

256. Hong, R., Kang, T. Y., Michels, C. A. & Gadura, N. Membrane lipid peroxidation in copper alloy-mediated contact killing of *Escherichia coli*. *Appl. Environ. Microbiol.* **78**(6), 1776–84 (2012).

257. San, K., Long, J., Michels, C. A. & Gadura, N. Antimicrobial copper alloy surfaces are effective against vegetative but not sporulated cells of Gram-positive *Bacillus subtilis*. *Microbiologyopen* **4**(5), 753–63 (2015).

258. Bragg, P. D. & Rainnie, D. J. The effect of silver ions on the respiratory chain of *Escherichia coli*. *Can. J. Microbiol.* **20**(6), 883–9 (1974).

259. Dibrov, P., Dzioba, J., Gosink, K. K. & Häse, C. C. Chemiosmotic mechanism of antimicrobial activity of Ag+ in *Vibrio cholerae*. *Antimicrob. Agents Chemother.* **46**(8), 2668–70 (2002).

260. Lok, C. N. *et al.* Proteomic analysis of the mode of antibacterial action of silver nanoparticles. *J. Proteome Res.* **5**(4), 916–24 (2006).

261. Fadeeva, M. S., Bertsova, Y. V., Euro, L. & Bogachev, A. V. Cys377 residue in NqrF subunit confers Ag + sensitivity of Na +-translocating NADH: Quinone oxidoreductase from *Vibrio harveyi*. *Biochem.* **5**(4), 916–24 (2011).

262. McDevitt, C. A. *et al.* A Molecular Mechanism for Bacterial Susceptibility to Zinc. *Plos Pathog.* **7**(11), e1002357 (2011).

263. Eijkelkamp, B. A. *et al.* Extracellular zinc competitively inhibits manganese uptake and compromises oxidative stress management in Streptococcus pneumoniae. *PLoS One* **9**(2), e89427 (2014).

264. Begg, S. L. *et al.* Dysregulation of transition metal ion homeostasis is the molecular basis for cadmium toxicity in *Streptococcus pneumoniae*. *Nat. Commun.* **6**, 6418 (2015).

265. Stout, J. E. & Yu, V. L. Experiences of the First 16 Hospitals Using Copper-Silver Ionization for *Legionella* Control: Implications for the Evaluation of Other Disinfection Modalities. *Infect. Control Hosp.*

Epidemiol. **24**(8), 563–8 (2003).

266. Dixon, B. Pushing Bordeaux mixture. *Lancet Infect. Dis.* **4**(9), 594 (2004).

267. Stevens, K. N. J. *et al.* Hydrophilic surface coatings with embedded biocidal silver nanoparticles and sodium heparin for central venous catheters. *Biomaterials* **32**(5), 1264–9 (2011).

268. Boonkaew, B., Kempf, M., Kimble, R., Supaphol, P. & Cuttle, L. Antimicrobial efficacy of a novel silver hydrogel dressing compared to two common silver burn wound dressings: Acticoat™ and PolyMem Silver ®. *Burns* **40**(1), 89–96 (2014).

269. Sun, Y. & Xia, Y. Shape-controlled synthesis of gold and silver nanoparticles. *Science.* **298**(5601), 2176–9 (2002).

270. Yu, D. & Yam, V. W. W. Hydrothermal-induced assembly of colloidal silver spheres into various nanoparticles on the basis of HTAB-modified silver mirror reaction. *J. Phys. Chem. B* **109**(12), 5497–503 (2005).

271. Applerot, G. *et al.* Enhanced antibacterial activity of nanocrystalline ZnO due to increased ROS-mediated cell injury. *Adv. Funct. Mater.* **19**(6), 842–52 (2009).

272. Li, W. R. *et al.* Antibacterial activity and mechanism of silver nanoparticles on *Escherichia coli*. *Appl. Microbiol. Biotechnol.* **85**(4), 1115–22 (2010).

273. Gunawan, C., Teoh, W. Y., Marquis, C. P. & Amal, R. Cytotoxic origin of copper(II) oxide nanoparticles: Comparative studies with micron-sized particles, leachate, and metal salts. *ACS Nano* **5**(9), 7214–25 (2011).

274. Applerot, G. *et al.* Understanding the antibacterial mechanism of CuO nanoparticles: Revealing the route of induced oxidative stress. *Small* **8**(21), 3326–37 (2012).

275. Verma, S. K. *et al.* Molecular aspects of core-shell intrinsic defect induced enhanced antibacterial activity of ZnO nanocrystals. *Nanomedicine* **13**(1), 43–68 (2018).

276. Bandyopadhyay, S., Peralta-Videa, J. R., Plascencia-Villa, G., José-Yacamán, M. & Gardea-Torresdey, J. L. Comparative toxicity assessment

of CeO2 and ZnO nanoparticles towards *Sinorhizobium meliloti*, a symbiotic alfalfa associated bacterium: Use of advanced microscopic and spectroscopic techniques. *J. Hazard. Mater.* **241-242**, 379–86 (2012).

277. Luef, B. *et al.* Iron-reducing bacteria accumulate ferric oxyhydroxide nanoparticle aggregates that may support planktonic growth. *ISME J.* **7**(2), 338–50 (2013).

278. Wilks, S. A., Michels, H. & Keevil, C. W. The survival of *Escherichia coli* O157 on a range of metal surfaces. *Int. J. Food Microbiol.* **105**(3), 445–54 (2005).

279. Wilks, S. A., Michels, H. T. & Keevil, C. W. Survival of *Listeria monocytogenes* Scott A on metal surfaces: Implications for cross-contamination. *Int. J. Food Microbiol.* **111**(2), 93-8 (2006).

280. Weaver, L., Michels, H. T. & Keevil, C. W. Survival of *Clostridium difficile* on copper and steel: futuristic options for hospital hygiene. *J. Hosp. Infect.* **68**(2), 145–51 (2008).

281. Michels, H. T., Noyce, J. O. & Keevil, C. W. Effects of temperature and humidity on the efficacy of methicillin- resistant *Staphylococcus aureus* challenged antimicrobial materials containing silver and copper. *Lett. Appl. Microbiol.* **49**(2), 191–5 (2009).

282. Mikolay, A. *et al.* Survival of bacteria on metallic copper surfaces in a hospital trial. *Appl. Microbiol. Biotechnol.* **87**(5), 1875–9 (2010).

283. Casey, A. L. *et al.* Role of copper in reducing hospital environment contamination. *J. Hosp. Infect.* **74**(1), 72–7 (2010).

284. Casey, A. L. *et al.* A comparative study to evaluate surface microbial contamination associated with copper-containing and stainless steel pens used by nurses in the critical care unit. *Am. J. Infect. Control* **39**(8), e52–e54 (2011).

285. Karpanen, T. J. *et al.* The Antimicrobial Efficacy of Copper Alloy Furnishing in the Clinical Environment: A Crossover Study. *Infect. Control Hosp. Epidemiol.* **33**(1), 3–9 (2012).

286. Schmidt, M. G. *et al.* Sustained reduction of microbial burden on common

hospital surfaces through introduction of copper. *J. Clin. Microbiol.* **50**(7), 2217–23 (2012).

287. Salgado, C. D. *et al.* Copper Surfaces Reduce the Rate of Healthcare-Acquired Infections in the Intensive Care Unit. *Infect. Control Hosp. Epidemiol.* **34**(5), 479–86 (2013).

288. Schmidt, M. G. *et al.* Copper Continuously Limits the Concentration of Bacteria Resident on Bed Rails within the Intensive Care Unit. *Infect. Control Hosp. Epidemiol.* **34**(5), 530–3 (2013).

289. Colin, M. *et al.* Copper alloy touch surfaces in healthcare facilities: An effective solution to prevent bacterial spreading. *Materials (Basel).* **11**(12), 2479 (2018).

290. Gabbay, J. *et al.* Copper oxide impregnated textiles with potent biocidal activities. *J. Ind. Text.* **35**(4), 323-335 (2006).

291. Zatcoff, R. C., Smith, M. S. & Borkow, G. Treatment of tinea pedis with socks containing copper-oxide impregnated fibers. *Foot* **18**(3), 136–41 (2008).

292. Borkow, G. Protection of soldiers' feet by copper oxide impregnated socks. *Adv. Mil. Technol.* **8**(2), 101–108 (2013).

293. Lazary, A. *et al.* Reduction of healthcare-associated infections in a long-term care brain injury ward by replacing regular linens with biocidal copper oxide impregnated linens. *Int. J. Infect. Dis.* **24**, 23–9 (2014).

294. Marcus, E. L. *et al.* Reduction of health care–associated infection indicators by copper oxide–impregnated textiles: Crossover, double-blind controlled study in chronic ventilator-dependent patients. *Am. J. Infect. Control* **45**(4), 401–3 (2017).

295. Kim, J., Pitts, B., Stewart, P. S., Camper, A. & Yoon, J. Comparison of the antimicrobial effects of chlorine, silver ion, and tobramycin on biofilm. *Antimicrob. Agents Chemother.* **52**(4), 1446–53 (2008).

296. Ruden, S., Hilpert, K., Berditsch, M., Wadhwani, P. & Ulrich, A. S. Synergistic interaction between silver nanoparticles and membrane-permeabilizing antimicrobial peptides. *Antimicrob. Agents Chemother.*

53(8), 3538–40 (2009).

297. Morones-Ramirez, J. R., Winkler, J. A., Spina, C. S. & Collins, J. J. Silver enhances antibiotic activity against Gram-negative bacteria. *Sci. Transl. Med.* **5**(190), 190ra81 (2013).

298. Zou, L. *et al.* Synergistic antibacterial effect of silver and ebselen against multidrug-resistant Gram-negative bacterial infections. *EMBO Mol. Med.* **9**(8), 1165–78 (2017).

299. Herisse, M., Duverger, Y., Martin-Verstraete, I., Barras, F. & Ezraty, B. Silver potentiates aminoglycoside toxicity by enhancing their uptake. *Mol. Microbiol.* **105**(1), 115–26 (2017).

300. Zou, L. *et al.* Synergistic antibacterial activity of silver with antibiotics correlating with the upregulation of the ROS production. *Sci. Rep.* **8**, 11131 (2018).

301. Allen, D. A., Austin, B. & Colwell, R. R. Antibiotic resistance patterns of metal-tolerant bacteria isolated from an estuary. *Antimicrob. Agents Chemother.* **12**(4), 545–7 (1977).

302. Calomiris, J. J., Armstrong, J. L. & Seidler, R. J. Association of metal tolerance with multiple antibiotic resistance of bacteria isolated from drinking water. *Appl. Environ. Microbiol.* **47**(6), 1238–42 (1984).

303. Huysman, F., Verstraete, W. & Brookes, P. C. Effect of manuring practices and increased copper concentrations on soil microbial populations. *Soil Biol. Biochem.* **26**(1), 103–10 (1994).

304. Stepanauskas, R. *et al.* Elevated microbial tolerance to metals and antibiotics in metal-contaminated industrial environments. *Environ. Sci. Technol.* **39**(10), 3671–8 (2005).

305. Stepanauskas, R. *et al.* Coselection for microbial resistance to metals and antibiotics in freshwater microcosms. *Environ. Microbiol.* **8**(9), 1510–4 (2006).

306. Resende, J. A. *et al.* Multidrug-resistance and toxic metal tolerance of medically important bacteria isolated from an aquaculture system. *Microbes Environ.* **27**(4), 449–55 (2012).

307. Ji, X. *et al.* Antibiotic resistance gene abundances associated with antibiotics and heavy metals in animal manures and agricultural soils adjacent to feedlots in Shanghai; China. *J. Hazard. Mater.* **235-6**, 178–85 (2012).

308. Devika, L., Rajaram, R. & Mathivanan, K. Multiple Heavy Metal and Antibiotic Tolerance Bacteria Isolated from Equatorial Indian Ocean. *Int. J. Micriobiological Res.* **4**, 212–8 (2013).

309. Manegabe, B. J., Marie-Médiatrice, N. K., Barr Dewar, J. & Christian, S. B. Antibiotic resistance and tolerance to heavy metals demonstrated by environmental pathogenic bacteria isolated from the Kahwa River, Bukavu Town, Democratic Republic of the Congo. *Int. J. Environ. Stud.* **74**(2), 290–302 (2017).

310. Sair, A. T. & Khan, Z. A. Prevalence of antibiotic and heavy metal resistance in Gram negative bacteria isolated from rivers in northern Pakistan. *Water Environ. J.* **32**(1), 51–7 (2018).

311. Charlesworth, S., de Miguel, E. & Ordóñez, A. A review of the distribution of particulate trace elements in urban terrestrial environments and its application to considerations of risk. *Environ. Geochem. Health* **33**(2), 103–23 (2011).

312. Li, Z., Ma, Z., van der Kuijp, T. J., Yuan, Z. & Huang, L. A review of soil heavy metal pollution from mines in China: Pollution and health risk assessment. *Sci. Total Environ.* **468-469**, 843–853 (2014).

313. Chen, H., Teng, Y., Lu, S., Wang, Y. & Wang, J. Contamination features and health risk of soil heavy metals in China. *Sci. Total Environ.* **512-513**, 143–53 (2015).

314. Baker-Austin, C., Wright, M. S., Stepanauskas, R. & McArthur, J. V. Co-selection of antibiotic and metal resistance. *Trends Microbiol.* **14**(4), 176–82 (2006).

315. Hasman, H. & Aarestrup, F. M. tcrb, a gene conferring transferable copper resistance in *Enterococcus faecium*: Occurrence, transferability, and linkage to macrolide and glycopeptide resistance. *Antimicrob. Agents Chemother.* **46**(5), 1410–6 (2002).

316. Martins, V. V., Zanetti, M. O. B., Pitondo-Silva, A. & Stehling, E. G. Aquatic environments polluted with antibiotics and heavy metals: A human health hazard. *Environ. Sci. Pollut. Res.* **21**(9), 5873–8 (2014).

317. Li, L. G., Xia, Y. & Zhang, T. Co-occurrence of antibiotic and metal resistance genes revealed in complete genome collection. *ISME J.* **11**(3), 651–62 (2017).

318. Mata, M. T., Baquero, F. & Pérez-Díaz, J. C. A multidrug efflux transporter in *Listeria monocytogenes*. *FEMS Microbiol. Lett.* **187**(2), 185–8 (2000).

319. Perron, K. *et al.* CzcR-CzcS, a Two-component System Involved in Heavy Metal and Carbapenem Resistance in *Pseudomonas aeruginosa*. *J. Biol. Chem.* **279**(10), 8761–8 (2004).

320. Caille, O., Rossier, C. & Perron, K. A copper-activated two-component system interacts with zinc and imipenem resistance in *Pseudomonas aeruginosa*. *J. Bacteriol.* **189**(13), 4561–8 (2007).

321. Plüddemann, A., Mukhopadhyay, S. & Gordon, S. Innate immunity to intracellular pathogens: Macrophage receptors and responses to microbial entry. *Immunol. Rev.* **240**(1), 11–24 (2011).

322. Botella, H., Stadthagen, G., Lugo-Villarino, G., de Chastellier, C. & Neyrolles, O. Metallobiology of host-pathogen interactions: an intoxicating new insight. *Trends Microbiol.* **20**(3), 106–12 (2012).

323. Vidal, S. *et al.* The ity/lsh/bcg locus: Natural resistance to infection with intracellular parasites is abrogated by disruption of the nrampl gene. *J. Exp. Med.* **182**(3), 655–66 (1995).

324. Gomes, M. S. & Appelberg, R. Evidence for a link between iron metabolism and Nramp1 gene function in innate resistance against *Mycobacterium avium*. *Immunology* **95**(2), 165–8 (1998).

325. Forbes, J. R. & Gros, P. Divalent-metal transport by NRAMP proteins at the interface of host-pathogen interactions. *Trends Microbiol.* **9**(8), 397–403 (2001).

326. Forbes, J. R. & Gros, P. Iron, manganese, and cobalt transport by

Nramp1 (Slc11a1) and Nramp2 (Slc11a2) expressed at the plasma membrane. *Blood* **102**(5), 1884–92 (2003).

327. Skamene, E., Schurr, E. & Gros, P. INFECTION GENOMICS: Nramp1 as a Major Determinant of Natural Resistance to Intracellular Infections. *Annu. Rev. Med.* **49**, 275–87 (1998).

328. Stagas, M. K. *et al.* Polymorphisms of the NRAMP1 gene: Distribution and susceptibility to the development of pulmonary tuberculosis in the Greek population. *Med. Sci. Monit.* **17**(1), PH1–6 (2011).

329. Li, X. W. *et al.* SLC11A1 (NRAMP1) polymorphisms and tuberculosis susceptibility: Updated systematic review and meta-analysis. *PLoS One* **6**(1), e15831 (2011).

330. Nairz, M. *et al.* The co-ordinated regulation of iron homeostasis in murine macrophages limits the availability of iron for intracellular *Salmonella* typhimurium. *Cell. Microbiol.* **9**(9), 2126–40 (2007).

331. Nairz, M. *et al.* Interferon-γ limits the availability of iron for intramacrophage *Salmonella* typhimurium. *Eur. J. Immunol.* **38**(7), 1923–36 (2008).

332. Golonka, R., Yeoh, B. S. & Vijay-Kumar, M. The Iron Tug-of-War between Bacterial Siderophores and Innate Immunity. *J. Innate Immun.* **11**(3), 249–262 (2019).

333. Wagner, D. *et al.* Elemental Analysis of *Mycobacterium avium* -, *Mycobacterium tuberculosis* -, and *Mycobacterium smegmatis* - Containing Phagosomes Indicates Pathogen-Induced Microenvironments within the Host Cell's Endosomal System . *J. Immunol.* **174**, 1491–500 (2005).

334. Botella, H. *et al.* Mycobacterial P 1 -Type ATPases mediate resistance to Zinc poisoning in human macrophages. *Cell Host Microbe* **10**, 248–59 (2011).

335. Schwan, W. R., Warrener, P., Keunz, E., Kendall Stover, C. & Folger, K. R. Mutations in the cueA gene encoding a copper homeostasis P-type ATPase reduce the pathogenicity of *Pseudomonas aeruginosa* in mice.

Int. J. Med. Microbiol. **295**(4), 237–42 (2005).

336. White, C., Lee, J., Kambe, T., Fritsche, K. & Petris, M. J. A role for the ATP7A copper-transporting ATPase in macrophage bactericidal activity. *J. Biol. Chem.* **284**(49), 33949–56 (2009).

337. Johnson, M. D. L. *et al.* Role of copper efflux in pneumococcal pathogenesis and resistance to macrophage-mediated immune clearance. *Infect. Immun.* **83**(4), 1684–94 (2015).

338. Saier, M. H., Tam, R., Reizer, A. & Reizer, J. Two novel families of bacterial membrane proteins concerned with nodulation, cell division and transport. *Mol. Microbiol.* **11**(5), 841–7 (1994).

339. Tseng, T. T. *et al.* The RND permease superfamily: An ancient, ubiquitous and diverse family that includes human disease and development proteins. *J. Mol. Microbiol. Biotechnol.* **1**(1), 107–25 (1999).

340. Nies, D. H. Efflux-mediated heavy metal resistance in prokaryotes. *Fems Microbiol. Rev.* **27**(2-3), 313–339 (2003).

341. Nies, D. H. The cobalt, zinc, and cadmium efflux system CzcABC from *Alcaligenes eutrophus* functions as a cation-proton antiporter in *Escherichia coli*. *J. Bacteriol.* **177**(10), 2707–12 (1995).

342. Hassan, M. e. T. *et al.* Identification of a gene cluster, czr, involved in cadmium and zinc resistance in *Pseudomonas aeruginosa*. *Gene* **238**(2), 417–25 (1999).

343. Franke, S., Grass, G., Rensing, C. & Nies, D. H. Molecular analysis of the copper-transporting efflux system CusCFBA of *Escherichia coli*. *J. Bacteriol.* **185**(13), 3804–12 (2003).

344. Bondarczuk, K. & Piotrowska-Seget, Z. Molecular basis of active copper resistance mechanisms in Gram-negative bacteria. *Cell Biol. Toxicol.* **29**(6), 397–405 (2013).

345. Kuroda, M., Hayashi, H. & Ohta, T. Chromosome-determined zinc-responsible operon czr in *Staphylococcus aureus* strain 912. *Microbiol. Immunol.* **43**(2), 115–25 (1999).

346. Grass, G. *et al.* ZitB (YbgR), a member of the cation diffusion facilitator family, is an additional zinc transporter in *Escherichia coli*. *J. Bacteriol.* **183**(15), 4664–7 (2001).

347. Argüello, J. M. Identification of Ion-Selectivity Determinants in Heavy-Metal Transport P1B-type ATPases. *J. Membr. Biol.* **195**(2), 93–108 (2003).

348. Argüello, J. M., González-Guerrero, M. & Raimunda, D. Bacterial transition metal P 1B-ATPases: Transport mechanism and roles in virulence. *Biochemistry* **50**(46), 9940–9 (2011).

349. Raimunda, D., Long, J. E., Padilla-Benavides, T., Sassetti, C. M. & Argüello, J. M. Differential roles for the Co2+/Ni2+ transporting ATPases, CtpD and CtpJ, in *Mycobacterium tuberculosis* virulence. *Mol. Microbiol.* **91**(1) (2014).

350. Padilla-Benavides, T., Thompson, A. M. G., McEvoy, M. M. & Argüello, J. M. Mechanism of ATPase-mediated Cu+ export and delivery to periplasmic chaperones: The interaction of *Escherichia coli* CopA and CusF. *J. Biol. Chem.* **289**(30), 20492–501 (2014).

351. Hassani, B. K., Astier, C., Nitschke, W. & Ouchane, S. CtpA, a copper-translocating P-type ATPase involved in the biogenesis of multiple copper-requiring enzymes. *J. Biol. Chem.* **285**(25), 19330–7 (2010).

352. González-Guerrero, M., Raimunda, D., Cheng, X. & Argüello, J. M. Distinct functional roles of homologous Cu+ efflux ATPases in *Pseudomonas aeruginosa*. *Mol. Microbiol.* **78**(5), 1246–58 (2010).

353. Grass, G. & Rensing, C. CueO is a multi-copper oxidase that confers copper tolerance in *Escherichia coli*. *Biochem. Biophys. Res. Commun.* **286**(5), 902–8 (2001).

354. Singh, S. K., Grass, G., Rensing, C. & Montfort, W. R. Cuprous oxidase activity of CueO from *Escherichia coli*. *J. Bacteriol.* **186**(22), 7815–7 (2004).

355. Carrondo, M. A. Ferritins, iron uptake and storage from the bacterioferritin viewpoint. *EMBO J.* **22**(9), 1959–68 (2003).

356. Blindauer, C. A. Bacterial metallothioneins: Past, present, and questions for the future. *J. Biol. Inorg. Chem.* **16**(7), 1011–24 (2011).

357. Rivera, M. Bacterioferritin: Structure, Dynamics, and Protein-Protein Interactions at Play in Iron Storage and Mobilization. *Acc. Chem. Res.* **50**(2), 331–40 (2017).

358. Chaturvedi, K. S., Hung, C. S., Crowley, J. R., Stapleton, A. E. & Henderson, J. P. The siderophore yersiniabactin binds copper to protect pathogens during infection. *Nat. Chem. Biol.* **8**(8), 731–6 (2012).

359. Chaturvedi, K. S. *et al.* Cupric yersiniabactin is a virulence-associated superoxide dismutase mimic. *ACS Chem. Biol.* **9**(2), 551–61 (2014).

360. Hannauer, M. *et al.* The PvdRT-OpmQ efflux pump controls the metal selectivity of the iron uptake pathway mediated by the siderophore pyoverdine in *Pseudomonas aeruginosa*. *Environ. Microbiol.* **14**(7), 1696–708 (2012).

361. Jiang, C. yu, Sheng, X. fang, Qian, M. & Wang, Q. ya. Isolation and characterization of a heavy metal-resistant *Burkholderia* sp. from heavy metal-contaminated paddy field soil and its potential in promoting plant growth and heavy metal accumulation in metal-polluted soil. *Chemosphere* **72**(2), 157–64 (2008).

362. Guo, J. K. *et al. Burkholderia metalliresistens* sp. nov., a multiple metal-resistant and phosphate-solubilising species isolated from heavy metal-polluted soil in Southeast China. *Antonie van Leeuwenhoek, Int. J. Gen. Mol. Microbiol.* **107**(6), 1591–8 (2015).

363. Pathak, A. *et al.* Genome-centric evaluation of *Burkholderia* sp. strain SRS-W-2-2016 resistant to high concentrations of uranium and nickel isolated from the Savannah River Site (SRS), USA. *Genomics Data* **12**, 62–8 (2017).

364. Peeters, E., Nelis, H. J. & Coenye, T. Resistance of planktonic and biofilm-grown *Burkholderia cepacia* complex isolates to the transition metal gallium. *J. Antimicrob. Chemother.* **61**(5), 1062–5 (2008).

365. Reid, D. E. W., Carroll, V., O'May, C., Champion, A. & Kirov, S. M.

Increased airway iron as a potential factor in the persistence of *Pseudomonas aeruginosa* infection in cystic fibrosis. *Eur. Respir. J.* **30**(2), 286–92 (2007).

366. Gray, R. D. *et al.* Sputum trace metals are biomarkers of inflammatory and suppurative lung disease. *Chest* **137**(3), 635–41 (2010).

367. Smith, D. J., Anderson, G. J., Bell, S. C. & Reid, D. W. Elevated metal concentrations in the CF airway correlate with cellular injury and disease severity. *J. Cyst. Fibros.* **13**(3), 289–295 (2014).

368. Schwager, S., Lumjiaktase, P., Stockli, M., Weisskopf, L. & Eberl, L. The genetic basis of cadmium resistance of *Burkholderia cenocepacia*. *Environ. Microbiol. Rep.* **4**(5), 562–568 (2012).

369. Higgins, S., Gualdi, S., Pinto-Carbó, M. & Eberl, L. Copper resistance genes of *Burkholderia cenocepacia* H111 identified by Transposon Sequencing. *Environ. Microbiol. Rep.* **12**(2), 241–9 (2020).

370. Routh, M. D. *et al.* Efflux pumps of the Resistance-nodulation-division family: A perspective of their structure, function, and regulation in gram-negative bacteria. *Adv. Enzymol. Relat. Areas Mol. Biol.* **77**, 109–46 (2010).

371. Anes, J., McCusker, M. P., Fanning, S. & Martins, M. The ins and outs of RND efflux pumps in *Escherichia coli*. *Frontiers in Microbiology* **6**, 587 (2015).

372. Guglierame, P. *et al.* Efflux pump genes of the resistance-nodulation-division family in *Burkholderia cenocepacia* genome. *Bmc Microbiol.* **6**, 66 (2006).

373. Jiang, M., Shao, W., Perego, M. & Hoch, J. A. Multiple histidine kinases regulate entry into stationary phase and sporulation in *Bacillus subtilis*. *Mol. Microbiol.* **6**, 22 (2000).

374. Francis, V. I., Stevenson, E. C. & Porter, S. L. Two-component systems required for virulence in *Pseudomonas aeruginosa*. *FEMS Microbiol. Lett.* **364**(11), fnx104 (2017).

375. Francis, V. I. & Porter, S. L. Multikinase Networks: Two-Component

Signaling Networks Integrating Multiple Stimuli. *Annu. Rev. Microbiol.* **73**, 199–223 (2019).

376. Galperin, M. Y. A census of membrane-bound and intracellular signal transduction proteins in bacteria: Bacterial IQ, extroverts and introverts. *BMC Microbiol.* **5**, 35 (2005).

377. Capra, E. J. & Laub, M. T. Evolution of two-component signal transduction systems. *Annu. Rev. Microbiol.* **66**, 325–47 (2012).

378. Thanbichler, M. Spatial regulation in *Caulobacter crescentus*. *Curr. Opin. Microbiol.* **12**(6), 715–21 (2009).

379. Sourjik, V. & Armitage, J. P. Spatial organization in bacterial chemotaxis. *EMBO J.* **29**(16), 2724–33 (2010).

380. Galperin, M. Y. Diversity of structure and function of response regulator output domains. *Curr. Opin. Microbiol.* **13**(2), 150–9 (2010).

381. Alm, E., Huang, K. & Arkin, A. The evolution of two-component systems in bacteria reveals different strategies for niche adaptation. *PLoS Comput. Biol.* **2**(11), e143 (2006).

382. Dutta, R. & Inouye, M. GHKL, an emergent ATPase/kinase superfamily. *Trends Biochem. Sci.* **25**(1), 24–8 (2000).

383. Ulrich, L. E., Koonin, E. V. & Zhulin, I. B. One-component systems dominate signal transduction in prokaryotes. *Trends Microbiol.* **13**(2), 52–6 (2005).

384. Krell, T., Busch, A., Lacal, J., Silva-Jiménez, H. & Ramos, J. L. The enigma of cytosolic two-component systems: A hypothesis. *Environ. Microbiol. Rep.* **1**(3), 171–6 (2009).

385. Wuichet, K., Cantwell, B. J. & Zhulin, I. B. Evolution and phyletic distribution of two-component signal transduction systems. *Curr. Opin. Microbiol.* **13**(2), 219–25 (2010).

386. Alvarez, A. F., Barba-Ostria, C., Silva-Jiménez, H. & Georgellis, D. Organization and mode of action of two component system signaling circuits from the various kingdoms of life. *Environ. Microbiol.* **18**(10),

3210–26 (2016).

387. Liu, Y., Harrison, P. M., Kunin, V. & Gerstein, M. Comprehensive analysis of pseudogenes in prokaryotes: widespread gene decay and failure of putative horizontally transferred genes. *Genome Biol.* **5**(9), R64 (2004).

388. Arthur, M., Molinas, C. & Courvalin, P. The VanS-VanR two-component regulatory system controls synthesis of depsipeptide peptidoglycan precursors in *Enterococcus faecium* BM4147. *J. Bacteriol.* **174**(8), 2582–91 (1992).

389. Khunajakr, N., Liu, C. Q., Charoenchai, P. & Dunn, N. W. A plasmid-encoded two-component regulatory system involved in copper- inducible transcription in *Lactococcus lactis*. *Gene* **229**(1-2), 229–35 (1999).

390. Deiwick, J., Nikolaus, T., Erdogan, S. & Hensel, M. Environmental regulation of *Salmonella* pathogenicity island 2 gene expression. *Mol. Microbiol.* **31**(6), 1759–73 (2003).

391. Fruci, M. & Poole, K. Bacterial Stress Responses as Determinants of Antimicrobial Resistance. *Stress Environ. Regul. Gene Expr. Adapt. Bact.* **67**(9), 2069–89 (2016).

392. Dubrac, S., Boneca, I. G., Poupel, O. & Msadek, T. New insights into the WalK/WalR (YycG/YycF) essential signal transduction pathway reveal a major role in controlling cell wall metabolism and biofilm formation in *Staphylococcus aureus*. *J. Bacteriol.* **189**(22), 8257–69 (2007).

393. Dubrac, S., Bisicchia, P., Devine, K. M. & Msadek, T. A matter of life and death: Cell wall homeostasis and the WalKR (YycGF) essential signal transduction pathway. *Mol. Microbiol.* **70**(6), 1307–22 (2008).

394. Utsumi, R. Bacterial signal transduction networks via connectors and development of the inhibitors as alternative antibiotics. *Biosci. Biotechnol. Biochem.* **81**(9), 1663–9 (2017).

395. Okada, A. *et al.* Walkmycin B targets WalK (YycG), a histidine kinase essential for bacterial cell growth. *J. Antibiot. (Tokyo).* **63**(2), 89–94 (2010).

396. Watanabe, T. *et al.* Isolation and characterization of signermycin B, an

antibiotic that targets the dimerization domain of histidine kinase WalK. *Antimicrob. Agents Chemother.* **56**(7), 3657–63 (2012).

397. Kato, A. *et al.* Characterization of H-box region mutants of WalK inert to the action of waldiomycin in *Bacillus subtilis*. *J. Gen. Appl. Microbiol.* **63**(4), 212–21 (2017).

398. Gotoh, Y. *et al.* Novel antibacterial compounds specifically targeting the essential WalR response regulator. *J. Antibiot. (Tokyo).* **63**(3), 127–34 (2010).

399. Choi, E., Groisman, E. A. & Shin, D. Activated by different signals, the PhoP/PhoQ two-component system differentially regulates metal uptake. *J. Bacteriol.* **191**(23), 7174–81 (2009).

400. Tang, Y. T. *et al.* Inhibition of Bacterial Virulence: Drug-Like Molecules Targeting the *Salmonella enterica* PhoP Response Regulator. *Chem. Biol. Drug Des.* **79**(6), 1007–17 (2012).

401. Galán, J. E. & Curtiss, R. Virulence and vaccine potential of phoP mutants of *Salmonella* typhimurium. *Microb. Pathog.* **6**(6), 433–43 (1989).

402. Miller, S. I., Loomis, W. P., Alpuche-Aranda, C., Behlau, I. & Hohmann, E. The PhoP virulence regulon and live oral *Salmonella* vaccines. *Vaccine* **11**(2), 122–5 (1993).

403. Martin, C. *et al.* The live *Mycobacterium tuberculosis* phoP mutant strain is more attenuated than BCG and confers protective immunity against tuberculosis in mice and guinea pigs. *Vaccine* **24**(17), 3408–19 (2006).

404. Tiwari, S. *et al. C. pseudotuberculosis* Phop confers virulence and may be targeted by natural compounds. *Integr. Biol. (United Kingdom)* **6**(11), 1088–99 (2014).

405. Eguchi, Y. *et al.* B1500, a small membrane protein, connects the two-component systems EvgS/EvgA and PhoQ/PhoP in *Escherichia coli*. *Proc. Natl. Acad. Sci.* **104**(47), 18712–17 (2007).

406. Eguchi, Y., Ishii, E., Yamane, M. & Utsumi, R. The connector SafA interacts with the multi-sensing domain of PhoQ in *Escherichia coli*. *Mol. Microbiol.* **85**(2), 299–313 (2012).

407. Minagawa, S. *et al.* Identification and molecular characterization of the Mg2+ stimulon of *Escherichia coli*. *J. Bacteriol.* **185**(13), 3696–702 (2003).

408. Rabin, R. S. & Stewart, V. Dual response regulators (NarL and NarP) interact with dual sensors (NarX and NarQ) to control nitrate- and nitrite-regulated gene expression in *Escherichia coli* K-12. *J. Bacteriol.* **175**(11), 3259–68 (1993).

409. Noriega, C. E., Lin, H. Y., Chen, L. L., Williams, S. B. & Stewart, V. Asymmetric cross-regulation between the nitrate-responsive NarX-NarL and NarQ-NarP two-component regulatory systems from *Escherichia coli* K-12. *Mol. Microbiol.* **75**(2), 394–412 (2010).

410. Francis, V. I. *et al.* Multiple communication mechanisms between sensor kinases are crucial for virulence in *Pseudomonas aeruginosa*. *Nat. Commun.* **9**(1), 2219 (2018).

411. Henke, J. M. & Bassler, B. L. Three parallel quorum-sensing systems regulate gene expression in *Vibrio harveyi*. *J. Bacteriol.* **186**(20), 6902–14 (2004).

412. Tsokos, C. G. & Laub, M. T. Polarity and cell fate asymmetry in *Caulobacter crescentus*. *Curr. Opin. Microbiol.* **15**(6), 744–50 (2012).

413. Heurlier, K. *et al.* Positive Control of Swarming, Rhamnolipid Synthesis, and Lipase Production by the Posttranscriptional RsmA/RsmZ System in *Pseudomonas aeruginosa* PAO1. *J. Bacteriol.* **186**(10), 2936–45 (2004).

414. Burrowes, E., Baysse, C., Adams, C. & O'Gara, F. Influence of the regulatory protein RsmA on cellular functions in *Pseudomonas aeruginosa* PAO1, as revealed by transcriptome analysis. *Microbiology* **152**(2), 405–18 (2006).

415. Ventre, I. *et al.* Multiple sensors control reciprocal expression of *Pseudomonas aeruginosa* regulatory RNA and virulence genes. *Proc. Natl. Acad. Sci.* **103**(1), 171–6 (2006).

416. Chambonnier, G. *et al.* The Hybrid Histidine Kinase LadS Forms a Multicomponent Signal Transduction System with the GacS/GacA Two-

Component System in *Pseudomonas aeruginosa*. *PLoS Genet.* **12**(5), e1006032 (2016).

417. Hsu, J. L., Chen, H. C., Peng, H. L. & Chang, H. Y. Characterization of the histidine-containing phosphotransfer protein B-mediated multistep phosphorelay system in *Pseudomonas aeruginosa* PAO1. *J. Biol. Chem.* **283**(15), 9933–44 (2008).

418. Bhuwan, M., Lees, H. J., Pengs, H. L. & Chang, H. Y. Histidine-containing phosphotransfer protein-B (HptB) regulates swarming motility through partner-switching system in *Pseudomonas aeruginosa* PAO1 strain. *J. Biol. Chem.* **287**(3), 1903–14 (2012).

419. Skerker, J. M., Prasol, M. S., Perchuk, B. S., Biondi, E. G. & Laub, M. T. Two-component signal transduction pathways regulating growth and cell cycle progression in a bacterium: A system-level analysis. *PLoS Biol.* **3**(10), e334 (2005).

420. Weigt, M., White, R. A., Szurmant, H., Hoch, J. A. & Hwa, T. Identification of direct residue contacts in protein-protein interaction by message passing. *Proc. Natl. Acad. Sci.* **106**(1), 67–72 (2009).

421. Skerker, J. M. *et al.* Rewiring the Specificity of Two-Component Signal Transduction Systems. *Cell* **133**(6), 1043–54 (2008).

422. Capra, E. J. *et al.* Systematic dissection and trajectory-scanning mutagenesis of the molecular interface that ensures specificity of two-component signaling pathways. *PLoS Genet.* **6**(11), e1001220 (2010).

423. Casino, P., Rubio, V. & Marina, A. Structural Insight into Partner Specificity and Phosphoryl Transfer in Two-Component Signal Transduction. *Cell* **139**(2), 325–36 (2009).

424. Willett, J. W. *et al.* Specificity residues determine binding affinity for two-component signal transduction systems. *MBio* **4**(6), e00420-13 (2013).

425. Ashenberg, O., Rozen-Gagnon, K., Laub, M. T. & Keating, A. E. Determinants of homodimerization specificity in histidine kinases. *J. Mol. Biol.* **413**(1), 222–35 (2011).

426. Galperin, M. Y., Higdon, R. & Kolker, E. Interplay of heritage and habitat

in the distribution of bacterial signal transduction systems. *Mol. Biosyst.* **6**(4), 721–8 (2010).

427. Gislason, A. S. *et al.* Competitive growth enhances conditional growth mutant sensitivity to antibiotics and exposes a two-component system as an emerging antibacterial target in *Burkholderia cenocepacia*. *Antimicrob. Agents Chemother.* **61**(1), e00790-16 (2017).

428. Cui, C. *et al.* A novel two-component system modulates quorum sensing and pathogenicity in *Burkholderia cenocepacia*. *Mol. Microbiol.* **108**(1), 32–44 (2018).

429. Flannagan, R. S., Aubert, D., Kooi, C., Sokol, P. A. & Valvano, M. A. *Burkholderia cenocepacia* requires a periplasmic HtrA protease for growth under thermal and osmotic stress and for survival in vivo. *Infect. Immun.* **75**(4), 1679–89 (2007).

430. Aubert, D. F., Flannagan, R. S. & Valvano, M. A. A novel sensor kinase-response regulator hybrid controls biofilm formation and type VI secretion system activity in *Burkholderia cenocepacia*. *Infect. Immun.* **76**(5), 1979–91 (2008).

431. Aubert, D. F., O'Grady, E. P., Hamad, M. A., Sokol, P. A. & Valvano, M. A. The *Burkholderia cenocepacia* sensor kinase hybrid AtsR is a global regulator modulating quorum-sensing signalling. *Environ. Microbiol.* **15**(2), 372–85 (2013).

432. Khodai-Kalaki, M., Aubert, D. F. & Valvano, M. A. Characterization of the AtsR hybrid sensor kinase phosphorelay pathway and identification of its response regulator in *Burkholderia cenocepacia*. *J. Biol. Chem.* **288**(42), 30473–84 (2013).

433. Merry, C. R. *et al.* Characterization of a Novel Two-Component System in *Burkholderia cenocepacia*. *Curr. Microbiol.* **70**(4), 556–61 (2015).

434. Tomich, M. & Mohr, C. D. Genetic characterization of a multicomponent signal transduction system controlling the expression of cable pili in *Burkholderia cenocepacia*. *J. Bacteriol.* **186**(12), 3826–36 (2004).

435. Trias, J. & Nikaido, H. Outer membrane protein D2 catalyzes facilitated

diffusion of carbapenems and penems through the outer membrane of *Pseudomonas aeruginosa*. *Antimicrob. Agents Chemother.* **34**(1), 52–7 (1990).

436. Ducret, V., Gonzalez, M. R., Scrignari, T. & Perron, K. OprD repression upon metal treatment requires the RNA chaperone Hfq in *Pseudomonas aeruginosa*. *Genes (Basel).* **7**(10), E82 (2016).

437. Jones, A. L., DeShazer, D. & Woods, D. E. Identification and characterization of a two-component regulatory system involved in invasion of eukaryotic cells and heavy-metal resistance in *Burkholderia pseudomallei*. *Infect. Immun.* **65**(12), 4972–7 (1997).

438. Dieppois, G., Ducret, V., Caille, O. & Perron, K. The Transcriptional Regulator CzcR Modulates Antibiotic Resistance and Quorum Sensing in *Pseudomonas aeruginosa*. *PLoS One* **7**(5), e38148 (2012).

439. Figurski, D. H. & Helinski, D. R. Replication of an origin-containing derivative of plasmid RK2 dependent on a plasmid function provided in trans. *Proc. Natl. Acad. Sci.* **76**(4), 1648–52 (1979).

440. Flannagan, R. S., Linn, T. & Valvano, M. A. A system for the construction of targeted unmarked gene deletions in the genus *Burkholderia*. *Environ. Microbiol.* **10**(6), 1652–60 (2008).

441. Cardona, S. T. & Valvano, M. A. An expression vector containing a rhamnose-inducible promoter provides tightly regulated gene expression in *Burkholderia cenocepacia*. *Plasmid* **54**(3), 219–228 (2005).

442. Lefebre, M. D. & Valvano, M. A. Construction and evaluation of plasmid vectors optimized for constitutive and regulated gene expression in *Burkholderia cepacia* complex isolates. *Appl. Environ. Microbiol.* **68**(12), 5956–64 (2002).

443. Schwager, S. *et al.* The genetic basis of cadmium resistance of *Burkholderia cenocepacia*. *Environ. Microbiol. Rep.* **4**(5), 562–8 (2012).

444. Hofmann, K. & Stoffel, W. TMbase: A Database of Membrane Spanning Protein Segments. *Biol. Chem.* **374**, 166 (1993).

445. Hess, J. F., Bourret, R. B. & Simon, M. I. Phosphorylation Assays for Proteins of the Two-Component Regulatory System Controlling Chemotaxis in *Escherichia coli*. *Methods Enzymol.* **200**, 188–204 (1991).

446. Porter, S. L., Wadhams, G. H. & Armitage, J. P. In Vivo and In Vitro Analysis of the *Rhodobacter sphaeroides* Chemotaxis Signaling Complexes. in *Methods in Enzymology* **423**, 392–413 (2007).

447. Meyer, M. & Hofherr, L. A broth-disc technique for the assay of antibiotic synergism. *Can. J. Microbiol.* **25**(11), 1232–8 (1979).

448. Christensen, G. D., Simpson, W. A., Bisno, A. L. & Beachey, E. H. Adherence of slime-producing strains of *Staphylococcus epidermidis* to smooth surfaces. *Infect. Immun.* **37**(1), 318–26 (1982).

449. Ceri, H. *et al.* The Calgary Biofilm Device: New technology for rapid determination of antibiotic susceptibilities of bacterial biofilms. *J. Clin. Microbiol.* **37**(6), 1771–6 (1999).

450. Huber, B. *et al.* The cep quorum-sensing system of *Burkholderia cepacia* H111 controls biofilm formation and swarming motility. *Microbiology* **147**(9), 2517–28 (2001).

451. Denman, C. C. & Brown, A. R. Mannitol promotes adherence of an outbreak strain of *Burkholderia multivorans* via an exopolysaccharide-independent mechanism that is associated with upregulation of newly identified fimbrial and afimbrial adhesins. *Microbiol. (United Kingdom)* **159**(4), 771–81 (2013).

452. Lysenko, O. & Weiser, J. Bacteria associated with the nematode *Neoaplectana carpocapsae* and the pathogenicity of this complex for *Galleria mellonella* larvae. *J. Invertebr. Pathol.* **24**(3), 332–6 (1974).

453. Seed, K. D. & Dennis, J. J. Development of *Galleria mellonella* as an alternative infection model for the *Burkholderia cepacia* complex. *Infect. Immun.* **76**(3), 1267–75 (2008).

454. Martin, M. Cutadapt removes adapter sequences from high-throughput sequencing reads. *EMBnet.journal* **17**(1), 10–12 (2011).

455. Patro, R., Duggal, G., Love, M. I., Irizarry, R. A. & Kingsford, C. Salmon

provides fast and bias-aware quantification of transcript expression. *Nat. Methods* **14**(4), 417–9 (2017).

456. Love, M. I., Huber, W. & Anders, S. Moderated estimation of fold change and dispersion for RNA-seq data with DESeq2. *Genome Biol.* **15**(12), 550 (2014).

457. LaVallie, E. R. *et al.* A thioredoxin gene fusion expression system that circumvents inclusion body formation in the *E*. *coli* cytoplasm. *Bio/Technology* **11**(2), 187–93 (1993).

458. Porter, S. L. *et al.* The CheYs of *Rhodobacter sphaeroides*. *J. Biol. Chem.* **281**(43), 32694–704 (2006).

459. Dutta, R. & Inouye, M. Reverse phosphotransfer from OmpR to EnvZ in a kinase-/phosphatase+ mutant of EnvZ (EnvZ·N347D), a bifunctional signal transducer of *Escherichia coli*. *J. Biol. Chem.* **271**(3), 1424–9 (1996).

460. Willett, J. W. & Kirby, J. R. Genetic and Biochemical Dissection of a HisKA Domain Identifies Residues Required Exclusively for Kinase and Phosphatase Activities. *PLoS Genet.* **8**(11), e1003084 (2012).

461. Pannen, D., Fabisch, M., Gausling, L. & Schnetz, K. Interaction of the RcsB response regulator with auxiliary transcription regulators in *Escherichia coli*. *J. Biol. Chem.* **291**(5), 2357–70 (2016).

462. Karimova, G., Pidoux, J., Ullmann, A. & Ladant, D. A bacterial two-hybrid system based on a reconstituted signal transduction pathway. *Proc. Natl. Acad. Sci. U. S. A.* **95**(10), 5752–6 (1998).

463. Elsinghorst, E. A. Measurement of invasion by gentamicin resistance. *Methods Enzymol.* **236**, 405–20 (1994).

464. Kobylka, J., Kuth, M. S., Müller, R. T., Geertsma, E. R. & Pos, K. M. AcrB: a mean, keen, drug efflux machine. *Ann. N. Y. Acad. Sci.* **1459**(1) 38–68 (2020).

465. Köhler, T., Epp, S. F., Curty, L. K. & Pechère, J. C. Characterization of MexT, the regulator of the MexE-MexF-OprN multidrug efflux system of *Pseudomonas aeruginosa*. *J. Bacteriol.* **181**(20), 6300–5 (1999).

466. Hamad, M. A., Skeldon, A. M. & Valvano, M. A. Construction of Aminoglycoside-Sensitive *Burkholderia cenocepacia* Strains for Use in Studies of Intracellular Bacteria with the Gentamicin Protection Assay. *Appl. Environ. Microbiol.* **76**(10), 3170–6 (2010).

467. Huerta-Cepas, J. *et al.* Fast genome-wide functional annotation through orthology assignment by eggNOG-mapper. *Mol. Biol. Evol.* **34**(8), 2115–22 (2017).

468. Munson, G. P., Lam, D. L., Outten, F. W. & O'Halloran, T. V. Identification of a copper-responsive two-component system on the chromosome of *Escherichia coli* K-12. *J. Bacteriol.* **182**(20), 5864–71 (2000).

469. Gudipaty, S. A., Larsen, A. S., Rensing, C. & Mcevoy, M. M. Regulation of Cu(I)/Ag(I) efflux genes in *Escherichia coli* by the sensor kinase CusS. *FEMS Microbiol. Lett.* **330**(1), 30–7 (2012).

470. Su, C. C., Long, F. & Yu, E. W. The cus efflux system removes toxic ions via a methionine shuttle. *Protein Sci.* **20**(1), 6–18 (2011).

471. Xue, Y. *et al.* Cu(I) recognition via cation-π and methionine interactions in CusF. *Nat. Chem. Biol.* **4**(2), 107–9 (2008).

472. Kittleson, J. T. *et al.* Periplasmic metal-resistance protein CusF exhibits high affinity and specificity for both Cu I and Ag I. *Biochemistry* **45**(37), 11096–102 (2006).

473. Bagai, I., Rensing, C., Blackburn, N. J. & McEvoy, M. M. Direct metal transfer between periplasmic proteins identifies a bacterial copper chaperone. *Biochemistry* **47**(44), 11408–14 (2008).

474. Kulathila, R., Kulathila, R., Indic, M. & van den Berg, B. Crystal structure of *Escherichia coli* CusC, the outer membrane component of a heavy metal efflux pump. *PLoS One* **6**(1), e15610 (2011).

475. Tetaz, T. J. & Luke, R. K. J. Plasmid-controlled resistance to copper in *Escherichia coli*. *J. Bacteriol.* **154**(3), 1263–8 (1983).

476. Brown, N. L., Barrett, S. R., Camakaris, J., Lee, B. T. O. & Rouch, D. A. Molecular genetics and transport analysis of the copper-resistance determinant (pco) from *Escherichia coli* plasmid pRJ1004. *Mol. Microbiol.*

17(6), 1153–66 (1995).

477. Argüello, J. M., Raimunda, D. & Padilla-Benavides, T. Mechanisms of copper homeostasis in bacteria. *Front. Cell. Infect. Microbiol.* **3**, 73 (2013).

478. Zhang, L., Koay, M., Maher, M. J., Xiao, Z. & Wedd, A. G. Intermolecular transfer of copper ions from the CopC protein of *Pseudomonas syringae*. Crystal structures of fully loaded CuICuII forms. *J. Am. Chem. Soc.* **128**(17), 5834–50 (2006).

479. Zimmermann, M. *et al.* PcoE - A metal sponge expressed to the periplasm of copper resistance *Escherichia coli*. Implication of its function role in copper resistance. *J. Inorg. Biochem.* **115**, 186–97 (2012).

480. Cha, J. S. & Cooksey, D. A. Copper hypersensitivity and uptake in *Pseudomonas syringae* containing cloned components of the copper resistance operon. *Appl. Environ. Microbiol.* **59**(5), 1671–4 (1993).

481. Arnesano, F., Banci, L., Bertini, I. & Thompsett, A. R. Solution structure of CopC: A cupredoxin-like protein involved in copper homeostasis. *Structure* **10**(10), 1337–47 (2002).

482. Outten, F. W., Outten, C. E., Hale, J. & O'Halloran, T. V. Transcriptional activation of an *Escherichia coli* copper efflux regulon by the chromosomal MerR homologue, CueR. *J. Biol. Chem.* **275**(40), 31024–9 (2000).

483. Rensing, C., Fan, B., Sharma, R., Mitra, B. & Rosen, B. P. CopA: An *Escherichia coli* Cu(I)-translocating P-type ATPase. *Proc. Natl. Acad. Sci. U. S. A.* **97**(2), 652–6 (2000).

484. Outten, F. W., Huffman, D. L., Hale, J. A. & O'Halloran, T. V. The Independent cue and cus Systems Confer Copper Tolerance during Aerobic and Anaerobic Growth in *Escherichia coli*. *J. Biol. Chem.* **276**(33), 30670–7 (2001).

485. Radford, D. S. *et al.* CopZ from *Bacillus subtilis* interacts in vivo with a copper exporting CPx-type ATPase CopA. *FEMS Microbiol. Lett.* **220**(1), 105–12 (2003).

486. Quintana, J., Novoa-Aponte, L. & Argüello, J. M. Copper homeostasis networks in the bacterium *Pseudomonas aeruginosa*. *J. Biol. Chem.* **292**(38), 15691–704 (2017).

487. Sass, A. M. *et al.* The unexpected discovery of a novel low-oxygen-activated locus for the anoxic persistence of *Burkholderia cenocepacia*. *ISME J.* **7**(8), 1568–81 (2013).

488. Cullen, L. *et al.* The involvement of the low-oxygen-activated locus of *Burkholderia cenocepacia* in adaptation during cystic fibrosis infection. *Sci. Rep.* **8**(1), 13386 (2018).

489. Peng, J., Miao, L., Chen, X. & Liu, P. Comparative transcriptome analysis of *Pseudomonas putida* KT2440 revealed its response mechanisms to elevated levels of zinc stress. *Front. Microbiol.* **9**, 1669 (2018).

490. Bailey, T. L. *et al.* MEME Suite: Tools for motif discovery and searching. *Nucleic Acids Res.* **37**, W202–8 (2009).

491. Coenye, T. *et al.* Identification of putative noncoding RNA genes in the *Burkholderia cenocepacia* J2315 genome. *FEMS Microbiol. Lett.* **276**(1), 83–92 (2007).

492. Mitchell, A. L. *et al.* InterPro in 2019: Improving coverage, classification and access to protein sequence annotations. *Nucleic Acids Res.* **47**(D1), D351–D360 (2019).

493. Nairn, B. L. *et al.* The Response of *Acinetobacter baumannii* to Zinc Starvation. *Cell Host Microbe* **19**(6), 826–36 (2016).

494. Capdevila, D. A., Edmonds, K. A. & Giedroc, D. P. Metallochaperones and metalloregulation in bacteria. *Essays in Biochemistry* **61**(2), 177–200 (2017).

495. Marchler-Bauer, A. *et al.* CDD: NCBI's conserved domain database. *Nucleic Acids Res.* **43**, D222–6 (2015).

496. Sievers, F. *et al.* Fast, scalable generation of high-quality protein multiple sequence alignments using Clustal Omega. *Mol. Syst. Biol.* **7**, 539 (2011).

497. Mahenthiralingam, E. *et al.* DNA-based diagnostic approaches for

identification of *Burkholderia cepacia* complex, *Burkholderia vietnamiensis*, *Burkholderia multivorans*, *Burkholderia stabilis*, and *Burkholderia cepacia* genomovars I and III. *J. Clin. Microbiol.* **38**(9), 3165–73 (2000).